GEORG-AUGUST-UNIVERSITÄT GÖTTINGEN

université de BORDEAUX

From the centrosome to the nuclear envelope and beyond: insights into the role of CRM1 in adenoviral genome delivery

Dissertation
for the award of the degree
"Doctor of Philosophy"

of the Georg-August-Universität, Göttingen
within the doctoral program *Molecular Medicine*
of the Georg-August University School of Science (GAUSS)
and

of the University of Bordeaux
within the Doctoral School Life and Health Sciences
with the Speciality *Microbiology - Immunology*

Submitted by Floriane Lagadec
From Landerneau, France

Göttingen, 2020

GEORG-AUGUST-UNIVERSITÄT
GÖTTINGEN

université de BORDEAUX

Du centrosome à l'enveloppe nucléaire et au-delà : un aperçu du rôle de CRM1 dans la libération du génome adénoviral

Thèse en cotutelle présentée pour obtenir
le grade de Docteur

de la Georg-August-Universität, Göttingen
au sein du programme doctoral *Molecular Medicine*
de la Georg-August University School of Science (GAUSS)
et

de l'Université de Bordeaux
Ecole Doctorale des Sciences de la Vie et de la Santé (SVS)
avec la spécialité *Microbiologie - Immunologie*

Par Floriane Lagadec
De Landerneau, France

Göttingen, 2020

Examination Board

Prof. Dr. med. Dörthe M. Katschinski (1st referee)

Institute of Cardiovascular Physiology

University Medical Center Göttingen

Prof. Dr. Beate Sodeik (2nd referee)

Institute of Virology

Medizinische Hochschule Hannover

Prof. Dr. Stefan Pöhlmann (3rd referee)

Abt. Infektionsbiologie

Deutsches Primatenzentrum, Göttingen

Dr. Anne Royou

Institut européen de chimie et biologie

Université de Bordeaux

Prof. Dr. Ralph H. Kehlenbach (PhD thesis co-supervisor)

Department of Molecular Biology

Georg-August-Universität Göttingen

Dr. Harald Wodrich (PhD thesis co-supervisor)

UMR 5234

Université de Bordeaux

Date of oral examination: 2nd June 2020

Declaration

I hereby declare that I have written this PhD thesis independently and with no other sources or aids than quoted.

Göttingen, April 2020

Floriane Lagadec

Table of contents

Acknowledgments

I would like first to thank Prof. D. Katschinski, Prof. B. Sodeik and Prof. S. Pöhlmann who kindly accepted to be the reviewers of my thesis manuscript. Thank you to Dr. A. Royou and to my two supervisors, Prof. R. Kehlenbach and Dr. H. Wodrich for evaluating my work.

As my time was shared between two places during these last years, I have twice as much people to thank. Harry and Ralph, thank you for offering me this opportunity, to work on this project. I am very thankful for your support, your help, to have given me the chance to travel, to initiate new projects, for the scientific freedom that you always gave us and for all these things that I have learnt. Vielen Dank!

I am very thankful to all the members of my “French lab” in Bordeaux. When I firstly joined the group back to my 1st year of Master, I would have never imagined ending up writing those lines… so thank you Fabienne to had given me the opportunity to join the Adeno team and for your help during these last 3 years. Thank you Benoît for your help purifying the TP antibodies and for our scientific (and less serious) discussions. Marie-Edith, thank you for your medical expertise that allows us to see viruses differently than from under our microscopes. Muriel and Jess, thank you for your help, our discussions and for facilitating our life in the lab. Cathy and Valérie thank you for your positive attitudes and your energy. Thank you to the members of the HBV team with whom we shared more than a lab, to all the past members of the lab and especially to Tetsuro for the generation of all these scientific tools.

A big thank you to, Noémie, Lara and Irene. Thank you for your presence, your help and your craziness. We shared much more than “la réalité de notre métier” together and I am very grateful to have had you by my side. I would also like to thank the team #CtrlT for all these talks and moments together.

Thank you to all the members of the UMR 5234. Sandrine, thank you for your help regarding all my travelling issues and your quick responsiveness. Thank you to Denis Dacheux for the generation of the TP antibodies. A special thanks to Vincent and Paul for welcoming me in your group and giving me the opportunity to develop collaborative projects. I am thankful to the members of the Bordeaux Imaging Center, for their availability and their help.

Thank you to the past and current members of my “German lab”. I would have never imagined coming back to Göttingen after my Master thesis, but thanks for your welcome and making me feel quickly part of the lab. Christiane thank you for your help and your kindness. Birgit, Mohamed, Imke, Christina and Mariuuuuus, thank you for your availability, your help (scientifically and German-wise!), our scientific talks and the moments spent together. I learnt a lot by your sides. I am also thankful to all the member of the Molecular Biology Department members, to maintain such a nice environment of work.

A special thanks to Maria and Renata for your friendship and your support. Renata, thank you for your motivation and all these crazy moments that we shared.

Je voudrais remercier mes amis de toujours, les “M”, de répondre toujours présents malgré la distance. Aude, Ju, Bogam, merci pour ces week-ends bordelais, rennais, vannetais et tous ces moments qui m’ont toujours reboosté. Laura, merci de m’avoir toujours aussi bien accueillie pendant mes transferts « franco-allemands », et merci pour tous ces moments partagés aux quatre coins de l’Europe (et crois moi mon soleil, ce n’est pas fini !). Camille, merci pour tes conseils avisés toujours très justes (oui, j’ai du mal à l’admettre mais merci de me connaître aussi bien…). Jo, un énorme merci pour ton soutien et toutes ces discussions sans fin qui me font toujours le plus grand bien. À vous tous, votre amitié m’est très chère !

Pour terminer, je tiens à remercier ma famille d’avoir cru en moi, de m’avoir soutenu et écouté dans les bons comme dans les moins bons moments. Papa, Maman, Damien, Victor et Louis, même si la distance n’a pas été facile tous les jours, il me tarde que l’on se retrouve pour désormais, ne profiter que des bons moments.

List of figures

List of tables

List of abbreviations

A

AP: aprotinin
ATP: adenosine-5-triphosphate
AVP: adenoviral protease
AdV: adenovirus
Ad5: adenovirus type 5
AdV pol: adenoviral DNA polymerase

B

bp: base pair

C

CRM1: chromosome region maintenance 1
CAR: coxsackievirus and adenovirus receptor
CD46: cluster of differentiation 46
CRIME: CRM1, Importin-β, Etc
CBS: chromatin binding site

D

DMEM: Dulbecco's modified eagles medium
DBP: DNA binding protein
DNA: desoxyribonucleic acid
dNTP: 2'-desoxynucleoside-5'-triphosphate
DTT: dithiothreitol
DAPI: 4',6-diamidino-2-phenylindole
DMSO: dimethyl sulfoxide

E

E1A: immediate early transcription unit A

F

FG: phenylalanine glycine
FCS: fetal calf serum
FACS: fluorescence-activated cell sorting

G

GTP: guanosine-5'-triphosphate
GDP: guanosine-5'-diphosphate
GFP: green fluorescence protein
GST: glutathione S-transferase
g: units of gravity

H

hCMV: human cytomegalovirus
HIV-1: human immunodefiency virus-1
His: Histidine Tag
HA: hemagglutinin
HSV-1: herpes simplex virus-1
HEAT: huntington, elongation factor 3, protein phosphatase 2A and TOR1
Hsc70: heat shock cognate 71 kDa protein
HFV: human foamy virus
HEK293: human embryonic kidney 293
hpi: hours post infection

I

IPTG: isopropyl b-D-1-thiogalactopyranoside
ITR: inverted terminal repeats

K

Kif5B: kinesin family member 5B

Kd: dissociation constant

KHSV: Kaposi's sarcoma-associated herpesvirus

kDa: kilo dalton

L

LMB: Leptomycin B

LP: Leupeptin Pepstatin

M

MAP: microtubule associated protein

MTOC: microtubule organisation center

MOI: multiplicity of infection

mRNA: messenger ribonucleic acid

M9: PY-NLS described in hnRNPA1

MW: molecular weight

N

NLS: nuclear localization signal

NES: nuclear export signal

NE: nuclear envelope

NPC: nuclear pore complex

NTF2: nuclear transport factor 2

Nup: nucleoporin

NEBD: nuclear envelope break down

NFAT: nuclear factor of activated T-cell

O

OD: optical density

P

PKI: protein kinase inhibitor

PBS: phosphate buffered saline

PCM: pericentriolar material

PCR: polymerase chain reaction

PFV: prototype foamy virus

PMSF: phenylmethylsulphonyl fluoride

pp: physical particle

PPxY: proline-proline-x-tyrosine

pTP: precursor TP

PFA: paraformaldehyde

R

RCC1: regulator of chromatin condensation 1

RanGAP: RanGTPase activating protein

RanBP: Ran binding protein

RNA: ribonucleic acid

rpm: rotations per minute

S

SAF: spindle assembly factor

SDS-PAGE: sodium-dodecyl-sulfate polyacrylamide gel electrophoresis

SPN1: snurportin 1

T

TAF-I: template activating factor-I

TP: terminal protein

U

U2OS: human osteosarcoma derived cells

V

vDNA: viral DNA

Abstracts

From the centrosome to the nuclear envelope and beyond: insights into the role of CRM1 in adenoviral genome delivery

Adenoviruses (AdV) are DNA viruses that replicate in the nucleus of their host cell. Due to the limited coding capacity, they have to take advantage of cellular mechanisms in order to perform their infection cycle. During entry, AdV particles use the microtubule transport machinery to reach the nucleus. AdVs interact with the microtubule motor dynein to be transported towards the nuclear compartment, where they dock to Nuclear Pore Complexes (NPCs), structures embedded into the nuclear envelop (NE). Once at the NPC, viral capsids disassemble to finally release and import their genome. Microtubule unloading, nuclear translocation and genome import of AdVs involve components of the nucleocytoplasmic transport machinery. However, the exact mechanism used by the virus to reach the NPC remains unclear. Nucleocytoplasmic transport involves different components and is tightly regulated. The active transport of cargoes is mediated by import and export factors interacting with RanGTP. The major cellular export factor CRM1 is known to be essential for targeting of AdVs to the NE. Pharmacological inhibition of CRM1 with Leptomycin B leads to the accumulation of AdVs at the centrosome, the major Microtubule Organisation Centre (MTOC) in mammalian cells. We thus investigated the role of CRM1 leading to AdV genome delivery. We analysed the interaction of AdV with the MTOC and observed that the absence of cytoplasmic factors and disruption of microtubules did not impair their accumulation at the MTOC. We identified and characterized a mutant of CRM1, functional for physiological export but inducing a strong delay in AdV NE translocation. We used live cell-imaging to analyse infections in mitotic cells, revealing a role of CRM1 in genome release from the capsid. Moreover, we identified a potential viral partner of CRM1 among the AdV genome associated core proteins, the Terminal Protein. Terminal protein contains a nuclear export signal and is a CRM1 export substrate. Taken together, our data highlight a possible role of CRM1 as an essential mediator for the complete dismantling of AdV capsid, promoting genome release and genome import.

Keywords: Adenovirus; nucleocytoplasmic transport; centrosome; CRM1

Universitätsmedizin Göttingen
Institut für Molekularbiologie
AG Kehlenbach
Humboldtallee 23
D-37 073 Göttingen
Germany

Laboratoire MFP
CNRS UMR 5234
Equipe SpacVir
146 rue Léo Saignat
33 076 Bordeaux Cedex
France

Du centrosome à l'enveloppe nucléaire et au-delà : un aperçu du rôle de CRM1 dans la libération du génome adénoviral

Les adénovirus (AdV) sont des virus à ADN se répliquant dans le noyau de la cellule hôte. Pour pouvoir se répliquer, ils détournent la machinerie cellulaire à leur profit. Au cours de l'entrée dans la cellule, les particules virales utilisent la machinerie de transport des microtubules pour rejoindre le noyau. Les AdV interagissent avec la dynéine, moteur moléculaire associé aux microtubules, pour être transportés vers le compartiment nucléaire. Ils se lient alors aux pores nucléaires, structures ancrées dans l'enveloppe nucléaire (EN). Une fois aux pores nucléaires, les capsides virales se désassemblent pour libérer et importer leur génome. Les mécanismes de détachement des microtubules, de translocation nucléaire et d'import du génome des AdV impliquent des facteurs de la machinerie de transport nucléocytoplasmique. Cependant, le mécanisme exact utilisé par les virus pour atteindre les pores nucléaires n'est pas clairement défini. Le transport nucléocytoplasmique est composé de différents facteurs et est hautement régulé dans les cellules. Le transport actif de cargos est dû à des facteurs d'import et d'export interagissant avec RanGTP. Le principal facteur d'export est CRM1 et il est connu pour être essentiel dans la translocation des AdV vers l'EN. L'inhibition de CRM1 par la Leptomycine B conduit à l'accumulation des AdV au centrosome, le principal Centre Organisateur des Microtubules (COMT) des cellules de mammifères. Nous avons donc étudié le rôle de CRM1 dans la libération du génome adénoviral. Nous avons analysé l'interaction des AdVs avec le COMT et nous avons observé que l'absence de facteurs cytoplasmiques ainsi que la perte d'intégrité des microtubules n'affectaient pas leur accumulation au COMT. En revanche, nous avons identifié et caractérisé un mutant de CRM1, qui reste fonctionnel pour l'export physiologique de cargo mais qui induit un retard important dans la translocation des AdV vers l'EN. Nous avons utilisé l'imagerie sur cellules vivantes pour analyser l'infection de l'AdV dans des cellules mitotiques et ceci a permis de révéler le rôle de CRM1 dans la libération du génome de ce virus. Nous avons également identifié un partenaire viral potentiel pour CRM1 parmi les protéines associées au génome viral, la Terminal Protein (TP). Cette protéine possède un signal d'export nucléaire et est un substrat de CRM1. Nos données soulignent le rôle de CRM1 comme un médiateur essentiel au désassemblage total de la capside adénovirale, qui favorise la libération du génome et son import.

Mots-clefs : Adénovirus ; transport nucléocytoplasmique ; centrosome ; CRM1

Vom Zentrosom zur Kernhülle und darüber hinaus: Einblicke in die Rolle von CRM1 im Transport adenoviraler Genome

Adenoviren (AdVs) sind DNA-Viren, die sich im Zellkern ihrer Wirtszelle replizieren. Wegen ihrer limitierten Verpackungskapazität müssen sie zelluläre Mechanismen ausnutzen, um ihren Infektionszyklus durchzuführen. AdV Partikel nutzen das Mikrotubuli-Transportsystem, um den Zellkern zu erreichen. Sie interagieren mit dem Motorprotein Dynein, um entlang der Mikrotubuli in Richtung des Zellkerns transportiert zu werden. Dort docken sie an Kernporen (NPCs) an, Strukturen die innerhalb der Kernhülle (NE) eingebettet sind. An den NPCs angekommen, lösen sich die virale Kapside auf, um schließlich ihr Genom freizusetzen und zu importieren. Für das Entladen von Mikrotubuli, die nukleare Translokation und den Genom-Import von AdVs wird die nukleozytoplasmatische Transportmaschinerie genutzt. Der exakte Mechanismus, der von den Viren verwendet wird, um die NPCs zu erreichen, ist jedoch unklar. Der nukleozytoplasmatische Transport beinhaltet verschiedene Komponenten und ist innerhalb der Zelle genau reguliert. Der aktive Transport von Proteinen wird durch Import- und Exportfaktoren vermittelt, die mit RanGTP interagieren. Der wichtige zelluläre Exportfaktor CRM1 hat eine essentielle Rolle beim Transport von AdVs zur Kernhülle. Pharmakologische Inhibition von CRM1 mittels Leptomycin B führt zu der Ansammlung von AdVs am Zentromer, dem primären Mikrotubuli-organisierenden Zentrum (MTOC) in Säugetierzellen. Wir haben deshalb die Rolle von CRM1 innerhalb von AdV Genomabgabe untersucht. Bei der Analyse der Interaktion von AdVs mit dem MTOC konnten wir feststellen, dass die Abwesenheit von zytoplasmatischen Faktoren und die Dissoziation von Mikrotubuli ihre Akkumulation am MTOC nicht beeinträchtigten. Wir identifizierten und charakterisierten eine Mutante von CRM1, die funktionell bezüglich Proteinexport aus dem Zellkern ist, aber eine Verzögerung von AdV NE-Translokation bewirkte. Wir nutzten Live-Cell-Imaging, um Infektionen in mitotischen Zellen zu analysieren, und deckten dabei eine Rolle von CRM1 bei der Genomfreisetzung aus dem Kapsid auf. Weiterhin identifizierten wir einen potentiellen viralen Partner von CRM1, das Terminal Protein, welches mit dem AdV Genom assoziiert ist. Das Terminal Protein enthält ein nukleares Exportsignal und ist ein CRM1-Exportsubstrat. Zusammenfassend zeigen unsere Daten eine mögliche Rolle von CRM1 als essentiellem Vermittler bei der vollständigen Auflösung des AdV Kapsids, wodurch die Genomfreisetzung und der Genomimport gefördert werden.

Stichwörter: Adenovirus; nukleozytoplasmatischer Transport; Zentrosom; CRM1

Substancial abstract in French

Les adénovirus (AdVs) sont des virus à ADN non enveloppés appartenant au genre des *Masteadenoviruses*. Ce genre est divisé en 7 espèces. Au sein de ces espèces, les AdV sont répartis par types selon leur tropisme et leurs propriétés biologiques physiques et chimiques. Ces virus ont un large tropisme (tractus respiratoire, gastro-intestinal, conjonctival…) et sont responsables d'infections modérées mais peuvent avoir de lourdes conséquences chez les enfants ou les personnes immunodéprimées. Leur ADN ne s'intègre pas dans celui de la cellule hôte, ils ne sont pas oncogènes pour l'Homme, ils ont une large capacité d'encapsidation ce qui en fait de bons outils pour la thérapie génique. Les types 2 et 5 sont les plus étudiés en recherche fondamentale. Notre étude ici se porte sur le type 5 (Ad5). L'Ad5 est constitué d'une capside icosaédrique de 90 nm de diamètre renfermant une molécule d'ADN linéaire double brin de 36 kpb, entourée de protéines « core ». Ces protéines core protègent l'ADN d'une dégradation cellulaire et sont indispensables pour le cycle viral. Parmi elles, la protéine VII (pVII) est la plus abondante avec environ 500 copies par particule virale, et forme des structures similaires aux histones cellulaires. La protéine terminale (TP) quant à elle est liée aux extrémités 5' de l'ADN viral et 2 copies sont ainsi retrouvées par virion.

Le cycle viral de l'Ad5 est initié par son attachement aux récepteurs de la cellule cible et est suivi par son entrée dans la cellule via l'endocytose. Une fois dans l'endosome, l'acidité du pH provoque un désassemblage partiel de la particule et l'exposition de protéines internes de la capside permet l'échappement endosomal de l'Ad5. Pour se répliquer, le virus doit ensuite atteindre le noyau pour y libérer son génome. Pour accéder au noyau, l'Ad5 utilise la voie de transport des microtubules. Sa liaison à la dynéine, moteur moléculaire, lui permet de rejoindre le centrosome, le principal Centre Organisateur des Microtubules (COMT). L'Ad5 va ensuite détourner la machinerie de transport nucléocytoplasmique pour importer son génome dans le noyau. Sachant que la taille de la capside ne permet pas son import nucléaire telle quelle, une étape préalable de désassemblage total de la capside et de libération de l'ADN viral est nécessaire pour l'import du génome dans le noyau. Une fois le génome importé, la réplication de l'ADN viral peut débuter, pour permettre la production de nouvelles particules virales. Ces premières étapes de transport de l'Ad5 jusqu'au noyau sont partiellement caractérisées, mais le mécanisme utilisé par ce virus pour se détacher des microtubules et rejoindre le noyau, ainsi que le mécanisme de désassemblage et de libération du génome restent encore mal connus.

La voie de transport nucléocytoplasmique est un mécanisme cellulaire bien régulé. En effet, des échanges constants entre le noyau et le cytoplasme sont nécessaires pour le bon fonctionnement de la cellule. Ce transport de molécules est réalisé au travers de pores nucléaires, structures intégrées dans l'enveloppe nucléaire.

Dans la cellule, les molécules de petite taille (< 40 kDa) sont transportées par diffusion passive alors qu'un transport actif impliquant différents facteurs cellulaires est requis pour les molécules les plus grandes. Le transport actif est facilité par des facteurs de transport. Les importines ou exportines se lient à des séquences spécifiques exposées par les protéines cargos nécessitant un transport : des Signaux de Localization Nucléaire (SLN) ou Signaux d'Export Nucléaire (SEN), respectivement. Le sens du transport est aussi régulé par RanGTP, une protéine de la famille Ran, capable de se lier à une molécule de GDP ou GTP. Un gradient de RanGTP est présent autour de l'enveloppe nucléaire, avec une concentration plus importante de RanGTP dans le noyau. Les facteurs de transport ont une forte affinité pour RanGTP. Ainsi, une fois le complexe d'import dans le noyau, la liaison de l'importine avec RanGTP induit la libération du cargo. Concernant le mécanisme d'export, le facteur majoritaire d'export est CRM1. CRM1 lie ses cargos dans le noyau de manière coopérative avec RanGTP. L'hydrolyse de GTP en GDP dans le cytoplasme conduit à la dissociation du complexe d'export et la libération du cargo. Ces facteurs de transport interagissent également avec les composants des pores nucléaires, les nucléoporines (Nups), afin de faciliter leur transport.

CRM1 lie ses cargos grâce à son interaction avec un SEN et son interaction simultanée avec RanGTP. Cette interaction induit un changement conformationnel de CRM1, qui stabilise le complexe et facilite son export. Le SEN est une séquence d'acides aminés hydrophobes avec un espacement typique suivant l'organisation $\Phi^{0}\Phi^{1}\text{-}(x)_{2\text{-}3}\text{-}\Phi^{2}\text{-}(x)_{2\text{-}3}\text{-}\Phi^{3}\text{-}x\text{-}\Phi^{4}$. L'interaction de CRM1 avec cette séquence a lieu au niveau de la partie centrale de CRM1, impliquant la Cystéine 528. La Leptomycine B (LMB) est une drogue connue pour cibler et modifier cette Cys528, empêchant l'interaction de CRM1 avec le SEN. Le traitement de cellules avec de la LMB inhibe donc la voie d'export dépendante de CRM1.

Des études précédentes ont montré que la LMB bloque les capsides de l'Ad5 au niveau du COMT dans les cellules. Ceci démontre le rôle essentiel de CRM1 dans cette translocation nucléaire. Cependant, le rôle exact de CRM1, ainsi que la nature de son interaction (directe ou indirecte) avec l'Ad5 ne sont pas connus. Dans cette étude, nous nous sommes intéressés au rôle de CRM1 dans l'infection par l'Ad5, ainsi qu'à ses mécanismes d'action dans ce contexte. Comme modèle cellulaire, nous avons utilisé des cellules épithéliales humaines d'ostéosarcome, U2OS.

Nous avons d'abord évalué l'interaction de l'Ad5 avec le COMT. En effet, l'intégrité des microtubules est connue pour être essentielle lors du transport de l'Ad5 mais les étapes après ce transport sont peu connues. Il a été montré que l'absence de noyau dans la cellule conduisait à la rétention de l'Ad5 au COMT.

Afin de caractériser plus précisément les interactions entre l'Ad5 et le COMT, nous avons dans un premier temps infecté des cellules énucléées (dépourvues de noyau) et nous avons pu confirmer la nécessité du noyau lui-même, ou de facteurs nucléaires, pour permettre la translocation de l'Ad5 depuis le COMT. De plus, afin d'évaluer le rôle des microtubules une fois l'Ad5 transporté au COMT, nous avons induit leur dépolymérisation et nous n'avons observé aucun effet sur la localization des virus. Nos résultats indiquent que l'interaction de l'Ad5 avec le COMT est indépendante des microtubules. Afin d'évaluer la nécessité d'une enveloppe nucléaire intègre pour la libération du génome de l'Ad5, nous avons également infecté des cellules en mitose et utilisé différentes techniques de détection du génome de l'Ad5, sur cellules fixées ou vivantes. Malgré l'absence de compartiment nucléaire en mitose (à l'inverse de l'interphase), l'ADN viral a pu être détecté, indiquant qu'une enveloppe nucléaire intacte n'est pas un prérequis pour l'exposition du génome de l'Ad5. Dans les cellules mitotiques, l'addition de LMB n'inhibe pas l'exposition du génome viral de l'Ad5 dans les cellules vivantes infectées. En revanche, elle entraîne un défaut de désassemblage total de la capside. L'ensemble de ces résultats indiquent que : i) l'interaction de l'Ad5 au COMT semble être indépendante des microtubules ; ii) la translocation du COMT vers le noyau requiert un ou des facteurs nucléaires ; iii) la libération du génome de l'Ad5 ne nécessite pas d'enveloppe nucléaire intacte ; iv) l'addition de LMB n'empêche pas l'exposition du génome de l'Ad5 mais empêche le désassemblage total de la capside permettant la libération de l'ADN viral.

CRM1 est donc essentiel pour la libération du génome de l'Ad5, étape indispensable à son import nucléaire. Afin de comprendre les mécanismes par lesquels CRM1 intervient lors du cycle de l'Ad5, nous avons étudié des mutants de cette protéine. La mutation de la Cys528 en Ser528 rend CRM1 insensible à la LMB, ce qui permet d'étudier l'impact de mutations ponctuelles de CRM1, lorsque CRM1 endogène est réprimé par la LMB. La combinaison de cette mutation C528S avec des mutations ponctuelles nous permet donc d'étudier leur impact sur CRM1, tout en étant dans des conditions où CRM1 endogène est réprimé par la LMB. Nous avons observé qu'un mutant de CRM1 retardait significativement les premières étapes du cycle de l'Ad5. En effet, une rétention transitoire au COMT a été observée, ce qui retardait donc l'import du génome ainsi que son expression. Les mutations en question, W142 et P143A, sont localisées à proximité du site de liaison de CRM1 avec la Nup214. La Nup214 est une nucléoporine cytoplasmique essentielle lors de l'export car elle permet la dissociation du complexe d'export.

Les mutations W142A et P143A ne sont pas impliquées dans la liaison de CRM1 avec les SEN. Afin de comprendre les effets de ces mutations, nous avons générer des cellules qui expriment de manière constitutive ce mutant et nous avons purifié cette protéine pour réaliser différentes études biochimiques afin de le caractériser pour ses capacités d'export. Nos résultats obtenus *in vivo* et *in vitro* ont montré que ce mutant est toujours fonctionnel pour l'export.

Cependant, un léger retard lors d'étude de cinétique d'export ainsi qu'un léger défaut de liaison aux SEN ont été observés. Ces résultats montrent que malgré un export efficace de cargos cellulaires par ce mutant, les premières étapes du cycle de l'Ad5 sont retardées. Nos résultats sont donc en faveur d'un rôle direct de CRM1 lors de l'infection par l'Ad5, et non d'un rôle indirect, qui serait assuré par un facteur exporté par CRM1.

La nature de l'interaction entre l'Ad5 et CRM1 reste cependant inconnue. Dans les cellules vivantes, nous avons montré qu'il y a toujours une exposition du génome détectable en présence de LMB. Ceci indique que des protéines core de l'Ad5 peuvent tout de même être exposées malgré la présence de LMB. En revanche, l'absence de désassemblage total de la capside en présence de LMB montre la nécessité de CRM1 pour la libération du génome. Nous nous sommes donc intéressés à TP, une protéine liée à l'ADN du génome de l'Ad5 et nous avons trouvé que cette protéine possède un SEN. Nos résultats indiquent que cette séquence d'export est fonctionnelle, et sensible à la LMB, ce qui en fait un partenaire potentiel de CRM1. Bien que préliminaires, nos résultats donc définiraient donc un nouveau modèle où, une fois au COMT, l'exposition du génome de l'Ad5, et donc l'exposition de TP serait responsable de l'interaction de l'Ad5 avec CRM1, afin de permettre sa translocation à l'enveloppe nucléaire.

La génération et la caractérisation du mutant W142A P143A de CRM1 ont permis d'étudier plus en détails le rôle de cette protéine lors des phases précoces de l'infection à l'Ad5. De plus, ces travaux ont également permis la génération d'anticorps monoclonaux dirigés contre TP, afin d'étudier en détails le rôle de cette protéine lors du cycle adénoviral.

INTRODUCTION

I. Nuclear transport machinery

Cell functionality relies on constant nucleocytoplasmic exchange of molecules between the cytoplasm and the nucleus. This process is highly regulated and involves specialized factors. Moreover, this cellular machinery can be hijacked by unphysiological substrates, such as viruses requiring a nuclear step during their infection cycle. The following sections describe the mechanism of active transport occurring at the nuclear envelope.

I.1 Nuclear Pore Complexes

Transports occur via passive diffusion or active transport of a large range of molecules between the nucleus and the cytoplasm. Active transport is facilitated by transport factors that cross the Nuclear Envelope (NE). The NE is composed of two lipid bilayers penetrated by Nuclear Pore Complexes (NPCs), large complexes with an 8-fold symmetry (Hinshaw et al. 1992), thereby connecting the nucleus and the cytoplasm. In addition, NPCs also regulate the permeability barrier of the nucleus and take part in transcriptional control during gene expression (Akhtar and Gasser 2007). NPCs are composed of around 30 different large proteins called nucleoporins (Nups). About one third of Nups contain hydrophobic segments called Phenylalanine-Glycine repeats (FG-repeats) (Rout and Wente 1994). Three groups of Nups can be distinguished according to their localization: cytosolic, nuclear or within the central channel (Figure 1).

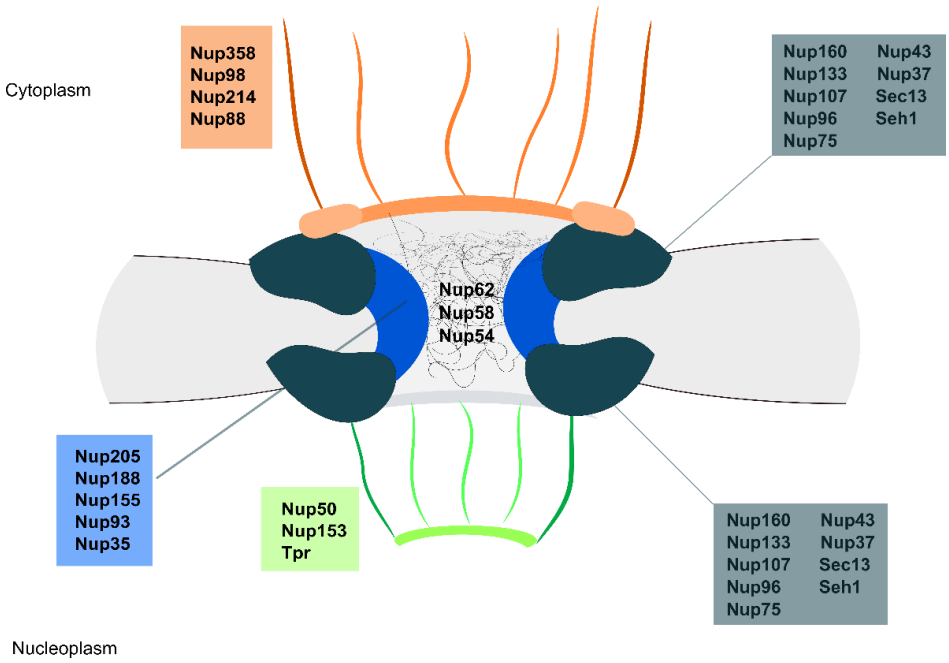

Figure 1. Distribution of nucleoporins within the Nuclear Pore Complex. Schematic representation of a NPC. Nups composing the nuclear basket are depicted in green; the central channel in blue and cytosolic Nups are depicted in orange (adapted from (Schwartz 2005)).

The disruption of hydrophobic interactions in the central channel, the loss of cohesion between the FG-repeats and the deletion of these domains in yeast have been shown to compromise the NPC permeability barrier (Ribbeck and Görlich 2002; Patel et al. 2007). Thus, the hydrophobic interactions that occur in the central channel of the NPCs would form a cohesive meshwork, controlling the permeability of NPCs. Several models have been proposed for the mechanism of selectivity control of FG-repeats in the central channel of NPCs. One of those model is called the “virtual gate” or “the polymer brush model” (Rout et al. 2003). FG-repeats of the central channel would form a repulsive network, implying for the molecule a decrease of its entropy (i.e release of energy), to diffuse through the NPC. Thus, macromolecular complexes would be less inclined to diffuse, compared to small cargoes for which a diminution of entropy is easier. In another model, the “forest model”, the FG-repeats of the central channel in the NPC would be organised in extended-coil or globular-coil conformations (Yamada et al. 2010). That organisation would divide the central channel into two zones, one central and two lateral zones of transport (for the transport of macromolecules or small molecules, respectively). Finally, in the “selective phase gel model”, the hydrophobic clusters of FG-repeats would form a three-dimensional meshwork, allowing only the diffusion of small molecules excluding diffusion of larger cargoes (Ribbeck and Görlich 2002; Mohr et al. 2009).

The selectivity of the nucleocytoplasmic transport across the NPC is regulated according to the molecular size of the cargo. This transport occurs via diffusion for small molecules (< 40 kDa) or via an active transport for larger molecules or bigger complexes. However, it has been reported that 90 to 110 kDa proteins are able to diffuse through NPCs (Wang and Brattain 2007). For large cargoes, an active transport facilitated by transport receptors is required to cross the NPCs. Transport factors recognise and bind their cargo via specific sequences and interact with FG-repeats to mediate nucleocytoplasmic transport (Ryan and Wente 2000).

I.2 Active transport

Unlike free diffusion, active transport requires energy and transport factors. The exposure of specific signals by the cargoes leads to their recognition and their transport. Two types of signals can be distinguished. Nuclear Localization Signals (NLS), leading to import, are composed of a set of basic amino acids. They were identified in the SV-40 T large antigen of the simian virus and in nucleoplasmin (Kalderon et al. 1984; Robbins et al. 1991). Nuclear Export Signals (NES) responsible for export, are composed of a set of hydrophobic amino acids and were first identified in the protein kinase inhibitor (PKI) and in the Human Immunodefiency Virus-1 Rev protein (HIV-1 Rev) (Wen et al. 1995; Fischer et al. 1995). Both signals are recognized by transport factors belonging to the same family of β-karyopherins and sharing some similarities.

In addition to comparable molecular weights and an acidic isoelectric point, β-karyopherins have a similar structural organisation. A motif of HEAT repeats (Huntingtin, Elongation factor 3, protein phosphatase 2A and TOR1) is highly conserved among the family. A HEAT motif is composed of two antiparallel helices α, linked by a loop. Thus, a repetition of HEAT motifs induces the formation of a flexible domain, often organized as a solenoid structure. The flexibility of β-karyopherins allows their interaction with several different partners (RanGTP, various cargoes, FG-repeats of Nups) to perform nucleocytoplasmic transport (Conti et al. 2006). The formation of transport complexes is driven by the Ran protein, a GTPase able to bind GDP or GTP. The presence of RanGTP is essential to modulate the conformation of transport factors. Upon binding of RanGTP, a structural reorganization of karyopherins is observed, either to allow their binding to cargoes, or to promote dissociation of the complex once the transport is over (reviewed in (Lui and Huang 2009)). RanGTP is asymmetrically distributed across the NPCs, with a higher concentration inside the nucleus (detailed below in section I.3 Ran gradient) (Moore and Blobel 1993; Izaurralde et al. 1997). Binding between karyopherins and RanGTP occurs at the N-terminal part of the transport factor, in a region named CRIME (CRM1, Importin-β, Etc) (Fornerod, et al. 1997a). Karyopherins are able to bind cargoes and RanGTP and also interact with FG-repeats of Nups (Rexach and Blobel 1995). Interaction of karyopherins with Nups has a dual role during nucleocytoplasmic transport. On one hand, interaction with FG-repeats mediates the passage across the central channel of the NPCs. On the other hand it allows the recruitment and the concentration of transport factors at the vicinity of the NPCs. Nup358 is known to promote the importin-β and transportin-1 pathways, by acting as a platform to concentrate import factors (Hutten et al. 2008; Hutten et al. 2009). Moreover, Nup358 and essentially Nup214 may play a role in the Chromosome Region Maintenance 1 (CRM1) dependent export pathway (detailed below in section I.4 CRM1) (Ritterhoff et al. 2016; Hutten and Kehlenbach 2006). A schematic representation of nuclear import and export pathway is depicted in Figure 2.

In nuclear import, cargoes are recognised by transport receptors named importins. Depending on the importin involved in transport, NLS binding is either direct or requires an adaptor (Görlich et al. 1995). Importins bind their cargoes in the cytoplasm, in a low RanGTP environment and mediate their translocation through NPCs. Once imported into the nucleus, the binding between importins and RanGTP leads to a structural conformation change of the importins, promoting dissociation of the complex and release of the cargo (Görlich et al. 1996; Rexach and Blobel 1995). On the other hand, exportins bind their cargo in the nucleus, in a highly concentrated RanGTP environment. The interaction between exportins and NESs is enhanced and stabilized by RanGTP.

In vitro experiments showed that absence of RanGTP impaired the binding between the exportin CRM1 and NESs (Fornerod et al. 1997b), since formation of the export complex occurs in a cooperative manner upon the binding of the different partners (detailed below in section I.4 CRM1).

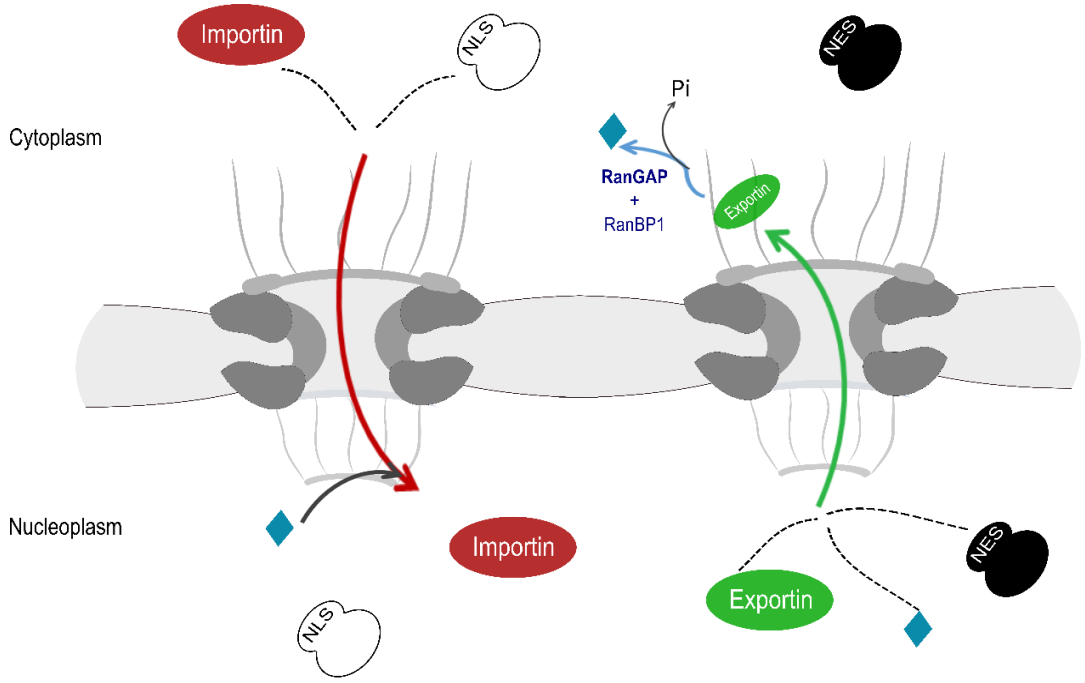

Figure 2. Nucleocytoplasmic transport pathway. Exportins recognise their cargo via an NES and form a complex stabilised by RanGTP (blue). After translocation through the NPC, the hydrolysis of RanGTP mediated by RanGAP and assisted by RanBP1 leads to the dissociation of the complex. In nuclear import, importins recognise cargoes via the binding with NLS and the complex is dissociated in the nucleus after binding of RanGTP.

After translocation through NPCs, the hydrolysis of RanGTP promoted by RanGTPase activating protein (RanGAP) leads to the dissociation of the complex, and the cytoplasmic release of the cargo (Bischoff et al. 1995; Kehlenbach et al. 1999). RanGTP hydrolysis is essential for the release of exported cargoes (Klebe et al. 1995). Export assays performed with RanQ69L, a mutant of Ran unable to hydrolyse GTP, showed a retention of the export complex at the NE, leading to a defect in the dissociation of the export complex (Klebe et al. 1995; Kehlenbach et al. 1999). Thus, the directionality of the nucleocytoplasmic transport is highly regulated via the asymmetric distribution of Ran across the NE.

I.3 Ran gradient

Ran belongs to the family of GTPase and can adopt two different conformations depending if it is in the RanGTP or RanGDP bound form. RanGTP is distributed in an asymmetric manner across the NE, with a higher concentration in the nucleus. To ensure the turnover of the GDP *vs* GTP bound forms of Ran and to maintain the gradient, several regulators are involved.

The nucleotide exchange from RanGDP to RanGTP is mediated via the regulator of chromatin condensation 1 (RCC1), a guanine nucleotide exchange factor (Bischoff and Ponstingl 1991). This factor has a restricted nuclear localization due to its interaction with mononucleosomes on chromatin (Bischoff and Ponstingl 1991; Nemergut et al. 2001). Thus, RCC1 maintains a high concentration of RanGTP in the nucleus. On the other hand, RanGAP promotes the hydrolysis of RanGTP to RanGDP (Coutavas et al. 1993). RanGAP interacts with Nup358 (also known as RanBP2), therefore it is concentrated at the cytoplasmic face of the NPC (Mahajan et al. 1997). RanGAP hydrolysis is further promoted by the Ran Binding Protein 1 (RanBP1), a co-factor of RanGAP (Bischoff et al. 1995; Kehlenbach et al. 1999). Cytoplasmic RanGDP is then recycled back to the nucleus via the Nuclear Transport Factor 2 (NTF2) (Smith et al. 1998), to be reloaded with GTP by RCC1 (Ribbeck et al. 1998) and to participate in a new round of export.

In interphase cells, a fraction of RanGTP and RanBP1 have been reported to be localized at the centrosome (detailed in section III.2.a The microtubule network) and to participate in microtubule nucleation (Keryer et al. 2003; Di Fiore et al. 2003). However, neither RanGAP nor RCC1 are localized at the centrosome in interphase cells (Joseph et al. 2002; Moore et al. 2002). Thus, the centrosomal localization of RanGTP is mostly not driven by a turnover involving RanGAP and RCC1, as observed across the NE. Although it is unclear how RanGTP is generated at the centrosome, it has been speculated that it could originate directly from the nucleus, and be anchored to the centrosome via its interaction with AKAP450, a centrosomal component (Lavia 2016; Keryer et al. 2003).

In addition to its role in nucleocytoplasmic transport, RanGTP and its regulator proteins are also involved in mitotic processes (Kalab et al. 2006) (detailed below in section I.5 Nuclear transport factors in mitotic cells). RanGTP promotes local nucleation of microtubules for mitotic spindle assembly and NE formation (Carazo-Salas et al. 1999; Hetzer et al. 2000). RCC1 maintains a high concentration of RanGTP in a close proximity of chromatin during mitosis, to enhance the formation of the mitotic spindle assembly. RanBP1 also participates in mitotic spindle and centrosomal assembly (Guarguaglini et al. 2000), by ensuring the correct localization of factors involved in microtubules generation (Tedeschi et al. 2007).

I.4 CRM1

CRM1 is the major exportin in cells, promoting export of nuclear cargoes to the cytoplasm. It was first identified for its role in the structure of chromosomes, in *Schizosaccharomyces pombe* (Adachi and Yanagida 1989) and later characterized for its role in nuclear export (Fornerod et al. 1997a; Kehlenbach et al. 1998; Fukuda et al. 1997).

CRM1 shares the characteristics of transport factors. It is composed of 21 HEAT repeats and binds RanGTP via the CRIME domain in the N-terminal part (Fornerod et al. 1997a; Ossareh-Nazari and Dargemont 1999). CRM1 recognises its cargoes via binding to NES and forms a trimeric complex with RanGTP. Moreover, RanGTP is kept in position within the export complex via bindings with other regions in CRM1 (Monecke et al. 2014) (Figure 3).

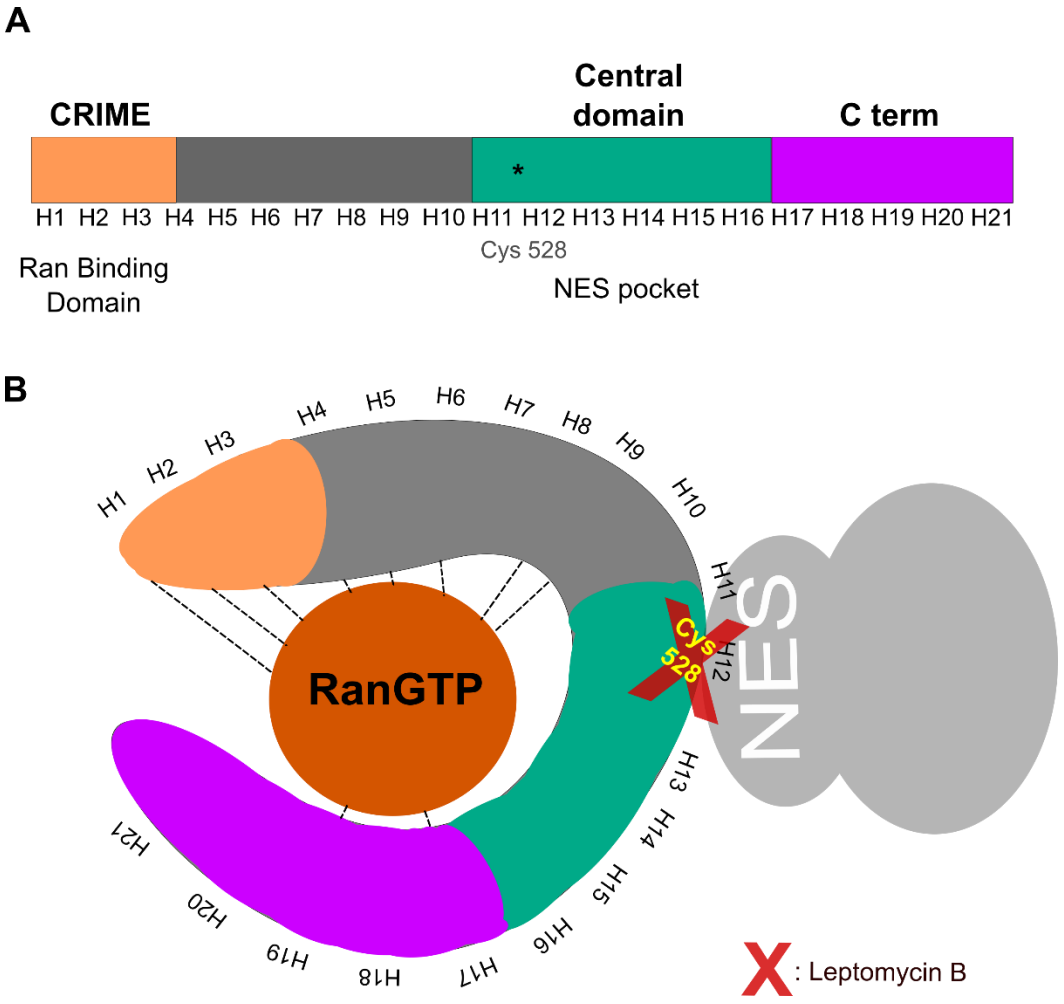

Figure 3. Schematic representation of the different domains of CRM1. (A) Different domains of CRM1 and the corresponding HEAT repeats (H1 to H21). Interaction of CRM1 with RanGTP occurs at the N-terminal part, via the CRIME domain (orange). The binding with NES cargoes involves cysteine 528 from the central domain (green), and the C-terminal part (purple) is known to stabilize the interaction with RanGTP, in a ring like structure (adapted from (Petosa et al. 2004)). (B) Ring-like structure of CRM1 interacting with RanGTP (orange) and an NES containing cargo (grey). Leptomycin B treatment impairs the binding between CRM1 and the NES by modifying cysteine 528. HEAT repeats interacting with RanGTP are depicted with black dot lines (adapted from (Monecke et al. 2014)).

Binding between the three partners occurs in a cooperative manner (Fornerod et al. 1997b). Ran Binding Protein 3 (RanBP3) is a cofactor of CRM1 and enhances the binding of CRM1 with RanGTP and NES (Lindsay et al. 2001). Leptomycin B (LMB), a fungal metabolite (Hamamoto et al. 1983), impairs the recognition of NES by CRM1, abolishing CRM1-mediated export (Hamamoto et al. 1983; Nishi et al. 1994; Kudo et al. 1998). LMB directly targets and covalently modifies cysteine 528 (Cys 528) localized within the hydrophobic pocket of CRM1 and therefore sterically hinders the interaction of CRM1 and NESs (Fornerod et al. 1997b; Kudo et al. 1999; Dong et al. 2009).

A consensus sequence for NES has been defined. This sequence consists of a set of five hydrophobic amino acids $\Phi^{0}\Phi^{1}\text{-}(x)_{2-3}\text{-}\Phi^{2}\text{-}(x)_{2-3}\text{-}\Phi^{3}\text{-}x\text{-}\Phi^{4}$ (Güttler et al. 2010). The nature and space between hydrophobic residues are diverse and the final affinity of CRM1 for an NES depends on this arrangement. Several cargoes of CRM1 have been identified (Thakar et al. 2013; Kirli et al. 2015; Xu et al. 2012). Some crystal structures of CRM1 in complex with its cargoes, in the presence or absence of RanGTP or bound to FG-repeats were solved in the past decades (Monecke et al. 2014; Port et al. 2015; Dong et al. 2009; Monecke et al. 2009; Güttler et al. 2010; Monecke et al. 2013). Thus, it is established that CRM1 in complex with RanGTP and an NES cargo adopts a close structure, different from its free cargo structure. The cooperative binding of RanGTP and the NES cargo on CRM1 induces a conformational change from an extended form, to a ring-like structure (Monecke et al. 2013). Once the export complex is formed in the nucleus, it is exported through NPCs and binds the Nup214 (Hutten and Kehlenbach 2006). This interaction promotes and stabilizes the export complex, but some cargoes have been shown to be exported in a CRM1 dependent pathway even in absence of Nup214 (Bernad et al. 2006). CRM1 binds some FG-repeats of Nup214 (Roloff et al. 2013). This interaction has been characterized and the crystal structure of CRM1 in complex with RanGTP, Snurportin 1 (SPN1) and FG-repeats of Nup214 has been solved (Port et al. 2015).

CRM1 has also been shown to be involved in the biogenesis of centrosomes, major site of microtubules nucleation in mammalian cells, and the maintenance of their integrity (Forgues et al. 2003; Neuber et al. 2008; Bao et al. 2018). Together with RanGTP, a fraction of CRM1 is found at the centrosome (Keryer et al. 2003; Liu et al. 2009).

I.5 Nuclear transport factors in mitotic cells

During mitosis, several changes occur within the cell (reviewed in (McIntosh 2016)). *Prior to* initiation of mitosis, the genetic material is duplicated to be further segregated between the mother and the daughter cells, during cell division. The centrosome, the organelle from where the microtubules originate is also duplicated.

Mitosis is then initiated by the condensation of DNA into structured chromosomes. The chromosomes consist of two chromatids bound to each other via the centromere. To ensure the correct distribution of the chromatids between the two newly divided cells, the segregation is performed via the assembly of mitotic spindles (reviewed in (Petry 2016)). These structures are composed of microtubules, originating from the centrosome on one side, and bound to the chromatids on the other side. Moreover, the association of chromatids with microtubules is performed via a macromolecular complex called the kinetochore. The polymerization of microtubules originating from centrosomes and bound to kinetochores leads to the segregation of the genetic information and to cell division. To separate the replicated chromosomes, the NE has to be dismantled first. This process is called nuclear envelope break down (NEBD). A succession of phosphorylation events destabilize interactions in the nuclear lamina and NPCs, leading to NE disassembly (Gerace and Blobel 1980; Beaudouin et al. 2002; Güttinger et al. 2009).

The compartmentalisation of nuclear and cytoplasmic factors does not longer exist in mitotic cells. However, Nups, RanGTP and karyopherins participate actively in mitosis progression. After NEBD, soluble Nup complexes are redistributed all over the cell. Nup358 in complex with RanGAP, and the Nup 107-160 complex, promote the microtubules-kinetochores interaction to form the mitotic spindle for chromosomal segregation (Joseph et al. 2004; Orjalo et al. 2006). RanGTP is involved in several steps of mitosis such as mitotic spindle assembly and NE (re)formation. As mention above (section I.3 Ran gradient), a high concentration of RanGTP is maintained at the vicinity of chromatin via RCC1 (Carazo-Salas et al. 1999) to mark its localization. Import factors such as importin-β prevent random formation of mitotic spindle by sequestering spindle assembly factors (SAFs). In a low RanGTP environment (i.e away from the vicinity of the chromatin), importin-β interacts with SAFs to prevent spindle assembly. On the other hand, in the vicinity of chromatin with a high RanGTP concentration, importin-β preferentially binds RanGTP. Thus, SAFs are released to drive spindle assembly (Nachury et al. 2001; Harel and Forbes 2004). In addition to importin-β, CRM1 also participates in the spindle assembly. The CDK1-cyclin B complex induces the phosphorylation of CRM1 on the serine 391, leading to the targeting of CRM1 to the mitotic spindle (Wu et al. 2013). CRM1 then promotes the recruitment of factors to the kinetochores, for the binding of chromatids with microtubules (Arnaoutov et al. 2005).

Nucleocytoplasmic transport through NPCs is essential to promote cellular functions. This process is highly regulated and involves different cellular factors. Active transport of cargoes requires karyopherins and RanGTP for the formation and dissociation of transport complexes. The asymmetric distribution of Ran across the NE and specific signals as NLS and NES drive the directionality of transport. Interestingly, in viral infections, many viruses that require a nuclear step for their replication highjack this transport pathway. Thus, the NPC also serves as a gateway for the import of several nuclear replicating viruses. Adenoviruses are a typical example of pathogens taking advantage of the nucleocytoplasmic transport pathway. The following sections describe the biology of adenoviruses, and their use of cellular pathways to perform their replication.

II. Adenovirus

II.1 History and classification

Adenovirus (AdV) was first discovered in human adenoid tissues in 1953 (Rowe et al. 1953). Rowe et al., discovered a new agent responsible for the degeneration of culture tissues and was transmissible to other cultures. In 1954, the same cytopathogenic effect was observed after the culture of a microbial agent from the throat of a patient with respiratory syndromes, during an epidemic peak of acute respiratory illness, in the U.S army (Hilleman and Werner 1954). Combining these similar observations, the official name of “Adenovirus” was chosen for this new pathogen, in 1956 (Enders et al. 1956). Since its discovery, AdV has been extensively studied.

The International Committee on Taxonomy of Viruses (Lefkowitz et al. 2018) provides a detailed database on the classification of viruses. According to the ICTV, human AdV belong to the family of *Adenoviridae* and the genus of *Masteadenoviruses.* They are divided into 7 species, from A to G and sub-divided into types according to their biological, chemical and physical properties (Table 1). Although 100 types have been identified, only 67 types are known to be pathogenic in humans (Crenshaw et al. 2019).

II.2 Pathogenicity

Depending on their type, AdVs have different tropisms and induce different clinical manifestations (Table 1). Common consequences of AdV infection are respiratory illnesses, conjunctivitis and acute gastroenteritis (source: Centres for Disease Control and Prevention. Adenovirus transmission, https://www.cdc.gov/adenovirus/). The AdV transmission occurs directly from an infected person to another one.

AdV infections are mild in most of the cases, but can induce severe complications in children or immuno-compromised patients. Moreover, emerging viruses with increased pathogenicity are observed worldwide (Cook and Radke 2017; Ghebremedhin 2014). There is no specific treatment for AdV infection.

AdVs are suitable to be used as vectors for viral gene therapy. The first vector therapy assay was performed in the early 90's (Jaffe et al. 1992). AdVs have a wide tropism of infection, are easy to manipulate and have a large capacity of encapsidation. They are non-oncogenic and not able to integrate in the host-DNA. Therefore, the episomal expression of transgenes encapsidated in AdV is considered safe (Ghosh et al. 2006; Lee et al. 2017). However, one of the disadvantages of such vectors is the strong immune response they induce. In 1999, a clinical assay was performed to test increasing doses of vectors, which led to the death of a patient (Raper et al. 2003).

Table 1. Classification of human AdVs. AdVs are classified according to their group, type and induced symptoms (modified from (Crenshaw et al. 2019)). AdV species type 5 from the Group C, used as a model for our AdV infections, is highlighted in red.

AdV group	Type	Type of infection
A	12, 18, 31, 61	gastrointestinal, respiratory, urinary, cryptic enteric infection, linked to obesity, meningoencephalitis
B	3, 7, 11, 14, 16, 21, 34, 35, 50, 55, 66	conjunctivitis, gastrointestinal, respiratory, urinary, pneumonia, meningoencephalitis, cystitis
C	1, 2, **5**, 6, 57	respiratory, gastrointestinal, obesity, pneumonia, hepatitis
D	8–10, 13, 15, 17, 19, 20, 22–30, 32, 33, 36–39, 42–49, 51, 53, 54, 56, 58-60, 63-67	conjunctivitis, gastrointestinal, linked to obesity, meningoencephalitis
E	4	conjunctivitis, respiratory, pneumonia
F	40, 41	gastrointestinal, infantile diarrhea
G	52	gastrointestinal

II.3 Structure

The AdV types 2 and 5 are the most studied. They share structural and pathogenesis properties and importantly can be predominantly found in patients (Berciaud et al. 2012). Our studies were based on the human AdV species serotype 5 (Ad5) hence the details below focus on Ad5.

Ad5 is a non-enveloped virus with an icosahedral capsid of approximatively 90 nm. The genome of Ad5 is a linear double stranded DNA molecule of 36 kb (Chroboczek et al. 1992). Two groups of proteins can be distinguished in the Ad5 particle. On one hand, the structural proteins, which form the capsid (including major and minor proteins), and on the other hand; the core proteins associated with the viral DNA (Figure 4). Moreover, the atomic structure of the Ad5 capsid solved by cryo-EM and its crystal structure have been determined (Liu et al. 2010; Reddy et al. 2010).

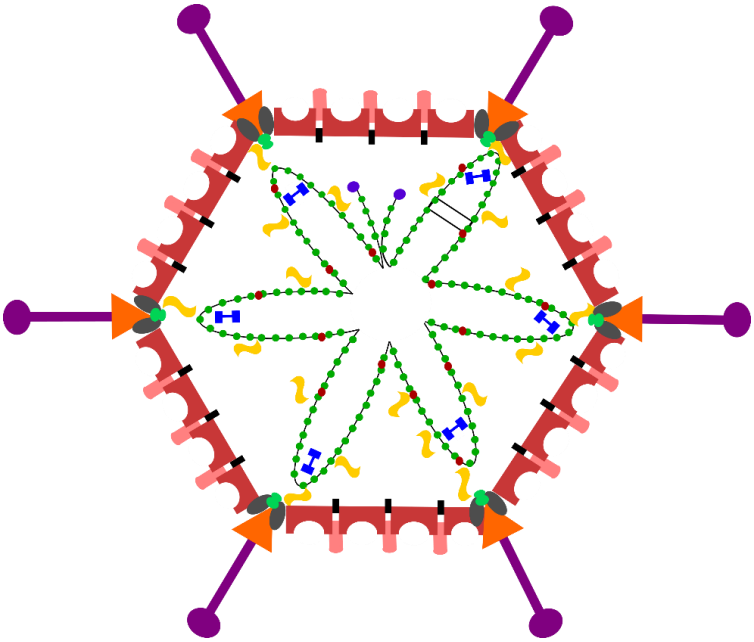

Figure 4. Structure of the adenovirus type 5. The organisation of the Ad5 is divided into structural proteins and core proteins. The corresponding proteins depicted on the scheme are listed in the table (adapted from (Russell 2009)).

II.3.a Capsid proteins

The Ad5 capsid is composed of at least seven different proteins. The three major proteins (hexon, penton base and fiber) and the four minor proteins (IIIa, VI, VIII, and IX) are assembled to form an icosahedral capsid with a pseudo-T=25 symmetry (Russell 2009). The major component of the Ad5 capsid is the hexon protein, assembled in trimers. In total, 240 trimers of hexon proteins are arranged and interact with a penton base (a pentamer of five pentons), at each vertex of the icosahedral capsid.

The trimeric fiber protein is found at every vertex of the capsid, interacting with the penton base structure (Reddy et al. 2010; Reddy and Nemerow 2014). The hexon is the major structural protein forming the capsid shell of the Ad5 particle and is also involved in docking Ad5 at the nuclear periphery (Trotman et al. 2001). Both the fiber protein and the penton-base structure are necessary for the interaction with cellular receptors (Mathias et al. 1994; Persson et al. 2007). The fiber protein promotes the cell attachment via its interaction with the coxsackievirus and adenovirus receptor (CAR) (Roelvink et al. 1998) whereas the penton-base structure binds to integrins αβ to further initiate the cell entry (Wickham et al. 1993).

The minor proteins are essential to maintain the integrity of the viral capsid, although their exact localization within the capsid are controversial (Liu et al. 2010; Reddy et al. 2010). In addition to provide structure to the capsid, the structural proteins are also involved in different steps of the viral life cycle. pVI maintains the capsid integrity via the interaction with the penton-base structure (Martinez et al. 2015). It has also been shown to promote Ad5 endosomal escape after its release from the capsid inside the endosome and to play a role in viral assembly (Wiethoff et al. 2005; Wodrich et al. 2003). pIX has been proposed to promote capsid disassembly at the NPC via interaction with Kinesin-1 (Strunze et al. 2011). The integrity of the Ad5 capsid is ensured by the capsid proteins, which surround the viral core with the genome.

II.3.b Core proteins

Early studies using electronic microscopy predicted an association of the Ad5 genome with core proteins (Epstein 1959). Several decades later, six core proteins interacting with Ad5 DNA were identified and extensively studied (pVII, pV, pIVa2, Mu, Terminal Protein (TP) and the adenoviral protease (AVP)).

pV is thought to provide a bridge between the capsid and the Ad5 genome via an interaction with pVI (capsid part) and pVII (genome part). Moreover, pV separates from the viral genome during entry *prior to* nuclear import but may enter the nucleus separately since, its accumulation in nucleoli is observed (Matthews and Russell 1998). pIVa2 directly interacts with the packaging sequence on the Ad5 genome (Zhang and Arcos 2005).

Therefore, it is involved in genome packaging during Ad5 assembly (Ostapchuk et al. 2005; Zhang and Imperiale 2003). pIVa2 is found at only one vertex of the Ad5 capsid (Christensen et al. 2008). Mu has also been shown to have a role during the packaging of Ad5 genome (Perez-Berna et al. 2009). AVP is important for the cleavage of the precursor of some proteins (pre-IIIa,VI, VII, VIII, TP and Mu), during the maturation of the capsid (Russell 2009) making it a protein that mediates the interplay between core and capsid.

The major core protein of the Ad5 is protein VII (pVII). pVII is found in 500 copies per particle (Benevento et al. 2014), surrounding the DNA molecule in a “histone-like” structure (Burg et al. 1983; Vayda et al. 1983). The condensation of the Ad5 DNA by pVII is necessary to protect the DNA from cellular degradation and to maintain the integrity of the capsid (Karen and Hearing 2011; Martin-Gonzalez et al. 2019). In addition, pVII has several roles during Ad5 infection. Three functional NLS were identified in pVII to promote nuclear genome import, via interactions with transport factors ((Russell et al. 1968; Wodrich et al. 2006). After import, pVII has been shown to enhance Ad5 gene expression via its interaction with the early viral transcription factor E1A and the Template Activating Factor-1 (TAF-I) (Komatsu et al. 2011; Haruki et al. 2003). While remodelling of Ad5 DNA is observed *prior to* viral DNA transcription or replication, the binding of pVII to the incoming genome and during later nuclear steps of Ad5 and its kinetics remain elusive (Giberson et al. 2012).

On the other hand, TP is found in only two copies *per* virion. TP is covalently bound to each extremity of the DNA via a phosphodiester bond between the serine 580 residue and the 5’-OH DNA extremity (Rekosh et al. 1977; Desiderio and Kelly 1981). TP is synthetized as a precursor (pTP), cleaved into TP by AVP upon maturation, and both proteins are involved in the DNA replication (Pronk and van der Vliet 1993; Challberg and Kelly 1981). TP is also responsible for viral DNA attachment to the nucleoplasmic protein network (also called the nuclear matrix), leading to the enhancement of viral transcription and replication (Schaack et al. 1990).

II.3.c Genome structure

The Ad5 genome encodes one immediate early transcription unit (encoding E1A), four early transcription units (E1B, E2, E3 and E4) and one late transcription unit (L1-L5) as shown in Figure 5 The genome is flanked by two Inverted Terminal Repeats (ITRs) of 100 bp. An extensive splicing of primary transcripts allows the expression of > 40 different Ad5 proteins, from the viral genome (Guimet)Guimet . Moreover, the splicing mechanism in itself was initially discovered in adenovirus, leading in 1993 to the Nobel Prize in Physiology or Medicine for Richard J. Roberts and Phillip A. Sharp (Chow et al. 1977; Berget et al. 1977). Although the kinetic of early genes expression was determined by hybridization-based system or PCR

(Binger and Flint 1984; Crisostomo et al. 2019), there is currently no study showing direct detection of mRNA transcripts by fluorescence microscopy (Pied and Wodrich 2019).

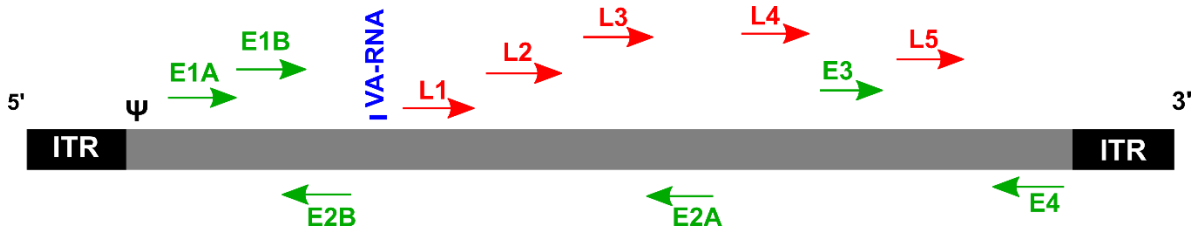

Figure 5. Organisation of the Ad5 genome. The Ad5 genome is flanked by two ITRs at each extremity, followed by the packaging sequence (Ψ) on the left end. Early genes are depicted in green, late genes in red and VA-RNA sequence in blue (adapted from (Lee et al. 2017))
.

The expression of early genes (E1A, E1B, E2, E3 and E4) occurs before DNA replication, and is initiated within two hours post-infection, starting with E1A (Crisostomo et al. 2019). Early genes encode proteins involved in the activation and stimulation of Ad5 transcription, the regulation of cellular immune responses and the initiation of viral DNA replication. In contrast, late genes (L1 to L5) are transcribed after initiation of the DNA replication (6 to 8 h pi) and code for most structural proteins. Both extremities of the DNA are composed of ITRs and are covalently bound to TP in the virion. These sequences contain the origin of replication of the Ad5 genome and have also been shown to enhance transcription (Guimet ; Hatfield and Hearing 1991). The packaging sequence (Ψ) controls viral DNA encapsidation upon assembly. Ψ is directly situated after the left end ITR and is the sole sequence responsible for genome packaging. The Ad5 genome also contains sequences coding for virus-associated RNAs (VA-RNAs), regulatory RNAs that modulate the immune response (Ma and Mathews 1996).

The first generation of AdV vectors used for gene therapy were deleted for the E1 region. However, at a high viral particles concentration, this region becomes dispensable for AdV replication and cytopathic effects were observed. Thus, to improve the safety of AdV vectors, second generation vectors were generated, lacking the early genes, or even more recently, just containing the ITRs and the packaging sequence in so called high-capacity vector (Lee et al. 2017).

III. Cycle of Adenovirus

III.1 Entry

The attachment of Ad5 to its target cell is mediated via the fiber protein and the coxsackievirus and adenovirus receptor (CAR) (Bergelson et al. 1997; Roelvink et al. 1998). Most of the AdVs use this receptor, except AdVs from the type B which preferentially binds the CD46 receptor (Gaggar et al. 2003). CAR was first discovered as the binding site of the coxsackievirus and adenovirus, but was later identified as a cell-adhesion molecule (Honda et al. 2000). This primary interaction requires the flexibility of the fiber protein to hold the virus at the vicinity of the cell surface (Wu et al. 2003). A second interaction occurs between the penton base and the cellular integrins αβ (Wickham et al. 1993). This binding induces a rearrangement of the actin cytoskeleton (Li et al. 1998a), leading to internalization of the Ad5 via clathrin-dependent endocytosis (Chardonnet and Dales 1970; Wang et al. 1998). Thus, an intact actin cytoskeleton is required for internalization of Ad5 (Patterson and Russell 1983; Li et al. 1998b).

Once in the endosomal vesicle, the endosome acidification and a drop in pH may help to destabilize the Ad5 capsid leading to its partial disassembly and the exposure of the internal protein VI (Wiethoff et al. 2005). The membrane lytic activity encoded in the N-terminus of pVI induces the disruption of the endosomal membrane. In addition, a conserved PPxY motif in pVI has been shown to promote the escape of Ad5 from the ruptured endosome (Wodrich et al. 2010). However, Ad5 remain associated with ruptured endosomes, before its total escape (Maier et al. 2012). Therefore, endosomal lysis and endosomal escape are two events separated in time and space. Thus, pVI is involved during both steps and is crucial for the virus to escape the endosomal degradation pathway.

III.2 Transport to the MTOC

Ad5 in the cytoplasm exploits the cytoskeleton for nuclear delivery. The cytoskeleton is primarily composed of an actin and a microtubule network. Together, these proteins maintain the organisation of the cell, drive the segregation of chromosomes during mitosis and interact with motor proteins. Both actin and microtubules are assembled in filaments, in a dynamic and energy dependent turn-over. We briefly reviewed here the organisation of the microtubule network in mammalian cells.

III.2.a The microtubule network

Microtubule assembly occurs through the polymerization of dimers of αβ-tubulin. The hydrolysis of GTP bound to β-tubulin leads to the depolymerization of tubulin filaments. Thus, the microtubule network is a dynamic balance between constant polymerization and depolarization of filaments (Akhmanova and Steinmetz 2015). Microtubules originate from Microtubule Organisation Centres (MTOCs), which are centres for nucleation, stabilization and anchoring of microtubules (Sanchez and Feldman 2017). The speed of polymerization of microtubules defines two orientations: the minus end at MTOCs, with a low rate of polymerization, and the plus end at the cell periphery. In mammalian cells, centrosomal and non-centrosomal MTOCs can be found (Sanchez and Feldman 2017). Both types of MTOCs are centres for microtubules nucleation, but centrosomal MTOCs contain the two centrioles, responsible for mitotic spindle assembly. Thus, the major MTOC in the cell is called the centrosome. In this study, we referred the term of MTOC as the centrosome. Centrosomes are composed of two centrioles embedded within pericentriolar material (PCM). During mitosis, centrioles duplicate in order to generate mitotic spindle poles. The PCM is composed of a matrix of proteins with coiled-coil motifs, to ensure the integrity of the centrosome (reviewed in (Woodruff et al. 2014)). Pericentrin is one of the major components of the centrosome, necessary for microtubule organisation (Doxsey et al. 1994). Centrosomal integrity is also mediated by centriolar satellites concentrated in the vicinity of centrosomes (Prosser and Pelletier 2020). Moreover, centriolar satellites interact with dynein to transport proteins towards the centrosome (Kubo et al. 1999). A schematic representation of a centrosome is depicted in Figure 6.

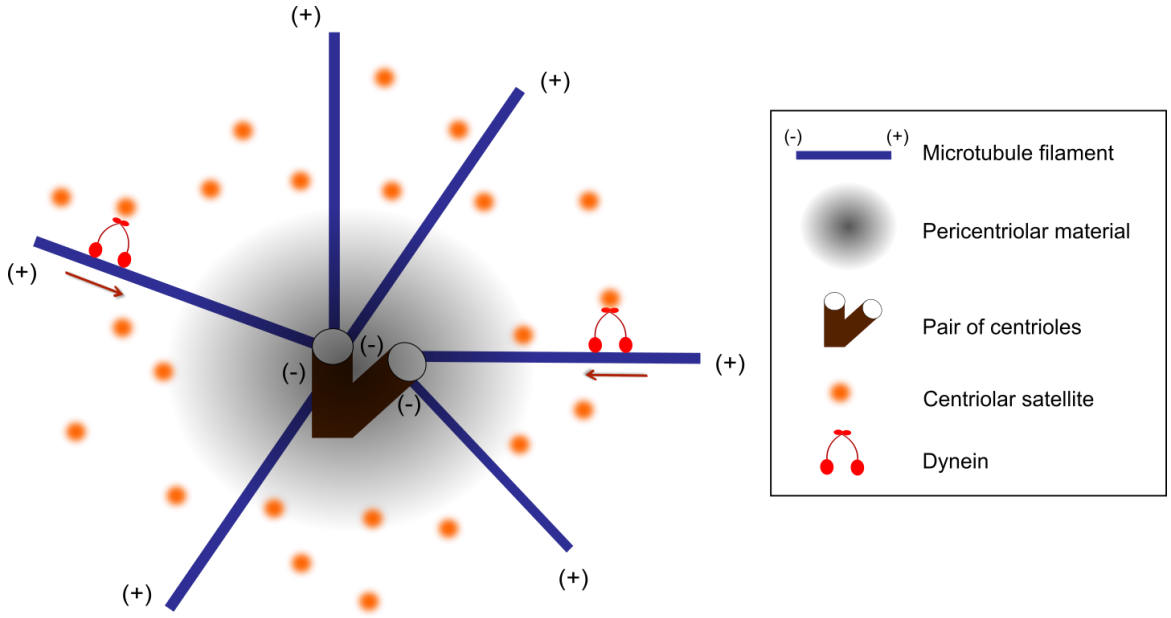

Figure 6. Schematic representation of a mammalian centrosome. Microtubule filaments nucleate from a pair of centrioles, embedded within the percientriolar material. Centrosome is surrounded by centriolar satellites, transported via the dynein motor (adapted from (Prosser and Pelletier 2020)).

Microtubules are associated with motor proteins and Microtubule Associated Proteins (MAPs) involved in the nucleation and stabilization of microtubule filaments (Bodakuntla et al. 2019). Among the motor proteins, two major families can be distinguished, with different directionality of transport. Kinesins perform anterograde transport, from the MTOC to the cell periphery ((-) end to (+) end) whereas dyneins perform retrograde transport of cargoes from the (+) end towards the MTOC (Lodish et al., 2000) (Figure 7). Microtubules integrity requires a balance between polymerization and depolymerization of tubulin filaments. Microtubule depolymerization can be artificially induced with cold or drug treatments like nocodazole or colcemid (Hoebeke et al. 1976).

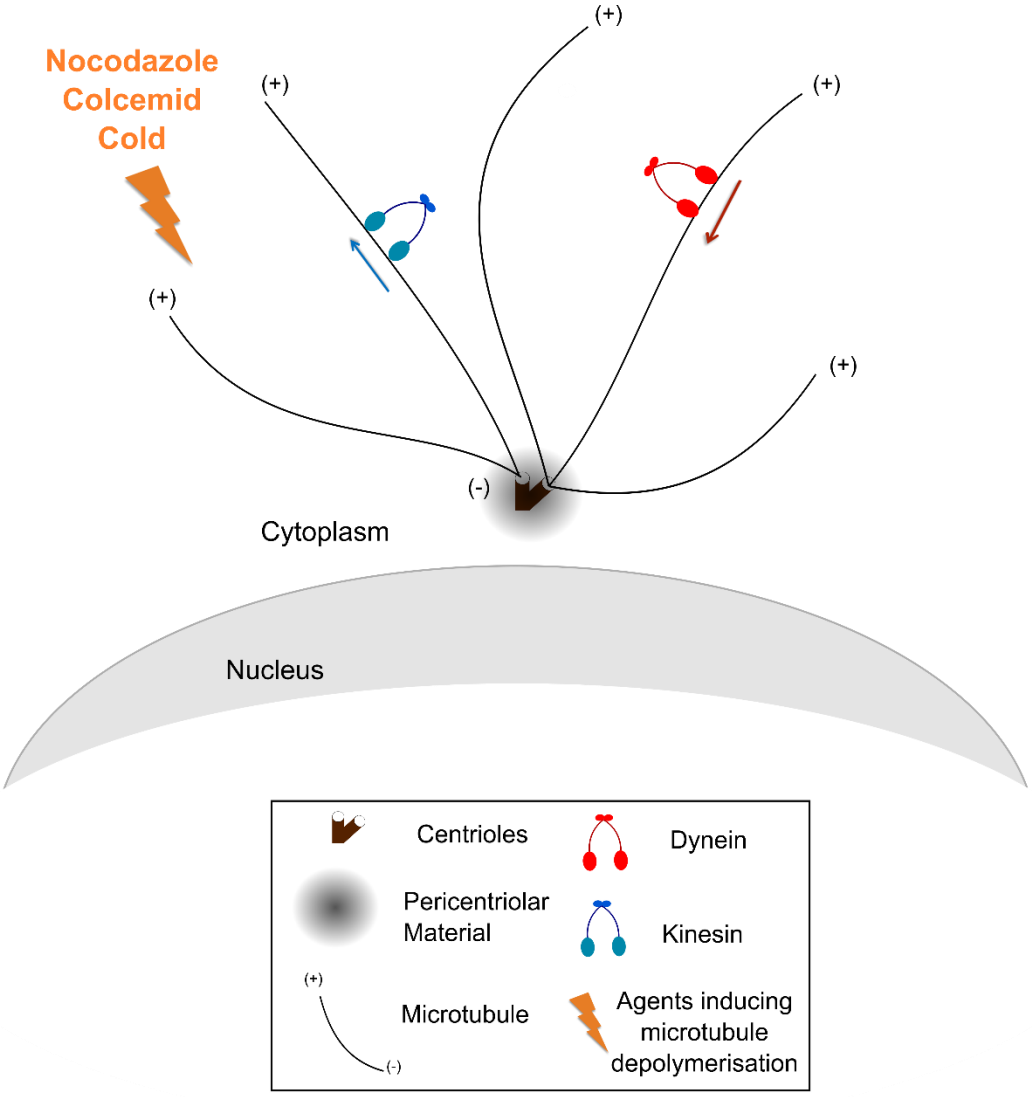

Figure 7. Organisation of the microtubule network. Microtubule filaments nucleate from the MTOC, composed of a pair of centrioles surrounded with pericentriolar material. Kinesin (in blue) or dynein (in red) are microtubule motors and transport cargoes from the (-) to the (+) or from the (+) to the (-) ends, respectively.

III.2.b Transport of Ad5 on microtubules

After endosomal escape, partially disassembled capsids of Ad5 are released into the cytoplasm. Early studies using electronic microscopy imaging visualized Ad5 particles associated with microtubules (Dales and Chardonnet 1973; Miles et al. 1980). Ad5 take advantage of the microtubule transport machinery in order to complete its life cycle. Other viruses like the Herpes-Simplex Virus 1 (HSV-1) or the retrovirus Human Foamy Virus (HFV), have been described to use a similar mode of transport machinery (Sodeik et al. 1997; Saib et al. 1997).

Actin disruption with cytochalasin treatment was shown to impair internalization of the virus, since the actin network is required for endocytosis of Ad5 (Patterson and Russell 1983; Li et al. 1998b). However, once inside the cell, the integrity of the actin network is not required for the nuclear targeting of Ad5 (Leopold et al. 2000). One the other hand, the disruption of microtubules with nocodazole has no effect on virus entry or on endosomal escape (Suomalainen et al. 1999), but does impair nuclear targeting, leading to gene expression defect (Mabit et al. 2002; Suomalainen et al. 1999). Thus, intact microtubules are required for nuclear targeting of the Ad5. However, once docked at the NE, the disruption of microtubules has been shown to not impair the localization of Ad5, remaining associated to the nucleus (Leopold et al. 2000). After translocation to the nuclear envelope, the integrity of the microtubule network is not required anymore.

Ad5 directly interacts with the dynein motor via the hexon protein to promote nuclear targeting of the capsid (Suomalainen et al. 1999; Bremner et al. 2009; Kelkar et al. 2004). Moreover, the microtubule motor dynein is also involved in endosomal escape *prior to* transport, probably for the actual escape process (Montespan et al. 2017). However, it remains to be shown how this first motor recruitment is regulated. Dynein transports Ad5 capsids towards the minus end of microtubules via a retrograde movement. Moreover, a bi-directional transport of capsid has been observed (Suomalainen et al. 1999). In addition to dynein, Ad5 also interacts with Kif5B, member of the kinesin-1 subfamily, and the absence of this factor retains Ad5 at the MTOC (Zhou et al. 2018). The role of such interaction is not well established. Several studies point to targeting and accumulation of Ad5 capsids at the MTOC (or at the mitotic spindle) *prior to* nuclear translocation (Suomalainen et al. 1999; Leopold et al. 2000). Nevertheless, there is no direct evidence whether a passage through the MTOC is required for every capsid to be delivered to the NPC.

Infection of cells lacking their nucleus showed a stable accumulation of Ad5 capsids at the MTOC (Bailey et al. 2003). Moreover, inhibition of the export factor CRM1 with LMB blocks the Ad5 capsids at the MTOC, presumably by preventing the uncoupling of Ad5 from microtubules (Strunze et al. 2005; Wang et al. 2017). The nuclear targeting defect induced upon inhibition of CRM1 also impairs capsid disassembly, although the mechanism of Ad5 capsid disassembly is not known (Strunze et al. 2005) and it is unclear if CRM1 plays a direct role or just prevents delivery to the nuclear envelope. Thus, CRM1 is involved in MTOC-removal of Ad5 but the exact role and the nature of the interaction with Ad5 (direct or indirect interaction) are currently unknown. The mechanism of Ad5 unloading from the microtubule transport machinery is also unclear, but seems to require nuclear factors. A schematic representation of the first steps of Ad5 cycle is depicted in Figure 8

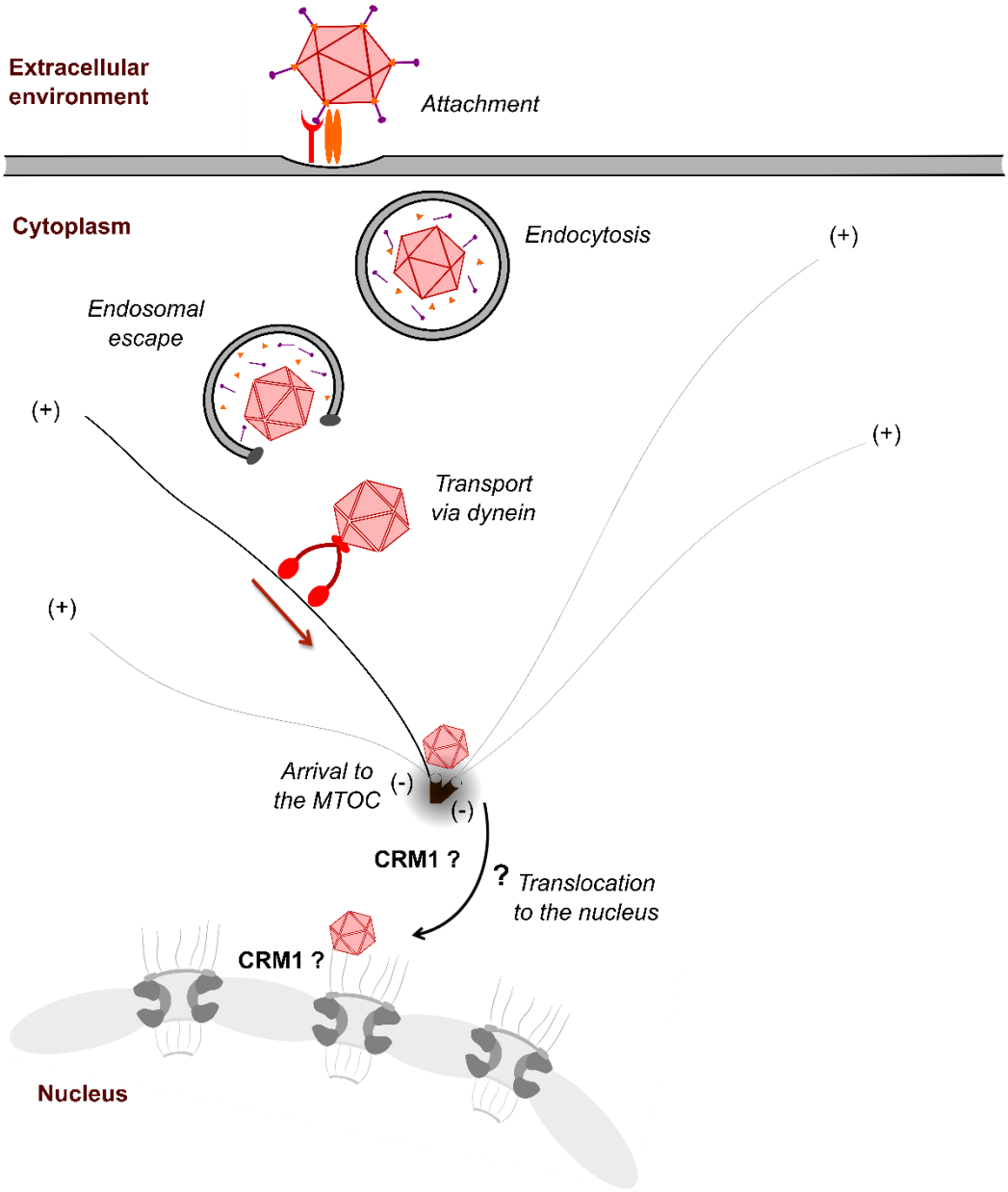

Figure 8. First steps of Ad5 cell cycle: from the cell entry to the nucleus. Ad5 binds to the cell via interactions between the fiber protein with CAR molecules and the penton-base with the integrins αβ on the cell surface. It enters the cytoplasm via clathrin-mediated endocytosis. Acidification of the endosome leads to a partial disassembly of the capsid. The exposure of pVI during this partial disassembly step promotes lysis of the endosomal membrane and allows the escape of the virus in the cytoplasm. Ad5 is then transported towards the MTOC via the microtubule motor dynein and the capsid is transferred to the NPC via an unknown mechanism. Moreover, CRM1 seems to be involved during these processes (Strunze et al. 2005).

III.3 Genome delivery

III.3.a Capsid disassembly

Translocation of Ad5 from microtubules to the nucleus and capsid disassembly are two steps required for Ad5 genome nuclear delivery. Although during the first steps of infection, the Ad5 capsid is subjected to partial disassembly events (Greber et al. 1993), the Ad5 genome remains protected inside the partially disassembled capsid until it reaches the NE. With a diameter of 90 nm, the capsid is too large to be imported intact through NPCs. Therefore, complete disassembly of the capsid is required to promote nuclear import of the genome. Partially intact Ad5 capsids directly bind NPCs via an interaction between the hexon protein and the N-terminal part of Nup214, independently of cytoplasmic factors (Trotman et al. 2001; Cassany et al. 2015). This interaction allows docking of Ad5 to NPCs and is a prerequisite for Ad5 capsid disassembly. Moreover, Ad5-NPC docking has been shown to decrease NE permeability by displacing some FG-Nups (Strunze et al. 2011). The Ad5 capsid disassembly mechanism is not well understood, but several factors have been suggested to promote this step. Histone H1 was identified as an interacting partner of the hexon protein and to participate in disassembly of the capsid, at least for AdV type 5 (Trotman et al. 2001). Another study showed that the mechanical force applied by the Nup358-Kinesin 1 complex bound to the outer capsid protein IX induces capsid disassembly by exerting mechanical force on Nup214 bound capsids. However, in a recent study, we showed that ΔpIX-Ad5 particles are less stable and subject to cytoplasmic premature disassembly. Moreover, particles that remained intact were able to deliver their genome without obvious differences to pIX containing particles suggesting that pIX does not play an important role in disassembly at the NPC (Carlon-Andres et al.2020).

In the past years, several novel technics have been developed to visualise the incoming Ad5 DNA by fluorescence microscopy. The vDNA can be indirectly detected via staining of pVII, the core protein bound to the Ad5 DNA, or the staining of pVII-interacting partners such as TAF-I (Komatsu et al. 2015). The direct detection of the Ad5 genome can be performed with fluorescence in situ hybridization (Cassany et al. 2015), EdU click chemistry by metabolic modification of nucleosides (Wang et al. 2013) or addition of fluorescently detectable sequences directly inserted in the Ad5 DNA (Glotzer et al. 2001; Komatsu et al. 2018). All of these technics use different ways and thresholds of detection. However, they all point to a nuclear detection of the vDNA, or at the edge of the NE. Thus, the disassembly of the Ad5 capsid and its genome exposure occur after docking of the capsid to the NPCs.

III.3.b Genome import

Nuclear import of the Ad5 DNA is not well characterized. Using fluorescence microscopy, nuclear dots representing Ad5 genomes have been identified 20 min post infection and kinetics analysis revealed a maximum number of imported genomes reached after 1 to 2 hours post infection (h pi) in classical cell line models (Komatsu et al. 2015). Several observations suggest an active nucleocytoplasmic transport of the Ad5 genome, using cellular factors. Docking of the capsid to NPCs and its disassembly lead to the exposure of the core-DNA. pV, the core protein that bridges the viral DNA with the capsid via the binding of pVI contains two NLS and is imported into the nucleus (Matthews and Russell 1998). Despite these NLS, the nuclear import of the Ad5 genome mediated by pV has not been reported. One the other hand, the core protein VII harbours several NLSs able to promote import of the core-DNA complex via the interaction with transport receptors such as importin-β, importin-7 and transportin-1 (Wodrich et al. 2006; Hindley et al. 2007). Moreover, an excess of RanGTP, which impairs the binding of import receptors with their cargoes, has been shown to block nuclear import of the Ad5 genome (Saphire et al. 2000). The Heat shock cognate 71 kDa protein (Hsc70) also contributes to nuclear import of the Ad5 genome, although its role remains unclear (Saphire et al. 2000). A small fraction of hexon protein has been reported to enter the nucleus, although mechanisms that trigger this nuclear entry are not known (Greber et al. 1993). We recently showed that the large cytoplasmic nucleoporin Nup358 promotes nuclear import of the Ad5 genome via the recruitment and the concentration of transport factors (i.e. transportin-1) at the NE edge (Carlon-Andres et al. 2020). In this study, we showed that the deletion of Nup358 delays the kinetic of nuclear Ad5 genomes import, whereas the number of disassembled capsids was increasing overtime. Thus, capsid disassembly and genome import are two distinct steps occurring at the NE that use distinct mechanisms. A schematic representation of the docking of Ad5 at the NPC is depicted in Figure 9

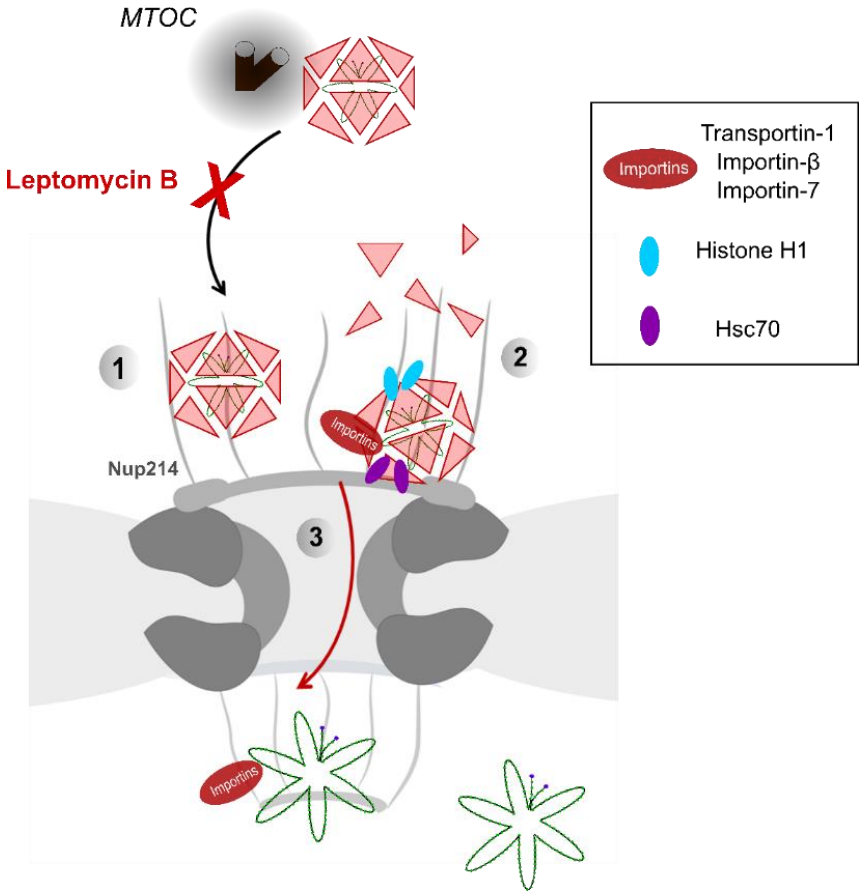

Figure 9. Docking of the Ad5 capsid to the NPC and nuclear import of the genome. The mechanism of translocation of the Ad5 capsid from the MTOC to the NPC is unknown but is impaired upon Leptomycin B (LMB) treatment (see section III.2.b Transport of Ad5 on microtubules), leading to the blocking of the Ad5 at the MTOC. (1) The docking of the partially disassembled Ad5 capsid at the NPC occurs via binding between the hexon protein and Nup214. (2) The exact mechanism of capsid disassembly is unknown but Histone H1 and the Hsc70 factors are involved in this process. (3) The exposure of pVII containing NLSs promotes the import of the genome via importins (transportin-1, importin- β, importin-7). Ad5 DNA is imported into the nucleus, where genome replication and expression are initiated.

III.4 Gene expression and replication

Within the first hours of infection, Ad5 early genes are expressed (Crisostomo et al. 2019). E1A is the first unit to be expressed and is required to activate the expression of the other early genes (Berk et al. 1979). The product of these early genes are proteins involved in the modulation of the immune response and in the replication of the Ad5 DNA. Late genes are only expressed after the initiation of the replication. The expression of the late genes is controlled by the major late promoter (Akusjarvi 2008) and they code for structural proteins. The late genes are expressed from a common primary transcript, spliced to generate five different units (Nevins and Darnell 1978).

The E2 gene codes for three proteins involve in replication: pTP, the adenoviral DNA polymerase (AdV pol) and the DNA Binding Protein (DBP). Initiation of replication starts with the formation of a complex at the origin of replication, i.e at the ITRs (Hoeben and Uil 2013). AdV pol initiates DNA synthesis at the 3'-OH extremity of DNA. Thus, pTP in complex with the AdV pol covalently binds its serine 580 to the 3'OH extremity of the viral DNA template (Desiderio and Kelly 1981). The DBP facilitates the formation of this initiation complex. Two cellular transcription factors, the Nuclear Factor I (NFI) and the Octamer binding protein (Oct-1) enhance the DNA replication (Mysiak et al. 2004). Once a few nucleotides are synthetized, AdV pol dissociates from the pTP to proceed the synthesis of the full DNA strand. Later during the maturation of the capsid, pTP is cleaved by the protease into TP. Therefore, TP is covalently bound to the 5' extremity of the newly synthetized Ad5 DNA molecules (Challberg and Kelly 1981). The replication of Ad5 is morphologically and spatiotemporally well organized. Recent studies performed in our group showed a biphasic replication with different rates of Ad5 genomes synthetized during a first and a second phase of replication (Komatsu et al. 2018). Moreover, the difference in replication rate is associated with distinct morphologies of replication centres during the viral life cycle raising the possibility that functionally different genomes can be replicated (Komatsu et al. 2016).

III.5 Assembly and egress

After DNA replication, the late genes coding for structural proteins are expressed and proteins are synthetized in the cytoplasm. Ad5 assembly takes place in the nucleus. Therefore, structural proteins need to be imported in the nucleus. The pre-pVI has been shown to promote nuclear import of the hexon protein, via the interaction of the NLS within its C-terminal part and importin-β (Wodrich et al. 2003). Thus, pre-pVI is a shuttling protein acting like an adaptor for the nuclear import of the hexon protein. The exact mechanism of Ad5 viral assembly is not known. However, it has been shown that the 52- and 55-kilodalton proteins (52/55K proteins), coded by the late L1 region, are essential for assembly of virions.

52/55K proteins are found in intermediate non-mature virions (see below) but they are absent in mature particles (Hasson et al. 1989). The co-staining of DBP, the protein involved in Ad5 DNA replication (see section III.4 Gene expression and replication) and the 52/55K proteins shows different nuclear localization, with an exclusion of 52/55K proteins from replication centres (Hasson et al. 1992). Thus, replication of the Ad5 genome and assembly of capsids are two separated events. In addition, the cellular protein nucleophosmin (NPM1/B23) appears to be essential for the regulation of the chromatinisation of the genome, therefore involved during the assembly process (Samad et al. 2012).

The packaging of the Ad5 DNA molecule into the newly assembled capsid require the encapsidation sequence (Ψ) and the pIVa2 (Zhang and Imperiale 2003). Interestingly, the major core protein VII condenses the DNA but is dispensable for the packaging of the Ad5 DNA into capsids upon assembly (Ostapchuk et al. 2017). The chronology of packaging and capsid assembly is not clear and there is no clear evidence of a simultaneous mechanism (San Martin 2012).

Intermediate immature virions are observed during the assembly of new Ad5 particles (Sundquist et al. 1973). The switch from an immature capsid to a mature capsid is operated by the cleavage of precursor proteins to mature proteins (pre-TP, pre-pVI, pre-pvII, pre-pVIII, pre-μ, pre-pIIIa), by the AVP (Mangel and San Martin 2014). The proteolytic activity of AVP is enhanced by the viral DNA and the C-terminal peptide of the pre-pVI (Mangel et al. 1993). The importance of the maturation of the Ad5 precursor proteins was studied using the AdV thermo-sensitive mutant ts1, a mutant lacking the AVP and therefore containing unprocessed precursors (Rancourt et al. 1995). The results of this study showed that in absence of AVP, no defect in genome packaging was observed, suggesting that maturation is not essential for particle assembly. In contrast, infectivity of the newly synthetized particles was impaired by the inability of immature particles to release protein VI, preventing them from escaping the endosomal compartment upon entry (Imelli et al. 2009). Moreover, AVP has been suggested to participate in early events of the Ad5 life cycle, during the uncoating process (Greber et al. 1996). Therefore, maturation of the capsid is a key step to ensure the infectivity of Ad5 particles and to maintain the architecture of the viral particle.

After assembly of newly synthetized particles, Ad5 virions induce the lysis of the host cell in order to spread in the extra-cellular environment. The mechanism used by Ad5 to induce the cell death is not clearly established. The Early gene E3 coding for the adenovirus death protein has been shown to promote cell lysis (Tollefson et al. 1996). Another study has implicated autophagy in inducing the cell lysis (Jiang et al. 2011).

Aim of the work

During its life cycle, Ad5 has to import its genome into the nucleus of the infected cell. In order to reach the nuclear compartment, Ad5 uses first the microtubule transport machinery to traffic towards the MTOC, requiring intact stable capsids that protect the genome. Following the MTOC mediated transport, Ad5 uses the nucleocytoplasmic transport to reach NPCs. The capsid has to be completely disassembled, to liberate the genome for import. The transport of the capsid on microtubules and the different interactions involved in this process are beginning to be characterized. However, the unloading of the virus from the microtubules and its translocation from the MTOC to the NE are not well understood. As mentioned, once at the NE, the capsid is disassembled to allow import of the Ad5 genome only. Like capsid unloading from the microtubules, capsid disassembly at the NPC is also not well understood. CRM1, a nuclear export factor, has been shown to be required for the MTOC-NE translocation of the capsid, *prior to* the capsid disassembly. However, the interaction between Ad5 and CRM1 and the exact function of this exportin during the Ad5 cycle are not characterized

The aims of this study were i) to characterize the interaction of Ad5 with microtubules at the MTOC area, ii) to analyse its removal from the MTOC for nuclear targeting and capsid disassembly, and iii) to gain more insights into the role of CRM1 during these early steps of Ad5 infection. The first part of this study focuses on early steps in Ad5 infection, from the MTOC arrival, to the NE targeting of Ad5 and especially the role of CRM1 in those steps. Different types of infection assays were performed, to individually analyse these steps, and the requirement of nuclear factors in those events. Infections of cells lacking their nucleus, live cell imaging on mitotic cells or immunostaining of fixed cells were performed. Moreover, we focused our analyses on a mutant of CRM1, showing a defect in the first steps of Ad5 infection. The second part of the work focuses on biochemical characterizations of the mutant of CRM1, to explain the effects that we observed during Ad5 infection. We generated cell lines constitutively expressing this CRM1 mutant, in order to analyse its export functions *in vivo*. We purified recombinant CRM1 to perform *in vitro* assays, and monitored the ability of this mutant to export substrates. We used *in vitro* export assays as well as anisotropy assays to characterize the formation of export complexes.

MATERIAL AND METHODS

I. Materials

I.1 Technical equipment

Equipment	Company
Agarose gel documentation GelSTICK touch	INTAS Science Imaging Instruments
Agarose gel running chamber	Home-made, Workshop, UMG
ÄKTA column MonoQ	GE Healthcare
ÄKTA HiTrap Prot G High Performance	GE Healthcare
ÄKTApurifier	Amersham Biosciences
Autoclave Sterilizer DX-200	Systec
BioPhotometer	Eppendorf
CASY 1	Schärfe System
Cell culture hood Herasafe™ KS	ThermoScientific
Cell culture incubator Heracell™ 150i	ThermoScientific
Centrifuge 5415R	Eppendorf
Centrifuge 5424	Eppendorf
Centrifuge Allegra® X-15R with rotor SX4750	Beckman Coulter
Centrifuge Avanti™ J-30I with rotor JA30.50Ti	Beckman Coulter
Centrifuge J6-MI with rotor TY-JS 4.2	Beckman Coulter
Centrifuge RC5B with rotor GSA	Sorvall
Certomat BS-1 Incubator Shaker	Sartorius
ChemiDoc MP Imaging System	BioRad
Dual Gel Caster for Mini Vertical Units	Hoefer
EmulsiFlex-C3	Avestin
FACSCanto™ II	BD Biosciences
Fluorescence microscope Axioskop 2	Zeiss
FluoroMax-4	Horiba
HybEZ™ II Hybridization System	ACDBio
Incubation/Inactivation Water Bath Model 1003	GFL
Incubator Heraeus function line	Heraeus
Incubator Shaker INNOVA 4430	New Brunswick Scientific
Inverted microscope Nikon Eclipse Ti2	Nikon
LAS-3000 Imaging System	Fujifilm
Leica DM6 CFS TCS SP8	Leica
Leica DMI6000 B	Leica
Mini Trans-Blot® Cell	Bio-Rad
Odyssey® CLx	LI-COR
Olympus CK40 Culture Microscope	Olympus
Photometrics Quantem 512	Teledyne Photometrics

Equipment	Company
SE250 Mighty Small II Mini Vertical Electrophoresis Unit	Hoefer
Spectrophotometer NanoDrop 2000c	ThermoScientific
Spinning-disk LIFA microscope	Leica
Thermocycler FlexCycler2	Analytik Jena AG
Thermomixer compact	Eppendorf
Trans-Blot Turbo Transfer System	BioRad
Ultracentrifuge Optima L-100 XP with rotor SW41	Beckman Coulter
UV quartz cuvette	Hellma® Analytics
UV Sterilizer	Biometra
UV transilluminator	Uvitec
Vortexer MS2 Minishaker	IKA
Western blot incubation boxes	LI-COR

I.2 Consumables

Consumable	Company
5 mL Polystyrene Round-Bottom Tubes	BD Biosciences
Amersham Protran 0.45 µm NC Nitrocellulose Blotting Membrane	GE Healthcare
Amicon Ultra UltraCel-50K	Merk
Casy cups with lids	Roche Diagnostics (Fisher Scientific)
Corning® Spin-X® UF Concentrators	Merk
Empty Gravity Flow Columns	BioRad
Ibidi® dishes and slides	Ibidi®
Microscope coverslips (12 or 15 mm Ø)	Marienfeld
Microscope slides (76 x 26 mm)	Thermo Scientific
Mini-PROTEAN® TGX Stain-Free™ (BioRad)	BioRad
Minisart RC 15, single use syringe filters (0.45 µm; 0.20 µm)	Sartorius stedim biotech
Parafilm "M"	Bemis Company, Inc.
PD-10 columns	GE Healthcare
Plastic consumables	Sarstedt, Nalge Nunc International, greiner bio-one
Polypropylene tubes	Beckman
Reaction tubes	Sarstedt, Greiner bio-one, Eppendorf
Slide-A-Lyzer™ Dialysis Cassettes	Thermo Fisher Scientific
Syringes and needles	Braun, Servoprax
Whatman gel blotting paper	GE Healthcare

I.3 Kits

Kit	Company
Alexa Fluor 488 Microscale Protein Labeling Kit	Life technologies Invitrogen
Alexa Fluor 594 Microscale Protein Labeling Kit	Life technologies Invitrogen
NucleoBond™ Xtra Mid	Macherey-Nagel
NucleoSpin® Gel and PCR Clean-up	Macherey-Nagel
NucleoSpin® Plasmid	Macherey-Nagel
Pierce® BCA Protein Assay Kit	ThermoScientific
RNAscope® Multiplex Fluorescent Assay	ACDBio
Trans-Blot Turbo RTA Mini 0.2 µm Nitrocellulose Transfer Kit	BioRad

I.4 Software

Software	Company
Endnote	Clarivate Analytics
FACS Diva 6.1.1	BD Biosciences
FluorEssence	Horiba
GraphPad Prism 7	GraphPad Software Inc.
Image J	NIH
Image Reader LAS-3000	Fujifilm
Image Studio Lite Ver 5.2	LI-COR
Inkscape 0.92.4	Inkscape
Leica LAS-X	Leica
MetaMorph	Molecular Devices LLC
NanoDrop 2000 Software	ThermoScientific
NetNES 1.1 Server	DTU Health Tech, University of Denmark
NIS-Elements AR 5.02	Nikon
Omega	GmbH
PyMOL	Schrödinger LLC
SerialCloner 2.6.1	SerialBasics
Unicorn	GE Healthcare

I.5 Chemicals and reagents

Chemicals, reagents and solvents not listed below were provided by AppliChem GmbH, Carl Roth GmbH, Merck, Sigma-Aldrich or Serva Electrophoresis GmbH.

Name	Company
5X Phusion Buffer	ThermoScientific
6X DNA Loading Dye	ThermoScientific
Acrylamide 4K Solution (30%)	AppliChem
Adenosine 5'-triphosphate disodium salt hydrate (A3377)	Sigma
Agarose 4%	Fisher
Bovine Serum Albumin (BSA) (20 mg/mL)	ThermoScientific
BSA, fraction V	AppliChem
Cesium Chloride	Sigma
CO2-Independent Medium	ThermoScientific
Colcemid	Sigma
cOmplete™, Mini, EDTA-free Protease Inhibitor Cocktail	Roche
Cyanogen bromide-activated Sepharose 4B beads	Sigma
Cytochalasin B	Enzo Life Sciences
Dako Fluorescent Mounting Medium	AGILET
DAPI	Sigma
Digitonin	Calbiochem
dNTP Set, 100 mM Solutions	ThermoScientific
Fast Digest restriction enzymes	ThermoScientific
FastAP Thermosensitive Alkaline Phosphatase	ThermoScientific
Fetal Calf Serum	Life Technologies
GeneRuler 100 bp DNA Ladder	ThermoScientific
GeneRuler 1 kb DNA Ladder	ThermoScientific
Geniticin	Fisher
Gibco® DMEM (1x)	Life Technologies
Gibco® Opti-MEM® (1x)	Life Technologies
Gibco® Penicillin Streptomycin (Pen Strep)	Life Technologies
Gibco® Trypsin/ EDTA 0.25% (1x)	Sigma
Glutamax	Life Technologies
Glutathione sepharose 4 fast flow	GE Healthcare
Guanosine 5'-diphosphate sodium salt	Sigma
Leptomycin B	Sigma; Enzo Life Sciences
Lipofectamine® 2000	Life Technologies
Milk powder	Sigma
MOWIOL® 4-88	Calbiochem
Ni-NTA Agarose	Quiagen
Oligonucleotides	Merk
PageRuler Plus Prestained Protein Ladder	ThermoScientific
PageRuler Unstained Protein Ladder	ThermoScientific

Name	Company
Paraformaldehyde 16 % EM grade	Delta microscopie
PBS (10x)	Life Technologies
Phusion® High-Fidelity DNA Polymerase	ThermoScientific
Pierce™ Coomassie Plus	ThermoScientific
Poly-L-lysine solution 0.1% (w/v)	Sigma
SafeView™ Classic DNA	Applied Biological Materials Inc.
Saponin	Sigma
SDS	Euromedex
T4 DNA Ligase	ThermoScientific
T4 DNA Ligase buffer	ThermoScientific
Trichostatin A	Sigma
β-Mercaptoethanol	Roth

I.6 Stock solutions

Stock solution	Composition
1.4-Dithiothreitol (DTT)	1 M diluted in H_2O
Adenosine triphosphate (ATP)	100 mM ATP; 100 mM $Mg(OAc)_2$; 20 mM HEPES (pH 7.4)
Ammonium persulfate (APS)	10% APS (Sigma) diluted in H_2O
Ampicillin	100 mg/mL diluted in H_2O
Aprotinin (AP)	1 mg/mL in 20 mM HEPES pH 7.4
Creatine Phosphate	80 mg/mL diluted in H_2O
Creatine phosphokinase	2000 U/mL; 50% glycerol; 20 mM HEPES pH 7.4
Ionomycin	1 mM diluted in DMSO
Isopropyl b-D-1-thiogalactopyranoside (IPTG)	1 M diluted in H_2O
Leupeptin/Pepstatin (LP/AP)	1 mg/mL each,diluted in DMSO
Phenylmethylsulfonyl fluoride (PMSF)	100 mM diluted in 2-propanol
Saponin	10% diluted in H_2O
Trichostatin A (TSA)	1 mM diluted in EtOH

I.7 Buffers and media

Solution	Composition
2YT-medium	1.6% (w/v) tryptone; 1% (w/v) yeast extract; 0.5% (w/v) NaCl; pH 7 adjusted with NaOH
Ad5 lysis buffer	10 mM Tris pH 7.4; 0.1% SDS; 1 mM EDTA
Anisotropy buffer.	20 mM Tris HCl pH 7.4; 50 mM NaCl; 1mM $Mg(OAc)_2$,

Solution	Composition
Calcium chloride buffer	250 mM $CaCl_2$ diluted in H_2O
Coomassie fixation solution	40% ethanol, 10% acetic acid
Coomassie staining solution	5% aluminum sulfate (14-18) hydrate; 10% ethanol; 2% ortho-phosphoric acid; 0.02% CBB-G250
CRM1 elution buffer	50 mM HEPES pH 7.8; 500 mM NaCl; 4 mM $MgCl_2$; 400 mM Imidazole; 3 mM β-mercaptoethanol
CRM1 lysis buffer	50 mM HEPES pH 7.8; 500 mM NaCl; 2 mM $MgCl_2$; 30 mM Imidazole; 10% glycerol; 4 mM β-mercaptoethanol
Desalting buffer	50 mM HEPES pH 7.8; 50 mM NaCl; 2 mM $MgCl_2$
Glycine elution buffer	100 mM glycine; pH 2.7 adjusted with HCl
GST buffer	50 mM Tris pH 6;8; 300 mM NaCl; 1mM $MgCl_2$; 0.25 mM EDTA
High salt buffer	50 mM HEPES pH 7.8; 500 mM NaCl; 2 mM $MgCl_2$
IF buffer	10% FCS; 0.01% Saponin diluted in 1x PBS
Laemmli buffer (10x)	250 mM Tris; 1.92 M glycine; 0.5% SDS
LB agar plates	LB supplemented with 1.5% (w/v) bacto-agar
LB medium	1% (w/v) bacto-tryptone; 0.5% (w/v) yeast extract; 1% (w/v) NaCl; pH 7
Neutralisation buffer	1M Tris pH 9.4 adjusted with HCl
PBS (10x)	1.37 M NaCl; 27 mM KCl; 100 mM Na_2HPO_4; 18 mM KH_2PO_4; pH 7.5
Phosphate buffer	20 mM Na-Phosphate pH 7
Ponceau staining solution	0.5% Ponceau in 1% acetic acid
SDS-reducing buffer (4x)	125 mM Tris pH 6.8; 4% SDS; 0.02% Bromophenol blue; 10% glycerol
SOC medium	2% (w/v) tryptone; 0.5% (w/v) yeast extract; 10 mM NaCl; 2.5 mM KaCl; 10 mM $MgCl_2$; 10 mM $MgSO_4$; 0.36% (w/v) glucose; pH 7
TAE (50x)	2 M Tris; 0.05 M EDTA; 5.71% acetic acid
TBS (10x)	1.37 M NaCl; 27 mM KCl; 250 mM Tris pH 7.4
Transport Buffer (10x)	200 mM HEPES; 1.1 M KOAc; 20 mM $Mg(OAc)_2$; 10 mM EGTA; pH 7.3
Tris-Glycine-SDS buffer (10x)	25 mM Tris; 192 mM glycine; 1% SDS; pH 8.3
WB blocking solution	TBS 1X -Tween 0.05%; 10% Milk
WB transfert buffer (10x)	250 mM Tris, 1.93 M glycine, 0.2% SDS

I.8 Mammalian cells

Cell line	Origin	Characteristics
U2OS	ATCC HTB-96 Provided by M.Piechaczyk, IGMM, Montpellier, France	Human bone osteosarcoma, epithelial cells
U2OS-TAF-I	(Komatsu et al. 2015)	Stably expressing TAF-I fused to GFP Maintained in cultured with 0.5 mg/mL of geneticine (G418)
U2OS-CRM1-HA	Generated in this study by J. Ragues	Stably expressing CRM1 C528S-HA or CRM1 W142A P143A C528S-HA Maintained in cultured with 2 nM of Leptomycin B
Hek293 αVβ5	ATCC CRL-1573 Provided by G.Nemerow, Scripps Research Institute La Jolla, USA	Human embryonic kidney cells Stably expressing the E1A and E1B AdV proteins Maintained in cultured with 0.5 mg/mL of geneticine (G418)
HeLa-NFAT	(Kehlenbach et al. 1998)	Human cervix carcinoma cells Stably expressing the nuclear factor of activated T-cell (NFAT) fused to GFP

I.9 Bacterial strains

Name	Genotype
DH5α	F- Φ80lacZΔM15 Δ (lacZYA-argF) U169 recA1 endA1 hsdR17 (rK-,mK+) phoA supE44 λ- thi-1 gyrA96 relA1
BL21 (DE3) codon+	F- ompT hsdS(rB- mB-) dcm+ Tetr gal l (DE3) endA Hte [argU proL Camr]

I.10 Antibodies

Table 2. List of primary antibodies.

Name	Species	Application	Dilution	Origin
α-Ad5	Rabbit	IF	1:1000	kindly provided by R. Iggo, Institut Bergonie, Bordeaux, France
α-CRM1	Goat	WB / IF	1:1000 / 1:500	Purified in this study
α-GST	Goat	WB	1:2000	sc459; Santa Cruz
α-HA	Rat	IF	1:500	Clone 3F10; Roche
α-HA	Rabbit	IF	1:1000	H6908; Sigma
α-HA	Mouse	WB	1:1000	HA.11 Clone 16B12; Biolegend
α-pericentrin	Rabbit	IF	1:500	ab4448; Abcam
α-pVII	Mouse	IF	1:100	Komatsu et al. 2015
α-RanBP1	Rabbit	IF	1:250	Kehlenbach et al. 1999
α-RanBP1	Mouse	IF	1:100	610756; BD Transduction Laboratories™
α-TP	Mouse	WB / IF	to be determined	Generated in this study

Name	Species	Application	Dilution	Origin
α-αtubulin	Mouse	IF	1:500	T6199; Sigma-Aldrich
α-αtubulin	Rabbit	WB	1:1000	11224-1-AP; ProteinTech

Table 3. List of secondary antibodies.

Name	Species	Application	Dilution	Origin
α-goat AlexaFluor® 594	donkey	IF	1:500	Life technologies Invitrogen
α-goat AlexaFluor® 647	donkey	IF	1:500	Life technologies Invitrogen
α-mouse AlexaFluor® 488	donkey	IF	1:500	Life technologies Invitrogen
α-mouse AlexaFluor® 488	donkey	IF	1:500	Life technologies Invitrogen
α-mouse AlexaFluor® 594	donkey	IF	1:500	Life technologies Invitrogen
α-mouse AlexaFluor® 647	donkey	IF	1:500	Life technologies Invitrogen
α-rabbit AlexaFluor® 488	donkey	IF	1:500	Life technologies Invitrogen
α-rabbit AlexaFluor® 647	donkey	IF	1:500	Life technologies Invitrogen
α-rabbit AlexaFluor® 647	donkey	IF	1:500	Life technologies Invitrogen
α-rat AlexaFluor® 647	donkey	IF	1:500	Life technologies Invitrogen
α-mouse 680	donkey	WB	1:10 000	LI-COR
α-goat 800	donkey	WB	1:10 000	LI-COR
α-rabbit 800	donkey	WB	1:10 000	LI-COR
α-rabbit StarBright Blue 700	goat	WB	1:10 000	BioRad

I.11 Primers

Table 4. List of primers used for PCR amplification.

Number	Name	Sequence
–	For TP_NES_AAA	CACTGTCGCCGAGCTCGCCCGTCTTCTGGAGGAGGAGG CAACCGCGTCGGCGCGCAACTCC
–	Rev TP_NES_AAA	GGAGTTGCGCGCCGACGCGGTTGCCTCCTCCTCCAGAA GACGGGCGAGCTCGGCGACAGTG
G2168	TP EcoRI_For	GCAGAATTCGCAATGGTCTTCCAACTGCGCCC
G2169	TP NotI_Rev	ACGGCGGCCGCACGCTAAAAGCGGTGACGCG
G2222	TP BamHI_Rev	ACGGGATCCGCACGCTAAAAGCGGTGACGCG
G2235	CRM1 codon optimized C528S for	GACCTGCTGGGTCTGAGTGAACAGAAACGTGGT
G2236	CRM1 codon optimized C528S rev	ACCACGTTTCTGTTCACTCAGACCCAGCAGGTC
G2237	CRM1 codon opt W142A P143A for	CAGATTCTGAAACAAGAAGCGGCGAAACATTGGCCGACC TTTA
G2238	CRM1 codon opt W142A P143A rev	TAAAGGTCGGCCAATGTTTCGCCGCTTCTTGTTTCAGAAT CTG

Number	Name	Sequence
G2244	5'_BamHI_CRM1 optimized	AAATGGGTCGCGGATCCATGCCTGCAATTATGACC
G2245	3'_XhoI_CRM1 optimized	GCACTCGAGTTAAGCGTAATCTGGAACATCGTATGGGTAGTGATGG TGATGGTGATG
G2254	TP_HindIII Rev	ACGAAGCTTACGCTAAAAGCGGTGACGCG
G2259	TP Nter AAAA_EcoRI	GCAGAATTCGCAATGGTCTTCCAACTGGCCGC

Table 5. List of primers used for sequencing.

Number	Name	Sequence
G2244	5'_BamHI_CRM1 optimized	AAATGGGTCGCGGATCCATGCCTGCAATTATGACC
G2246	3'_XhoI_CRM1 optimized	TGTACAAAAATATGCGCGAAACACT
GATC	pEGFP-C2-FP	GATCACATGGTCCTGCTG
GATC	pET-RP	CTAGTTATTGCTCAGCGG
GATC	pGEX5	GGGCTGGCAAGCCACGTTTGGTG
GATC	pMalE	TCAGACTGTCGATGAAGC
_	TP NES mut_for	GTCTTCCAACTGCGCCCCCG
_	TP NES mut_rev	CTGCGAGAAGGCGTTGAGGC

I.12 Plasmids

Table 6. List of plasmids used in this study, already available.

Number	Name	Origin	Application
46	pGex-6P-1	Amersham	Expression
75	pMal-PreScission	S. Port	Expression
290	pEGFP-GST	D. Doenecke	Transfection
623	pEGFP-C1-Rev68-90-GFP2-M9core	S. Hutten	Transfection
628	pcDNA3.1(+)-CRM1-C528S-HA	S. Roloff	Transfection
857	pEGFP-C1-SPN1	I. Waldmann	Transfection
1331	pcDNA3.1(+)-CRM1-W142-P143A-C528S-HA	S. Port	Transfection
1979	pET21a-Hs-CRM1-His	T.Monecke	Expression
2054	pEGFP-C1-TP-full length	T. Komatsu	Transfection
2055	pEGFP-C1-TP-full length-Nterm AAAA	T. Komatsu	Transfection
_	pCAG-ME-IP-H2B-tdiRFP	Addgene	Transfection

Table 7. List of plasmids generated in this study.

Number	Name	Cloning	Application
2056	pEGFP-C1-TP-full length-Nterm AAAA - NES (I432A/L439A/V441A)	PCR on #2054 with "For TP_NES_AAA" and "Rev TP_NES_AAA"	Transfection
2070	pcDNA5-FRT-3x Flag GFP-TRAK1	Montpellier Genomic Collection (MGC)	Transfection
2071	pcDNA3-mCherry TRAK1	Montpellier Genomic Collection (MGC)	Transfection
2095	pGEX-6P1-TP FL Nterm AAAA	PCR on #2118 with (G2168; G2169), cloned into #46 (EcoRI, NotI)	Expression
2118	pEGFP-GST TP FL N term AAAA	PCR on #2055 with (G2168; G2222), cloned into #290 (EcoRI, BamHI)	Transfection
2131	pGEX-6P1-TP FL Nterm AAAA NES AAA	PCR on #2056 with (G2168; G2169) cloned into #46 (EcoRI, NotI)	Expression
2132	pGEX-6P1-TP FL wt	PCR on #2054 with (G2168; G2169), cloned into #46 (EcoRI, NotI)	Expression
2133	pEGFP-GST TP FL N term AAAA NES AAA	PCR on #2056 with (G2168; G2222), cloned into #290 (EcoRI, BamHI)	Transfection
2148	pET21a-Hs-CRM1-His-HA	PCR on #1979 with (G2244; G2245), cloned back to #1979 digested with BamHI and XhoI	Expression
2149	pET21a-Hs-CRM1-C528S-His	Mutagenesis on #1979 with (G2235; G2236)	Expression
2150	pET21a-Hs-CRM1-C528S-His-HA	Mutagenesis on #2148 with (G2235; G2236)	Expression
2151	pET21a-Hs-CRM1-W142A P143A-His	Mutagenesis on #1979 with (G2237; G2238)	Expression
2152	pET21a-Hs-CRM1-W142A P143A-His-HA	Mutagenesis on #2148 with (G2237; G2238)	Expression
2153	pET21a-Hs-CRM1-C528S W142A P143A-His	Mutagenesis on #2151 with (G2235; G2236)	Expression
2154	pET21a-Hs-CRM1-C528S W142A P143A-His-HA	Mutagenesis on #2150 with (G2237; G2238)	Expression
2163	pMal-PreScission-TP wt	PCR on #2054 with (G2168; G2254) cloned into #75 (EcoRI and Hind III) (K. Kostadinovska)	Expression

Number	Name	Cloning	Application
2164	pMal-PreScission-TP Nterm AAAA	PCR on #2055 with (G2259; G2254) cloned into #75 (EcoRI and Hind III) (K. Kostadinovska)	Expression
2165	pMal-PreScission-TP Nterm AAAA NES AAA	PCR on #2056 with (G2259; G2254) cloned into #75 (EcoRI and Hind III) (K. Kostadinovska)	Expression
2170	pMal-PreScission-TP NES mut	Mutagenesis on MBP-TP, with “For TP_NES_AAA" and "Rev TP_NES_AAA"	Expression
2171	pGEX-6P1-TP NES mut	Mutagenesis on #2132, with “For TP_NES_AAA" and "Rev TP_NES_AAA"	Expression
2207	pEGFP-GST TP FL wt	PCR on #2054 with (G2168; G2222), cloned into #290 (EcoRI, BamHI)	Transfection

II. Cell biology

II.1 Cell maintenance

All the cell lines were maintained in Dulbecco's modified Eagle Medium (DMEM), supplemented with 100 U/mL of penicillin, 100 µg/mL of streptomycin and 10% of Fetal Calf Serum (FCS). Geneticin or Leptomycin B (LMB) were added (see section I.8 Mammalian cells) to maintain the selection. Cells were incubated in a humidified cell incubator at 37 °C, with 5% CO_2. Twice a week, when ~80% confluency was reached, cells were washed with 1x PBS, detached by the addition of 0.05% trypsin/EDTA and splitted approximatively 1/10 into fresh medium.

II.2 Coating of coverslips with poly-L-lysine

To limit the detachment of cells, coverslips were coated with poly-L-lysine. Coverslips were washed 20 min with isopropanol, dried and incubated at room temperature with 0.01% poly-L-lysine. After 30 min, the poly-L-lysine solution was removed, the coverslips were washed twice with sterile water and dried. Coverslips were sterilized with UV in an UV sterilizer *prior to* their use.

II.3 DNA transfection

For transient expression of DNA, cells were either transfected with the calcium phosphate method described in (Chen and Okayama 1987) or with lipofectamine 2000. The conditions used in both methods are summarized in the Table 8 and Table 9.

Transfections with lipofectamine 2000 were performed by mixing the DNA with lipofectamine and optimem. The solutions 1 and 2 were incubated for 20 min at room temperature and added on cells. The transfection mix was incubated with the cells for 3 h at 37 °C, removed and replaced with fresh DMEM for 24 h.

Table 8. Lipofectamine transfection method. Conditions used for transfections with Lipofectamin 2000.

Conditions	6 wells	12 wells	24 wells
Number of cells	$2x10^5$	$8x10^4$	$5x10^4$
Solution 1	200 µL Optimem + DNA (2 – 3 µg)	100 µL Optimem + DNA (0.8 – 1.5 µg)	50 µL Optimem + DNA (0.5 – 1 µg)
Solution 2	200 µL Optimem + 3 µL lipofectamine	100 µL Optimem + 1.5 µL lipofectamine	50 µL Optimem + 1 µL lipofectamine
Addition on cells	+ 800 µL Optimem	+ 400 µL Optimem	+ 200 µL Optimem

Transfections with calcium phosphate were performed by mixing the DNA with $CaCl_2$ (250 mM) and the solution was mixed by vortexing for 10 sec. Hepes pH 6.98 was added, the total solution was mixed 5 sec by vortexing and incubated for 20 min at room temperature. The transfection mix was added for 24 h to the cells pre-incubated in DMEM.

Table 9. Calcium phosphate transfection method. Conditions used for transfections with calcium phosphate.

Conditions	6 wells	12 wells	24 wells
Number of cells	$2x10^5$	$8x10^4$	$5x10^4$
Solution 1	80 µL $CaCl_2$ + DNA (2 - 3 µg)	40 µL $CaCl_2$ + DNA (0.8 – 1.5 µg)	20 µL $CaCl_2$ + DNA (0.5 – 1 µg)
Solution 2	80 µL Hepes	40 µL Hepes	20 µL Hepes
Addition on cells	+ 2 mL DMEM	+ 1 mL DMEM	+ 0.5 mL DMEM

II.4 Leptomycin B treatment

CRM1 dependent export was blocked by LMB. LMB targets the cysteine 528 on the NES binding pocket of CRM1 therefore inducing the blocking of the export function (Kudo et al. 1999). Cells were incubated in DMEM containing 20 nM of LMB for 45 min at 37 °C *prior to* fixation or *prior to* Ad5 infections. When mitotic cells were infected, the LMB treatment was performed in the presence of colcemid before infection. Throughout Ad5 infections, a concentration of 20 nM of LMB was kept in the medium.

II.5 Generation of U2OS CRM1-HA cells

The U2OS cells constitutively expressing constructs coding for CRM1-HA were generated by Dr. H. Wodrich. $2.5x10^5$ U2OS cells were seeded in DMEM, in a 6 well plate. The day after, cells were transfected with 2 µg of the corresponding pc.DNA3.1 CRM1-HA construct (see Table 6), using lipofectamine 2000. 48 h post-transfection, cells were washed once with 1x PBS and 20 nM of LMB was added in fresh DMEM. LMB was added to allow the selection of cells having incorporated the constructs coding for CRM1-HA. Every two days, cells were washed once with 1x PBS and fresh medium containing 20 nM of LMB was added. After a few days of culture with LMB, when the confluency of the cells was reached, cells were detached and seeded in a T25 culture flask. The cells were then amplified and maintained in DMEM containing 2 nM of LMB.

II.6 Cell growth U2OS expressing CRM1-HA cells

Cell viability and cell growth were monitored overtime by cell counting. On day 1, $2x10^5$ cells were seeded into a 6 well plate in DMEM for U2OS or DMEM with 2 nM of LMB for U2OS expressing CRM1-HA. On day 3, 2 nM of LMB was added to U2OS cells not expressing CRM1-HA constructs to monitor the effect of LMB, as a control condition. Every 3 days, cells were detached by the addition of trypsin and counted using the CASY cell counter. After counting, the total amount of cells collected cells was seeded *de novo* on new plates.

II.7 Synchronisation of cells in mitosis

Coverslips coated with poly-L-lysine were placed in a 12 well plate. $1.5x10^5$ U2OS cells were seeded *per* well in a total volume of 1 mL of DMEM. The day after, cells were washed once with 1x PBS and fresh medium containing 40 µg/mL of colcemid was added for 14 to 16 h. Upon infections of mitotic cells with Ad5, colcemid was kept in the medium during LMB treatment but was removed before the addition of viruses.

II.8 Enucleation of cells

The protocol for the enucleation of cells was established by Dr. Q. Osseman during his PhD thesis (Quentin Osseman., 2014). Nuclei of U2OS cells were removed by depolymerization of the actin network, followed by high-speed centrifugation (see also Figure 12). $3x10^5$ U2OS cells were seeded in a 35 mm^2 ibidi dish in a total volume of 1 mL of DMEM. The day after, cells were washed once with 1x PBS and 1 mL of DMEM containing 10 µg/mL of cytochalasin B was added for 45 min, at 37 °C. After incubation, fresh medium containing 10 µg/mL of cytochalasin B was added to entirely fill the dish with liquid. The lid of the ibidi dish was carefully screwed and sealed with parafilm to close the plate without any air bubble. The dishes were placed upside-down (cells on the top) in centrifuge bottles of 250 mL filled with paper to wedge the dishes horizontally. The cells were centrifuged using the Rotor GSA Sorvall at 11.000 rpm for 50 min, at room temperature. Due to the disruption of the actin network, the nuclei were no longer supported by the cytoskeleton. Thus, the centrifuge force applied on cells with a disrupted actin network led to the mechanical removal of the nuclei. After centrifugation, cells were washed three times with 1x PBS to remove the cellular debris and incubated at 37 °C with DMEM, for at least 90 min before being infected.

II.9 Depolymerization of microtubules

U2OS cells grown on coverslips were infected with Ad5 for 2 h at 37 °C in the presence or absence of LMB. 2 h post-infection (pi), cells were washed with pre-warmed 1x PBS and incubated with approximatively 100 µL of fresh DMEM (to cover entirely the cells) in the absence or presence of LMB.

The coverslips were placed in a humidity chamber either at 37 °C for the control conditions, or on ice for the depolymerization of microtubules, for 30 min. Cells were fixed with 4% paraformaldehyde (PFA) either for 15 min at room temperature for the control conditions, or for 40 min on ice for the condition with depolymerized microtubules.

II.10 Digitonin treatment

U2OS cells grown on coverslips were infected with Ad5 for 2 h at 37 °C in the presence or absence of LMB. 2 h pi, cells were washed once with 1x PBS and incubated with 0.1% of digitonin diluted in 1x transport buffer (1x TPB), freshly supplemented with a cocktail of protease inhibitor, for 5 min at 37 °C. After permeabilization, cells were washed three times with 1x PBS and fixed with 4% PFA in 1x PBS, for 15 min at room temperature.

II.11 Seeding cells for live cell imaging

U2OS cells constitutively expressing the TAF I-GFP construct were seeded in a 6 well plate. The day after, cells were transfected with the construct coding for the H2B-tdiRFP using the lipofectamin 2000 method (see condition in Table 8). After 24 h of transfection, cells were detached with 0.05% trypsin/EDTA and $3x10^5$ cells were seeded on imaging ibidi µ-slides. After 3 to 4 h, the time to allow cell attachment, fresh DMEM medium containing 40 µg/mL of colcemid was added to the cells for 14 to 16 h at 37 °C. Fresh DMEM medium containing 40 µg/mL of colcemid in the presence or absence of 20 nM of LMB was added for 45 min at 37 °C. Cells were then washed three times with imaging medium (CO_2 independent medium) in the absence or presence of LMB and kept in this medium for infection with Ad5.

II.12 Immunofluorescence staining

Cells grown on 12 mm or 15 mm coverslips were washed three times with 1x PBS *prior to* fixation. Fixation was performed at room temperature for 15 min by the addition of 100 µL of 4% PFA in 1x PBS, to entirely cover the cells. After fixation, cells were washed three times with 1x PBS and either directly processed for immunostaining or kept at 4 °C in 1x PBS for few days. The following steps were performed with the coverslips in a humidity chamber, to prevent cells from drying out. 100 µL of fresh immunofluorescence buffer (IF buffer) containing 10% of FCS and 0.1% of saponin diluted into 1x PBS, were added on each coverslip for 15 min at room temperature. FCS and saponin were added to reduce unspecific bindings of antibodies and gently permeabilize the cells, respectively.

Primary antibodies were diluted in IF buffer (for dilutions see Table 2) and 50 µL per coverslip were added for 1 h at 37 °C. Cells were washed three times with 1x PBS for 5 min at room temperature with gentle agitation. Secondary antibodies (for dilutions see Table 3Table 3. List of secondary antibodies.) were diluted 1:500 in IF buffer and 50 µL were added for 1 h at 37 °C.

Cells were washed three times for 5 min with 1x PBS at room temperature and the coverslips were shortly immerged in water and pure ethanol and left to air dry. Once they were dry, 5 µL of the mounting medium containing either DAKO or Mowiol mixed with 1 µg/mL of DAPI, were applied on microscopy slides and the coverslips were dropped upside down, with the cells in contact with the mounting medium. The slides were dried in the dark overnight before microscopy imaging and kept at 4 °C in the dark for longer storage.

II.13 RNAscope

The RNAscope assay was performed in order to visualize the Ad5 E1A mRNAs transcripts by fluorescence microscopy, at the single cell level. To this end, we adapted the protocol from the RNAscope® Multiplex Fluorescent Assay (Company ACDBio; https://acdbio.com) (Wang et al. 2012) to our infection assays, in combination with IF staining. The assay required several steps of incubation with different compounds. First, the Ad5 E1A mRNAs were detected by a set of probes hybridizing specifically the E1A mRNA sequences of the Ad5. The probes were designed by the manufacturer in a way to hybridize mRNA in tandem, to avoid unspecific bindings. Each probe was organised as a "Z", with the lower region complementary to the RNA sequence target and the upper region composed of a 14-base tail sequence. The hybridization of tandem-probes on E1A mRNA sequences formed thus a 28-base sequence. Pre-amplifiers were then added to hybridize the 28-base tail sequence formed by the tandem-probes. These compounds were organised as a platform containing several sites for the binding of amplifier sequences. Amplifiers were then added, to bind the pre-amplifier platform on one hand, and to bind labelled probes on the other hand. As a last step, labelled probes were added to bind the amplifiers. To this end, the signal of detection was amplified thanks to the high number of labelled probes. As a result, a single target RNA molecule was represented by an individual dot visualized by fluorescence microscopy.

Cells grown on 15 mm coverslips were infected, washed once with 1x PBS and fixed with 100 µL of 4% PFA in 1x PBS for 10 min at room temperature. After fixation, cells were washed three times with 1x PBS and incubated for 5 min with successive baths of 50% and 70% ethanol and for 10 min with 100% ethanol. Coverslips were stored at -20 °C in 100% ethanol before performing the RNAscope assay. The storage of coverslips can be done up to 6 months in these conditions. On the day of the assay, cells were incubated for 2 min with 70% ethanol, followed by 2 min of incubation with 50% ethanol. A final bath of 10 min with 1x PBS was performed to progressively rehydrate the cells. The following steps were performed with the coverslips in a humidity chamber, to prevent cells from drying out. 100 µL of protease III (provided in the kit) freshly diluted 1:30 in 1x PBS was added for 15 min at room temperature to allow the entry of the probes into the cells, and washed 3 times with 1x PBS.

The commercial solution containing the probes was applied pure to entirely cover the cells, for 2 h at 40 °C, incubated into an incubator provided by ACDBio. Cells were then washed twice for 2 min with the provided wash buffer initially diluted 1:50 in water and hybridized with the "amplifiers", following the manufacturer's instructions. Solutions were added pure, to entirely cover the cells. The "Amp 4 AltB-FL" containing the labelled Alexa 488 probes was chosen. After the last washing step with the wash buffer, two washing steps using 1x PBS were performed. The coverslips were directly processed for IF staining (see section II.12 Immunofluorescence staining), starting with an incubation with IF buffer.

II.14 *In vitro* export assays

In vitro export assays were performed to measure export functions of CRM1, following an adapted protocol established by Kehlenbach et al., in 1998. HeLa cells constitutively expressing the construct coding for GFP-NFAT were seeded in DMEM, in a 15 cm diameter plate. The day after, 1 µM of trichostatin A was added to the cells to induce GFP-NFAT expression, and incubated overnight at 37 °C. The following day, 1 µM of ionomycin was added to the cells for 25 min, to induce nuclear import of GFP-NFAT. Cells were then washed once with 1x PBS, detached with addition of 0.05% trypsin/EDTA and re-suspended in 1x TPB supplemented with 10% FCS. After 5 min of centrifugation at 4 °C, 300 g, cells were washed once, re-suspended in 20 mL of cold 1x TPB and counted with the CASY cell counter. Cells were pelleted by centrifugation at 300 g for 5 min, 4 °C and 1x TPB was added to the pellet to reach a concentration of $1x10^7$ cell/mL. Cells were permeabilized by addition of 100 µg/mL of digitonin (0.7 µL of a 1% stock solution *per* 10^6 cells) for 3 min on ice and permeabilization was confirmed under a microscope by mixing 5 µL of cell suspension to 5 µL of a trypan blue solution. Permeabilized cells were washed twice with 1x TPB and diluted to reach a concentration of $2x10^7$ cells/mL. For each condition, $2x10^5$ cells (10 µL of the permeabilized cell solution) were incubated with 1 µL ATP regenerating system (1 mM ATP, 5 mM Creatine Phosphate, 20 U/mL creatine phosphokinase) in a total volume of 40 µL of 1x TPB, for 15 min at 30 °C, under agitation. After incubation, cells were washed twice with 1x TPB and re-suspended in 10 µL of 1x TPB. Export reaction mix was added to the cells: 1 µL of ATP regenerating system, 1 µM of NFAT oligonucleotides, 1 µM of RanGTP and various concentrations of recombinant CRM1, in a final volume of 40 µL. Reaction mixes were incubated for 25 min (or various amount of time for kinetic experiments), at 30 °C under agitation and reactions were stopped by the addition of 500 µL of cold 1x TPB. Samples were transferred into Fluorescence-activated cell sorting (FACS) tubes and GFP fluorescence of 10.000 cells was analyzed by flow cytometry, using a FACS CantoTM II flow cytometer.

III. Molecular biology

III.1 Polymerase chain reaction (PCR)

DNA sequence amplifications were performed by PCR, with the Phusion® High-Fidelity DNA Polymerase The mix reactions were prepared in a total volume of 50 µL, according to the manufacturer's guidelines (ThermoScientific) and are detailed in the Table 10. The primers and templates used for the PCR reactions are listed in the Table 4. The annealing temperatures for each pair of primers were set according to the tool "Tm calculator" from Thermo Fisher Scientific. DNA amplifications were performed in a thermocycler following the cycling instructions specifics for the Phusion® High-Fidelity DNA Polymerase, from the manufacturer. Extension time of the amplification reactions were determined according to the expected size of the PCR product (i.e 15 to 30 sec/kb). 30 cycles of amplification were performed for each amplification reaction except for the mutagenesis, where only 20 cycles were performed.

Table 10. Composition of one PCR mix.

Component	Final concentration
5x Buffer	1X
dNTP	200 µM each
Primer 1	0.5 µM
Primer 2	0.5 µM
Template DNA	100 ng
Enzyme Phusion	0.02 U/µL
H_2O	qsp 50 µL

III.2 Purification PCR products

The PCR amplification products were separated by electrophoresis on agarose gels. Depending on the size of the DNA fragment, 0.8 to 2% agarose gels were prepared by dissolving agarose powder with Tris Acetate EDTA 1X (1x TAE) buffer and heating the mix in a microwave. To visualize the DNA with UV illumination, SafeView™ Classic DNA stain was added to the agarose melt solution to a dilution 1:10.000. After solidification, the agarose gel was placed in a running chamber, immerged in 1x TAE buffer. DNA loading buffer 1X was added to DNA samples and loaded on the gel. A molecular weight marker was loaded in parallel, to control the size of DNA fragments. Size separation of the samples was performed at 120 V. After migration, agarose gels were subjected to UV illumination and the DNA fragments of interest were cut from the gel.

The DNA was extracted and purified with the NucleoSpin® Gel and PCR Clean-up kit, following the manufacturer's instructions, and eluted in a final volume of 15 µL. The concentration of DNA after purification was measured with a NanoDrop 2000c.

III.3 Digestion of DNA

Purified PCR products were digested with Fast Digest restriction enzymes. The optimal conditions for the digestion reaction (buffer, final volume, time of digestion, temperature of enzymatic inactivation) were determined according to the manufacturer's instructions. Between 100 to 500 ng of purified PCR product and 1 µg of the selected vector were digested at 37 °C. Digested vectors were dephosphorylated for 10 min at 37 °C with 1 µL of FastAP Thermosensitive Alkaline Phosphatase, to prevent their re-circularization. After enzymatic inactivation, digested vectors were loaded on an agarose gel, cut and purified using the NucleoSpin® Gel and PCR Clean-up kit following the "Gel clean up" protocol. Digested PCR products were directly purified with the same kit, following the "PCR clean up" protocol. For mutagenesis reactions, PCR products were directly incubated after the PCR reaction with 1 µL of DpnI for 1 h at 37 °C, to digest the methylated DNA from the template.

III.4 Ligation

The digested DNA fragments and vectors were ligated using the T4 DNA Ligase. In addition to the vector and DNA fragments, the reaction mix was composed of 1X T4 DNA Ligase buffer, 250 µM of ATP and 1 µL of the T4 DNA Ligase enzyme, in a final volume of 20 µL. 50 µg of the vector was used in the ligation reaction, with a 5x molar excess of the DNA insert. The reaction was performed for 1 h at room temperature and transformed into *Escherichia coli* DH5 α.

III.5 Transformation of bacteria

For plasmid amplifications, chemically competent *E. coli* DH5 α strains were used. Bacteria (~100 µL) were thawed on ice and the entire ligation reaction was added. In the case of amplification of a pure plasmid, 200 to 500 ng of DNA were added to the cells. DNA and bacteria were incubated on ice for 15 min and placed at 42 °C for 1 min, to induce a heat shock. Cells were then immediately placed on ice for 2 min before the addition of 900 µL of SOC-medium. The bacterial suspension was incubated in heating blocks at 37 °C for 1 h at 750 rpm. 100 µL of the bacterial suspension were plated on LB-agar plate, supplemented with the corresponding selection antibiotic. For bacteria incubated with the ligation reaction, before plating, cells were centrifuged at 300 g for 5 min, 800 µL of the supernatant were removed and the bacterial pellet was re-suspended with the 100 µL of remaining SOC-medium. For amplification of plasmid, no centrifugation was performed and 100 µL of the suspension was directly processed. LB-medium plate were incubated overnight at 37 °C.

III.6 Isolation and selection of positive clones

To isolate amplified plasmids in *E. coli* grown on LB-medium plates, bacteria colonies were picked and incubated in 7 mL of LB-medium supplemented with the corresponding antibiotic, overnight at 37 °C at 180 rpm. The day after, bacteria cells were pelleted and plasmid DNA was extracted and purified using the NucleoSpin® Plasmid kit, according to the manufacturer's instructions. Extracted DNA was digested with restriction enzymes used during the previous steps (section III.3 Digestion of DNA) and digestion products were analysed with electrophoresis on agarose gels. The DNA extracted from clones harbouring fragments with expected molecular sizes after digestion were sent to sequencing to the Eurofins genomic company. Sequencing primers used in this study are summarized in the Table 5. Plasmids with the correct expected sequence were amplified in large scale (200 mL of LB-medium supplemented with the selection antibiotic) and purified using the NucleoBond ™ Xtra Midi kit, according to the manufacturer's instructions.

IV. Biochemistry

IV.1 Electrophoresis of proteins

Proteins were separated according to their molecular size using sodium-dodecyl-sulfate polyacrylamide gel electrophoresis (SDS-PAGE). Depending on the molecular weight of the proteins of interest, acrylamide gels with a concentration of 8 to 15% were prepared. Protein samples (recombinant proteins or cells lysates) were incubated with SDS-reducing buffer for 5 min at 95 °C before loading on a polyacrylamide gel. Molecular weight ladders were loaded next to the protein samples to check molecular sizes. Electrophoresis was performed in 1x Laemmli Buffer, at 25 mA, 300 V, for 1 h, at room temperature. After electrophoresis, acrylamide gels were either incubated with a coomassie solution (section IV.2 Coomassie staining) or processed for Western blotting (section IV.3 Western blot (WB)).

When the TP antibodies purification was performed, pre-casted gels Mini-PROTEAN® TGX Stain-Free™ with a gradient resolution of 4 to 15% were used. Electrophoresis was performed at 90 V and constant voltage, in Tris-Glycine-SDS (TGS) 1X buffer.

IV.2 Coomassie staining

For the visualization of proteins directly on the acrylamide gel, coomassie staining was performed. Gels were rinsed with water and incubated with comassie fixing solution, under agitation. After a minimum of 10 min of incubation, gels were rinsed with water and incubated with the coomassie staining solution for at least 1 h. When the proteins were sufficiently stained to be visualised, gels were incubated with water to remove the residual background.

Gels were then documented using the LAS-3000 imaging system and analysed using the Image J software.

IV.3 Western blot (WB)

Immuno-detection of specific proteins in a protein sample was performed by Western blotting. After electrophoretic separation (section IV.1 Electrophoresis of proteins), gels were rinsed with water before being processed for protein transfer on nitrocellulose membrane. The transfer was performed in 1x WB transfer buffer, supplemented with 15% ethanol, on Amersham Protran 0.45 µm NC Nitrocellulose Blotting Membranes, in a cold room, at 400 mA, 300 V, for at least 90 min. The efficiency of the transfer was controlled by Ponceau staining. Nitrocellulose membranes were incubated for two minutes with Ponceau solution and rinsed with water until disappearance of the background. Nitrocellulose membranes were incubated for 30 min with WB blocking solution at room temperature, under agitation. Primary antibodies were diluted in blocking solution (for dilutions, see Table 2).

Nitrocellulose membranes were incubated with primary antibodies overnight at 4 °C, under rotation. Membranes were washed three times with TBS 1X-Tween 0.05% for 5 min, at room temperature under agitation. Secondary antibodies, coupled with fluorescent dyes (Table 3), were diluted 1:10.000 in blocking solution and incubated with membranes for 1 h at room temperature under agitation, in the dark. Three washes of 5 min with TBS 1X-Tween 0.05% were performed at room temperature before detection of fluorescent secondary antibodies, using the Odyssey® CLx system. Images were analysed using the Image Studio Lite Version 5.2 software.

Pre-casted gels from BioRad were activated with UV lights, on the ChemiDoc MP Imaging System *prior to* their transfer on nitrocellulose membranes. This step allows the detection of total proteins, to later control the efficiency of transfer (i.e replaces the Ponceau staining). Nitrocellulose membranes and transfer buffers were provided by the manufacturer. Transfers were performed using the Trans-Blot Turbo Transfer System (BioRad), according to the manufacturer's instructions. Antibody incubations were performed as described above and fluorescent detection of secondary antibodies was performed using the ChemiDoc MP Imaging System.

IV.4 Protein purifications

IV.4.a Ran proteins

RanQ69L, used for NFAT assays, was expressed, purified and loaded with GTP by C. Spillner following the protocol described in (Melchior et al. 1995).

The short version of Ran, RanQ69L $^{1-180}$, was truncated at the C-terminal part, to enhance the GTP bound form of Ran (Nilsson et al. 2002). This truncated version of Ran was used for anisotropy assays. RanQ69L $^{1-180}$ was expressed, purified and loaded with GTP by M. Hamed, following the protocol described in (Monecke et al. 2009).

IV.4.b Protein expression

E. coli BL21 (DE3) strains were transformed with DNA constructs coding for the protein of interest and plated on LB medium plates containing ampicillin. The day after, one colony was picked and incubated into 100 mL of 2YT medium supplemented with 100 µg/mL of ampicillin, overnight at 37 °C, 150 rpm. Protein expressions were performed in 5 L flasks with (CRM1 expression), or without baffles (TP expression). 1 L of 2YT medium, supplemented with 100 µg/mL of ampicillin was added per flask. 10 mL of the starter culture suspension was added *per* flask and incubated at 37 °C, 110 rpm. When an OD of 0.5 was reached, bacterial suspensions were moved to 18 °C and protein expressions were induced by the addition of 100 µM of IPTG per litre of medium, overnight at 110 rpm. The day after, cells were collected by centrifugation at 4200 g, for 20 min at 4 °C. Bacterial pellets were washed once with 1x PBS and stored at -80 °C until purification.

IV.4.c Purification of CRM1

The vector containing the construct coding for the codon optimized *Homo sapiens* CRM1 wild type was provided by Prof. Dr. R. Ficner. Mutants used in our study were generated using the construct #1979 as a template (Table 6). Expression (as described above) and purification of these constructs were performed following an adapted protocol optimized by A. Shaikqasem (lab of Prof. Dr. R. Ficner). In total, 2 L of medium for CRM1 wild type and CRM1 C528S and 6 L of medium for CRM1 W142A P143A C528S were used for expression for one set of purification.

For CRM1 purification, each pellet was re-suspended with 35 mL of CRM1 lysis buffer (freshly supplemented with 1 mM of PMSF, AP and LP). Bacterial lysis was performed using an Emusiflex-C3 and lysates were cleared at 30.000 g for 45 min, at 4 °C. Nickel beads were equilibrated in CRM1 lysis buffer and incubated with supernatants for 90 min at 4 °C, on a rotation wheel.

Beads were washed three times with CRM1 lysis buffer, until no protein were detectable in supernatants. Beads were transferred into empty columns (BioRad) pre-equilibrated with CRM1 lysis buffer and proteins were eluted with CRM1 elution buffer (freshly supplemented with 1 mM PMSF, AP and LP). Eluted proteins were changed into desalting buffer (freshly supplemented with 2 mM DTT) using PD-10 desalting columns.

Protein solutions were filter with 0.2 µm filters before their loading to a MonoQ anion exchange column, equilibrated with desalting buffer. Elution was performed by increasing salt concentrations (gradient from 0 to 250 nM) of high salt buffer (freshly supplemented with 2 mM DTT). 10 µL of each peak fractions were loaded on an acrylamide gel and fractions containing CRM1 were pooled. Finally, the buffer was exchanged to 1x TPB containing 1 mM of DTT, using PD-10 desalting columns and proteins were concentrated using Amicon Ultra UltraCel-50K filters, aliquoted, snap-frozen in liquid nitrogen and stored at -80 °C.

IV.4.d Purification of Terminal Protein

For purification of TP, each bacterial pellet was re-suspended in 35 mL of GST buffer supplemented with 0.1% of Triton (and freshly supplemented with 1 mM DTT, AP and LP). Bacterial lysis was performed using an Emusiflex-C3 (Avestin) and lysates were cleared by centrifugation at 30.000 g for 45 min, at 4 °C.

Glutathione beads (glutathione sepharose 4 fast flow) were equilibrated in GST buffer and incubated with supernatants for 2 h at 4 °C, on a rotation wheel. Beads were washed three times with GST buffer and transferred into an empty column. Elution of GST-TP protein was performed by the addition of GST buffer supplemented with 15 mM of glutathione. Eluted proteins were concentrated with Corning ® Spin-X® UF concentrators 30K and changed into GST buffer, without glutathione, using PD-10 desalting columns. GST-TP were aliquoted, snap-frozen in liquid nitrogen before and stored at -80 °C.

IV.5 Antibodies purification

IV.5.a CRM1 antibody

The anti-CRM1 antibodies were purified from goat serum that has previously been obtained by Dr. S. Roloff. The goat had been immunized with the C-terminal peptide of CRM1 “GIFNPHEIPEEMCD” coupled to keyhole limpet hemocyanin (KLH) (Kehlenbach et al. 1998). 30 mL of goat serum was used for the purification of anti-CRM1 antibodies. 1 mg of recombinant His-CRM1 (purified by C.Spillner) was dialyzed against 0.2 M $NaHCO_3$, pH 8.9 overnight at 4 °C, using a Slide-A-Lyzer™ Dialysis Cassettes, 20K MWCO, 3 mL. The day after, the dialysis buffer was replaced with fresh 0.2 M $NaHCO_3$, pH 8.9 and incubated for 2 h at 4 °C.

This washing step was repeated once. 0.75 g of Cyanogen Bromide activated sepharose 4B beads (CNBr beads) were swelled in 3 mL of 1 mM HCl for 10 min. The CNBr beads were washed twice with 0.2 M $NaHCO_3$, pH 8.9, with 2 min of centrifugation at 200 g between each washing step. Dialysed His-CRM1 was added to the beads. The volume of the incubation solution was filled up to 15 mL with addition of 0.2 M $NaHCO_3$, pH 8.9. The mix containing His-CRM1 with the beads was incubated overnight at 4 °C, on a rotation wheel. The day after, beads were collected and washed twice with 15 mL of 0.2 M $NaHCO_3$, pH 8.9. The beads were then incubated under rotation for 1 h at room temperature with 100 mM Ethanolamine diluted into 0.2 M $NaHCO_3$, pH 8.9. After 1 h, three washes were performed with 0.2 M $NaHCO_3$, pH 8.9 and one wash with 0.5 M of NaCl diluted into 1x PBS. The serum was diluted 1:1 with 1x PBS and filtered through 0.2 µm filter. The filtered serum was added to the beads and incubated overnight at 4 °C, on a rotation wheel. The day after, beads were transferred into an empty column (BioRad) and washed with 0.5 M NaCl diluted with 1x PBS. The elution of antibodies was performed by the addition of 0.5 M NaCl diluted into 0.2 M acetic acid pH 2.5 and fractions of 500 µL were collected into tubes containing 100 µL of 1 M Tris pH 7.4. The presence of proteins was confirmed using the Pierce™ Coomassie Plus (Bradford) Assay Reagent and fractions containing proteins were pooled. The pool of eluted fractions was concentrated using centrifugal filter units (Corning® Spin-X® UF concentrators; 30K MWCO). The buffer was changed to 1x PBS, using PD-10 desalting column and glycerol was added to a final concentration of 50%. Purified antibodies were then tested by immunofluorescence and Western blotting, to determine the optimal concentration to be used.

IV.5.b TP antibody

TP antibodies were generated by Dr. D. Dacheux, hybridomas cloning was performed by Dr. H. Wodrich and antibodies were purified by Dr. B. Roger. TP antibodies were raised against the recombinant GST-TP purified in this study, in mice, following the protocol described in (Martinez et al. 2015). Hybridomas were cloned and amplified by limiting dilution. Culture supernatants were screened by immunofluorescence on infected cells and cells transfected for a construct coding for GFP-TP, as by Western blotting on recombinant GST-TP. Two clones were selected for their specificity and purified on Protein G- Sepharose beads. Briefly, 250 mL of hybridomas culture supernatant were cleared by centrifugation at 10 000g for 30 min at 4 °C. The purification was performed on an ÄKTA purifier, with a HiTrap Prot G High Performance column. The column was equilibrated with phosphate buffer and the cleared supernatant was loaded on the column. The elution was performed by the addition of glycine elution buffer, and collected in 500 µL fractions.

The pH was neutralised by the addition of 50 µL of neutralisation buffer *per* fraction. 5 µL of each fraction were loaded on an acrylamide gel and fractions containing TP antibodies were pooled. 10% glycerol was added before storage of purified antibodies at -20 °C.

IV.6 Anisotropy assay

Anisotropy assays (or polarization assays) were performed to measure the affinity of recombinant CRM1 for the PKI-NES. Recombinant CRM1 was purified in this study, RanQ69L $^{1\text{-}180}$ loaded with GTP was purified by M. Hamed and the PKI-NES fluorescent peptide (synthetized by EMC microcollections GmbH) was provided by Prof. Dr. R. Ficner. The excitation wavelength of the PKI-NES peptide was 470 nm and its emission wavelength was 520 nm. The entire assay was performed in anisotropy buffer (freshly supplemented with 0.005% digitonin and 2 mM DTT). 40 nM of PKI-NES fluorescent peptide was mixed with increasing concentrations of recombinant CRM1, with an excess of 3 µM of RanGTP (or 6 µM of RanGTP when the concentration of CRM1 was higher than 1 µM), in a final volume of 150 µL. Reactions were incubated at 25 °C for 30 min in the dark. Samples were gently mixed and transferred into a UV quartz cuvette. The ratio of polarized light emitted by the fluorophore related to the total light intensity was measured using the FluoroMax-4 spectrofluorometer.

V. Ad5 related experiments

V.1 Ad5 production

Ad5 replicative and non-replicative particles were used in this study. Both viruses were depleted for the E3 region. The E1A region in non-replicative viruses was replaced by a CMV driven GFP expression cassette. Viral particles were produced in Hek293 αVβ5 cells. These cells stably overexpress the AdV αVβ5 receptor and the E1 region to complement the deletion in Ad5 vectors. Cells were grown in five 15 cm diameter plates. When a confluence of 80 to 90% was reached, cells were infected with 10^9 particles *per* dish and incubated at 37 °C. After 48 to 96 h, when the cells started to detach, they were collected and pelleted by centrifugation at 3.500 g for 5 min at room temperature and re-suspended in 20 mL of fresh DMEM. Cells were frozen at -80 °C and three cycles of freeze/thaw (-80 °C/27 °C) were performed to break the cells and liberate virus particles. After the last cycle of freeze/thaw, cells were pelleted by 10 min of centrifugation at 3.500 g, at room temperature and the supernatant containing viruses was kept. Ad5 amplification was then performed on twenty 15 cm diameter plates seeded with Hek293 αVβ5 cells. 1 mL of the supernatant containing Ad5 particles was added *per* plates and cells were incubated at 37 °C for 48 to 96 h, until cellular detachment. Cells were collected and pelleted by centrifugation at 3.500 g for 5 min at room temperature and re-suspended in 40 mL of fresh DMEM.

A second step of three cycles of freeze/thaw was performed and cells were centrifuged for 10 min at 3.500 g, at room temperature. The supernatant was frozen at -80 °C and kept for further Ad5 purification.

V.2 Ad5 purification

Ad5 were purified using a cesium chloride (CsCl) step gradient followed by a continious gradient, using ultracentrifugation. Three solutions of CsCl were freshly prepared in 50 mM of Tris pH 8.1 and 150 mM of NaCl; 1.25 g/mL, 1.40 g/mL and 1.34 g/mL. The first step gradient was carefully prepared by overlaying 2 mL of the CsCl solution at 1.40 g/mL with 2 mL of the 1.25 g/mL solution, into a polypropylene tube.

Three tubes in total were prepared to purify approximatively 20 mL supernatant containing Ad5 particles. 8 mL of the supernatant were then added *per* tube, and centrifuged at 35.000 rpm for 2 h at 18 °C, using a SW41 rotor. After centrifugation, virus particles were accumulated between the two CsCl fractions. Two bands could be distinguished: the thinner one on the top was containing empty capsids and the thicker one below was containing Ad5 particles. Viruses were collected in a syringe by perforation of the tubes using a 21 G needle and aspiration of the thicker band. Viruses collected from three gradients were pooled and transferred into a new polypropylene tube. Approximatively 12 mL of the solution at 1.34 g/mL of CsCl was added to viruses, to fill the tube and a second centrifugation at 35.000 rpm was performed, for 18 h at 18 °C. During this time a, continuous gradient formed and the virus band concentrated at its density. The lower band was collected as before using a syringe, and transferred into a Slide-A-Lyzer™ Dialysis Cassettes, 10K MWCO, 3 mL, pre-hydrated with 1x PBS. Viruses were dialysed against 1x PBS, two times for 2 and 3 h to remove the CsCl. A last dialysis was performed overnight against 1x PBS supplemented with 10% of glycerol. The day after, viruses were collected, aliquoted and stored at -80 °C.

V.3 Ad5 quantification

The number of physical Ad5 particles was quantified by OD measurements, following the protocol described in (Mittereder et al. 1996). Ad5 capsids were disrupted in an Ad5 lysis buffer, to release the vDNA and the OD_{260} was measured. 10 µL of -pure or diluted- purified particles solution were lysed in 90 µL of Ad5 lysis buffer and incubated for 10 min at 56 °C. The OD_{260} was then measured and the number of physical particles (pp) was determined using the equation 1 OD_{260} = 1.16×10^{12} physical particles/mL.

The number of infectious particles was determined by plaque assays. 10^6 Hek293 αVβ5 cells were seeded *per* well in 2 mL of DMEM, in a 6 well plate. The day after, when ~90% of confluence was reached, cells were infected overnight with 1, 0.1 or 0.01 estimated physical particles *per* cell (determined by OD_{260}, see above) and incubated at 37 °C. Cells were then washed once with 1x PBS and 2 mL of DMEM containing 1% of agarose (Stock solution 4%) were added *per* well, to form a layer preventing Ad5 dissemination.

Once the layer was solidified, cells were incubated at 37 °C for several days until the formation of lysis plaques could be observed and quantified by microscopy. One lysis plaque was considered as one Ad5 particle. Thus, the number of infectious particles contained in the stock solution can be determined by the average of each dilution condition.

V.4 Ad5 labelling

Ad5 particles were fluorescently labelled using micro-scale protein labelling kits, using Alexa 488 and Alexa 594 dyes. Alexa dyes were freshly re-suspended with 10 µL of DMSO. 100 µL of purified Ad5 (containing approximatively 10^9 pp/µL, purified as detail above) were mixed with 12 µL of 1 M Na-bicarbonate buffer pH 8.3 (provided in the kit) and 2 µL of the desired dye. The mix reaction was incubated for 15 min in the dark, on a roll-incubator at room temperature. A BioRad Micro Bio-Spin™ 6 column (provided in the kit) was equilibrated with 1x PBS supplemented with 10 % of glycerol. After incubation, the reaction mix was loaded on the column and centrifuged at full speed for 2 min, to remove the excess of dye. The flow through was collected, aliquoted and stored at – 80 °C.

V.5 Ad5 infections

V.5.a Synchronous infections

$0.8x10^5$ U2OS cells were seeded on coverslips, in 12 well plates. The day after, $1.5x10^5$ cells *per* well were considered for the infection. Infections were performed by the addition of 3.000 pp/cell, *per* 100 µl. Cells were washed once with 1x PBS and the coverslips were placed in a humidity chamber. Ad5 particles were diluted in pre-warmed DMEM and 100 µL of the solution was added to the cells for 30 min at 37 °C, to keep the microtubule network intact. The medium was then removed and the coverslips were placed back to their initial well on the 12 well plate, containing 1 mL of fresh warm DMEM. This was considered at the time point zero of the infection, to analyse the particles that entered synchronously to the cells. This step was performed to synchronize infections. Cells were incubated at 37 °C and fixed at different time point.

Infections of mitotic cells (see section II.7 Synchronisation of cells in mitosis) were performed using the same protocol, except for the synchronisation of infections. The 30 min of incubation were performed at 4 °C, to avoid re-polymerization of microtubules. Cells were then incubated in 1 mL of fresh DMEM at 37 °C.

V.6.b Infection of enucleated cells

After enucleation of cells (see section II.8 Enucleation of cells), they were incubated in DMEM for at least 90 min at 37 °C before Ad5 infection. Cells were infected with 3.000 pp/cell of Alexa 488 labelled Ad5 particles in a total volume of 500 µL of DMEM for 30 min, at 37 °C. The medium was then removed and replaced with 1 mL of fresh DMEM. Cells were incubated for 2 h at 37 °C, washed three times with 1x PBS before fixation with 500 µL of 4% PFA in 1x PBS.

V.6.c Infection for live-cell imaging analysis

Mitotic cells were grown on imaging ibidi µ-slides (see section II.11 Seeding cells for live cell imaging). DMEM was replaced by a medium suitable for live cell-imaging, a CO_2-independent medium supplemented with 4 mM Glutamax and 10% FCS. Infections were performed in this medium, in the presence or absence of LMB, depending on the conditions. Approximatively 3.000 pp/cell were added to the cells, in a total volume of 500 µL. Cells were kept at 37 °C and directly imaged, without removal of the inoculum (asynchronous infections).

VI. Data analyses

VI.1 Image acquisition

VI.1.a Fixed cells imaging

IF samples were imaged using fluorescence microscopes, either using a Leica DMI6000 B microscope equipped with the MetaMorph software or a Nikon Eclipse Ti2 inverted microscope, equipped with the NIS-Elements AR 5.02. One stack section was taken *per* image.

Confocal imaging was performed at the Bordeaux Imaging Center (BIC), using a Leica DM6 CFS TCS SP8 equipped with the Leica LAS-X software. The pinhole was set to 1 and samples were imaged every 0.3 µm, with a total of 10 stacks for image analysing. Images were acquired with a resolution of 16 bits and a pixel size of 80 nm. Images were analysed with the software Image J.

VI.1.b Live cell imaging

Live cell imaging was performed with the help of Dr. H. Wodrich on a Spinning-disk LIFA microscope (Leica) equipped with a heating chamber and an EMCCD camera Photometrics Quantum 512. The MetaMorph software was used. Seven stacks of 0.3 µm were taken every 5 sec for each channel using a 100X objective.

VI.2 Image quantification

Quantifications of the number of pVII, Ad5 capsids or E1A dots were performed using the Image J software. Channels were splitted and analyses were performed on Z-projections of 10 stacks. Cell periphery was first determined by drawing manually the outline. A threshold was applied to every channel, to select signals of interest in each channel.

Objects exceeding a pixel size of 5 were considered as positive for Ad5 capsids and E1A channels, but a minimal pixel size of 10 was determined for pVII signals. A minimal pixel size of 500 was determined to identify nuclei. These settings automatically created a “mask” with all the positive signals identified. A semi-automated macro was developed to automatize quantifications of these positive signals. For colocalization analyses, signals obtained in two different masks were superposed and structures with at least 5 pixels in common were considered as positive.

For Western blot analysis, signal quantifications were performed using the Image Studio Lite Version 5.2 software and results were represented as the mean of the ratio of HA signals, normalised to the level of tubulin (+/- standard deviation (SD)), in arbitrary units.

VI.3 Statistical analyses

Statistical analyses were performed using the Graph Pad Prism 7 software. Image quantifications were performed on 30 cells *per* condition. Results of quantifications were represented as scatter plot with the mean values +/-SD. Statistical analyses were performed using one-way ANOVA test. For cell growth analysis, the total number of cells was plotted on the graph and statistical analyses were performed using two-way ANOVA test.

Multi-comparison post-hoc tests were performed to compare the groups between themselves. Sidak’s post-hoc test was used after one-way ANOVA tests whereas Tukey’s post-hoc test was used after two-way ANOVA tests. Multi-comparison post-hoc test results were indicated on the graphs with the following nomenclature: ns: non-significant; *: P< 0.05; **: P< 0.01; ***: P< 0.001; ****: P< 0.0001.

RESULTS

I. At the MTOC, CRM1 is required for genome delivery

After cell entry and endosomal escape, Ad5 needs to traffic towards the nucleus to ultimately import its genome. To reach the nuclear vicinity, Ad5 requires intact microtubules and motor proteins from the cytoskeleton retrograde transport machinery (Suomalainen et al. 1999; Leopold et al. 2000; Kelkar et al. 2004). This interaction is well characterized and involves direct interactions between Ad5-hexon protein and dynein (Smith et al. 2008; Bremner et al. 2009). Several studies in A549, TC7 or HeLa cells showed that *prior to* nuclear targeting, Ad5 localizes at the MTOC area (Suomalainen et al. 1999; Leopold et al. 2000; Wang et al. 2017) Kinesin 1 knockdown or LMB treatment have been shown to arrest Ad5 at the MTOC, producing a nuclear transport block that impairs Ad5 genome import (Zhou et al. 2018; Strunze et al. 2005). Although Ad5 capsid transport along microtubules after endosomal escape is well established, removal from microtubules and NPC translocation mechanisms remain unclear. Using U2OS cells, we investigated the implication of CRM1 in these two processes. To discriminate between the different steps of infection, we used enucleated cells and synchronised mitotic U2OS cells.

I.1 Role of CRM1 in Ad5-MTOC removal

Previous studies performed with AdV types 2 or 5 in different cell lines pointed to an active transport of capsids ending at the (-) end of microtubules, i.e. to the MTOC (Suomalainen et al. 1999; Leopold et al. 2000; Strunze et al. 2005; Wang et al. 2017). There is no direct evidence if such a MTOC localization is required before nuclear targeting of every capsid or if their centrosomal localization represents a dead-end product. However, Ad5 capsids can be artificially blocked at the MTOC upon infection in enucleated cells (Bailey et al. 2003), following LMB treatment (Strunze et al. 2005) or Kinesin 1 deletion (Zhou et al. 2018). Furthermore, CRM1 was suggested to be required for Ad5 capsid MTOC removal (Strunze et al. 2005). To gain more insights into Ad5-MTOC interactions and the role of CRM1 in this MTOC removal, we performed infection assays in U2OS cells and analysed the Ad5 capsid localization.

I.1.a Ad5 are trafficking to the MTOC area in U2OS

We infected U2OS cells with Ad5 particles and analysed capsids distribution after 1 h of infection. As shown in Figure 10, Ad5 capsids were spread throughout the cytoplasm, but enrichment in proximity to pericentrin was observed for most of the capsids. Such staining, with capsids enrichment at the MTOC was observed in every infected cell.

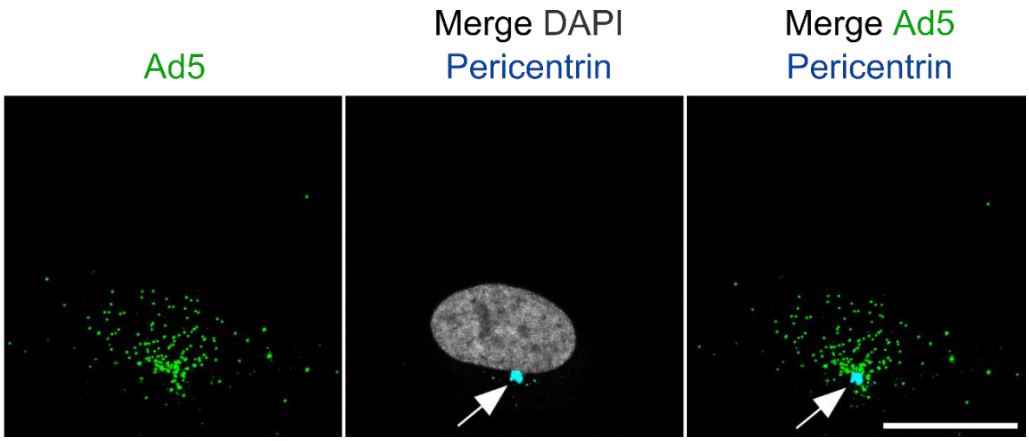

Figure 10. Ad5 capsids traffic to the MTOC area. U2OS cells were infected with Alexa 488 labelled Ad5-GFP particles for 1 h. Cells were fixed and stained with anti-pericentrin (cyan) and DAPI (grey) for chromatin staining. Cells were imaged by confocal microscopy and maximal projection images are shown. Pericentrin position is indicated by the white arrow. (Scale bar, 20 µm).

It is not clear whether every new entering particle requires to pass by the MTOC before nuclear targeting. To further investigate Ad5 capsids MTOC localization, we performed a double Ad5 infection with two subsequent waves of differently labelled viruses (Figure 11), to analyse if after a first wave of infection, new particles can be visualized as well at the MTOC. U2OS cells were first infected with Alexa 488 Ad5-GFP particles and 1 h later, the same cells were infected with Alexa 594 Ad5-GFP particles.

Both labelled viruses were found in proximity of the MTOC area. These results suggested that the microtubule transport machinery used by viruses from the first wave of infection was not rate limiting and could be used by viruses from the second wave of infection. Our microscopy imaging analyses thus favour a dynamic transport of Ad5 towards the MTOC, in order to reach the nucleus, in U2OS cells.

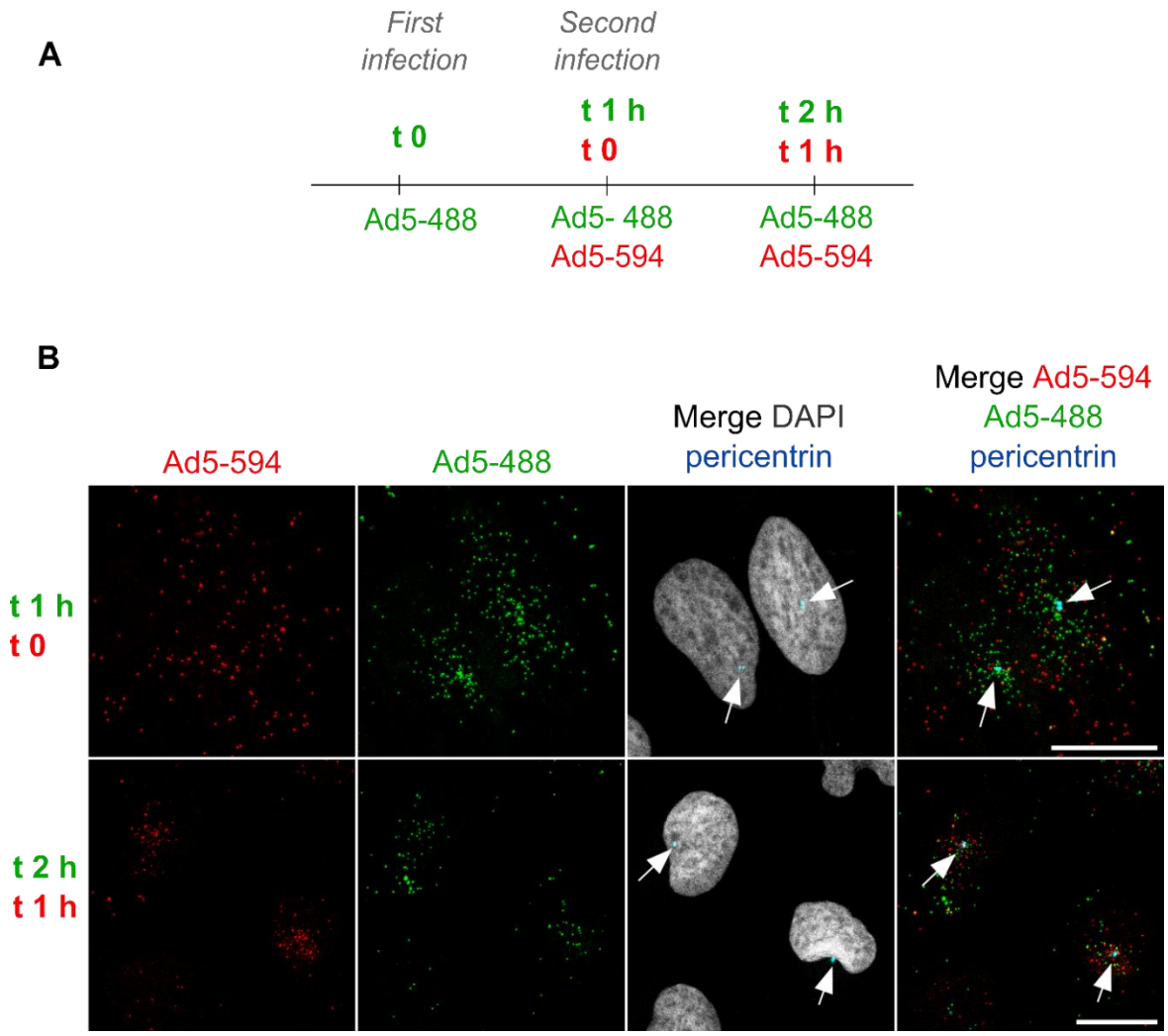

Figure 11. Ad5 capsids are able to reach the MTOC area even after asynchronous infections. U2OS cells were infected with Alexa 488 labelled Ad5-GFP particles and after 1 h, a second infection with Alexa 594 labelled Ad5-GFP particles was performed. Chromatin was stained using DAPI (grey). (A) Timeline of the experiment. (B) Top row: Alexa 488 Ad5-GFP 1 h pi; Alexa 594 Ad5-GFP t0. Bottom row: Alexa 488 Ad5-GFP 2 h pi; Alexa 594 Ad5-GFP 1 h pi. Cells were imaged by confocal microscopy and maximal projection images are shown. Pericentrin positions indicating the MTOC are shown with white arrows. (Scale bars, 20 µm).

I.1.b Ad5 do not require nuclear factors to reach the MTOC

After endosomal escape, free Ad5 capsids traffic on microtubules in the cytoplasm (Leopold et al. 2000; Bremner et al. 2009; Montespan et al. 2017). These first steps during Ad5 infection are cytosolic events and do not involve apparent nuclear factors. Previous studies in A549 cells (Bailey et al. 2003) showed Ad5 capsids accumulation at the MTOC after infection of enucleated cells. In this assay, nuclei were removed by Cytochalasin B treatment and high-speed centrifugation, followed by Ad5 infection.

In the absence of nuclei, Ad5 capsids accumulated at the MTOC, compared to a more spread distribution in cells with a remaining nucleus. We adapted this enucleation experiment to U2OS cells and analysed Ad5 capsids localization (Figure 12).

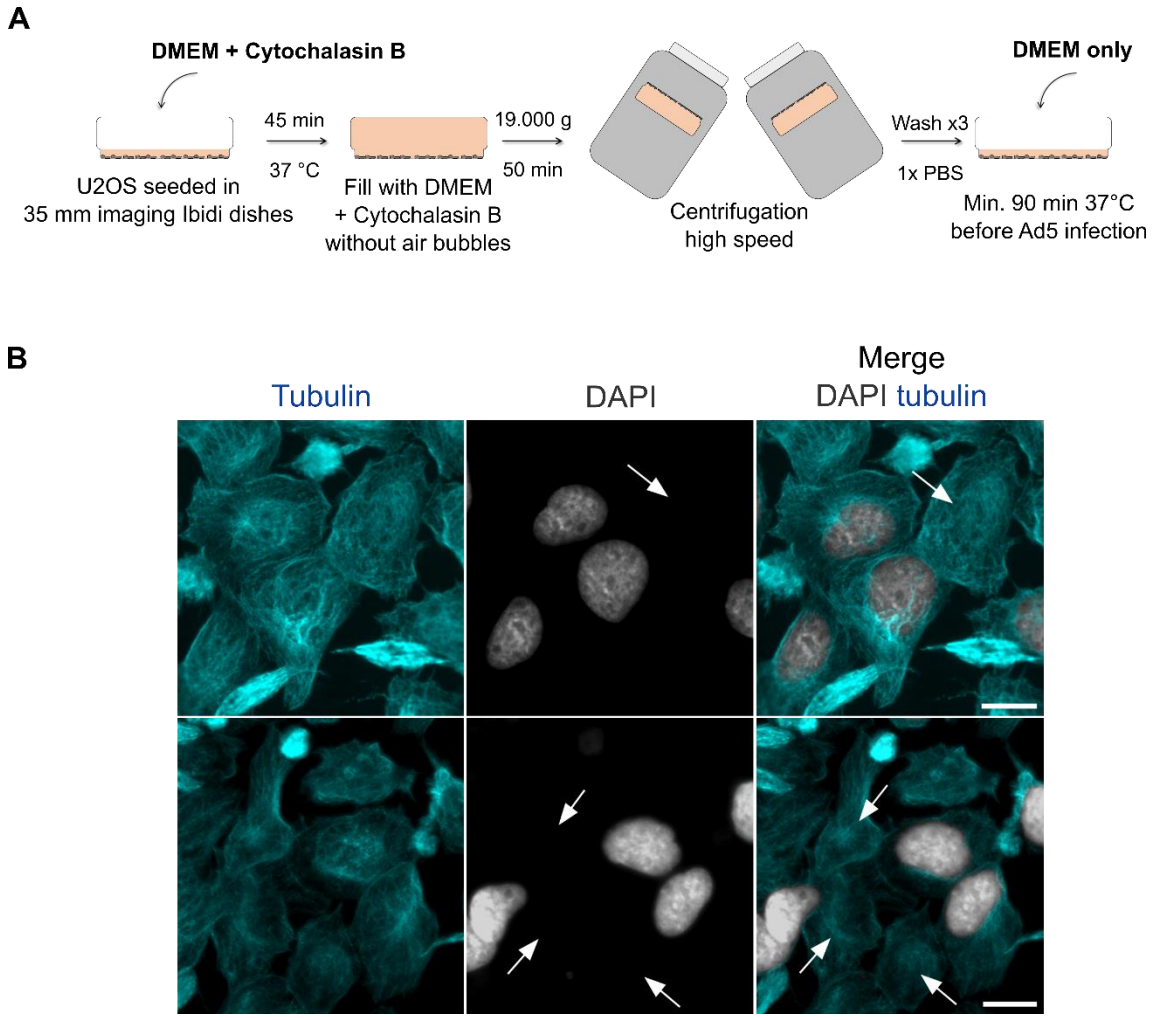

Figure 12. Enucleation of U2OS cells. Enucleation of U2OS was performed by Cytochalasin B treatment followed by centrifugation. (A) Scheme of enucleation protocol. (B) After enucleation, U2OS cells were fixed and stained with anti-tubulin (cyan) to control their global shape and DAPI (grey) to identify remaining nuclei. Cells without a nucleus are pointed with white filled arrows. Cells were imaged by fluorescence microscopy and one plane is shown. (Scale bars, 50 µm).

Cytochalasin B treatment induces actin filaments depolymerization, removing some of the cellular scaffold and lowering viscosity of the cytoplasm within the cell (MacLean-Fletcher and Pollard 1980). Under this condition, nuclei are no longer strongly supported by the cytoskeleton. After Cytochalasin B treatment, cells grown on small dishes (35 mm² ibidi) were centrifuged upside down, with cells on the top. The absence of air bubbles is one of the crucial step before centrifugation, as cells need to be in contact with medium to avoid drying.

Nuclei were mechanically removed by high speed centrifugation. Cells were then washed and incubated for at least 90 min with DMEM before any further analysis. We used live cell imaging to control the membrane permeability. Fluorescently labelled antibodies were not able to enter the cells, demonstrating that they remained intact under these conditions (data not shown). The efficiency of enucleation was about 50%. Intact cells with a remaining nucleus in the same sample were used as controls.

As shown on microscopy images (Figure 12; Figure 13 A), the microtubule network in enucleated cells was comparable to control cells: tubulin filaments can be detected. Integrity of microtubules is required for Ad5 infection (Leopold et al. 2000). Nuclear factors such as CRM1 were removed beyond the detection limit in cells lacking their nucleus. Cytochalasin B treatment did not change the apparent tubulin organisation and did not induce leakage of CRM1 into the cytoplasm.

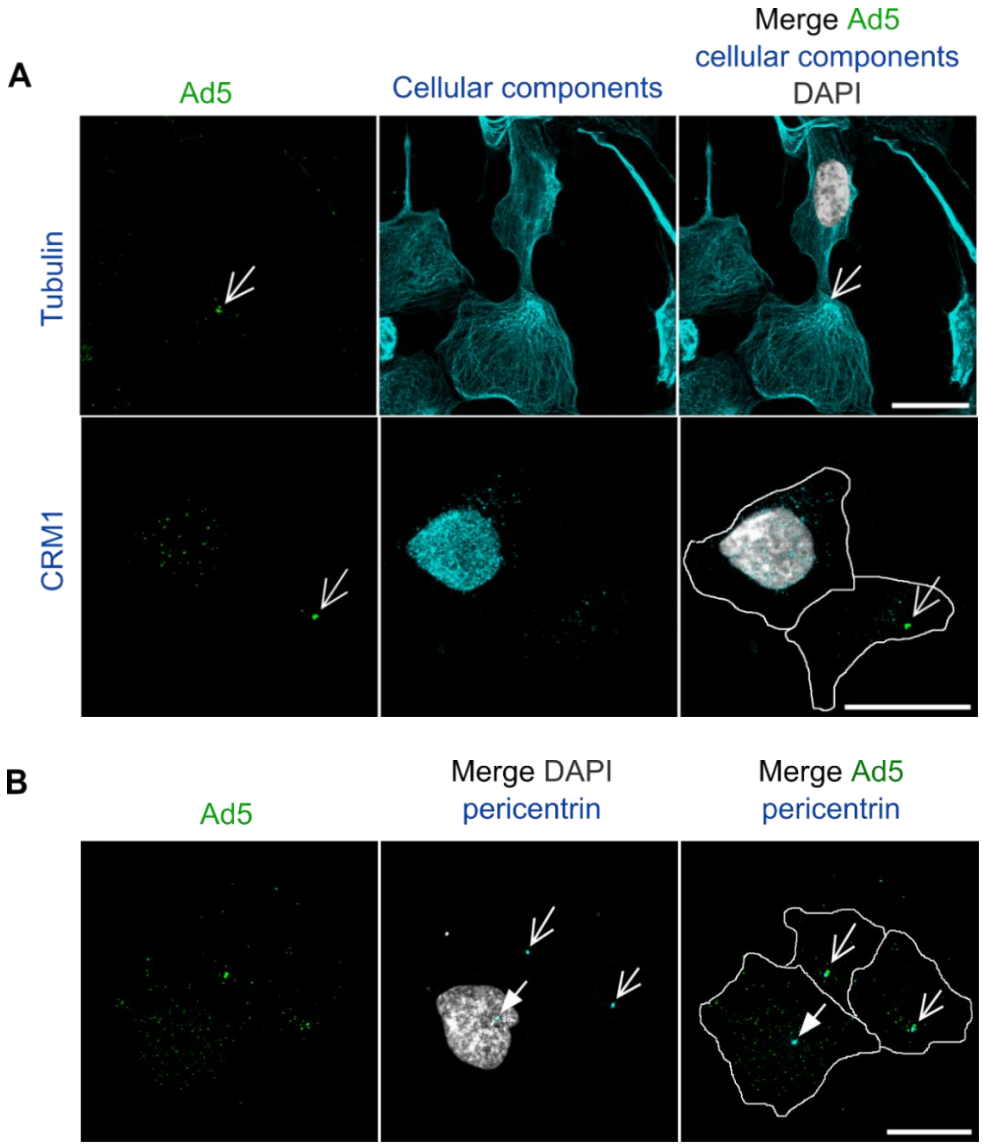

Figure 13. Ad5 do not require nuclear factors to reach the MTOC. (previous page) Enucleated U2OS cells were infected for 2 h with Alexa 488 labelled Ad5-GFP particles, fixed and stained for different cellular components (cyan): anti-tubulin and anti-CRM1 (A) as anti-pericentrin (B) antibodies were used. DAPI staining (grey) is used to identify remaining nuclei. The cell periphery was manually drawn after increasing the contrast of the Ad5-channel image in the Image J software. Pericentrin staining in cells with a remaining nucleus are shown with filled white arrows. Ad5 accumulation (A) or pericentrin staining (B) in enucleated cells are shown with empty white arrows. Cells were imaged by confocal microscopy and maximal projection images are shown. (Scale bars, 20 µm).

After establishing the enucleation protocol, we infected cells with fluorescently-labelled Ad5 particles. In nuclei-containing control cells, Ad5 capsids were evenly distributed within the cytoplasm whereas they strongly colocalized with pericentrin in enucleated cells (Figure 13 B). Thus, following Ad5 cell entry, trafficking on microtubules toward the MTOC does not require nuclear factors. Our analyses were done up to 2 h pi but previous studies, (Bailey et al. 2003) performed infections of A549 enucleated cells up to 10 h pi and Ad5 MTOC accumulation was still detectable. This interaction is quite stable overtime. The strong stability of Ad5 MTOC accumulation in cells without nuclei indicates that nuclear factors are not required for MTOC arrival, but rather suggests that they are required for MTOC removal.

I.1.c Blocking of CRM1 with Leptomycin B leads to Ad5 MTOC accumulation

Upon LMB treatment of cells, Ad5 infection leads to MTOC accumulation of viruses (Strunze et al. 2005). Previous observations suggest that blocking CRM1 retains Ad5 on microtubules and that uncoupling is prevented (Wang et al. 2017). In order to further study the role of CRM1, we repeated this assay in our model U2OS cells.

Cells were pre-incubated with 20 nM of LMB and infected with Ad5 in the continued presence of LMB. RanBP1, a known cargo of CRM1, was used as a control for the LMB effect: nuclear retention of RanBP1 was observed upon LMB treatment (Figure 14 A). Moreover, the localization of CRM1 was not impaired with LMB treatment, and CRM1 remained nuclear. Infected U2OS cells treated with LMB showed a strong accumulation of Ad5 capsids at the MTOC (Figure 14 A and B), marked by colocalization with pericentrin. These results confirm that Ad5 requires functional CRM1 to be removed from the MTOC. This accumulation induced by LMB treatment is quite stable, as it was still detectable 8 h pi (data not shown).

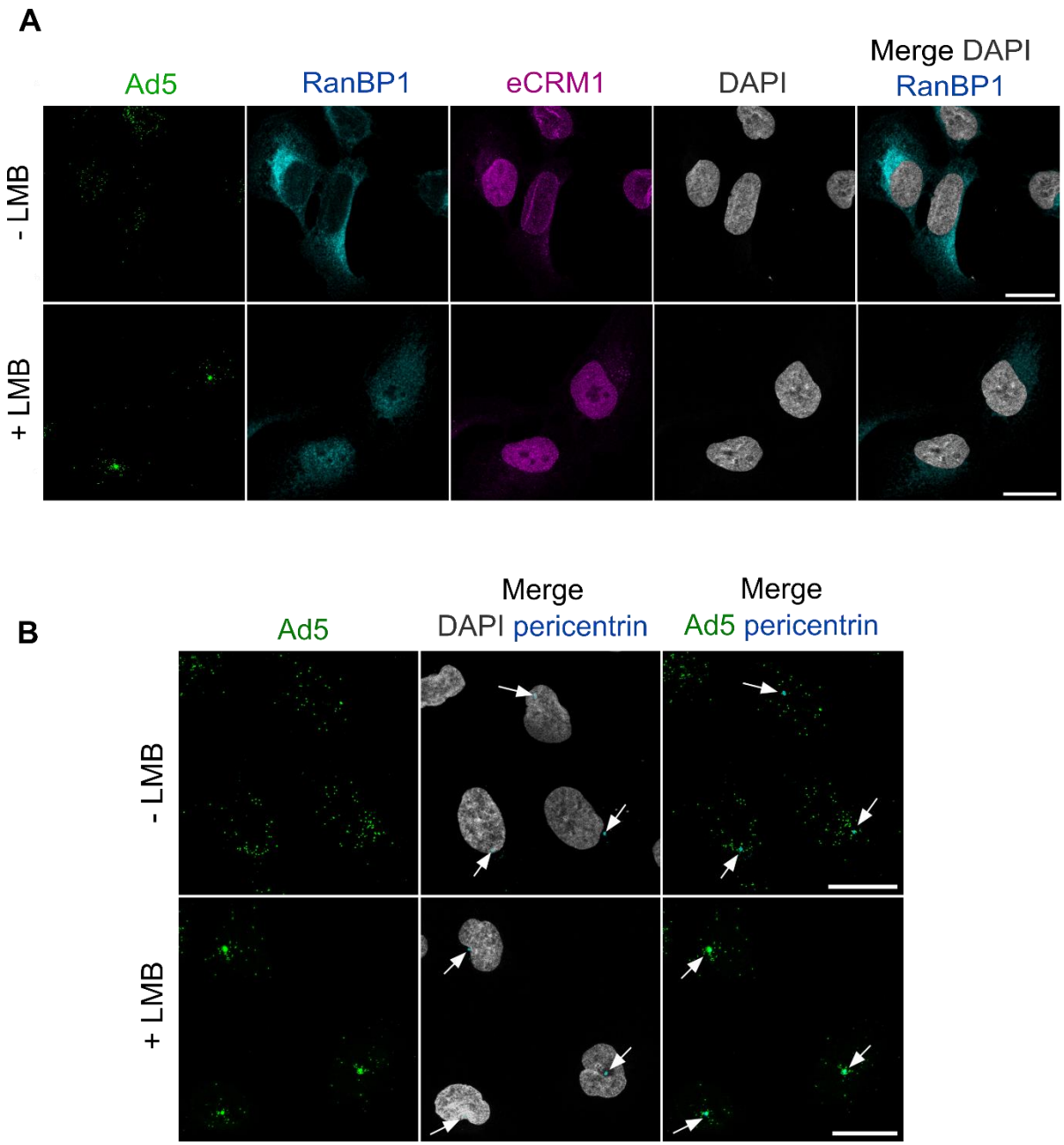

Figure 14. Blocking of CRM1 with Leptomycin B leads to Ad5-MTOC accumulation. U2OS cells were treated with (+ LMB) or without LMB (- LMB) for 45 min. Infections with Alexa 488 labelled Ad5-GFP particles were performed in the presence (+ LMB) or absence (-LMB) of LMB for 1 h. Cells were fixed and stained for different cellular components: RanBP1 (cyan) and CRM1 (magenta) (A), pericentrin (cyan) (B) and DAPI (grey) for chromatin staining. Pericentrin positions are shown with white arrows (B). Cells were imaged by confocal microscopy and maximal projection images are shown. (Scale bars, 20 µm).

I.1.d Association of Ad5 with MTOC is stable and independent of the integrity of microtubules

We previously showed that Ad5 reached the MTOC during the initial steps of infection. Enucleation or LMB treatment blocked Ad5 capsids at the MTOC (Figure 13 and Figure 14). While several studies showed that intact microtubules are required for Ad5 trafficking to reach the MTOC (Suomalainen et al. 1999; Leopold et al. 2000), the question if intact microtubules are still required once Ad5 reached the MTOC is poorly studied. In infected enucleated cells, Bailey et al. (Bailey et al. 2003) showed that depolymerization of microtubules via Nocodazole treatment disrupted Ad5-MTOC localization and pericentrin distribution. To address this question, we infected U2OS cells with Ad5, in the absence or presence of LMB, and microtubules were depolymerized after infection with cold treatment (Figure 15 A). Cold treatment is known to disrupt the microtubule network, by slowing down the addition of αβ-tubulin dimer, thus promoting depolymerization of microtubule filaments (Hoebeke et al. 1976).

In control cells (Figure 15 A a and c), tubulin staining showed filaments of polymerized microtubules. In cold-treated cells (Figure 15 B b and d), tubulin filaments were largely absent, indicating depolymerized microtubules. In both cases, with or without LMB, Ad5 capsids were still detectable at the MTOC after microtubules depolymerization.

We then analysed the requirement of soluble cytoplasmic components to maintain the association of Ad5 with the MTOC (Figure 15 B). U2OS cells were infected in the absence or presence of LMB and treated with digitonin to permeabilize the cells. In permeabilized cells, Ad5 capsids still accumulated at the MTOC, even without LMB treatment. The microtubule network was completely disrupted after digitonin treatment, but MTOCs remained intact, as indicated by pericentrin staining.

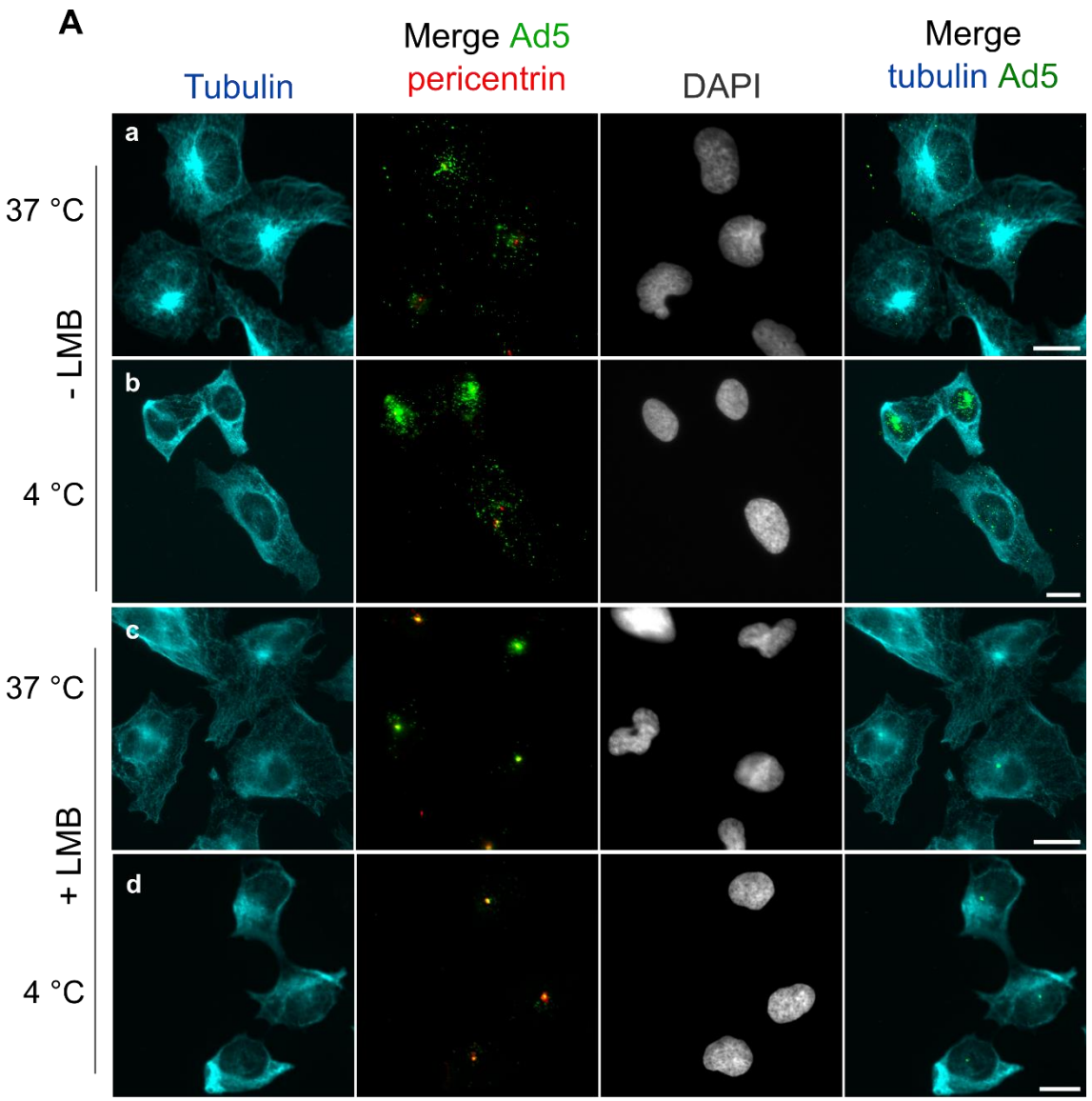
A
Tubulin
Merge Ad5 pericentrin
DAPI
Merge tubulin Ad5
a
b
c
d
37 °C
- LMB
4 °C
37 °C
+ LMB
4 °C

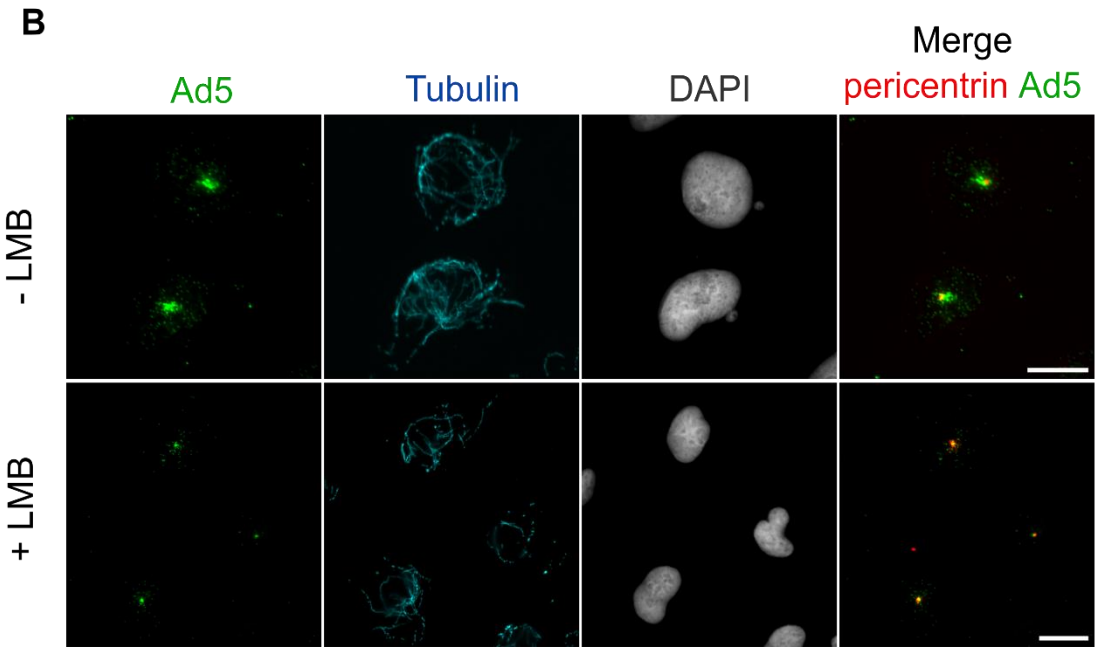
B
Ad5
Tubulin
DAPI
Merge pericentrin Ad5
- LMB
+ LMB

Figure 15. Ad5 capsids remain associated to the MTOC independently of microtubules integrity. (previous page) U2OS cells were treated with (+ LMB) or without LMB (- LMB) for 45 min. Infection with Alexa 488 labelled Ad5-GFP particles was performed in the presence (+ LMB) or absence (- LMB) of LMB for 2 h. (A) Microtubule depolymerization was induced by cold treatment (4 °C) for 30 min (b and d) and cells were compared to controls (a and c) where they stayed at 37 °C in DMEM. (B) After infection, cells were permeabilized with Digitonin for 5 min at 37 °C. (A and B) After fixation, cells were stained with anti-tubulin (cyan) and anti-pericentrin (red) antibodies and with DAPI (grey) for staining chromatin. Cells were imaged by fluorescence microscopy and one plane is shown. (Scale bars, 50 µm).

Our results suggested that polymerized microtubules are required for Ad5 to reach the MTOC, but association of Ad5 with MTOC does not rely on microtubules integrity. Moreover, after digitonin permeabilization, cells were washed three times before fixation. Despite absence of cytosolic components due to cell permeabilization, Ad5 stayed attach to the MTOC, suggesting a very stable interaction.

I.1.e Removal of Ad5 from MTOC depends on functional CRM1

As LMB treatment specifically impairs binding between CRM1 and NES containing cargo proteins, the blocking of Ad5 at the MTOC in the presence of LMB suggests that such interaction might be involved in Ad5-MTOC removal. We next performed a rescue experiment with a mutant of CRM1 insensitive to LMB. In this mutant, cysteine 528 (the target of LMB), was mutated to a serine, preventing binding of LMB to CRM1 (Fornerod et al. 1997b; Kudo et al. 1999). In cells overexpressing the HA tagged CRM1 C528S, export of RanBP1 was rescued (Figure 16), showing that this mutant was functional under LMB treatment. U2OS cells were infected with Ad5 upon LMB treatment (Figure 16 B). U2OS overexpressing the CRM1 C528S-HA construct did not accumulate Ad5 at their MTOC, compared to control cells. This result demonstrates that restoring CRM1 functionality with this mutation was sufficient to restore MTOC removal, hence CRM1 function is essential and sufficient for Ad5 MTOC removal. Such rescue of Ad5-MTOC removal, upon expression of the construct coding for CRM1 C528S in the presence of LMB was also observed by Wang et al. in 2017.

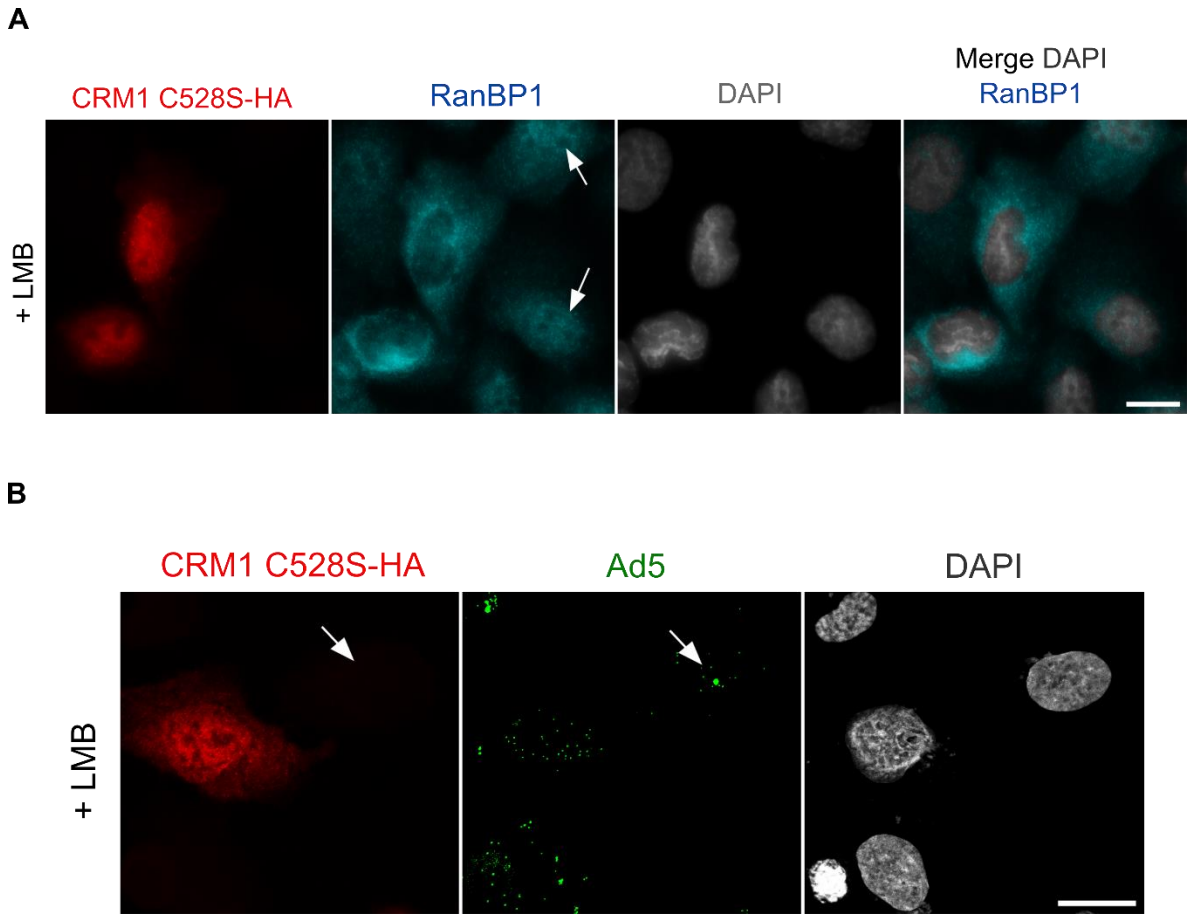

Figure 16. Removal of Ad5 from MTOC depends on functional CRM1. U2OS cells were transfected with CRM1 C528S-HA construct. 24 h post transfection cells were treated with LMB for 45 min. (A) Cells were fixed and stained with anti-RanBP1 (cyan) and anti-HA (red) antibodies as well as with DAPI (grey) for chromatin staining. Non-transfected cells with nuclear retention of RanBP1 are pointed with white filled arrows.(B) Cells were infected for 1 h in the presence of LMB with Ad5-GFP particles, fixed and stained with anti-HA (red) and anti-Ad5 capsids (green) antibodies, and a DAPI (grey) staining for chromatin. Non-transfected cells with accumulation of Ad5 at the MTOC are pointed with white filled arrows. Cells were imaged by fluorescence microscopy (A) or confocal microscopy (B). (Scale bars, 50 µm (A), 20 µm (B)).

Using our U2OS cell model, we confirmed previous results and established conditions for Ad5 MTOC accumulation. After endosomal escape, Ad5 traffics to reach the MTOC and this step does not require nuclear factors but needs intact microtubules. This step is likely a prerequisite for nuclear delivery of Ad5. In contrast, interaction with the MTOC itself is stable and microtubule integrity is not required. CRM1 is involved in the subsequent removal of Ad5 capsids from the MTOC. Blocking CRM1 with LMB induces accumulation of capsids at the MTOC and can be rescued with overexpression of an LMB insensitive CRM1 mutant.

I.2 Role of CRM1 in Ad5 genome nuclear import

After MTOC arrival, Ad5 capsids are translocated to the nucleus to dock at NPCs where they disintegrate and liberate their genomes for import. Ad5 NPC docking is mediated via an interaction between the hexon protein and Nup214 (Trotman et al. 2001; Cassany et al. 2015). Our groups recently showed that Nup358 is also involved in Ad5-NPC interactions, because Nup358 deletion leads to a delay in genome delivery (Carlon-Andres et al. 2020). Nup358 concentrates several transport factors at the cytoplasmic face of the NPCs (Hutten et al. 2008; Hutten et al. 2009; Wälde et al. 2012), which support Ad5 genome delivery. So far we showed that LMB treatment blocks Ad5-NPC translocation, revealing a role for CRM1 upstream of genome delivery (sections I.1.c Blocking of CRM1 with Leptomycin B leads to Ad5 MTOC accumulationand I.1.e Removal of Ad5 from MTOC depends on functional CRM1). However, nothing is known about the exact mechanism: does CRM1 interact directly with Ad5 or is the translocation mediated by one of the cargoes of CRM1? Using LMB treatments and mitotic cells as a model of infection, we performed infection experiments to better characterize the role of CRM1 after MTOC arrival.

I.2.a Ad5 genome detection: pVII as a tool to indirectly detect Ad5 genomes

Nuclear import through NPCs is restricted to cargoes with a maximum size of ~40 nm (Pante and Kann 2002). Ad5 capsids have a diameter of about ~90nm, exceeding the import size. Thus, capsid disassembly is required to release the genome before import. Ad5 genomes can be detected by antibody staining of genome associated protein VII, a core protein attached to the viral DNA (Komatsu et al. 2015). In intact Ad5 capsids, the genome is not exposed and cannot be detected via antibodies. However, when the capsid is partially disassembled (i.e at the NE edge), Ad5 genome is exposed and pVII becomes detectable by antibodies. As a schematic representation, in Figure 17, intact or partially disassembled capsids were detected by specific antibodies against capsids and Ad5 genomes via pVII antibodies. Colocalization events between Ad5 capsid and pVII signals were considered as disassembled capsids exposing genomes, whereas free pVII dots were considered as genome completely released from the capsid.

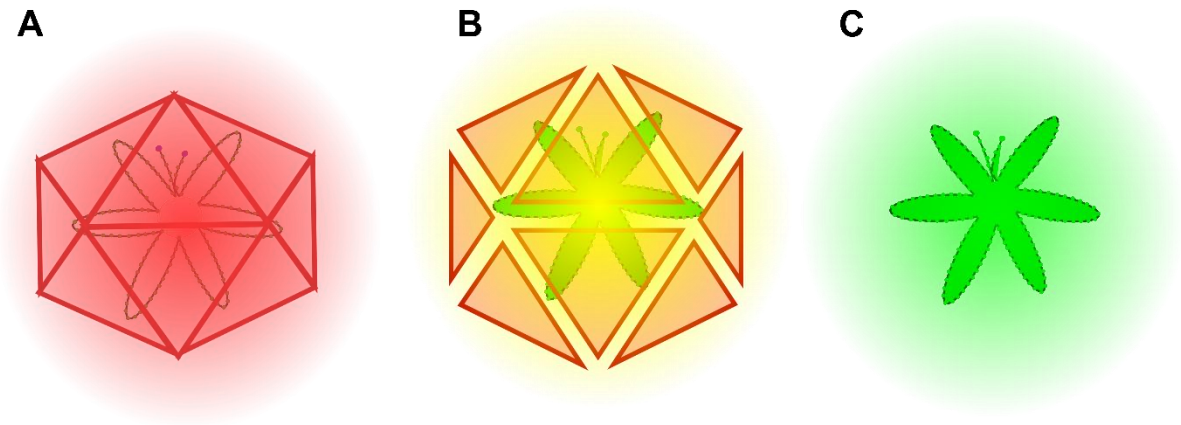

Figure 17. Types of signals observed upon the detection of Ad5 capsids and their associated genome by immunofluorescence. Intact (A) or partially disassembled (B) Ad5 capsids are depicted in red. Ad5 genome stained with pVII antibodies, partially exposed (B) or released from the capsid (C) are depicted in green. Signals for the partially disassembled Ad5 capsid and its exposed genome lead to colocalization events between the red and green channel, depicted in yellow signals.

For quantitative analyses, it was shown that one dot of pVII can be considered as one Ad5 infectious genome (Walkiewicz et al. 2009). To monitor Ad5 genome delivery overtime, we thus performed Ad5 infections and fixed the cells at different time points (Figure 18 A). In interphase cells, pVII was exclusively nuclear, since the disassembly of Ad5 takes place at the NE (Trotman et al. 2001). We next quantified genome import up to 4 h pi. Results showed that genome import started at 30 min pi, with a peak of imported genomes reached after 2 h pi (Figure 18 B). Capsid disassembly events could also be detected overtime (Figure 18 B, white arrows).

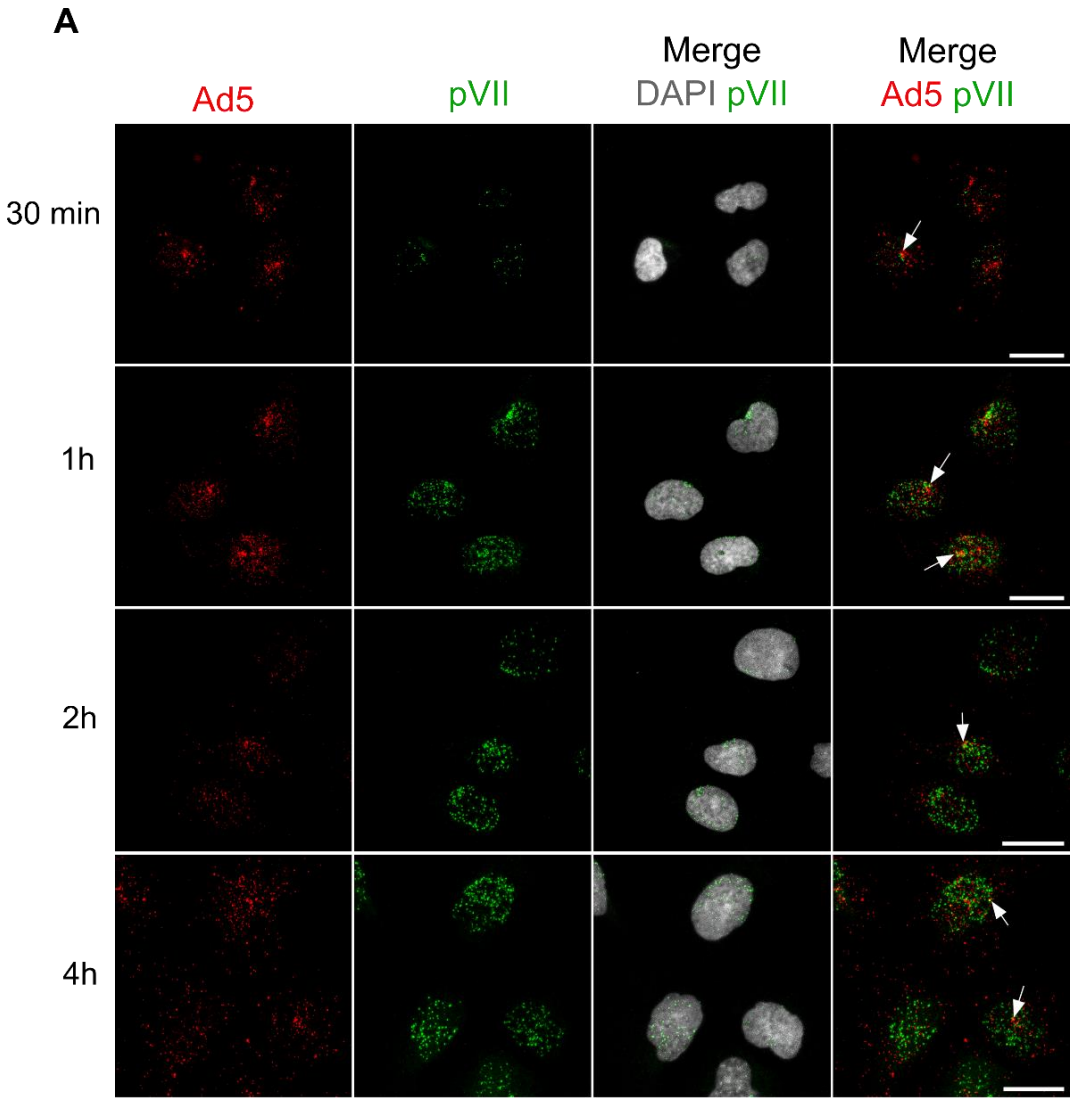
A
Ad5
pVII
Merge
DAPI pVII
Merge
Ad5 pVII
30 min
1h
2h
4h

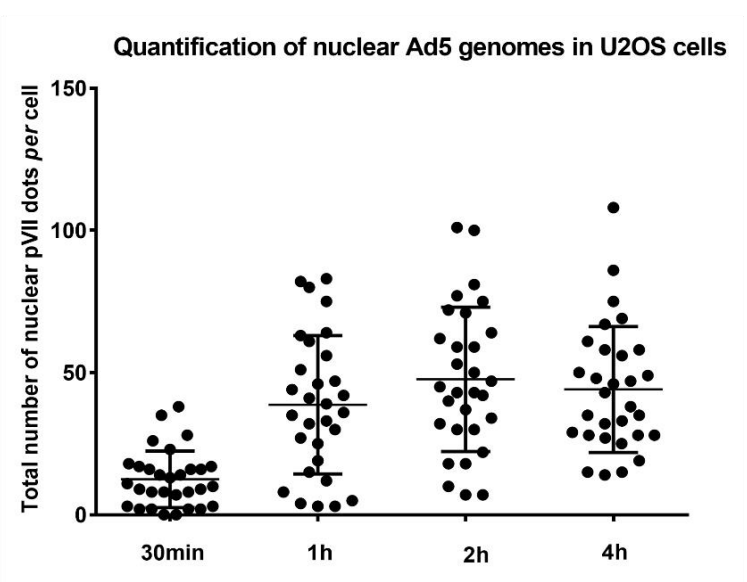
B
Quantification of nuclear Ad5 genomes in U2OS cells
Total number of nuclear pVII dots per cell
150
100
50
0
30min
1h
2h
4h

Figure 18. Kinetic of Ad5 genome nuclear import. (previous page) U2OS cells were infected with Ad5-GFP particles for 30 min up to 4 h. (A) Cells were fixed and stained with anti-Ad5 capsids (red) and anti-pVII (green) antibodies and with DAPI (grey) for chromatin staining. Colocalization events between Ad5 capsids and pVII are shown with white arrows. Cells were imaged by confocal microscopy and maximal projection images are shown. (Scale bars, 20 µm). (B) Scatter plot showing the quantification of the total number of pVII foci colocalizing with DAPI signal per cell (depicted in (A): Merge DAPI / pVII). Mean values (+/- SD) of 30 cells per condition are shown.

I.2.b Accumulation of Ad5 at the MTOC impairs Ad5 genome import

We previously showed a blocking of Ad5 at the MTOC upon LMB treatment, leading to a defect in NPC translocation (Figure 14). Blocking of this step is expected to have an impact on downstream events, i.e nuclear import of Ad5 genomes. To confirm this, we analysed the effect of CRM1 inhibition by LMB treatment on Ad5 genome import. We performed Ad5 infections in the presence of LMB and quantified the number of nuclear pVII dots (Figure 19). No signal for pVII was detectable upon infection with LMB, even after 4 h pi. Moreover, capsids trapped at the MTOC were intact, since no pVII signal was detectable neither in the nucleus nor at the MTOC area.

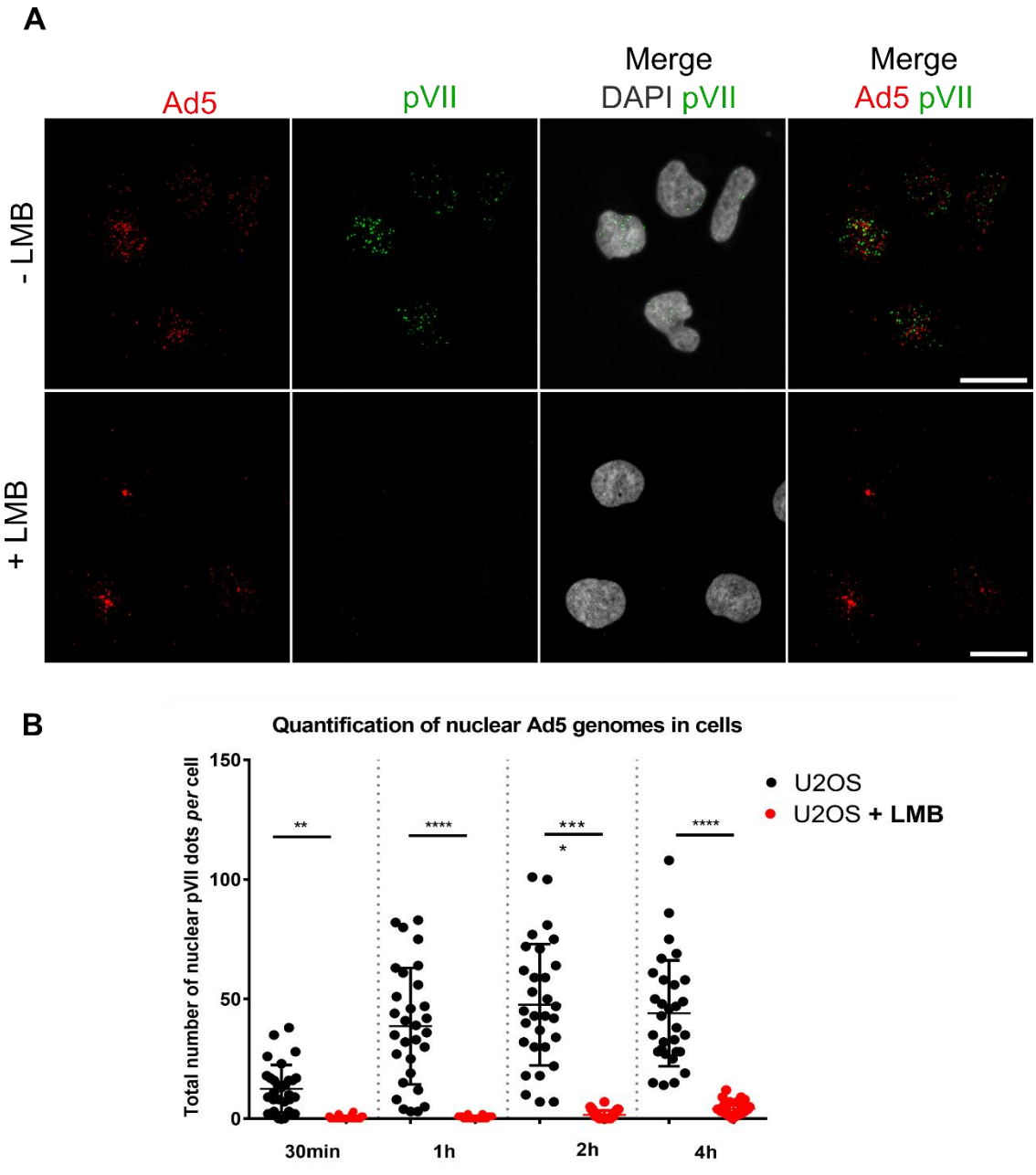

Figure 19. MTOC accumulation caused by LMB treatment leads to a defect in Ad5 genome import. U2OS cells were treated with (+ LMB) or without LMB (- LMB) for 45 min. Infections with Ad5-GFP particles were performed in the presence (+ LMB) or absence of LMB (- LMB) for 30 min up to 4 h. (A) Cells were fixed and stained with anti-Ad5 capsids (red) and anti-pVII (green) antibodies and with DAPI (grey) for chromatin staining. Images represent cells after 1 h of infection. Cells were imaged by confocal microscopy and maximal projection images are shown. (Scale bars, 20 µm). (B) Scatter plot showing the quantification of the total number of pVII foci colocalizing with DAPI signal per cell (depicted in (A): Merge DAPI/pVII), in the absence (black dots) or presence (red dots) of LMB. Mean values (+/- SD) of 30 cells per condition are shown. Statistical analysis was performed using one-way ANOVA multicomparison test.

I.2.c CRM1 is required for genome import and gene expression

Ad5 genome has to be delivered in the nucleus in order to initiate genome replication and expression. As previously showed, blocking of Ad5 capsids at the MTOC lead to a defect in Ad5 genome delivery. Thus, this MTOC retention inhibits nuclear steps of Ad5. Transcription of early genes is required to promote total transcription of Ad5 genes. 1 to 2 h pi, immediate early transcripts (E1A) can be detected (Berk et al. 1979; Glenn and Ricciardi 1988). However, up to now there is no available tool for the direct detection of Ad5 transcript via fluorescence microscopy.

We therefore developed and optimized a new protocol to visualize Ad5 E1A mRNA molecules at the single cell level. We adapted the RNAscope® Multiplex Fluorescent Assay (from ACDBio) in our infection model (see II.13 RNAscopeof Material and Methods section, for a detailed description). Cells were infected with Ad5 and fixed at different time points. Briefly, a probe mixture of 17 individual target sequences specifically designed to hybridize to Ad5 E1A mRNA transcripts was added for 2 h at 40 °C to the cells. Hybridized probes on the target were detected and signals were amplified with amplifiers in order to be detected by fluorescence microscopy. One fluorescent dot was considered as one E1A transcript, thus the total number of E1A transcription products can be quantified by fluorescence microscopy. Such assays can be combined with immunofluorescence staining, in order to visualize Ad5 capsids and genomes. As a specificity control, we infected U2OS with Ad5 vector lacking the coding E1A region (Figure 20). These cells were infected and Ad5 genomes correctly imported as Ad5 capsids and pVII signals were detectable. However, no signal for E1A mRNA was detectable. When cells were infected with replicative Ad5 particles (comprising the E1A coding region), E1A dots were detected, after 2 h pi. This new method can be used to monitor gene expression overtime.

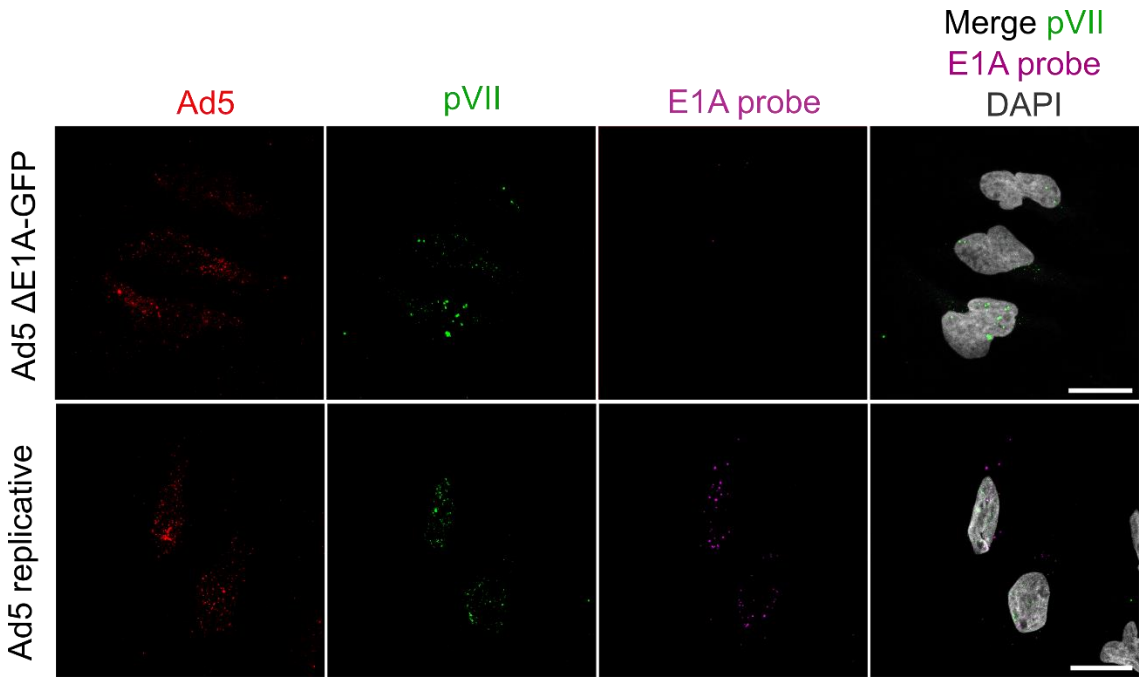

Figure 20. Identification of Ad5 E1A mRNA by fluorescence microscopy is specific. U2OS cells were infected with Ad5-GFP vector deleted for the E1A region (top row) or Ad5 replicative particles (bottom row) for 2 h. Cells were fixed and E1A transcripts (magenta) were detected using specific RNA probes (RNAscope). A second staining using antibodies was used to detect Ad5 capsids (red) and pVII (green) and DAPI (grey) was used to stain chromatin. Cells were imaged by confocal microscopy and maximal projection images are shown. (Scale bars, 20 µm).

We then performed RNAscope assays upon LMB treatment (Figure 21). In the absence of LMB, nuclear E1A mRNA dots started to be detectable after 2 h pi. The number of E1A dots increased overtime, and 6 h pi E1A signals were mostly found in the cytoplasm. In comparison, MTOC accumulation of Ad5 capsids induced by LMB treatment led to impaired gene expression, as no E1A mRNA molecules were detected under these conditions.

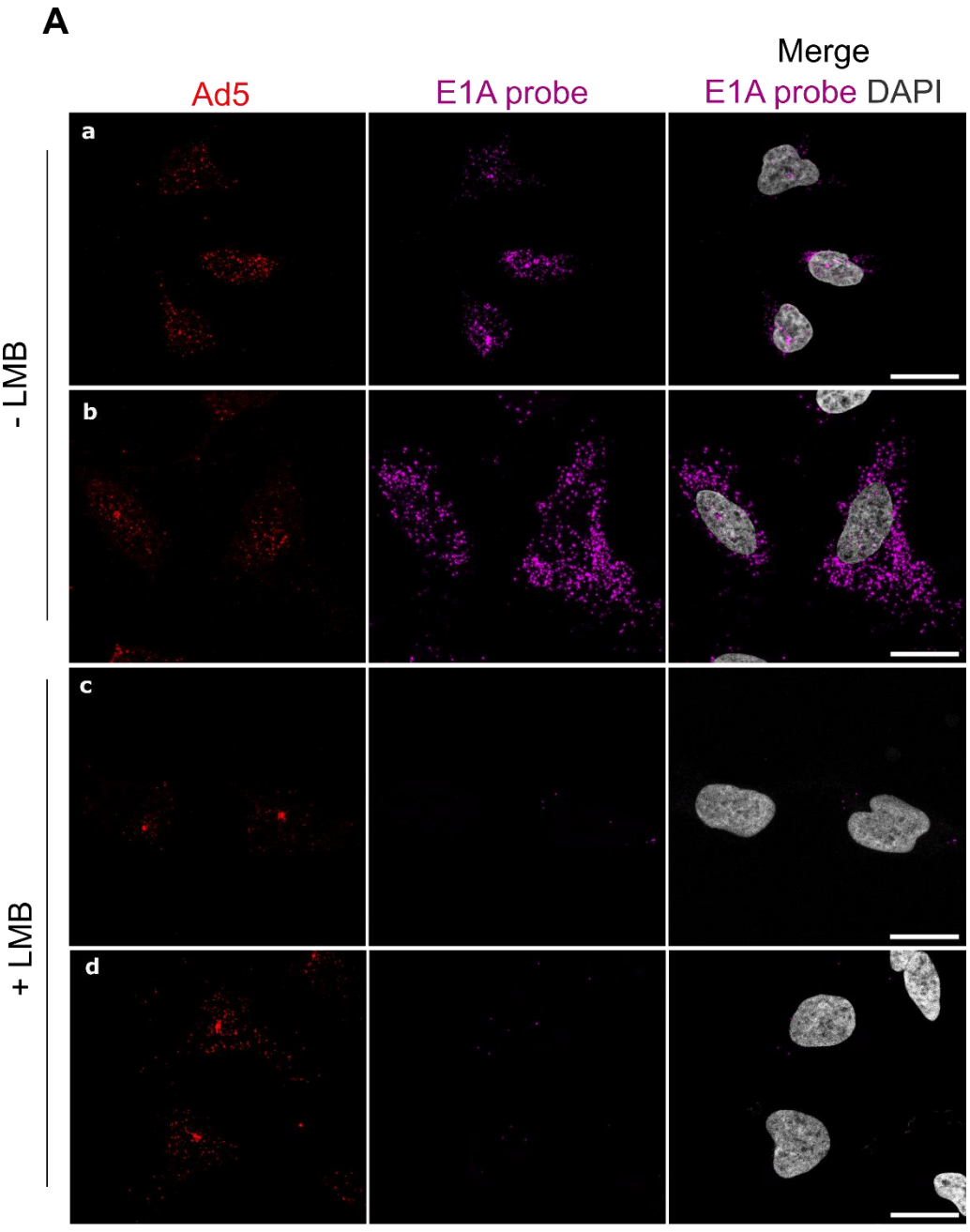
A
Ad5
E1A probe
Merge
E1A probe DAPI
- LMB
+ LMB
a
b
c
d
B
Number of total E1A mRNA dots in cells
E1A mRNA foci per cell
350
300
250
200
150
100
50
0
ns
****
****
U2OS
U2OS + LMB
2h
4h
6h

Figure 21. Functional CRM1 is required for Ad5 gene expression. (previous page) U2OS cells were infected with Ad5 replicative particles for 4 h (a and c) or 6 h (b and d) in the absence (-LMB) or presence (+ LMB) of LMB. Cells were fixed and E1A transcripts (magenta) were detected using specific RNA probes (RNAscope). A second staining using antibodies was used to detect Ad5 capsids (red) and pVII (green) and DAPI (grey) was used to stain chromatin. Cells were imaged by confocal microscopy and maximal projection images are shown. (Scale bars, 20 µm). (B) Scatter plot showing the quantification of the total number of E1A foci signal *per* cell in the absence (black dots) or presence (red dots) of LMB (pictures depicted in (A)). Mean values (+/- SD) of 30 cells *per* condition are shown. Statistical analysis was performed using one-way ANOVA multicomparison test.

We confirmed with quantitative data that functional CRM1 is required for NPC translocation, leading to genome import and gene transcription. Upon LMB treatment, Ad5 genome was not detectable via pVII staining: core DNA is not exposed due to Ad5 capsid protection. We then focused our experiments to study the role of CRM1 in Ad5-genome release.

I.2.d CRM1 affects Ad5 capsid disassembly in mitotic cells

Several studies demonstrated a role for NPCs in capsid disassembly, e.g. via binding with Nup214 (Greber et al. 1997; Trotman et al. 2001; Strunze et al. 2011; Cassany et al. 2015). It was shown that the N-terminal part of Nup214 is required for the docking of Ad5, via the hexon protein, before genome release. These studies were performed in the context of intact NE, with assembled NPCs. In order to bypass this physical barrier of NE and to study if CRM1 possesses a role in capsid disassembly independent of the NPC, we established a protocol for Ad5 infection of mitotic cells (protocol established by Dr. I. Carlón Andrés, PhD thesis Irene Carlón-Andrés, 2017). In such a cellular model, every component of the NE and NPCs should be available in the cell, but not in the physiological context of an intact nucleus. Therefore, detection of pVII in mitotic cells is the result of direct capsid disassembly and not genome import because the NE barrier is absent.

Cells were synchronised in mitosis with colcemid (also known as demecolcine) treatment. This drug induces microtubules depolymerization and blocks cells in metaphase. Before Ad5 infection, cells were treated with or without LMB to analyse the role of CRM1 in Ad5 capsid disassembly. Infections of mitotic cells were done in colcemid-free medium and were analysed for up to 2 h pi, since after 2 h cells started to divide due to the reversibility of the colcemid block. pVII dots were detectable in mitotic infected cells 1 h pi, and increased overtime, resulting from capsid disassembly (Figure 22 A and B). Capsid disassembly can be observed in fixed cells by colocalization events between pVII and Ad5 capsids (Figure 22 A, upper row). However, upon LMB treatment, no pVII were detectable, even at 2 h pi.

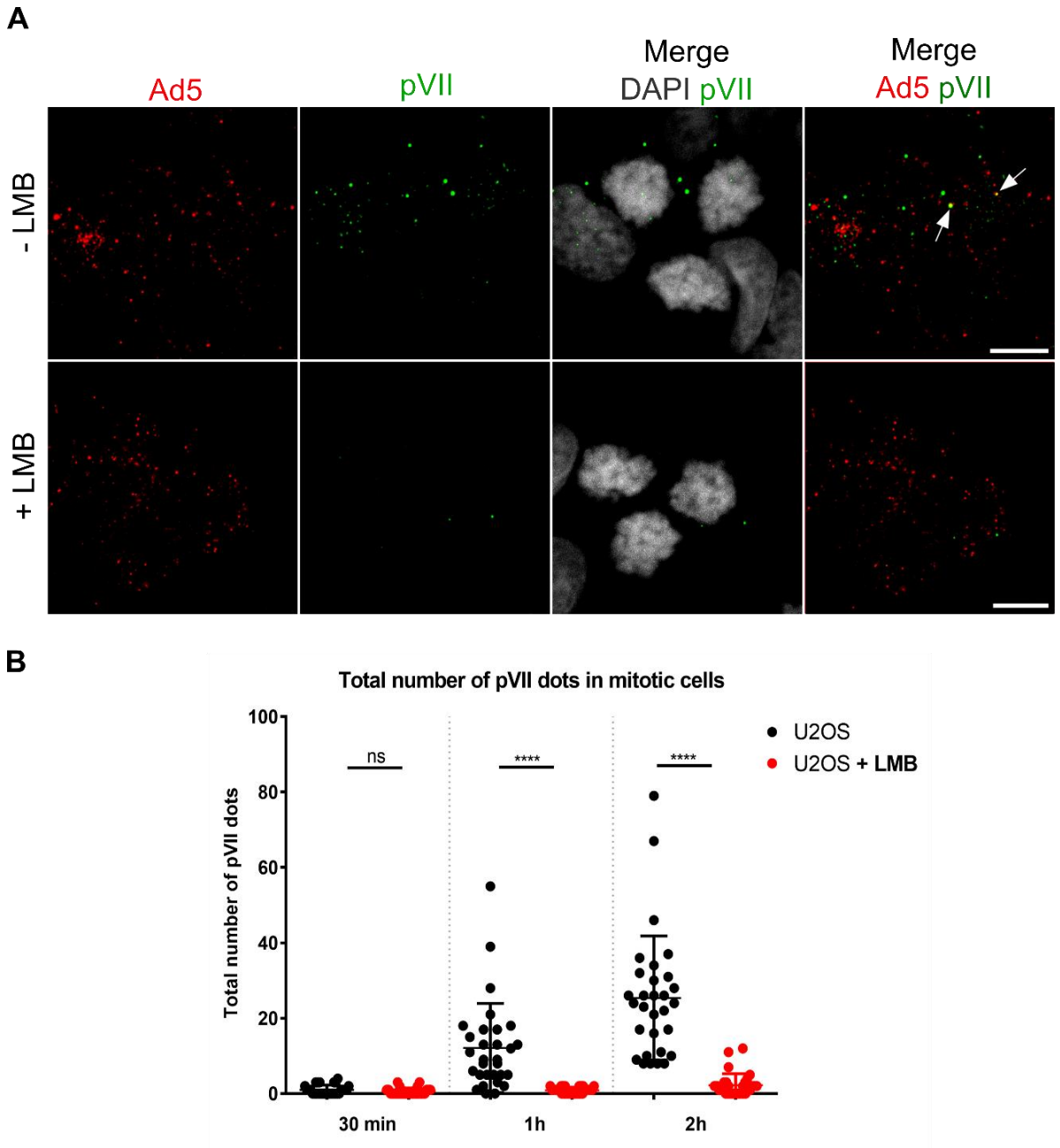

Figure 22. Intact nuclear envelope is not required for Ad5 capsid disassembly. U2OS cells were treated with colcemid for 14 to 16 h to synchronise cells in mitosis. Cells were treated with (+ LMB) or without LMB (- LMB) for 45 min in the presence of colcemid. Synchronised cells were infected with Ad5-GFP particles with (+ LMB) or without LMB (-LMB) but in the absence of colcemid for 30 min up to 2 h. (A) Cells were fixed and stained with anti-Ad5 capsids (red) and anti-pVII (green) antibodies and with DAPI (grey) for chromatin staining. Colocalization events between Ad5 capsids and pVII are shown with white arrows. Cells were imaged by confocal microscopy and maximal projection images are shown. (Scale bars, 10 µm). (B) Scatter plot showing the quantification of the total number of pVII foci signal per cell in the absence (black dots) or presence (red dots) of LMB (pictures depicted in (A)). Mean values (+/- SD) of 30 cells per condition are shown. Statistical analysis was performed using one-way ANOVA multicomparison test.

Our results showed that the addition of LMB impaired capsid disassembly and genome release in mitotic cells. In mitotic cells, there is no compartmentalisation between cytoplasmic and nuclear factors. Therefore, CRM1 cargoes blocked in the nucleus upon LMB treatment of interphase cells are found everywhere in mitotic cells and should be available for virus disassembly. Thus, it is unlikely that CRM1 cargoes sequestration in the nucleus induced by LMB is responsible for the disassembly defect. Our results strongly favour a direct role of CRM1 during capsid disassembly, where CRM1 dependent nuclear export is not required. Moreover, an intact NE is also not required to perform Ad5 capsid disassembly.

I.2.e CRM1 promotes the total Ad5 genome release from the capsid

Our capsid disassembly analyses were based on antibody detection of pVII in fixed cells. Fixation of cells can impair or hide some epitopes and the sensitivity of detection relies on the accessibility of these epitopes for antibodies. Moreover, single particle track analysis require live cell imaging experiments. To bypass these issues, our group had developed another indirect way of Ad5 genome detection, applicable to living cells (Komatsu et al. 2015). This system involves again pVII detection, but this time, via the detection of TAF-I. TAF-I is a cellular factor known to form ternary complexes with pVII on incoming genomes (Haruki et al. 2003). Binding of TAF-I molecules to pVII upon genome exposure can then be monitored by fluorescence microscopy using U2OS TAF-I GFP expressing cell lines, generated in our lab by Dr. T. Komatsu.

Upon infection of these cells with Ad5, we clearly observed nuclear TAF-I GFP dots and all of them corresponded to pVII dots, as shown by the merge between TAF-I GFP and pVII channels (Figure 23, upper row). This system is specific, as TAF-I GFP dots were not detectable upon LMB treatment (Figure 23, lower row).

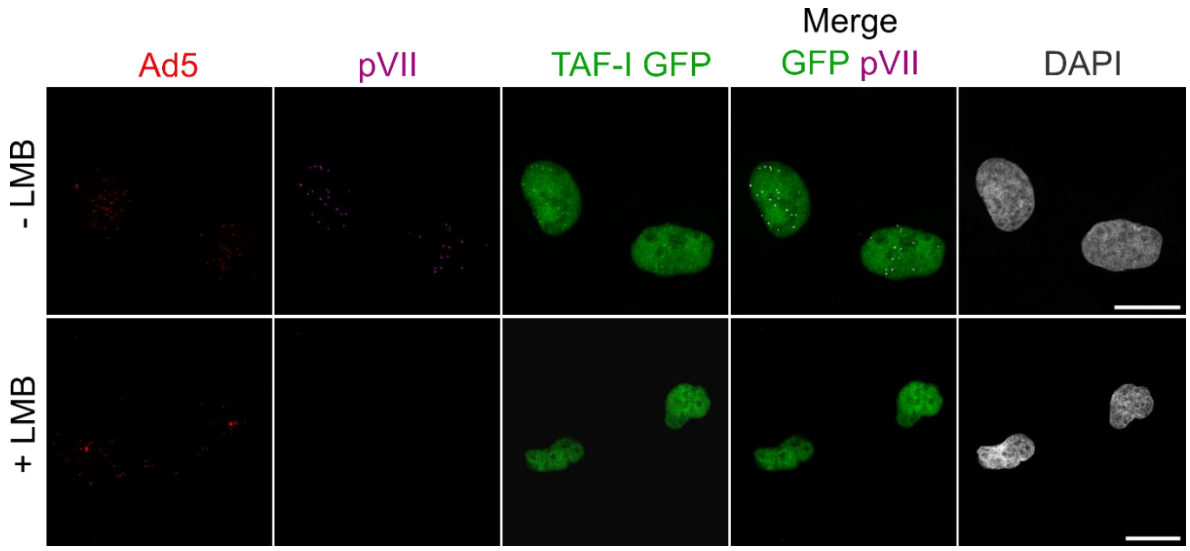

Figure 23. TAF-I staining can be used for pVII detection. (previous page) U2OS cells stably transfected with a construct coding for TAF-I GFP were treated with (+ LMB) or without LMB (- LMB) for 45 min. Infection with Alexa 594 labelled Ad5-GFP particles was performed in the presence (+ LMB) or absence (- LMB) of LMB for 1 h. Cells were fixed and stained with anti-pVII (magenta) antibodies and with DAPI (grey) for chromatin staining. TAF-I was detected by GFP signal. Cells were imaged by confocal microscopy and maximal projection images are shown. (Scale bars, 20 µm).

We used TAF-I GFP U2OS cells in order to study the role of CRM1 in capsid disassembly in living cells. In this assay, the dynamic of capsid disassembly is resulting in pVII exposure and is monitored via the detection of TAF-I GFP dots overtime, by live cell imaging microscopy. Cells were transfected with a construct coding for tagged Histone2B-tdiRFP to stain chromatin. Cells were synchronised via colcemid treatment (as shown in section I.2.d CRM1 affects Ad5 capsid disassembly in mitotic cells), and infected with Alexa-594 labelled Ad5-GFP particles. Infections were performed in the presence or absence of LMB. Mitotic cells were identified according to their chromatin staining (condensed chromosomes) and overall round shape. Single cells were selected and followed overtime. Colocalization events between TAF-I and Ad5 capsid signals were considered as partial disassembled capsids. Under these conditions pVII (i.e Ad5 genome) was enough exposed to interact with TAF-I GFP, but the capsid remained partially intact to be detected via Alexa-594 labelling fluorophore. On the other hand, free TAF-I GFP dots were considered as completely released genomes, separated from capsids.

In non LMB treated control cells, approximatively 1 h 30 to 2 h pi, green TAF-I dots were detectable (Figure 24 A). Within the cell population several TAF-I dots were free from capsids (highlighted with filled white arrows), whereas some dots remained associated with capsids (highlighted with empty white arrows). The number of TAF-I dots free from capsid increased overtime (Figure 24 B). Moreover, virtually all free TAF-I dots and some TAF-I Ad5 associated dots were observed with a restricted mobility associated to cellular chromatin, implying that the genomes became stably anchored to the chromatin (zoom Figure 24 A).

In cells treated with LMB, TAF-I dots were also detectable. However, these TAF-I were exclusively associated with capsids (yellow dots, Figure 24 C), and the number of accumulating free TAF-I dots overtime was strongly decreased compared to control cells (Figure 24 D). However, in the presence of LMB, chromatin targeting of partially disassembled capsids was also observed (zoom Figure 24 C).

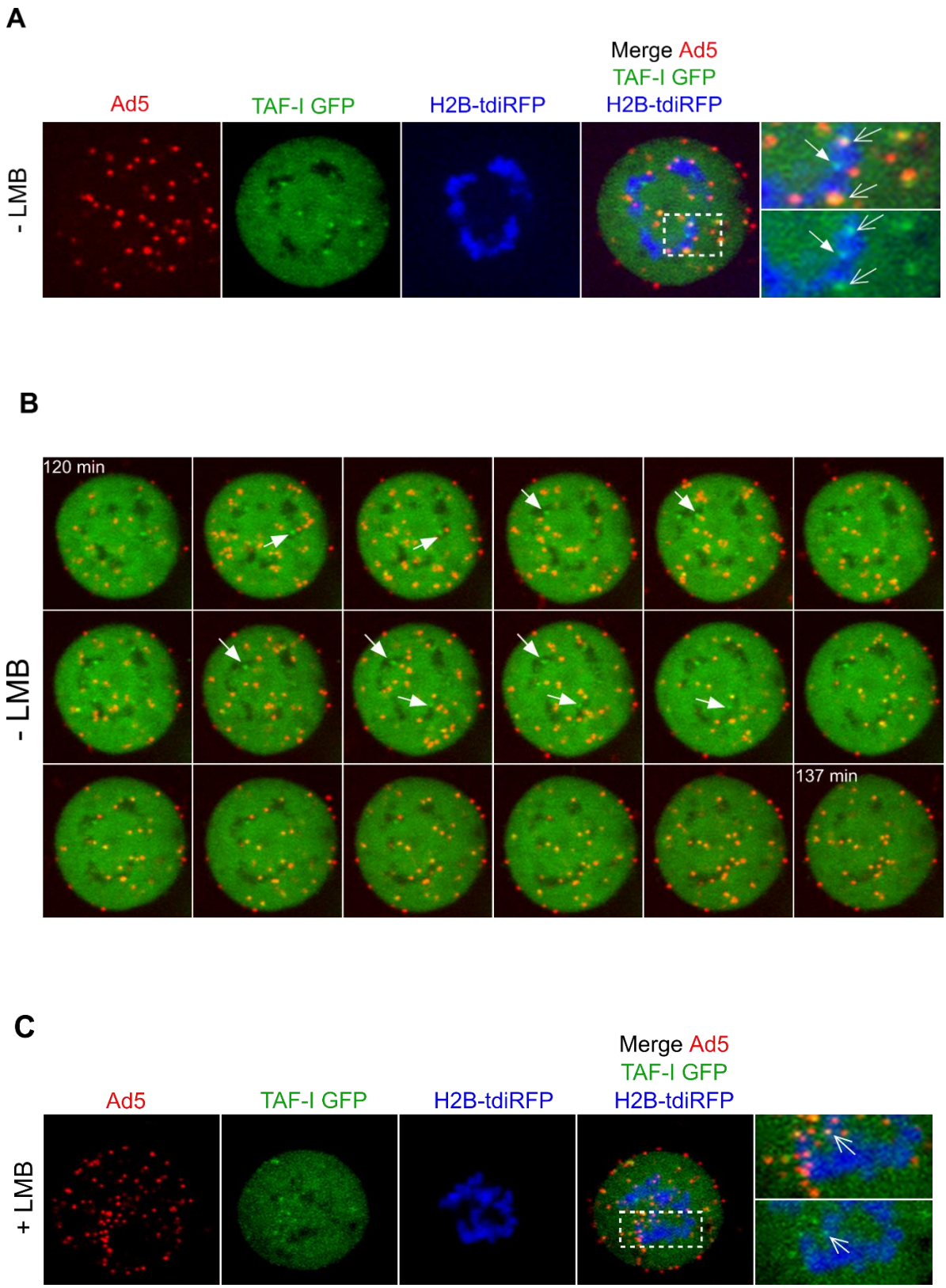
A
Ad5
TAF-I GFP
H2B-tdiRFP
Merge Ad5
TAF-I GFP
H2B-tdiRFP
- LMB
B
120 min
137 min
- LMB
C
Ad5
TAF-I GFP
H2B-tdiRFP
Merge Ad5
TAF-I GFP
H2B-tdiRFP
+ LMB

D

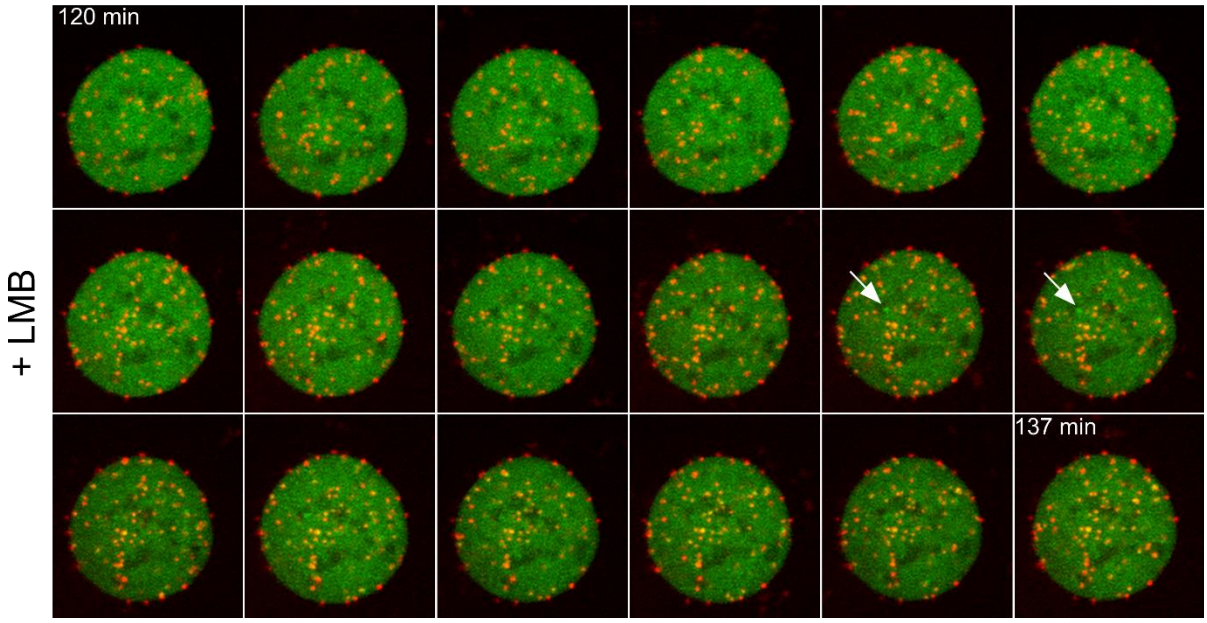

Figure 24. Functional CRM1 is required for total Ad5 capsid disassembly in mitotic cells. (Fig A, B and C previous page) U2OS TAF-I GFP expressing cells were transfected with H2B-tdiRFP construct (blue) to stain chromatin. After 24 h of transfection, cells were treated with colcemid for 14 to16 h to be synchronised in mitosis. Cells were treated with or without LMB for 45 min in the presence of colcemid. Infection with Alexa-594 labelled Ad5-GFP particles was performed without colcemid but in the absence or presence of LMB. Mitotic cells were identified according to their chromatin staining (blue) and Ad5 capsids (red) as Ad5 genomes (TAF-I GFP dots; green) are depicted on the pictures. Cells were imaged by spinning disk confocal microscopy. Maximal projection images are shown. (A) and (C) Mitotic U2OS TAF-I GFP cell treated without (A) or with (C) LMB. Maximal projection of signals detected in each channel at 130 min pi. TAF-I GFP dots free from Ad5 colocalization are shown with filled white arrows whereas TAF-I GFP dots colocalizing with Ad5 are shown with empty white arrows. (B) and (D) Overlay of TAF-I GFP (green) and Ad5 capsids (red) signals in one single cell in absence (B) or presence (D) of LMB overtime. From the top left corner (120 min) to the bottom right (137 min) each frame is separated by 1 min. TAF-I GFP dots free from Ad5 colocalization are shown with white arrows.

These results showed that capsid disassembly and genome separation in mitotic cells require functional CRM1. The strong reduction of free TAF-I dots observed upon LMB treatment suggests that inhibition of CRM1 impairs Ad5 genome capsid-release. In contrast, in mitotic cells, partially disassembled capsids were targeted to the chromatin, even in the presence of LMB. One hypothesis is that a partially exposed core-genome is sufficient to target the genome to chromatin, dragging the attached capsid with it. Complete genome release and capsid disassembly, however, would need functional CRM1. In fixed mitotic cells, antibody detection of pVII in LMB treated cells did not give any signal (Figure 22), whereas pVII could be detected using the TAF-I GFP system. The TAF-I GFP pVII detection system appears thus more sensitive and does not rely on epitope recognition. However, we have not tested pVII detection in TAF-I GFP U2OS mitotic fixed cells.

Our analyses in U2OS cells confirmed previous studies about the role of CRM1 in efficient nuclear genome import. During the first steps of infection, neither CRM1 nor other nuclear factors are required for Ad5 trafficking to the MTOC. Ad5-MTOC interaction is not well characterized but our data are in favour of an interaction independent of the integrity of the microtubule network. However, functional CRM1 is needed to mediate Ad5-MTOC removal for NPC translocation. Inhibition of CRM1 with LMB impairs nuclear genome import, leading to a defect in Ad5 gene expression. Our model of mitotic infected cells gave us more insights into the role of CRM1. Total genome release from Ad5 capsid requires functional CRM1 and it seems to directly involve CRM1 and none of its cargoes.

II. A new CRM1 mutant as a tool to study Ad5 genome import

CRM1, the major cellular export factor, is known to form a ternary complex together with RanGTP and NES-containing cargoes (Ossareh-Nazari and Dargemont 1999; Fornerod et al. 1997b; Monecke et al. 2013). Its final binding site on Nup214 has been shown to promote the efficient release of some export complexes (Kehlenbach et al. 1999; Bernad et al. 2006; Hutten and Kehlenbach 2006). Moreover, our group showed that CRM1 binds some FG-repeats of Nup214 (Roloff et al. 2013) and solved the crystal structure of the export complex CRM1-RanGTP-SPN1 associated with FG-repeats fragment of Nup214 (Port et al. 2015). Based on this study, several mutants of CRM1 were generated. In order to study CRM1 and its interacting partners upon Ad5 infection, we tested a batch of these mutants in our infection assays. Interestingly, one of these mutants did not show any defect in Nup214 binding assays (data not shown) but was found to impair Ad5 genome delivery. We chose to study in details this CRM1 mutant in order to better characterize its role upon Ad5 infection. We generated and characterized new cell lines constitutively expressing the CRM1 mutant. We also performed export assays and biochemical studies with recombinant proteins to characterize the export kinetic and the binding with NES in this mutant, in comparison to the wild type protein.

II.1 CRM1 W142A P143A mutation

A CRM1 mutant library was initially generated by Dr. S. A. Port, to study the interaction between CRM1 and Nup214-FG repeats. Based on the predicted structure of CRM1 in complex with RanGTP and SPN1, bound to an FG-repeats fragment of Nup214, point mutations were introduced on CRM1 at the predicted binding site of Nup214. In export complexes, RanGTP is found in the central domain of CRM1 whereas the NES cargo interacts with the outer surface of CRM1 (reviewed in (Monecke et al.2014)).

Therefore, as an example for one of the CRM1 generated mutants, W142 P143A mutations are located close to the site of interaction between CRM1 and Nup214 (but not overlapping) (Figure 25).

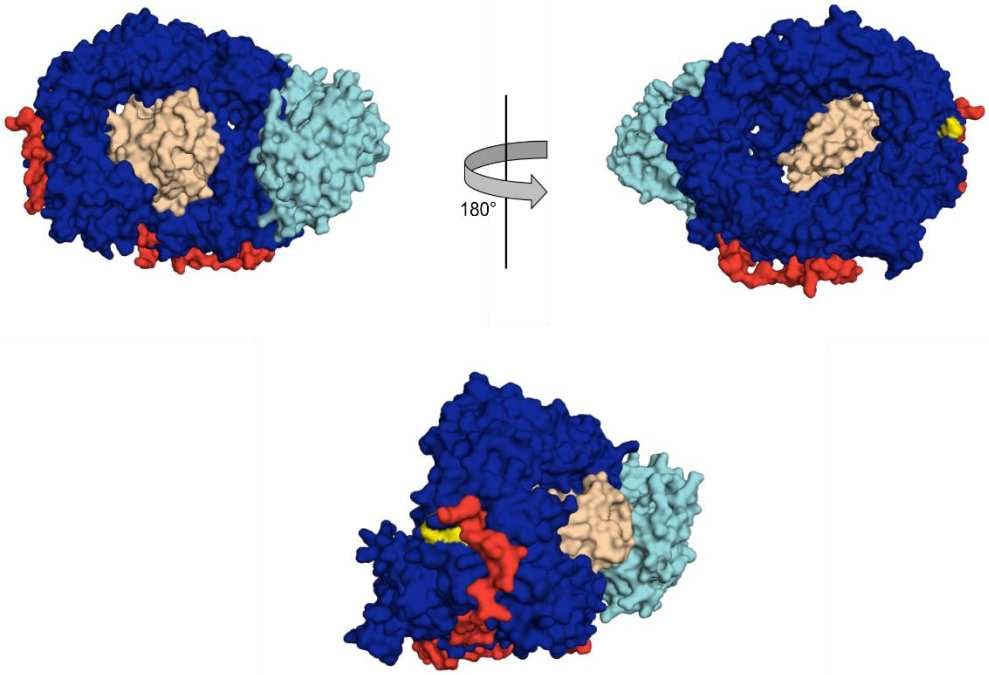

Figure 25. Mutations W142A P143A are close to the binding region of Nup214 FG-repeats. Overall structure of CRM1 (blue) in complex with RanGTP (light orange), the cargo SPN1 (cyan) and Nup214-FG repeats (red). Different orientations of the complex are depicted. Mutations W142A P143A on CRM1 are highlighted in yellow (Port et al. 2015).

In order to study the impact of a mutation on CRM1 function in the cell, endogenous CRM1 has to be inactivated with LMB treatment. In this context, all mutants tested had to be LMB resistant. Therefore, the C528S mutation was introduced in addition to other mutated sites in every CRM1-mutant tested. A preliminary screening of several CRM1 mutants from the mutant library mentioned above was done by Dr. I. Carlón-Andrés. U2OS cells were transfected with various HA-tagged and LMB-resistant CRM1 and infected with Ad5. The efficiency of capsid disassembly in mitotic cells was quantified according to the number of pVII dots normalised to the total number of Ad5 capsids *per* cells, after 1 h of infection, upon LMB treatment (Figure 26, adapted from PhD thesis Irene Carlón-Andrés, 2017).CRM1 C528S (conferring the LMB resistance) increased the capsid disassembly efficiency, compared to cells non-treated with LMB, confirming a role of CRM1 during this process. Five other mutants holding 2 (or 4) extra mutations were able to rescue capsid disassembly upon LMB treatment. Only CRM1 with W142A P143A mutations was not able to rescue the LMB inhibition effect on capsid disassembly.

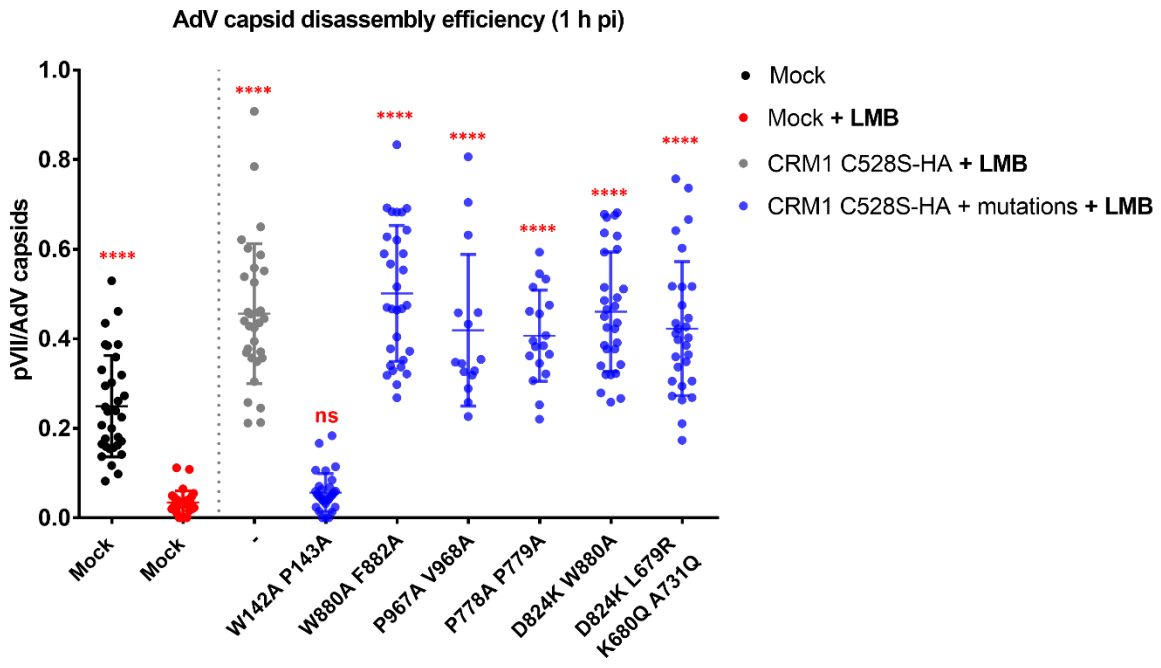

Figure 26. CRM1 W142A P143A C528S is not able to rescue Ad5 capsid disassembly upon LMB treatment. U2OS cells were transfected with empty plasmid (mock) or with CRM1 C528S-HA constructs with specific mutations, indicated below the X axis. Cells were treated with colcemid for 14 to 16 h to synchronise cells in mitosis and treated with LMB (red, grey and blue conditions) or without (black condition) for 45 min prior to infection. Synchronised cells were infected for 1 h with Alexa 594 labelled Ad5-GFP particles with or without LMB but in absence of colcemid. Cells were fixed and stained with anti-HA antibodies to identify transfected cells. Ad5 genomes were identified via anti-pVII antibodies and DAPI was used for chromatin staining. Cells were imaged by confocal microscopy and the quantification of the number of pVII foci normalised to the number of Ad5 capsid per cell was performed on maximal projection images. Results are depicted with a scatter plot. Mean values (+/- SD) of 30 cells per condition are shown. Statistical analysis was performed using one-way ANOVA multicomparison test, comparing every condition to mock transfected LMB treated U2OS cells (red condition on the graph) (modified from PhD thesis Irene Carlón-Andrés, 2017).

II.2 Generation and characterization of CRM1 mutant expressing cell lines

To further analyse the Ad5 capsid disassembly defect observed upon expression of the CRM1 W142A P143A C528S mutant, we generated U2OS cells constitutively expressing this mutant form of CRM1. The CRM1-HA construct was transfected in U2OS and after few days of culture, LMB was added to the medium, to select cells that had incorporated the LMB resistant form of CRM1. Indeed, random events of integration can be observed upon transfection of mammalian cells (Murnane 1990). A concentration of 2 nM of LMB was added to the medium to maintain the shut-down of endogenous CRM1 and to keep the selection of transfected cells. Such concentration has been shown to be cytotoxic for cells (Wolff et al. 1997).

We first monitored the cell growth of these new cell lines (Figure 27). U2OS non-transfected cells and cells transfected with CRM1 C528S-HA as a control were compared to the CRM1 triple mutant cell lines. Addition of 2 nM of LMB after 3 days of culture led to the death of non-transfected cells. This concentration was sufficient to be used as a selection tool. Moreover, this result shows that functional CRM1 is essential for cell survival. Both CRM1-HA expressing cells showed an exponential growth overtime, although they grew slower than U2OS control cells. After 9 days of culture, almost 10 times more U2OS cells were counted. Among the two populations of transfected cells, U2OS expressing CRM1 W142A P143A C528S-HA grew slightly slower compared to control cells. These new U2OS cell lines are viable and able to grow upon LMB treatment.

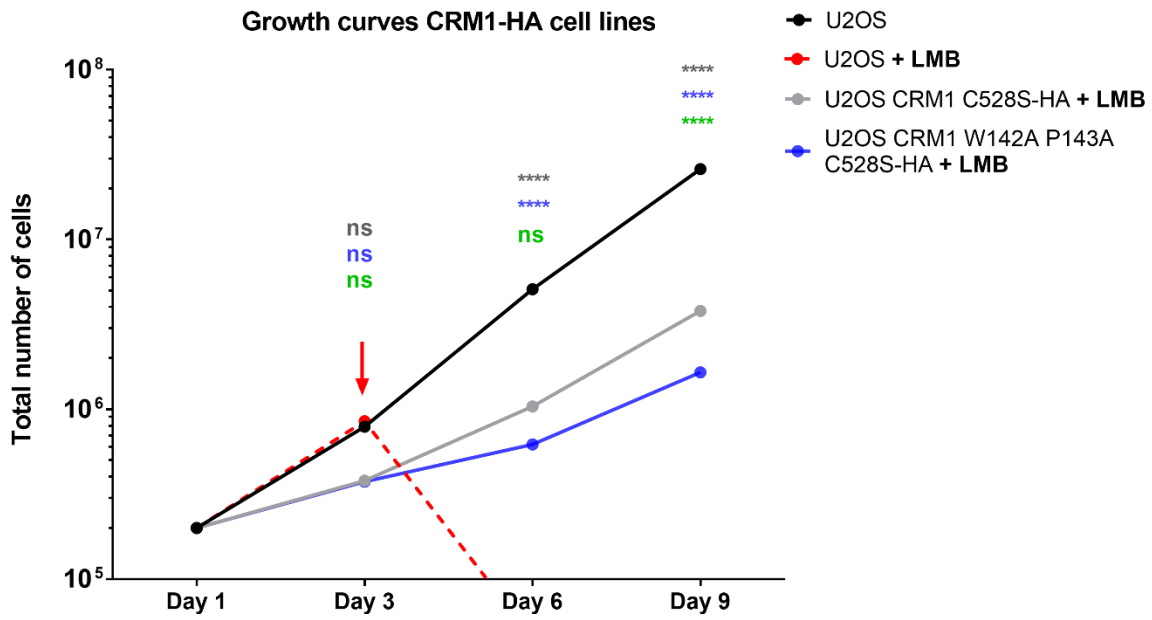

Figure 27. U2OS cells expressing CRM1 W142A P143A C528S-HA are viable. On day 1, 2x10^5 U2OS cells or CRM1-HA expressing U2OS cells were seeded into a 6 well plate. Every 3 days, cells were detached with trypsin, counted using the CASY cell counter and the totality of cells was seeded on new plates. No LMB was added to U2OS (black dots); 2 nM of LMB was added on U2OS + LMB (red dots) after 3 days of culture (depicted with the red arrow). U2OS CRM1-HA expressing cells (CRM1 C528S-HA grey dots; CRM1 W142A P143A C528S-HA blue dots) were maintained from day 1 with 2 nM of LMB. Graph showing the total number of cells counted over time, resulting from one experiment. Statistical analysis was done using two-way ANOVA multicomparison test; CRM1 C528S-HA and CRM1 W142A P143A C528S-HA conditions were compared to U2OS cells (* in grey and blue respectively) and also compared between themselves (* in green).

To further characterize these cell lines, we were interested in the level of expression and the localization of CRM1-HA within these cells. Endogenous CRM1 is found in the nucleus (see Figure 14 A). Immunofluorescence staining with anti-HA antibodies showed a similar pattern of expression in both cell lines: the majority of CRM1-HA was found in the nucleus, with most of the cells showing a nuclear rim staining (Figure 28 A).

However, the signal intensity was very heterogeneous among each population, with a cytoplasmic localization of CRM1-HA in some cells. Moreover, the signal intensity was stronger in cells expressing CRM1 W142A P143A C528S-HA compared to cells expressing CRM1 C528S-HA. Indeed, integration events are random and do not take place at the same position in cellular DNA. Thus, within the cell population, expression of CRM1 constructs is not controlled by the same promotors.

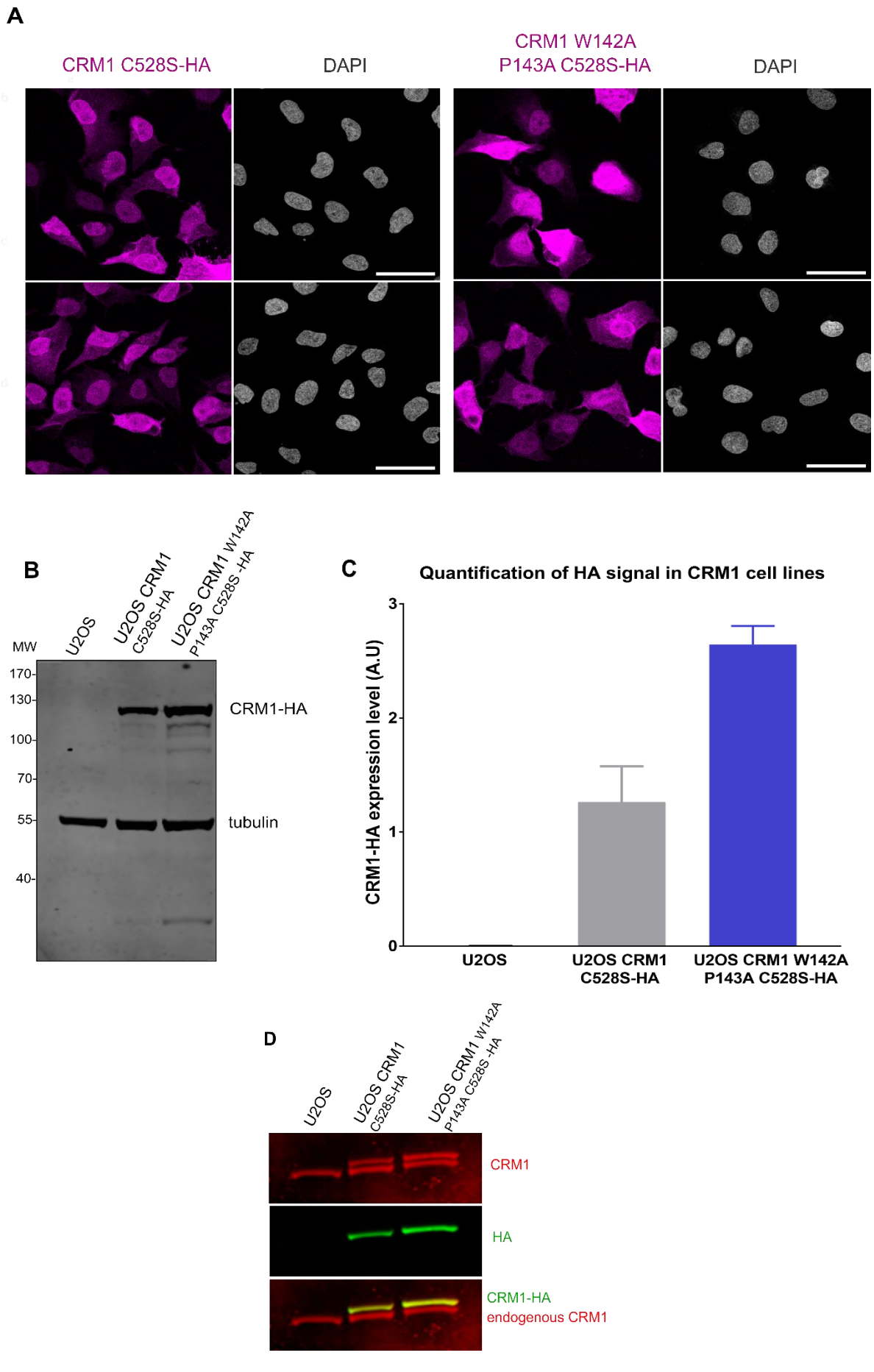
A
CRM1 C528S-HA
DAPI
CRM1 W142A
P143A C528S-HA
DAPI
B
MW
U2OS
U2OS CRM1 C528S-HA
U2OS CRM1 W142A P143A C528S -HA
170-
130-
100-
70-
55-
40-
CRM1-HA
tubulin
C
Quantification of HA signal in CRM1 cell lines
CRM1-HA expression level (A.U)
0
1
2
3
U2OS
U2OS CRM1 C528S-HA
U2OS CRM1 W142A P143A C528S-HA
D
U2OS
U2OS CRM1 C528S-HA
U2OS CRM1 W142A P143A C528S -HA
CRM1
HA
CRM1-HA
endogenous CRM1

Figure 28. CRM1-HA is correctly expressed in both cell lines. (previous page) (A) U2OS CRM1-HA expressing cell lines were fixed and stained using anti-HA antibodies (magenta) to visualize overexpressed CRM1-HA constructs and DAPI (grey) for chromatin staining (Scale bars, 50 µm). Cells were imaged by confocal microscopy and maximal projection images are shown. (B) Detection of CRM1-HA expression within U2OS cell lines using anti-HA antibodies (upper band), by Western blotting. Tubulin (lower band) was used as a loading control. (C) Graph showing the quantification of HA signal intensities, normalized to the level of tubulin (quantification of Western blotting in (B); Arbitrary Units (AU)). (D) Detection of CRM1 (red) and CRM1-HA (green) by Western blotting. Merge of both signals is depicted in the lower panel.

A higher level of expression in U2OS CRM1 W142A P143A C528S-HA was confirmed by Western blotting analysis (Figure 28 B and C). Upon LMB treatment, synthesis of endogenous CRM1 is not impaired, only its NES binding capacity is inhibited. To check if endogenous CRM1 could be distinguished from the overexpressed mutant in these cells, we performed Western blotting of cellular extracts and used anti-CRM1 and anti-HA antibodies (Figure 28 D). Expression of endogenous CRM1 could still be detected with the same intensity between cell lines. Taken these results together, we confirmed the viability and the correct expression of CRM1 mutants in these new cell lines. Thus, they can be used to perform our *in cellulo* analyses.

II.3 CRM1 W142A P143A is functional for export

We previously showed that U2OS CRM1-HA expressing cells were viable under LMB treatment (section II.2 Generation and characterization of CRM1 mutant expressing cell lines). The export function of CRM1 is essential for cell viability. The fact that U2OS CRM1 W142A P143A C528S-HA cells survived and grew upon LMB treatment suggests that this CRM1 mutant was physiologically active. We thus analysed export functions of this mutant by testing the export of several NES cargoes in these cell lines, with immunofluorescence analyses. As negative and positive controls, we used U2OS cells, treated or not with LMB. We first analysed the distribution of an endogenous cargo of CRM1, RanBP1 known to be sensitive to LMB treatment (Plafker and Macara 2000). In U2OS, RanBP1 was correctly exported since most of the signal was cytoplasmic (Figure 29 A). Upon LMB treatment, RanBP1 was trapped in the nucleus. In both U2OS CRM1-HA cell lines treated with 20 nM of LMB, RanBP1 was correctly exported. Similar results were observed upon overexpression of a GFP-fused cargo of CRM1, SPN1 (Paraskeva et al. 1999). Export was rescued in U2OS CRM1-HA cells (Figure 29 B). We then overexpressed a shuttling construct, containing an NLS (M9 peptide) and the CRM1 dependent NES of HIV-1 Rev, fused to GFP. This construct was homogeneously distributed within U2OS, but LMB treatment led to its nuclear retention (Figure 29 C). Again, in both CRM1-HA cell lines, the export was rescued. These results showed a functional export of different NES cargoes in CRM1-HA cell lines. It also confirmed that W142A P143A mutations did not impair CRM1 cargoes export functions under steady state conditions.

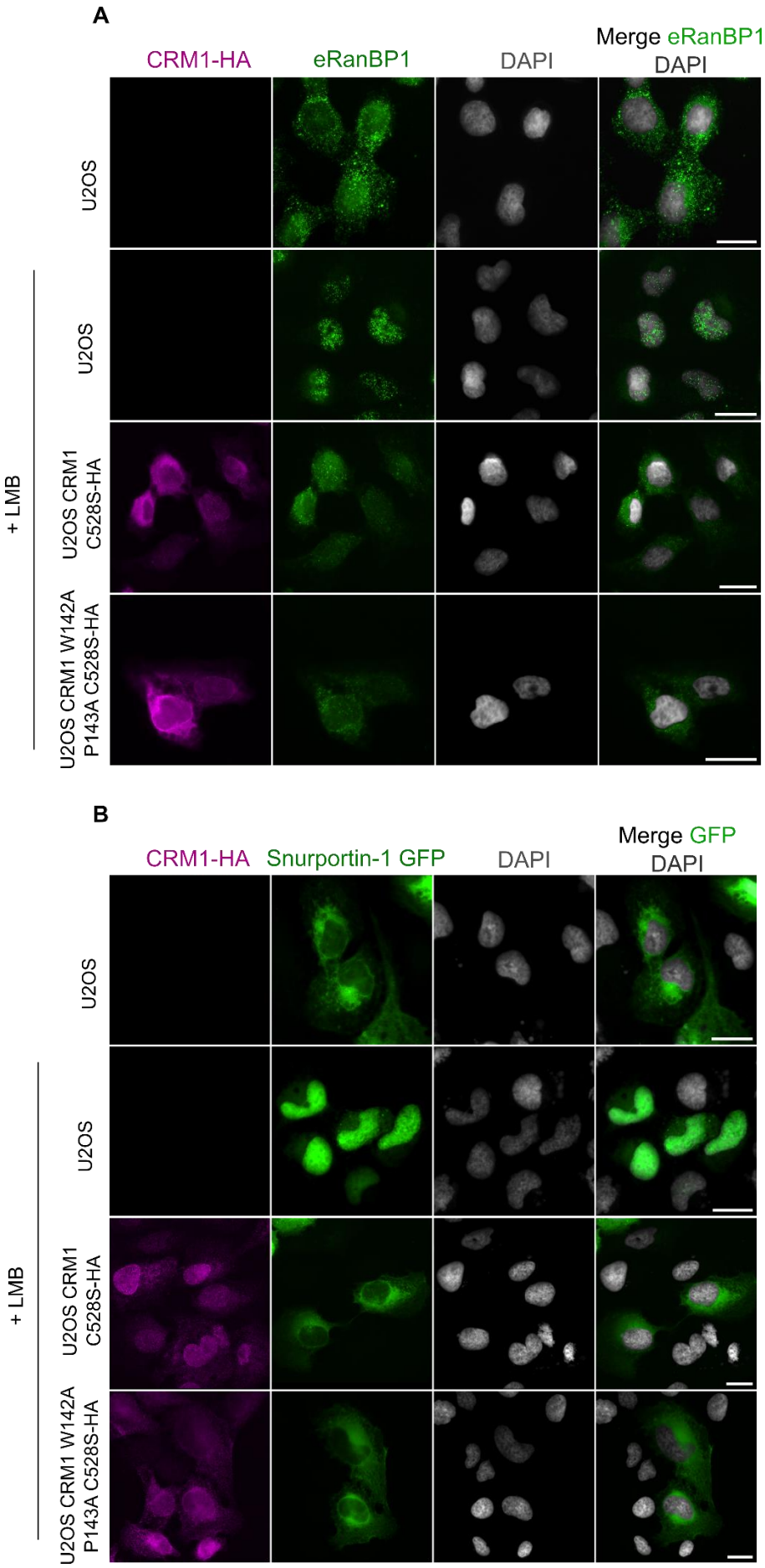
A
CRM1-HA
eRanBP1
DAPI
Merge eRanBP1 DAPI
U2OS
U2OS
U2OS CRM1 C528S-HA
U2OS CRM1 W142A P143A C528S-HA
+ LMB
B
CRM1-HA
Snurportin-1 GFP
DAPI
Merge GFP DAPI
U2OS
U2OS
U2OS CRM1 C528S-HA
U2OS CRM1 W142A P143A C528S-HA
+ LMB

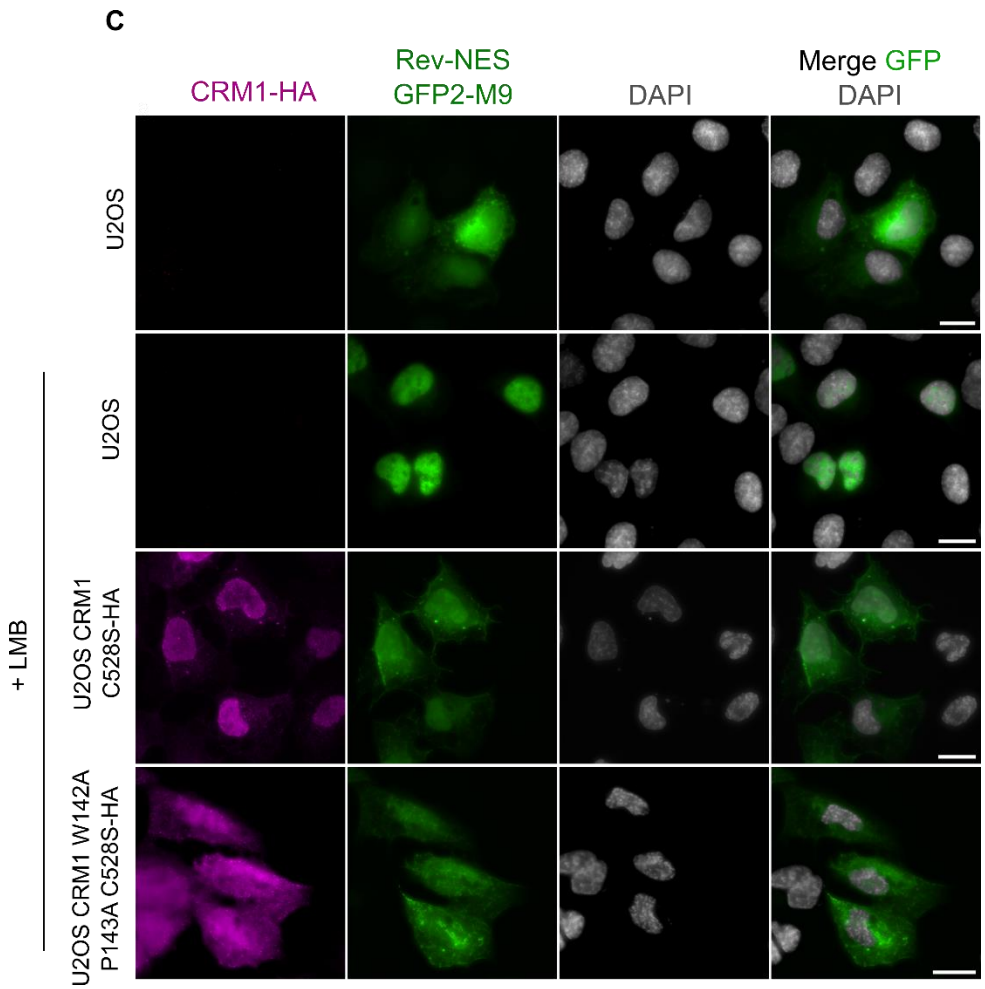

Figure 29. CRM1 dependent export is functional in both CRM1-HA cell lines. (Fig A and B on previous page) U2OS, U2OS CRM1 C528S-HA or U2OS CRM1 W142A P143A C528S-HA expressing cells were seeded and either non-transfected (A) or transfected with constructs coding for SPN1 GFP (B) or Rev-NES-GFP2-M9 (C). 24 h post-transfection, LMB was added (+ LMB) for 45 min or not. Cells were fixed and stained with anti-HA (magenta), anti-RanBP1 ((A); green) antibodies and with DAPI (grey) for chromatin staining. SPN1-GFP (B) or Rev-NES-GFP2-M9 (C) were detected via their GFP signals. Cells were imaged by fluorescence microscopy and one plane is shown. (Scale bars, 20 µm).

II.4 CRM1 W142A P143A impairs Ad5 capsid disassembly

To better understand the defect observed upon overexpression of the triple mutant in the Ad5 capsid disassembly (Figure 26), we performed infection assays. During all our infection assays, 20 nM LMB was added to CRM1-HA cells, to block endogenous CRM1. We first studied capsid disassembly in mitotic CRM1-HA cell lines, to control whether we were able to reproduce the results obtained upon transient expression of CRM1-HA constructs (Figure 26). Cells were synchronised with colcemid and infected with Ad5 (Figure 30).

Ad5 genome release was monitored overtime (from 30 min to 2 h) by quantification of pVII dots *per* cell. As previously shown (Figure 22), Ad5 genome release increased overtime and was completely blocked upon LMB treatment. The LMB effect in CRM1 C528S-HA expressing cells was rescued and the capsid disassembly efficiency 1 h pi was even increased compare to control cells, highlighting the role of CRM1 in this process (Figure 30 B and C). Constitutive expression of CRM1-HA construct did not impair Ad5 infectivity. However, no pVII signal was detectable in CRM1 W142A P143A C528S-HA U2OS cells (Figure 30 A) 1 h pi, confirming previous results (Figure 26). Despite its LMB resistance, this mutant was not able to rescue the defect of Ad5 capsid disassembly due to the presence of LMB, up to 2 h pi (Figure 30 D and E). Later point could not be analysed since after 2 h cells started to divide. Within these 2 h of infection, the lack of effect of the CRM1 triple on Ad5 capsid disassembly, compared to CRM1 C528S-HA, was quite striking.

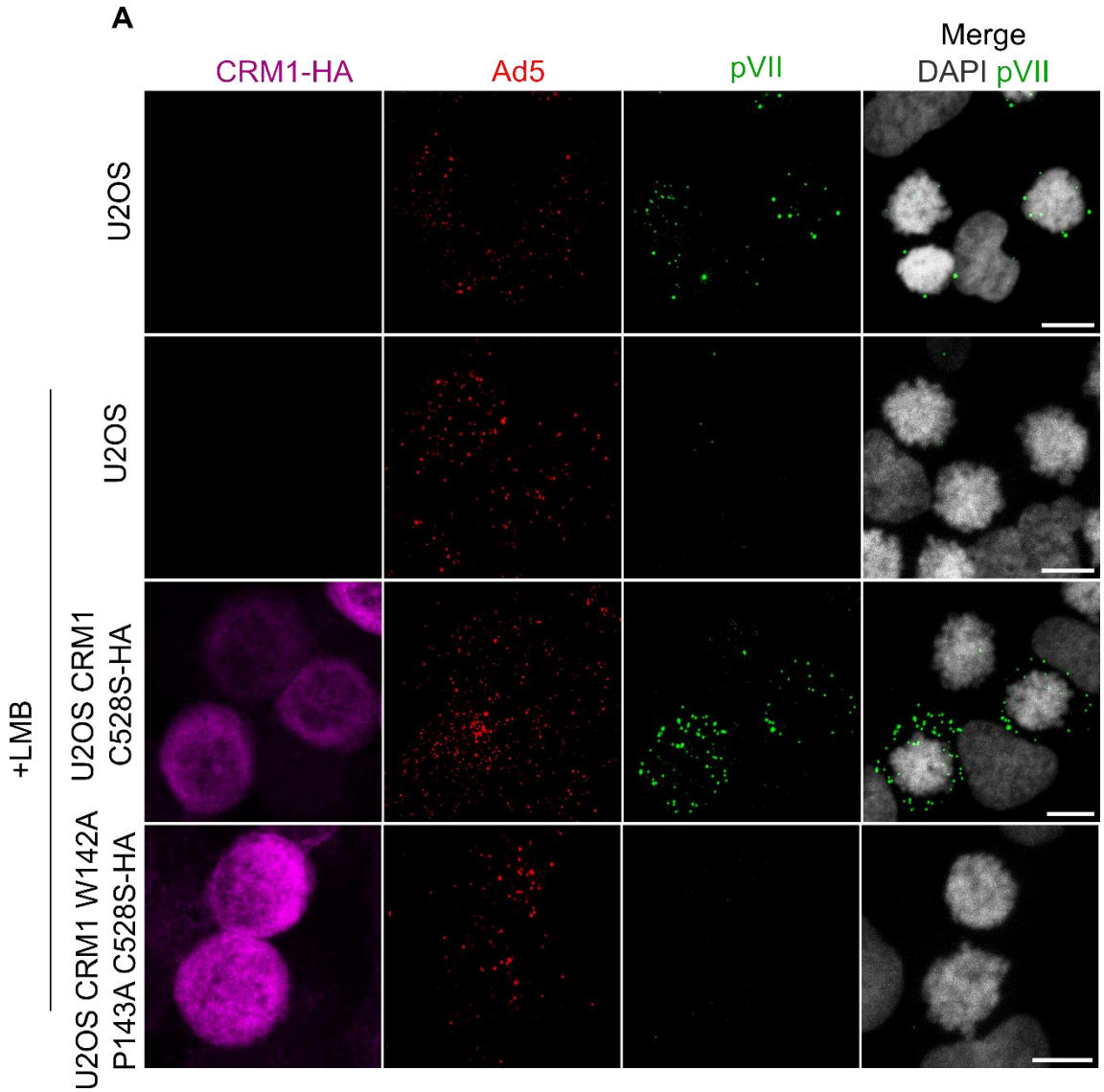

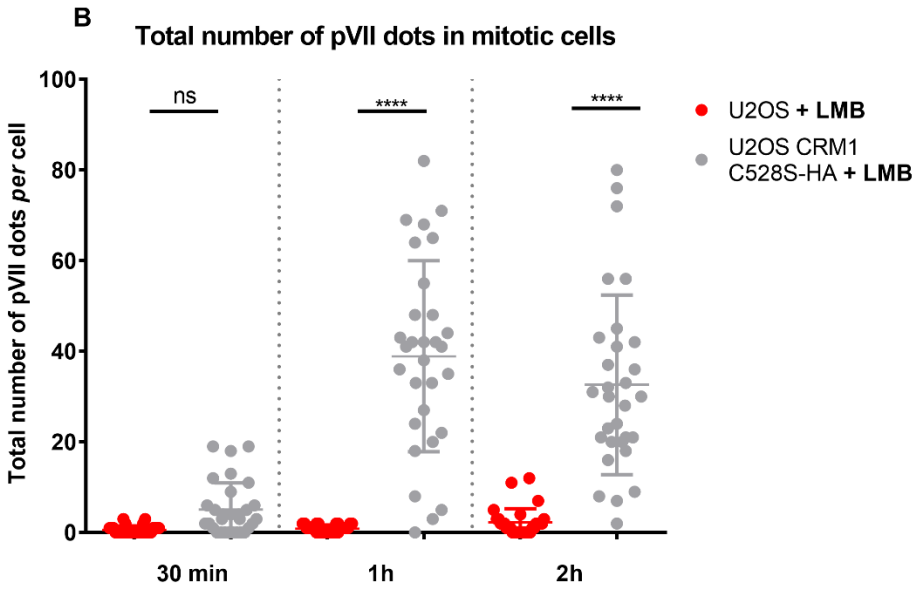
B
Total number of pVII dots in mitotic cells
Total number of pVII dots per cell
100
80
60
40
20
0
ns
****
****
30 min
1h
2h
U2OS + LMB
U2OS CRM1
C528S-HA + LMB

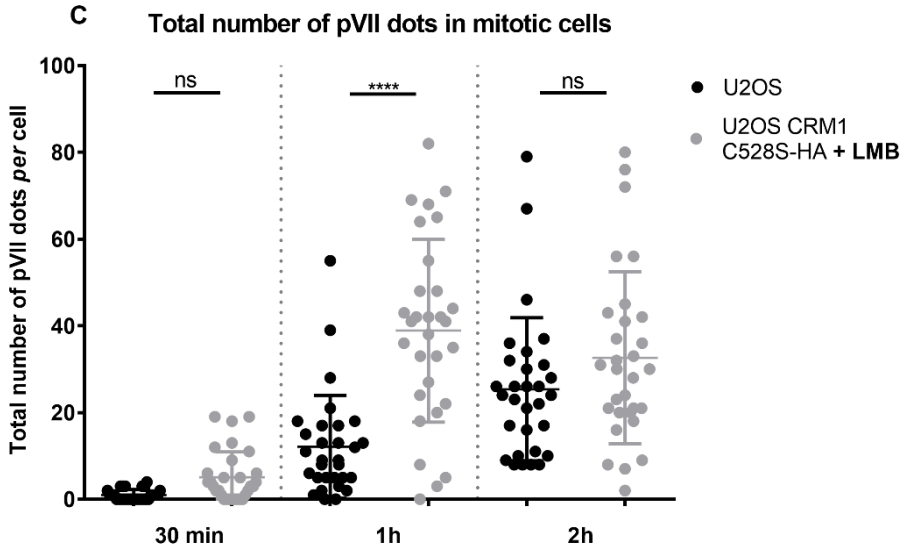
C
Total number of pVII dots in mitotic cells
Total number of pVII dots per cell
100
80
60
40
20
0
ns
****
ns
30 min
1h
2h
U2OS
U2OS CRM1
C528S-HA + LMB

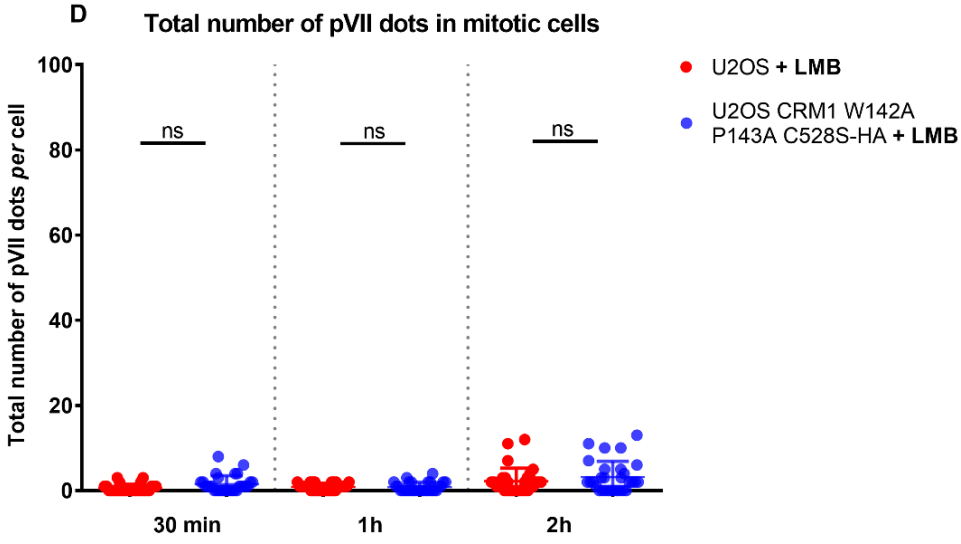
D
Total number of pVII dots in mitotic cells
Total number of pVII dots per cell
100
80
60
40
20
0
ns
ns
ns
30 min
1h
2h
U2OS + LMB
U2OS CRM1 W142A
P143A C528S-HA + LMB

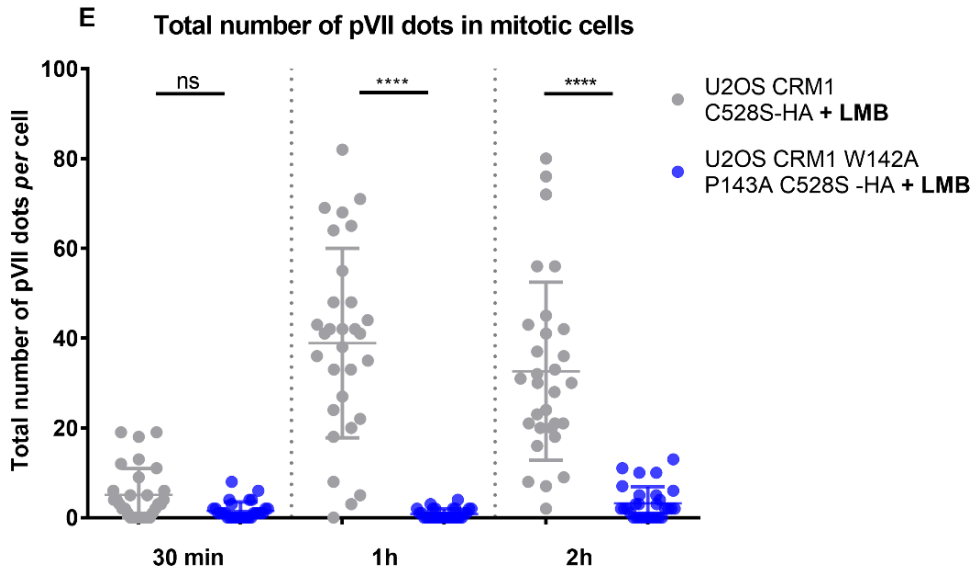

Figure 30. Ad5 genome release cannot be rescued after 2 h of infection in mitotic CRM1 W142A P143A C528S-HA expressing cells. (Fig A p111 ; Fig B, C and D p112) U2OS or U2OS CRM1-HA expressing cells were treated with colcemid for 14 to 16h to synchronise cells in mitosis. Infection with Ad5-GFP particles was performed for 30 min to 2 h in the absence (U2OS cells) or presence (+ LMB) of LMB. Cells were fixed and stained with anti-HA (magenta), anti-Ad5 capsids (red), anti-pVII (green) antibodies and with DAPI (grey) for chromatin staining. (A) Confocal images of cells after 1 h of infection. Cells were imaged by confocal microscopy and maximal projection images of cells are shown. (Scale bars,10 µm). (B, C, D, E) Scatter plots showing quantifications of total pVII foci per cell. Quantifications of U2OS not treated with LMB are depicted in black; U2OS LMB treated cells in red; U2OS CRM1 C528S-HA in grey and U2OS CRM1 W142A P143A C528S-HA in blue. Mean values (+/- SD) of 30 cells per condition are shown. Statistical analysis was performed using one-way ANOVA multicomparison test.

II.5 CRM1 W142A P143A delays the first steps of Ad5 infection

The next step after capsid disassembly is genome nuclear import, leading to Ad5 gene expression. As at 2 h pi capsid disassembly is strongly impaired in CRM1 W142A P143A C528S-HA cells, we analysed Ad5 genome import, expecting the same phenotype as in LMB treated U2OS cells: accumulation at the MTOC and no genome imported. We infected and fixed U2OS and CRM1-HA cells at different time points and monitored the number of nuclear genomes by quantifying nuclear pVII dots overtime (Figure 31). Again, in CRM1 C528S-HA cells, the effect of LMB was rescued (Figure 31 B and C). In CRM1 W142A P143A C528S-HA cells, Ad5 capsids accumulated initially to similar levels observed in U2OS cells treated with LMB. Co-staining of Ad5 capsids and pericentrin (Figure 32) showed an accumulation at the MTOC, like in LMB treated U2OS cells. Only when we analysed later time points in such cells, genomes started to be imported. At 2 h pi, nuclear pVII dots started to be detected, and this number increased at 4 h pi. The LMB phenotype observed during the first 2 h pi was rescued, but this rescue was severely delayed compared to control cells (Figure 31 D and E).

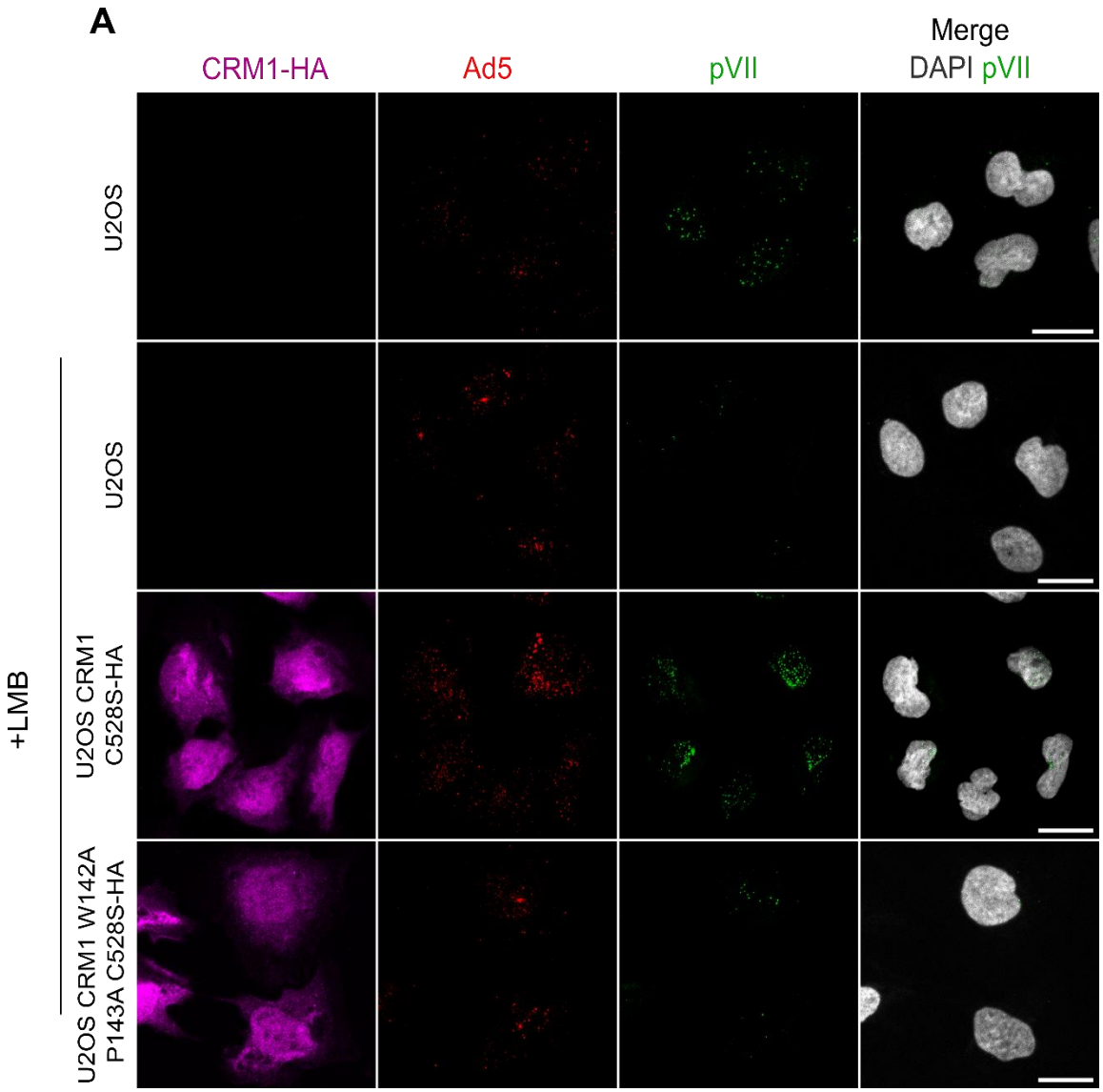
A
CRM1-HA
Ad5
pVII
Merge
DAPI pVII
U2OS
U2OS
U2OS CRM1 C528S-HA
U2OS CRM1 W142A P143A C528S-HA
+LMB
B
Quantification of nuclear Ad5 genomes in cells
Total number of nuclear pVII dots per cell
150
100
50
0
****
****
****
****
30min
1h
2h
4h
U2OS + LMB
U2OS CRM1 C528S-HA + LMB

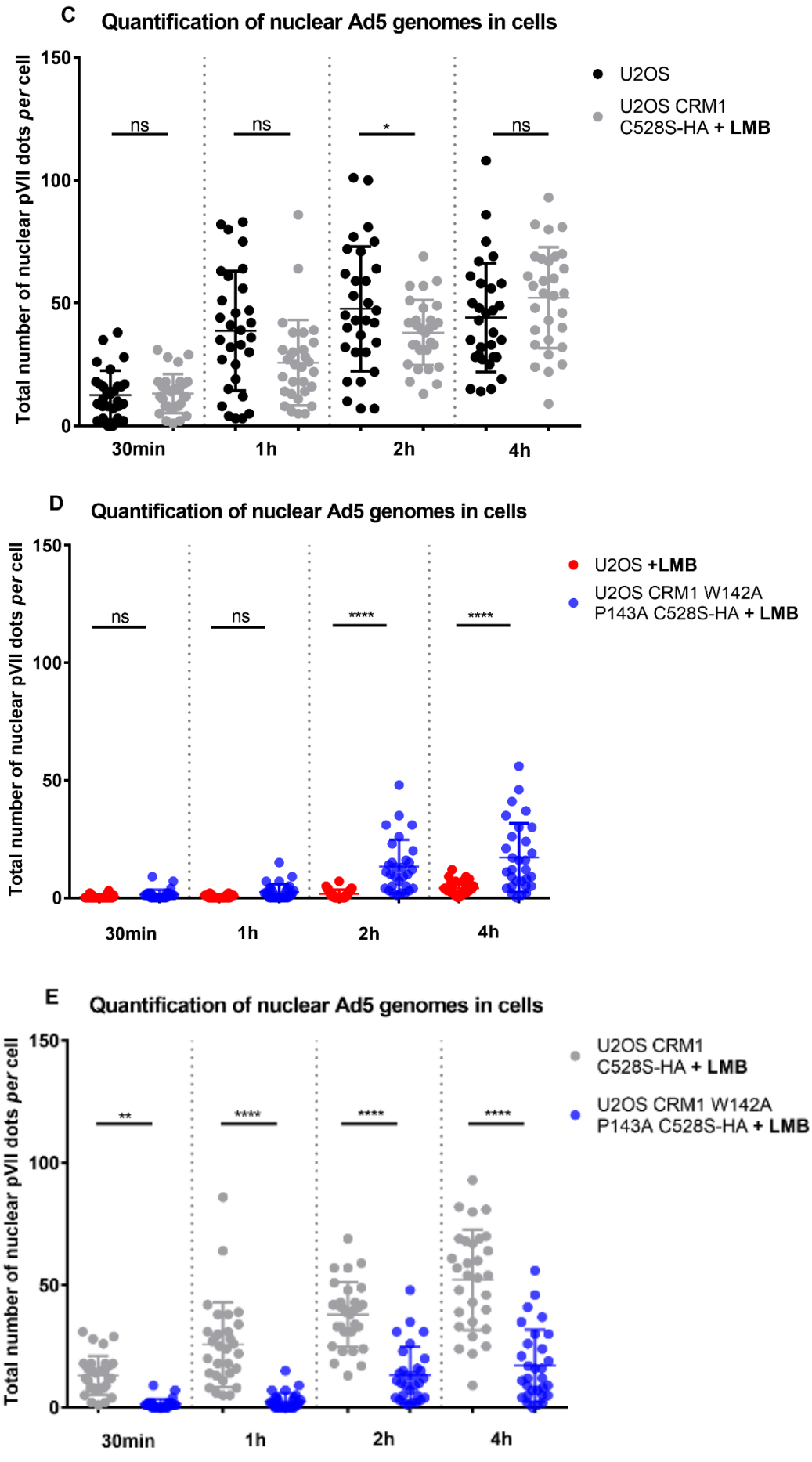
C
Quantification of nuclear Ad5 genomes in cells
Total number of nuclear pVII dots per cell
150
100
50
0
ns
ns
*
ns
30min
1h
2h
4h
U2OS
U2OS CRM1
C528S-HA + LMB
D
Quantification of nuclear Ad5 genomes in cells
Total number of nuclear pVII dots per cell
150
100
50
0
ns
ns
****
****
30min
1h
2h
4h
U2OS +LMB
U2OS CRM1 W142A
P143A C528S-HA + LMB
E
Quantification of nuclear Ad5 genomes in cells
Total number of nuclear pVII dots per cell
150
100
50
0
**
****
****
****
30min
1h
2h
4h
U2OS CRM1
C528S-HA + LMB
U2OS CRM1 W142A
P143A C528S-HA + LMB

Figure 31. Ad5 genome import is slower in CRM1 C528SW142A P143A-HA expressing U2OS. (Fig A and B p 115; Fig C, D and E p116) U2OS or U2OS CRM1-HA expressing cells were infected with Ad5-GFP particles for 30 min to 4 h in the absence (U2OS cells) or presence (+ LMB) of LMB. Cells were fixed and stained with anti-HA (magenta), anti-Ad5 capsids (red), anti-pVII (green) antibodies and with DAPI (grey) for chromatin staining. (A) Confocal images of cells after 2 h of infection. Cells were imaged by confocal microscopy and maximal projection images of cells are shown. (Scale bars, 20 µm). (B, C, D, E) Scatter plots showing quantifications of total number of pVII foci colocalizing with DAPI signal *per* cell. Quantifications of U2OS not treated with LMB are depicted in black; U2OS LMB treated cells in red; U2OS CRM1 C528S-HA in grey and U2OS CRM1 W142A P143A C528S-HA in blue. Mean values (+/- SD) of 30 cells *per* condition are shown. Statistical analysis was performed using one-way ANOVA multicomparison test.

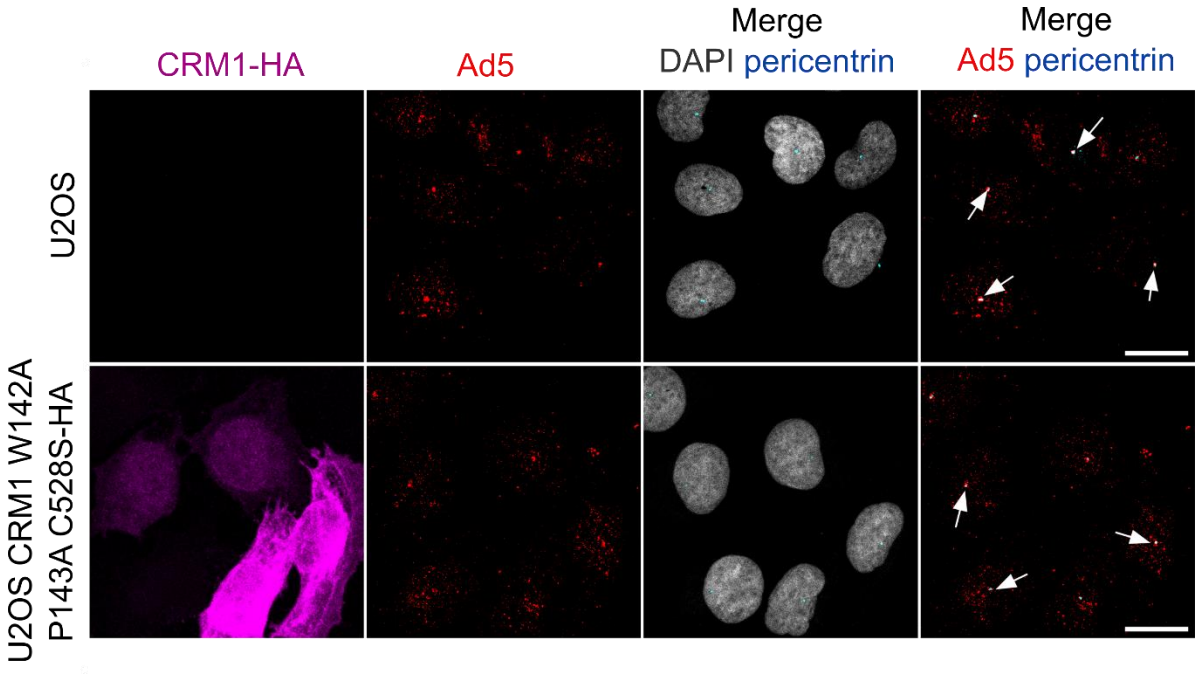

Figure 32. Infection of CRM1 W142A P143A C528S-HA cells leads to accumulation of Ad5 at the MTOC. U2OS cells or U2OS CRM1 W142A P143A C528S-HA expressing cells were treated with LMB for 45 min. Infections with Ad5-GFP particles were performed in the presence of LMB for 1 h. Cells were fixed and stained with anti-HA (magenta), anti-Ad5 capsids (red), anti-pericentrin (cyan) antibodies and DAPI (grey) for chromatin staining. Pericentrin positions and/or colocalization events between pericentrin and Ad5 capsids are shown with white arrows Cells were imaged by confocal microscopy and maximal projection images are shown. (Scale bars, 20 µm).

Ad5 genome nuclear import was not totally blocked in CRM1 W142A P143A C528S-HA cells upon LMB treatment. Indeed, after 2 h pi, genomes started to be imported, suggesting that this mutant induced a slowdown of the genome delivery, but was still functional. To confirm that CRM1 W142A P143A C528S-HA could overcome the LMB phenotype with a delay, we monitored E1A mRNA transcription using the RNAscope technology (Figure 33). As expected, CRM1 C528S-HA rescued LMB effect and promoted E1A transcription (Figure 33 B and C). Regarding the CRM1-HA triple mutant, the effect of rescue was only observed later, 6 h pi (Figure 33D and E).

Together, these results show that genome import and downstream E1A gene expression steps were delayed upon expression of the CRM1 W142A P143A C528S-HA mutant.

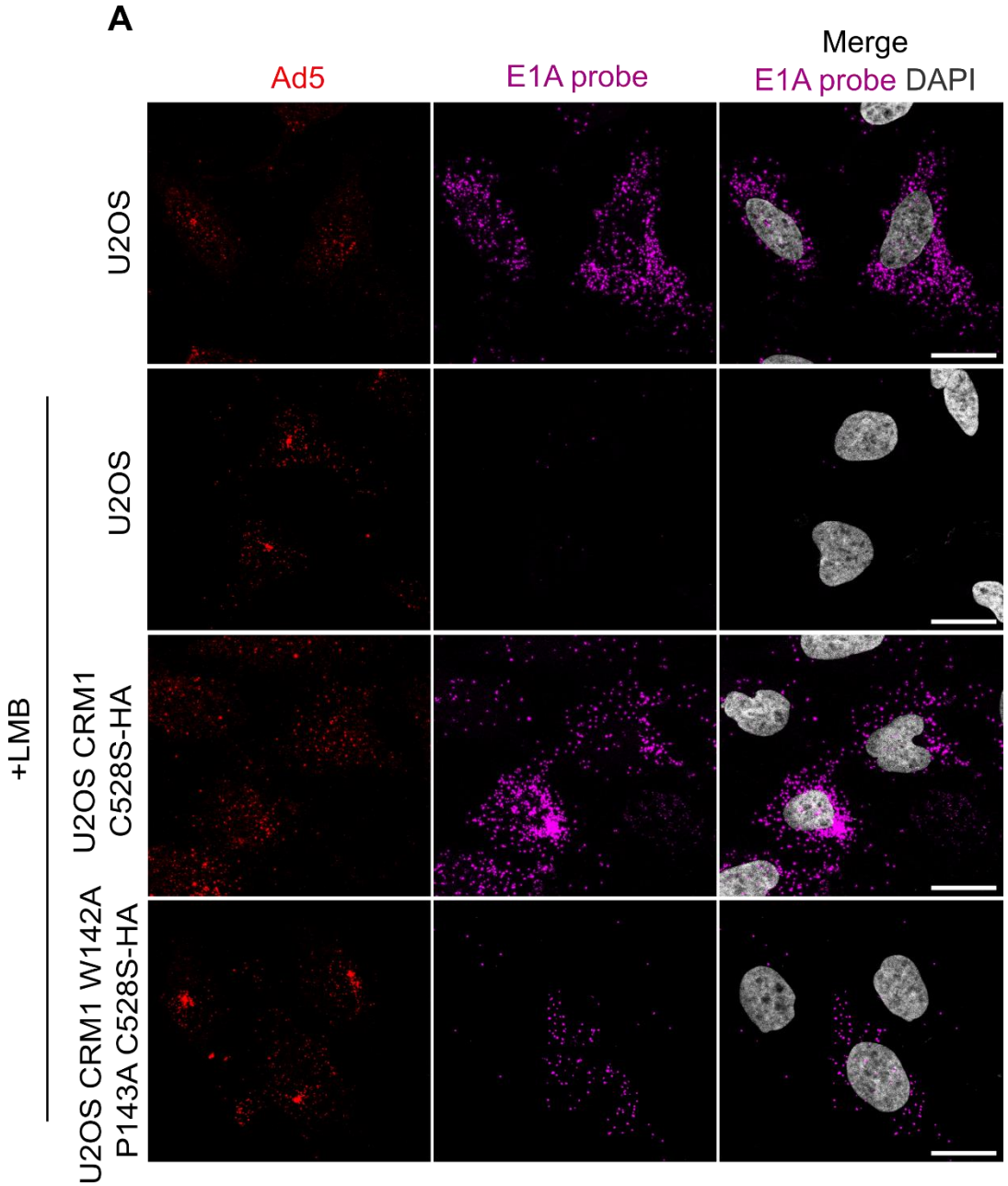

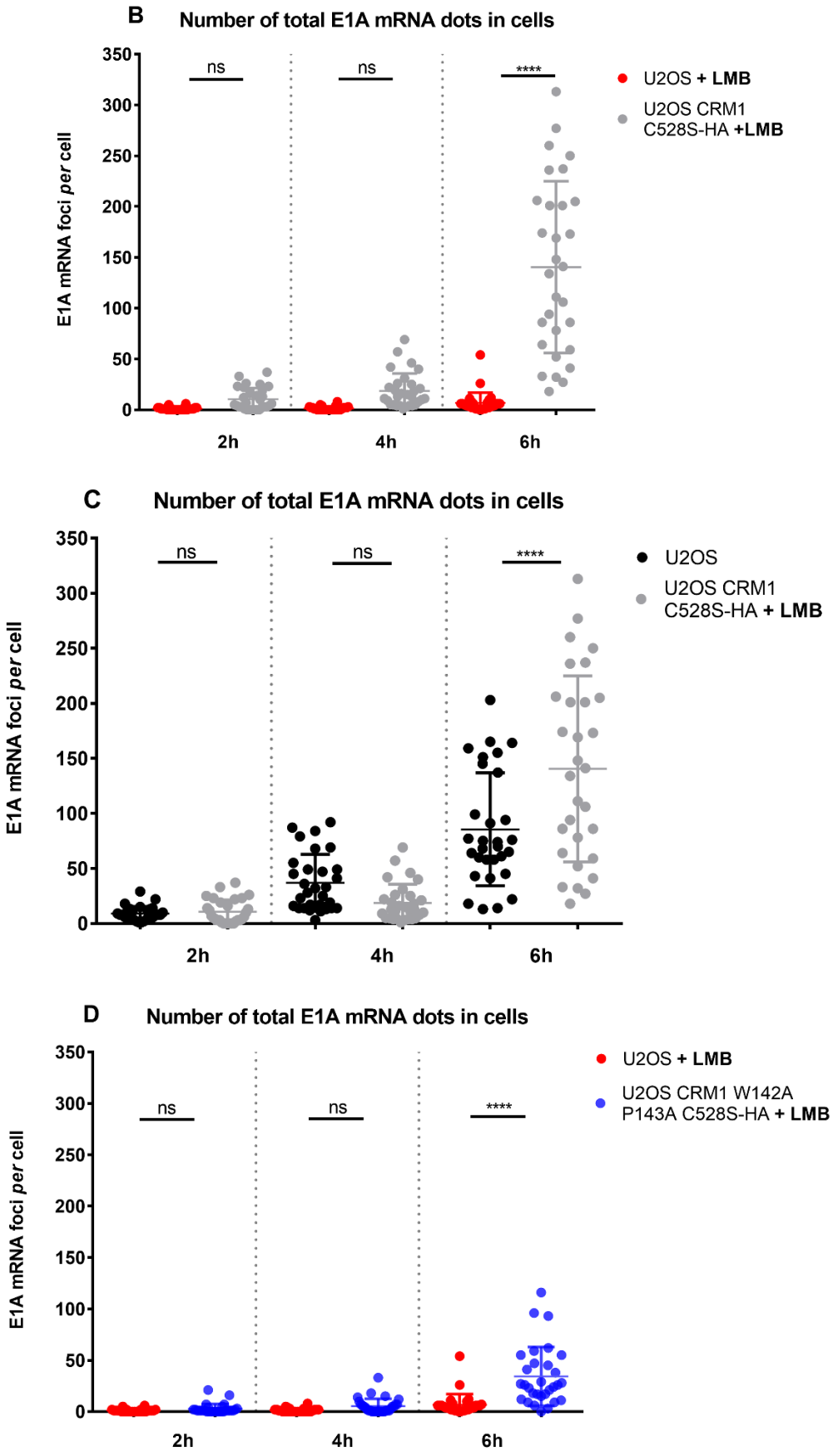
B
Number of total E1A mRNA dots in cells
E1A mRNA foci per cell
350
300
250
200
150
100
50
0
ns
ns
****
2h
4h
6h
U2OS + LMB
U2OS CRM1 C528S-HA +LMB
C
Number of total E1A mRNA dots in cells
E1A mRNA foci per cell
ns
ns
****
2h
4h
6h
U2OS
U2OS CRM1 C528S-HA + LMB
D
Number of total E1A mRNA dots in cells
E1A mRNA foci per cell
ns
ns
****
2h
4h
6h
U2OS + LMB
U2OS CRM1 W142A P143A C528S-HA + LMB

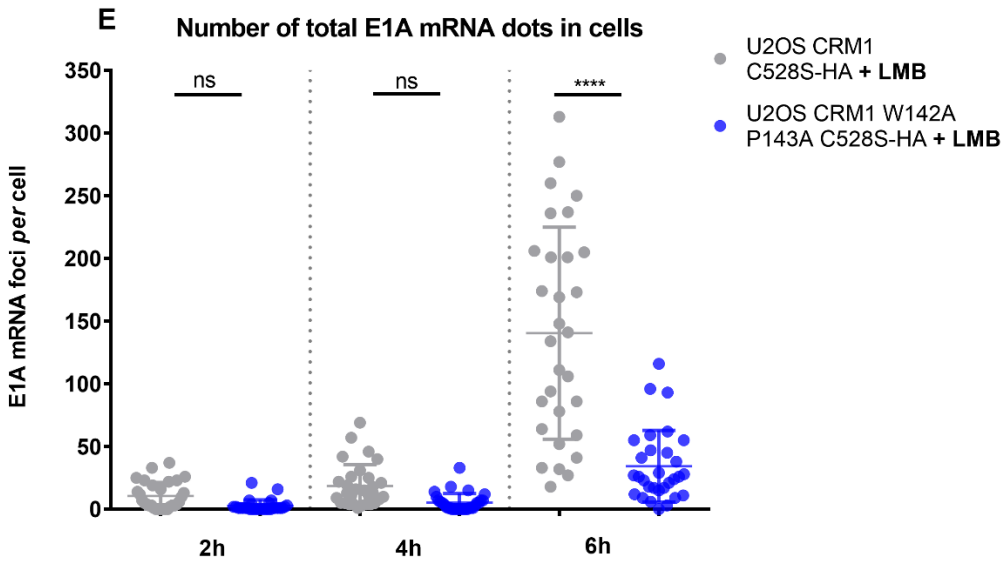

Figure 33. Ad5 E1A gene expression is delayed in U2OS CRM1 W142A P143A C528S-HA cells. (Fig A p 118; Fig B, C and D p 119) U2OS cells or U2OS CRM1-HA expressing cells were infected with Ad5 replicative particles for 2 h to 6 h in the absence (U2OS cells) or presence (+ LMB) of LMB. Cells were fixed and E1A transcripts (magenta) were detected using specific RNA probes (RNAscope). A second staining using antibodies was used to detect Ad5 capsids (red) and a DAPI (grey) staining for chromatin. (A) Confocal images of cells after 6 h of infection. Cells were imaged by confocal microscopy and maximal projection images of cells are shown. (Scale bars, 20 µm). (B, C, D,E) Scatter plot showing the quantification of the total number of E1A foci signal per cell. Quantifications of U2OS not treated with LMB are depicted in black; U2OS LMB treated cells in red; U2OS CRM1 C528S-HA in grey and U2OS CRM1 W142A P143A C528S-HA. Mean values (+/- SD) of 30 cells per condition are shown. Statistical analysis was performed using one-way ANOVA multicomparison test.

As a last assay to monitor Ad5 infection in U2OS CRM1-HA cells, we performed a plaque assay experiment. In this assay, cells were infected with different low Multiplicity of Infection (MOI) (1; 0.1 and 0.01). 24 h pi, cells were overlayed with agarose to prevent dissemination of viruses so that only the cells in a close proximity of an initially infected cell can be infected, and form a plaque. Five to six days later, plaques can be observed under a microscope. A plaque is resulting from the infection of one cell and the dissemination of newly synthetized viruses to the neighbour cells. We performed this assay in U2OS CRM1-HA cells in order to compare their infectivity. We infected cells with different MOIs and 6 days pi the total number of plaques *per* condition was counted (Figure 34).

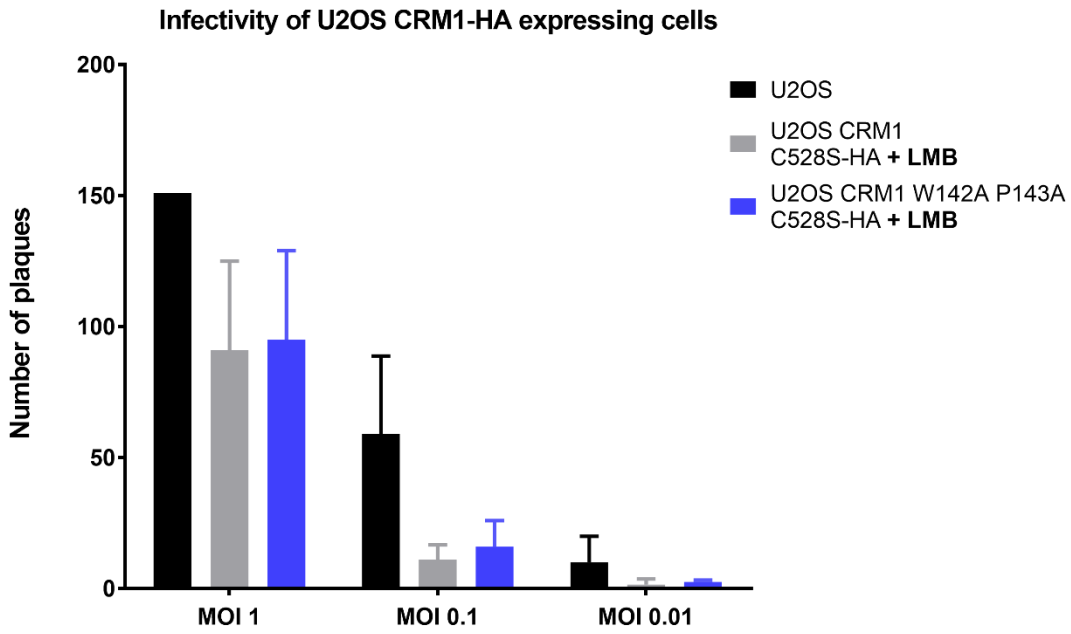

Figure 34. Both CRM1-HA U2OS cell lines have the same infectivity. Plaque assays were performed on U2OS, U2OS CRM1 C528S-HA (grey) and U2OS CRM1 W142A P143A C528S-HA (blue) cells. Ad5 was added at different MOI: 0, 0.1 and 0.01. 2 nM of LMB was added to CRM1-HA expressing cells whereas no LMB treatment was performed on U2OS cells. 6 days post-infection, plaques were counted using bright field microscopy and the total number of plaques per condition was plotted on the graph. Bars depict the standard deviation from the mean of two independent experiments.

As shown above, significant differences were observed between U2OS CRM1-HA cells within the first steps of infection resulting in a delayed infection and gene expression for the W142A P143A mutant. However, 6 days pi no difference was observed in number of plaque formed, suggesting that in the late phase of infection, the delay observed after few hours of infection has no consequences. These results show that the delay induced by the mutant of CRM1 impacts only early phases of infection. Interestingly, during our kinetic analyses of genome import and gene expression, CRM1 C528S-HA was found to promote these steps, compared to U2OS cells. However, much more plaques were counted in the population of U2OS infected cells compared to CRM1 C28S cells-HA. This observation is in line with the cell growth analysis that we performed (Figure 27). This artificial system has limits and cannot totally rescue the phenotype observed in U2OS cells.

Interestingly, CRM1 W142A P143A C528S is also able to promote genome import and gene expression, downstream events of capsid disassembly. This mutant is functional, but somewhat slower than CRM1 wild type. The proteins with an NES were correctly exported in these CRM1 triple mutant cells (Figure 29), thus were available in the cytoplasm for a hypothetical interaction with Ad5. However, despite the availability of the cargoes of CRM1, a delay was observed upon Ad5 infection. This result reinforces the idea of a direct interaction between Ad5 and CRM1.

II.6 Purification of recombinant CRM1

We further investigated potential reasons for the export delay observed with the CRM1-HA triple mutant using biochemical assays. To perform our biochemical studies, we used a codon optimized version of CRM1 (gift from Prof. Dr. R. Ficner). We introduced the corresponding mutations and an HA-tag in addition to a His-tag, to the C-terminal part (Figure 35).

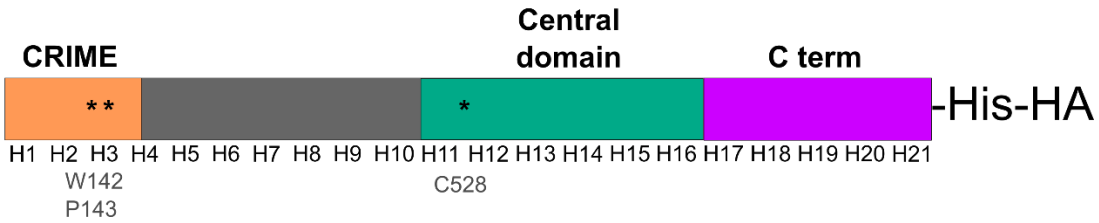

Figure 35. Introduction of point mutations in CRM1. Structure of the CRM1 W142A P143A C528S mutant, with the introduced point mutations depicted with (*).

Purification of recombinant CRM1 was performed based on previous established protocols (see section IV.4.c Purification of CRM1 in Material and Methods). Coomassie staining of eluted fractions from the MonoQ column revealed the presence of CRM1 (band ~120kDa) but in addition, contamination products (band ~70 kDa) were collected for each construct (Figure 36 A to D). Moreover, the intensity of this lower band was higher upon the purification of the triple mutant of CRM1 compared to the two others. These contamination products were the result of degradation of CRM1, since they reacted with anti-CRM1 antibodies in Western blotting analyses (Figure 36 E). To get rid of this degradation product and increasing the purity of CRM1, only the first eluted fractions were pooled (B10 to C1) and concentrated for our further assays.

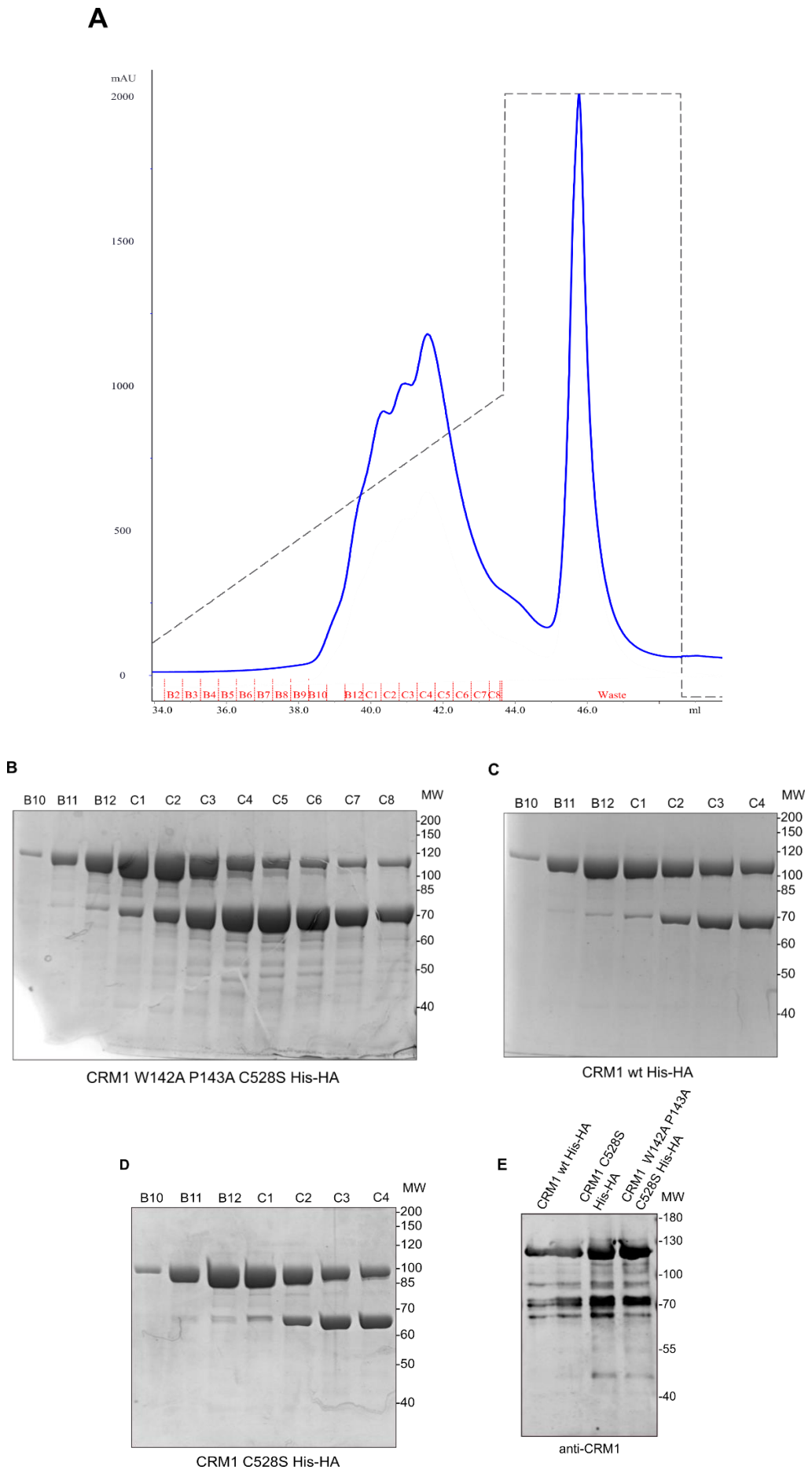
A
mAU
2000
1500
1000
500
0
B2 B3 B4 B5 B6 B7 B8 B9 B10 B12 C1 C2 C3 C4 C5 C6 C7 C8
Waste
34.0
36.0
38.0
40.0
42.0
44.0
46.0
ml
B
B10 B11 B12 C1 C2 C3 C4 C5 C6 C7 C8
MW
200
150
120
100
85
70
60
50
40
CRM1 W142A P143A C528S His-HA
C
B10 B11 B12 C1 C2 C3 C4
MW
200
150
120
100
85
70
60
50
40
CRM1 wt His-HA
D
B10 B11 B12 C1 C2 C3 C4
MW
200
150
120
100
85
70
60
50
40
CRM1 C528S His-HA
E
CRM1 wt His-HA
CRM1 C528S His-HA
CRM1 W142A P143A C528S His-HA
MW
180
130
100
70
55
40
anti-CRM1

Figure 36. Purification of CRM1 His-HA proteins leads to degradation products. (previous page) Purification of CRM1 His-HA tagged proteins were performed using a MonoQ anion exchange column and 500 µL fractions were eluted with a salt gradient. (A) Graph showing the elution profile (blue line) of CRM1 W142A P143A C528S His-HA from the MonoQ column. The salt concentration is depicted by the grey dotted line. (B) 10 µL of fractions B10 to C8 from the MonoQ elution (graph (A)) were analysed by SDS-PAGE electrophoresis followed by coomassie staining. (C and D) Same as (B), for CRM1 His-HA wt (C) and CRM1 C528S His-HA (D). (E) Western blotting analysis of recombinant CRM1 His-HA tagged proteins using anti-CRM1 antibodies.

II.7 CRM1 W142A P143A C528S has slight export kinetic defects

Our *in vivo* data using transfected cells showed that CRM1 mutants C528S and W142A P143A C528S were functional with respect to nuclear export of different cargoes (Figure 29). For a more quantitative analysis, we performed *in vitro* export assays (Kehlenbach et a.1998). Briefly, HeLa cells expressing the CRM1 cargo NFAT tagged with GFP were permeabilized using digitonin, and incubated with a reaction mix containing an ATP-regenerating system, Ran wt loaded with GTP and recombinant CRM1 (Figure 37). Export of GFP-NFAT was analysed by FACS and a decrease of the GFP signal was the result of GFP-NFAT nuclear export.

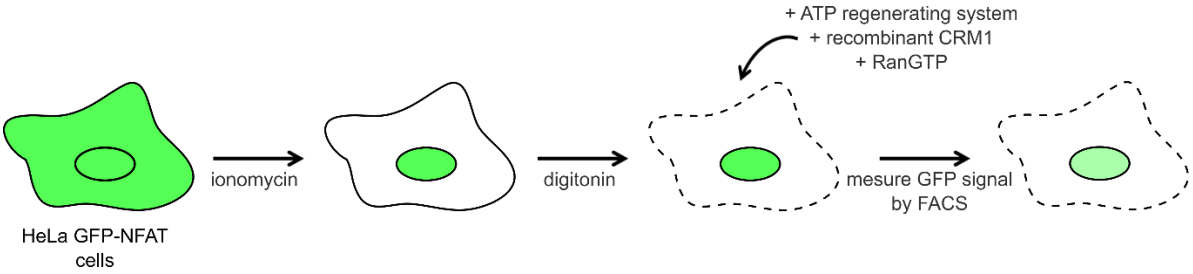

Figure 37. NFAT export assay to measure the CRM1 mediated export. HeLa GFP-NFAT expressing cells were treated with ionomycin to induce import of the GFP-NFAT construct and treated with digitonin to permeablize the cells and remove the cytosolic components. A mix containing an ATP renegerating system, recombinant CRM1 and RanGTP was added and the GFP fluorescence signal was measued by flow cytometry. A decrease in the GFP signal indicated nuclear export of GFP-NFAT.

To compare the efficiency of CRM1 in export reactions, we first performed a titration assay (Figure 38 A), with increased concentrations of recombinant CRM1 (wild type, C528S or W142A P143A C528S). A decrease of the GFP signal was observed under every condition, showing that the recombinant CRM1 variants were functional for export. However, the efficiency of export upon addition of the triple mutant was weaker than the wild type and C528S. A plateau of maximum export was reached with a concentration of 125 nM of CRM1 wild type and CRM1 C528S but the same level of export required addition of around 3 times more of the CRM1 triple mutant (~415 nM). 20% more of GFP fluorescence was observed all along this assay with CRM1 W142A P143A C528S compared to the controls.

A higher concentration of this mutant was necessary to reach the same export ratio than CRM1 wild type.

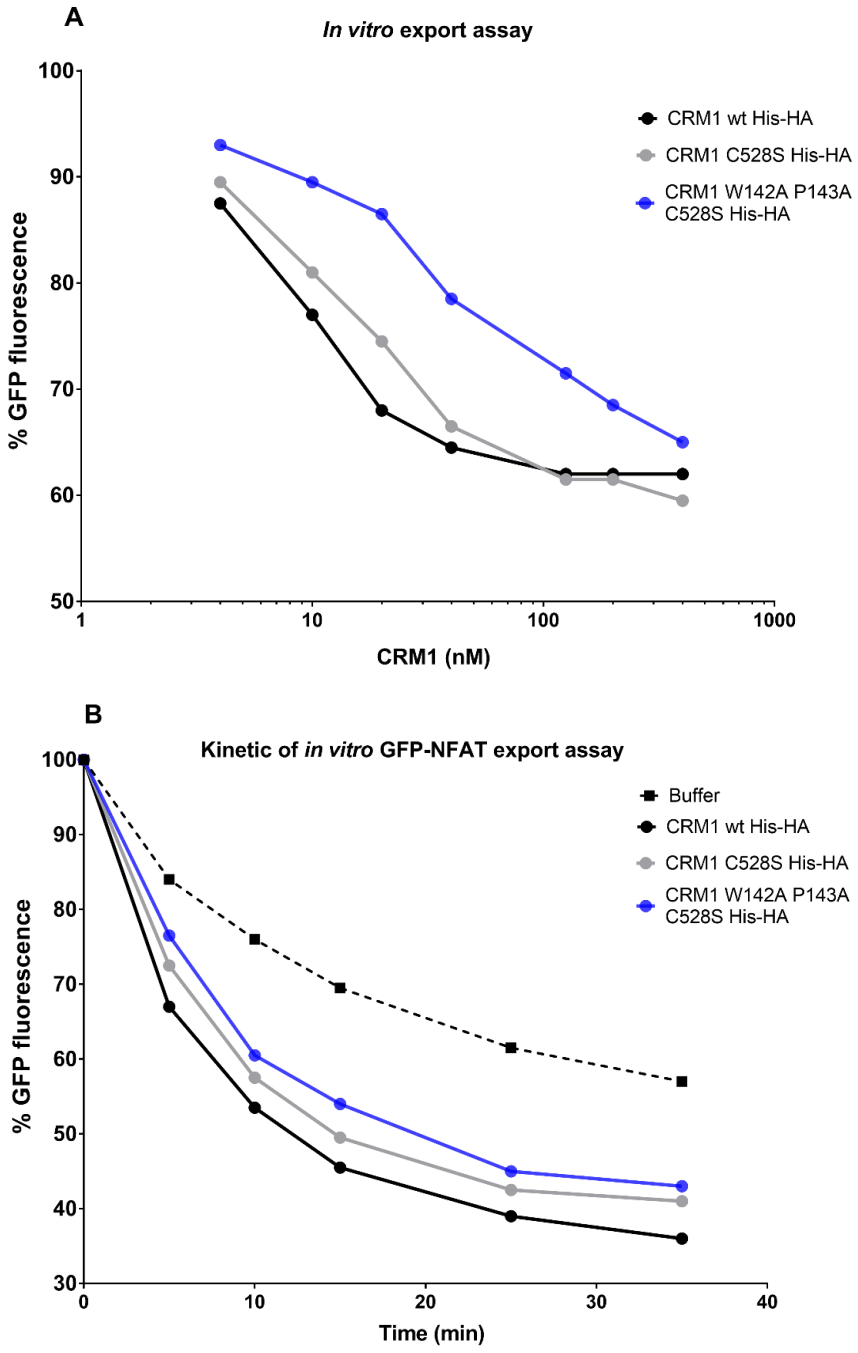

Figure 38. Recombinant CRM1 W142A P143A C528S is functional for export. GFP-NFAT fluorescence was measured by flow cytometry analysis after export reactions with recombinant CRM1 proteins: CRM1 wild type (black dots), CRM1 C528S (grey dots) and CRM1 W142A P143A C528S (blue dots). Means of the median GFP signals from 2 independent experiments were normalized to the fluorescence value obtained without addition of CRM1 and plotted on the graph. (A) GFP fluorescence was measured after 35 min with increasing concentrations of recombinant CRM1 proteins and an excess of RanGTP. (B) GFP fluorescence was measured over time (0 to 35 min) after addition of 125 nM of CRM1 and an excess of RanGTP. Transport buffer (black squares) was added as a control.

As the plateau was reached with addition of 125 nM of recombinant CRM1 wild type, we chose this condition to perform kinetics export assay (Figure 38 B). Buffer alone was added as a negative control. The export reaction was stopped at different time points and the residual GFP fluorescence was measured. As shown before, export of GFP-NFAT could be observed upon addition of the three different forms of CRM1. In our titration assay (Figure 38 A), upon addition of 125 nM of protein, about 10% more GFP fluorescence signal was measured when CRM1 W142A P143A C528S was added compared to CRM1 wild type. This result was consistent with the previous kinetic assay, where at every time point 10% more GFP fluorescence was measured. Taken together, these results showed that CRM1 W142A P143A C528S is functional for export *in vitro*, but is less efficient than CRM1 wild type.

II.8 CRM1 W142A P143A has a lower affinity for NES

The defect observed upon infection of CRM1 W142A P143A C528S U2OS cell lines was not due to an absolute lack of export function in this CRM1 mutant Figure 29and Figure 38). However, quantitative export assays revealed a less efficient export of the GFP-NFAT construct with this mutant. Although the mutations are far away from the NES-binding cleft (see Figure 25 and Figure 35), this difference could be explained by a weaker affinity for NESs in general. To test this hypothesis, and compare the Kd of CRM1 wild type and CRM1 mutant for an NES, we performed fluorescence polarization assays with recombinant CRM1 and a fluorescent NES-peptide. We chose to analyse the affinity of CRM1 for the NES of the PKI (PKI-NES), known to have a high affinity for CRM1 (Paraskeva et al. 1999; Fu et al. 2018).

The assay relies on the ratio between the emission of polarized light used to excite a fluorophore, and the actual polarized light emitted after excitation of the fluorophore. Molecular complexes in solution have a slow motion compared to free molecules: the quantity of polarized light emitted by a fluorophore within a complex is higher than a free fluorophore in solution. An increase of the polarized light signal thus indicates complex formation (i.e between CRM1, RanGTP and the NES peptide). The PKI-NES sequence was synthetized as a 17 mer sequence, bound to a fluorophore. To determine the Kd, increasing concentrations of recombinant CRM1 were added to the peptide, in the presence of the C-terminal truncated version of RanQ69L-GTP$^{1-180}$ (Monecke et al. 2009) to induce complex formation. The binding of CRM1 to NESs is dependent on RanGTP (Fornerod et al. 1997b). In our assay, binding affinities between CRM1 wild type and CRM1 C528S with PKI-NES were comparable (Kd ≈ 35 nM; Kd ≈ 40 nM respectively) (Figure 39). However, this affinity was three times lower for the CRM1 triple mutant (Kd ≈105 nM).

These results confirmed our hypothesis about a weaker affinity for NESs in the CRM1 triple mutant. However, from the structure (Figure 25) it is obvious that W142 and P143 are not part of the NES-binding pocket of CRM1.

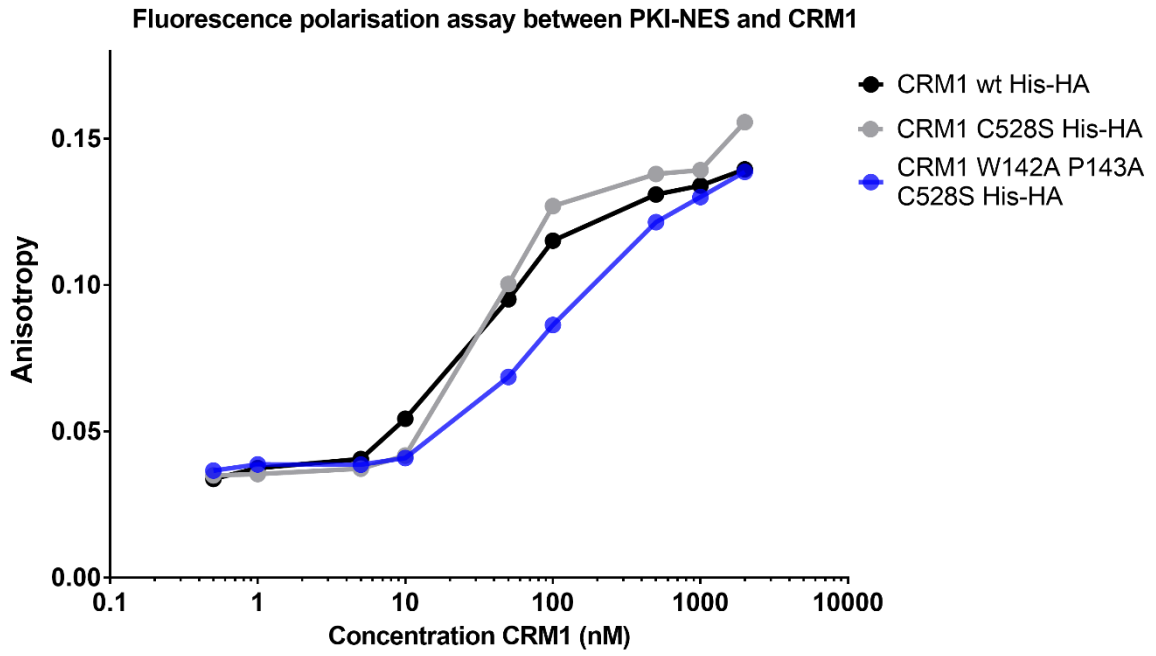

Figure 39. Anisotropy assays reveal a lower affinity of CRM1 W142A P143A C528S for PKI-NES. The PKI-NES peptide tagged with 6-carboxyfluorescein was incubated with increasing concentrations of CRM1 wild type (black dots), CRM1 C528S (grey dots) or CRM1 W142A P143A C528S (blue dots), in the presence of 3 µM RanQ69L-GTP1-180 (or 6 µM of RanQ69L-GTP1-180 for concentrations of CRM1 higher than 1000 nM). The ratio of the polarized light to the total light intensity (Anisotropy) was measured with a FluoroMax-4 device and plotted on the graph.

Our biochemical analyses revealed an efficient export of GFP-NFAT upon addition of the CRM1 triple mutant. However, at the same concentration, the level of export was weaker with this mutant compared to CRM1 wt. This defect was also identified in kinetics measurements. CRM1 W142A P143A C528S-HA showed a weaker affinity for the PKI-NES, compared to the Kd measured with CRM1C528S-HA. Thus, differences in Kds measured upon our anisotropy assays could explained the slight effects measured during our *in vitro* export assay.

III. Terminal Protein as a potential substrate of CRM1

After cell entry, the release of the pVI structural protein and the disruption of endosomes impair capsid integrity, leading to partial capsid disassembly (Wiethoff et al. 2005). As shown with our live cell-imaging data (Figure 24), partially disassembled capsids expose their genomes before their total release. Total genome-capsid dissociation is blocked by LMB, suggesting a role for CRM1 during this process. Moreover, such effects of LMB suggest the requirement for a CRM1-NES interaction for the total dismantling of the Ad5 capsid. Little is known about Ad5 proteins harbouring NESs. E1A, E1B-55K and E4orf6 are AdV proteins known to contain an NES (Jiang et al. 2006; Kindsmüller et al. 2007; Weigel and Dobbelstein 2000). However, these proteins are expressed in late stages of AdV cycle, after nuclear genome import, therefore not present in newly infectious particles.

To explain the inhibition of genome release upon LMB treatment, we hypothesized that within the partially disassembled state of Ad5 capsid upon entry, a virally encoded and virion associated NES might be sufficiently exposed to be recognised by CRM1. This NES could be found either on a structural protein (capsid protein) or directly on a core protein. Interestingly, we found a predicted NES in the TP, a core protein of Ad5 that is covalently attached to each end of the viral genome (Rekosh et al. 1977). We focused our next analysis on the study of this predicted NES to investigate if this intricate link to the viral genome could explain the role of CRM1 in capsid disassembly and genome release.

III.1 Terminal Protein interacts with chromatin

TP is found in two copies *per* virion, covalently bound to both extremities of the Ad5 genome. TP protects Ad5 genome from exonuclease degradation and promotes vDNA replication by stabilizing the replication complex and anchoring the genome to the nuclear matrix (Rekosh et al. 1977; Schaack et al. 1990; Komatsu et al. 2018). Synthetized as a precursor (pTP), this protein is cleaved by the AdV protease before the release of newly synthetized virions. The site of cleavage in pTP has been mapped in its N-terminal part (Webster et al. 1994). pTP contains an NLS and the function of this sequence in nuclear import of the AdV polymerase has been discussed (Zhao and Padmanabhan 1988). The site of cleavage in pTP is placed upstream of this NLS (Webster et al. 1994). Therefore, this NLS is conserved in the mature form of TP. When GFP-TP construct was transfected in U2OS cells, it showed a clear interaction with chromatin, in interphase and mitotic cells (Figure 40). Mutation of this Chromatin Binding Site (CBS) domain led to the loss of interaction with cellular chromatin and to the homogeneous redistribution of TP within the cell.

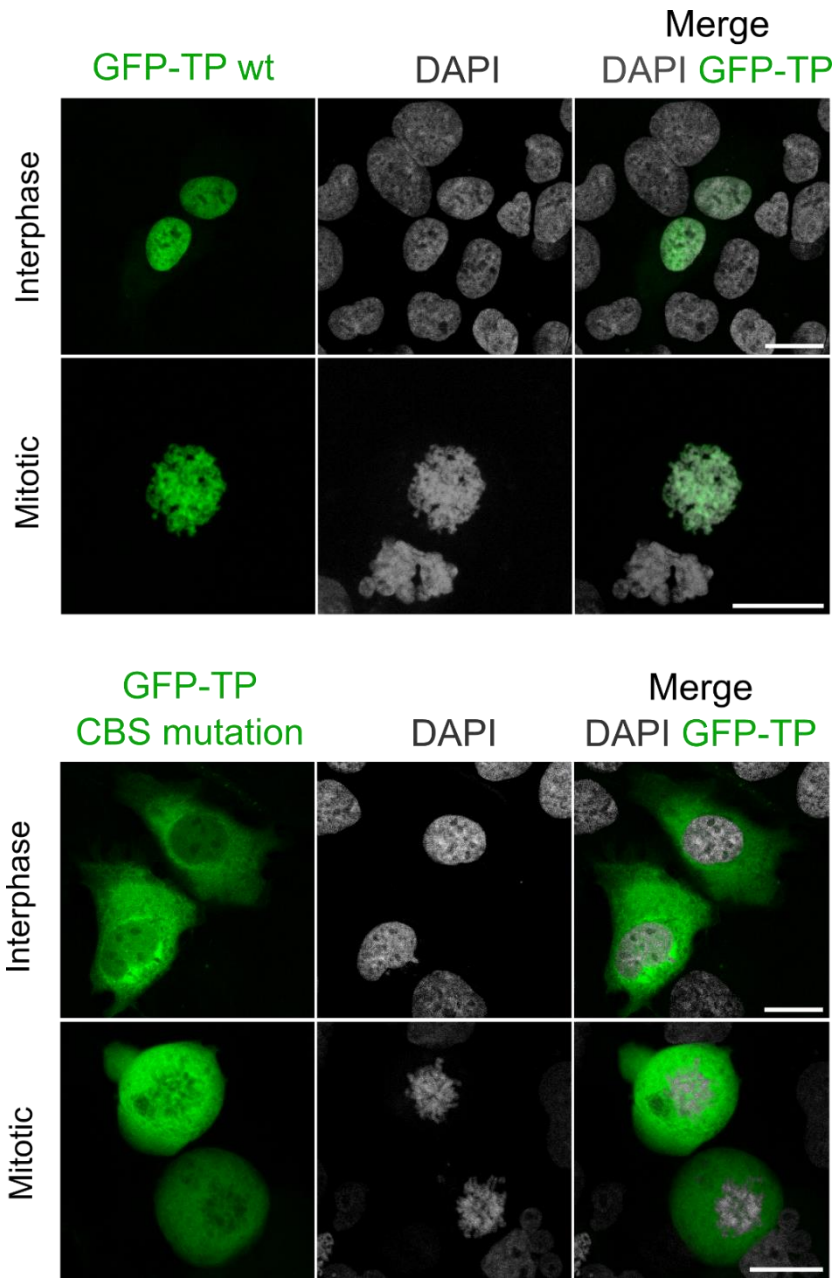

Figure 40. The chromatin binding site targets Ad5 Terminal Protein to chromatin. U2OS cells were transfected with a construct coding for GFP-TP, TP wild type (upper panel) or TP mutated for its CBS (lower panel). Mitotic cells (lower row) were synchronised with colcemid treatment for 14 to 16 h prior to fixation. GFP-TP signals (green) and DAPI (grey) staining for chromatin visualisation were used. Cells were imaged by confocal microscopy and maximal projection images of cells are shown. (Scale bars, 20 µm).

Due to the strong affinity of this CBS with the chromatin, we performed our following analyses with the GFP-TP constructs mutated for the CBS.

III.2 Terminal Protein is sensitive to LMB treatment

To test the possible interaction of CRM1 with TP, we transfected cells with a construct coding for GFP-TP (mutated for CBS) and analysed TP localization after LMB treatment. Upon addition of LMB, the homogeneous distribution of GFP-TP was impaired, in favour of a nuclear retention of GFP-TP (Figure 41). Such phenotype reminds the nuclear retention of RanBP1 upon LMB treatment (see Figure 14). TP is sensitive to LMB effect. This result suggests that TP could be an interacting partner for CRM1 and a CRM1 export cargo.

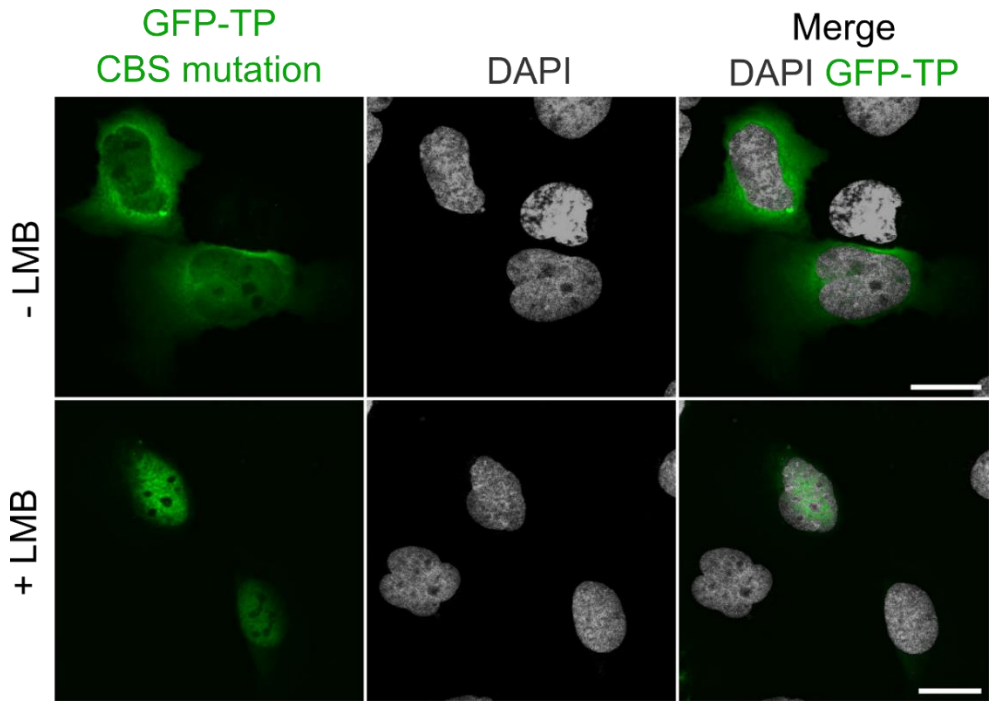

Figure 41. Ad5 Terminal Protein is sensitive to LMB treatment. U2OS cells were transfected with a construct coding for GFP-TP mutated for its chromatin binding site. 24 h post-transfection, cells were treated (+ LMB) or not (- LMB) with LMB for 45 min. Cells were fixed and stained with DAPI (grey) for chromatin staining. GFP-TP signals are depicted in green. Confocal images of transfected cells imaged by confocal microscopy. Maximal projection images of cells are shown. (Scale bars, 20 µm).

III.3 NES of Terminal Protein is functional

CRM1 recognises its cargo via the binding of a consensus NES. These sequences contain a set of five spaced hydrophobic amino acids. The nature of these hydrophobic residues and the spacing between them define the affinity of the sequence for CRM1. Consensus NES have been redefined as $\Phi^0\Phi^1\text{-}(x)_{2-3}\text{-}\Phi^2\text{-}(x)_{2-3}\text{-}\Phi^3\text{-}x\text{-}\Phi^4$ (Güttler et al. 2010). The predicted NES of TP is as followed: **L**IR**LL**EEE**L**T**V** (with the critical hydrophobic residues underlined). Spacing between hydrophobic residues deviates from the consensus (no spacing between Φ^1 and Φ^2).

To test the functionality of the TP-NES, we introduced point mutations in this sequence: L**A**RLLEEE**A**T**A**. Transfection of this mutant led to a higher GFP nuclear signal, showing a defect in the export of this construct (Figure 42). Inactivation of this NES did not impair the NLS, which explains the nuclear localization of TP. The effect observed upon mutation of the NES was the same than what we observed upon transfection of the wild-type construct in cells treated with LMB, as just shown before (Figure 41), it also induced the nuclear retention of TP. This result confirms the functionality of the TP-NES. TP could indeed be a partner of CRM1, via the binding with this NES sequence.

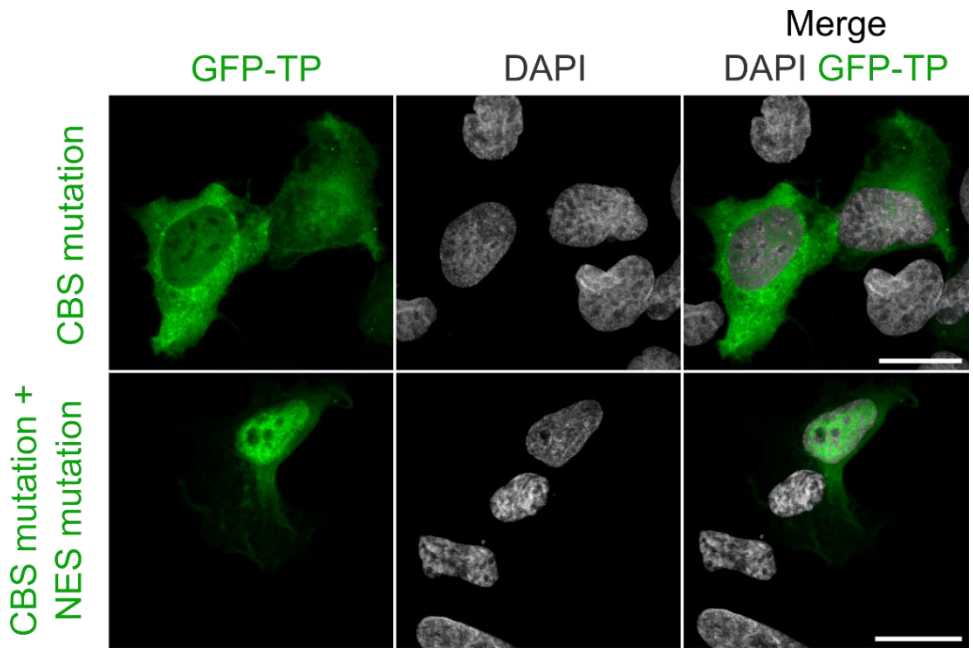

Figure 42. The Nuclear Export Signal of Ad5 Terminal Protein is functional. U2OS cells were transfected with constructs coding for GFP-TP mutated for its chromatin binding site, with (NES mutation) or without a mutation in the NES domain. 24 h post-transfection, cells were fixed and stained with DAPI (grey) for chromatin staining. GFP-TP signals are depicted in green. Confocal images of transfected cells imaged by confocal microscopy. Maximal projection images of cells are shown. (Scale bars, 20 µm).

The presence of an NES in the mature TP has never been studied. The functionality of this NES and the nuclear retention of TP upon LMB treatment are in favour of a CRM1-TP interaction. Further biochemical analyses need to be performed to study in details CRM1-TP interaction, but we developed some tools to confirm these preliminary data (see Appendix).

DISCUSSION

I. Interaction of Ad5 at the MTOC

Replication of Ad5 takes place in the nucleus. After cell entry, Ad5 needs to reach the nuclear compartment. Despite some controversies about a microtubule-independent transport of Ad5 (Glotzer et al. 2001; Yea et al. 2007), most scientists agree that traffic of Ad5 towards the nucleus is a movement mediated by the microtubule transport machinery. This mechanism of transport involves interactions between the microtubule motor dynein and the Ad5 capsid protein hexon (Suomalainen et al. 1999; Bremner et al. 2009; Kelkar et al. 2004). In addition, the anterograde transport motor Kinesin-1 also interacts with Ad5 (Strunze et al. 2011; Gazzola et al. 2009; Zhou et al. 2018). Thus, Ad5 is subject to a bi-directional transport in the cytoplasm. Several aspects of this traffic are characterized in detail. Physical integrity of microtubules is required for nuclear targeting of Ad5 (Suomalainen et al. 1999; Mabit et al. 2002). In contrast, the dynamic (balance of polymerization-depolymerization of tubulin) of this network is not necessary for Ad5 trafficking (Suomalainen et al. 1999; Mabit et al. 2002; Giannakakou et al. 2002). Moreover, once Ad5 reached the NE, right before nuclear import of viral DNA, the integrity of microtubules is not required anymore (Mabit et al. 2002; Leopold et al. 2000). Although some studies point to a passage through the MTOC before NE targeting (Suomalainen et al. 1999; Glotzer et al. 2001; Yea et al. 2007), the reason (if any) for this step is not very well characterized. In mammalian cells, the centrosome is the major MTOC. Thus, the term MTOC referees in the context of this study, to the centrosome. We addressed the question about the nature of interactions occurring at the MTOC and the key players involved in this step during Ad5 infection.

I.1 Ad5 traffic towards the MTOC *prior to* NE targeting

The movement of Ad5 capsids towards and away from the MTOC (Suomalainen et al. 1999), or accumulation of capsids at the mitotic spindle pole in mitotic cells (Leopold et al. 2000) were observed upon Ad5 infections. Depending on the cell lines used, formation of a cluster of Ad5 particles at the MTOC was more or less evident (Yea et al. 2007). During our infection assays, we used U2OS cell lines. 30 min to 1 h pi, immunostainings of Ad5 capsids showed that capsids were localized in close proximity of the MTOC. We also performed asynchronous infections, consisting of a first infection of cells with Ad5 particles, followed 1 h later by a second infection, with new and distinguishable infectious particles. Even after two waves of infection, Ad5 capsids were localized at the MTOC area, showing the tendency of Ad5 to be transported towards the MTOC. Moreover, this assay also showed that cellular factors used for the transport of Ad5 from the first infection were not rate limiting for the particles of the second wave of infection.

Bailey et al. in 2003 showed that absence of nuclear factors (in cells lacking their nucleus) does not impair Ad5 capsids traffic towards the MTOC, but traps viral particles at the MTOC. The authors concluded that nuclear factors are required for removal of Ad5 from the MTOC. Moreover, integrity of the MTOC was required for a stable accumulation in those enucleated cells. Our results in enucleated cells (see Figure 13) confirmed that nuclear factors are not required for transport of Ad5 along microtubules to reach the MTOC after infection. However, the nucleus itself or nuclear factors are involved in translocation of Ad5 from the MTOC to the NE and their absence leads to MTOC accumulation. Thus, most likely, in the absence of a nucleus, the MTOC is the end point of dynein-mediated transport of Ad5.

Microtubule associated proteins or microtubule motor proteins have been shown to be required for the transport and/or uncoating of some viruses. Human Immunodeficiency Virus-1 (HIV-1) and Herpes Simplex Virus -1 (HSV-1) have been shown to interact with dynein and kinesin 1 (Lukic et al. 2014; McDonald et al. 2002; Döhner et al. 2002; DuRaine et al. 2018). Therefore, a bi-directional transport of HIV-1 and HSV-1 has been observed *prior to* their nuclear targeting. Moreover, MTOC localization of HIV-1 particles has been reported after infection (McDonald et al. 2002).

Analysis of Ad5 transport shows also an “exploratory” movement of capsids, a bi-directional transport from the cell periphery to the MTOC and *vice versa* (Suomalainen et al. 1999; Zhou et al. 2018). Several binding sites have been identified on Ad5 capsid, to promote the binding with dynein and kinesin (Gazzola et al. 2009). The role of such switch in the directionality of transport of Ad5 is not clear but may reflect the binding of opposing motors. These observations could reflect a mechanism of defence for the cell, to keep Ad5 away from the nucleus. This bi-directional movement could also avoid a “saturation of system”, to ensure the availability of cellular factors for Ad5. The deletion of Kif5B, a member of the kinesin motor family, induces the blocking of Ad5 capsids at the MTOC (Zhou et al. 2018), and this effect is even increased upon LMB treatment. Hence, binding of Ad5 with Kif5B seems to be required for nuclear translocation. In Ad5 infection, the lack of nuclear factors abolishes Ad5 nuclear targeting and leads to accumulation of capsids at the MTOC. Inhibition of CRM1, a nuclear export factor, has been shown to increase the rate of capsids engaged with microtubules at the MTOC (Strunze et al. 2005; Wang et al. 2017). Taken together, the proximity of Ad5 with the MTOC upon infection and the blocking of Ad5 at the MTOC in absence of a nucleus, absence of functional CRM1 or deletion of Kif5B, show that transport of Ad5 towards the MTOC, *prior to* their nuclear targeting appears to be essential for Ad5, in order to be translocated to the NE. However, it is not known if under these conditions (i.e lack of nucleus, deletion of Kif5B and CRM1 inhibition), Ad5 remain associated with dynein.

An association with components of the MTOC can be envisaged as an intermediate *prior to* NE targeting and may reflect a motor switching at the MTOC.

I.2 Microtubule integrity is not required to maintain the MTOC accumulation of Ad5

The absence of a nucleus, deletion of Kif5B or inhibition of the major exportin CRM1 have been shown to induce MTOC accumulation of Ad5 (Bailey et al. 2003; Strunze et al. 2005). Integrity of microtubules is required for NE targeting of Ad5 (Suomalainen et al. 1999; Mabit et al. 2002), and integrity of the MTOC itself (Bailey et al. 2003) is required to maintain accumulation of Ad5 capsids in enucleated cells. We thus investigated whether microtubules integrity is required once Ad5 reached the MTOC. In our assays, MTOC accumulation of Ad5 was still observed after microtubules depolymerization, independently of the presence or absence of LMB. In addition, removal of cytoplasmic components following cell permeabilization did not disrupt Ad5-MTOC accumulation. Under these conditions, cold incubation or digitonin treatment did not disrupt the integrity of MTOCs, since pericentrin was still detectable. We concluded that integrity of microtubules is not required once Ad5 reached the MTOC and soluble cytoplasmic components are not required to maintain Ad5 at the MTOC. Thus, interaction of Ad5 with the MTOC under these conditions seems to involve factors from the MTOC itself, independently of the microtubule network.

In U2OS cells, the MTOC is composed of two centrioles surrounded by PCM and centriolar satellites (reviewed in (Woodruff et al. 2014; Prosser and Pelletier 2020)). Centriolar satellites are transported towards the MTOC to achieve their function via their interaction with dynein (Kubo et al. 1999). Thus, we cannot exclude a mechanism of unloading of Ad5 from dynein via a competition with centriolar satellites and an interaction of Ad5 capsids with components of the PCM, as intermediates before their NE targeting.

I.3 CRM1 is essential for translocation of Ad5 from the MTOC to the NE

After arrival at the MTOC, Ad5 are unloaded from dynein via an unknown mechanism, before being targeted to the NE. Moreover, it is not clear whether microtubule unloading and NE targeting are mediated by the same factor or are performed via two distinct mechanisms. Our Ad5 infection assays performed in the absence of nuclear factors (in enucleated cells) led to the accumulation of capsids at the MTOC, confirming previous data (Bailey et al. 2003). In 2005, Strunze et al. identified CRM1 as a nuclear factor involved in translocation of Ad5 from the MTOC to the NE. When the recognition of NESs by CRM1 was inhibited via LMB treatment, Ad5 capsids were trapped at the MTOC. Later on, in 2017, Wang et al. analysed the motion of Ad5 at the MTOC. They concluded that in close proximity of the MTOC, the motion of Ad5 was slowed-down, to probably promote their unloading from microtubules, *prior to* NE translocation.

CRM1 inhibition enhanced this motion and inhibited unloading of Ad5 from microtubules. CRM1 is the major exportin in the cell, and forms a trimeric complex with NES cargoes and RanGTP (Fornerod et al. 1997b). Together with RanGTP, a fraction of CRM1 is localized at the centrosome (Liu et al. 2009; Keryer et al. 2003). Although there is no direct evidence, these proteins mostly originate directly from the nucleus. Therefore, unloading of Ad5 from microtubules occurring at the MTOC, observed by Wang et al., and marking the end point of trafficking could be explained by the availability of CRM1 at the MTOC. RanGTP and CRM1 are nuclear factors and removal of nuclei during our assays could also disrupt their localization at the MTOC, explaining the centrosomal retention of Ad5 observed under these conditions.

Infections performed upon LMB treatment showed a clear retention of Ad5 at the MTOC. Expression of a mutant of CRM1, insensitive to LMB (CRM1 C528S-HA) was able to rescue this blocking, confirming the involvement of CRM1 in Ad5-MTOC removal. However, whether CRM1 interacts alone or if the translocation is mediated by a cargo previously exported by CRM1, is still unknown. Analyses performed with the expression of a mutant of CRM1, also insensitive to LMB but with two extra mutations in the N-terminal part (CRM1 W142A P143A C528S-HA) showed that Ad5 genome delivery was delayed, due to a delay in Ad5-NE translocation. We showed that the CRM1 dependent export pathway was functional within these cells. Hence, cargoes of CRM1 were correctly exported into the cytoplasm and should be available for Ad5. Thus, if we assume that Ad5 requires a nuclear factor exported by CRM1 to be translocated to the NE, the availability of CRM1 cargoes in the cytoplasm of those CRM1 mutant cells should not induce MTOC retention.

Centrosomal accumulation of Ad5 observed in these cells are in favour of a direct role of CRM1 in promoting nuclear targeting of Ad5 rather than mediated by a nuclear factor exported by CRM1. Still, the remaining question at this step is the number of partners involve in the interaction between Ad5 and CRM1 (direct or indirect). Addition of LMB impairs the recognition of CRM1 with NES (Kudo et al. 1999) and impairs the NE translocation of Ad5 (Strunze et al. 2005). Thus, if the CRM1-NES interaction required by Ad5 for its translocation towards the nucleus occurs directly with a viral protein, or is mediated via a cellular NES-containing protein, localized at the MTOC, is not known. In a deep proteomic analysis, high-scoring CRM1 cargoes have been found among components of the centrosome, e.g PCM or MAPs (Kirli et al. 2015). Thus, components of the MTOC could be binding intermediates between Ad5 and CRM1. As an example, the yeast protein complex Mto1/Mto2 (CDK5RAP2 in human) is involved in nucleation of microtubules in the fission yeast *Schizosaccharomyces pombe.* This complex holds an NES and is docked at the NE via its interaction with CRM1 and Nup146, the homologue of Nup214 in human (Bao et al. 2018). Moreover, this interaction is RanGTP dependent.

Therefore, formation of complexes between CRM1, RanGTP and a third partner can occur at the MTOC, to be further docked at the NE. We can thus speculate about such mechanism for nuclear targeting of Ad5.

I.4 Conclusion

After cell entry, Ad5 use the microtubule transport machinery to reach the nucleus. Using U2OS, we observed traffic of Ad5 towards the MTOC, *prior to* its NE targeting, confirming previous observations. Moreover, we showed that once the end point of traffic is reached at the centrosome, integrity of microtubules is not required anymore, nor the presence of cytoplasmic components. These results highlight a possible interaction of Ad5 with centrosomal proteins, *prior to* or upon unloading of Ad5 form microtubules. CRM1 was already known as an essential factor to promote the removal of Ad5 from the MTOC, but our infection assays performed in cells expressing a mutant of CRM1 functional for export showed a transient retention of Ad5 at the MTOC. Our results are in favour of the direct involvement of CRM1 rather than one nuclear factor exported by this exportin.

II. CRM1 is involved in Ad5 genome release

During the first steps of Ad5 infection, from cell entry to NE targeting, several but discrete steps participate in the dismantling of the viral capsid shell (cell entry itself, endosomal escape…) (Greber et al. 1993). However, once at the NE, the size of the capsid remains too large to allow its nuclear entry through NPCs. Thus, Ad5 capsid is disassembled, via an unknown mechanism, to expose and release the viral genome associated with the core proteins. Ad5 capsid is docked at NPCs, via interactions between Nup214 and the hexon protein (Trotman et al. 2001; Cassany et al. 2015). Total dismantling of the capsid is then promoted at the NE and leads to the exposure of the core-DNA. pVII, the major core protein surrounding the Ad5 DNA (Benevento et al. 2014) contains NLSs (Wodrich et al. 2006). Exposure of these sequences promote the binding of different transport factors on pVII, to perform import of Ad5 genome (Wodrich et al. 2006; Hindley et al. 2007; Saphire et al. 2000; Trotman et al. 2001). The nuclear edge is an environment highly concentrated in transport factors. Nup358, a cytoplasmic Nup, is known to promote import of cargoes by acting like a platform to concentrate transport factors at the nuclear edge (Hutten et al. 2008; Hutten et al. 2009; Wälde et al. 2012). Recently, our groups showed that capsid disassembly and nuclear genome import are two distinct mechanistic steps (Carlon-Andres et al. 2020). The deletion of Nup358 induced a delay in genome import, but the number of disassembled capsids was not impaired.

Moreover, we showed that Nup358 and the capsid protein IX are dispensable for capsid disassembly, which is in contradiction with a previous study (Strunze et al. 2011). In the current study, we analysed the role of CRM1 in capsid disassembly. We used mitotic cells and live-cell imaging assays to perform our analyses.

II.1 Mitotic cells as a model to study Ad5 capsid disassembly

Nup214 and Nup358 are two cytoplasmic Nups described to be required for NE docking of Ad5, *prior to* genome import (Trotman et al. 2001; Strunze et al. 2011). While the interaction between the Ad5 hexon protein with Nup214 was mapped at the N-terminal part of this Nup (Cassany et al. 2015), Nup358 was however found dispensable for genome import (Cassany et al. 2015; Carlon-Andres et al. 2020). In order to study the requirement of intact NE to perform capsid disassembly of Ad5, we developed an infection assay in mitotic cells (established by Dr. I Carlón-Andrés). Infection of mitotic cells represent a great model to study i) the requirement of intact NE for Ad5 disassembly/genome delivery and ii) the role of nuclear factors (i.e CRM1 in this study) in upstream events of genome import. The disruption of NE during mitosis induced a homogeneously distribution of cytoplasmic and nuclear factors within the cells. NPCs are no longer assembled, but soluble Nups or sub-complexes of Nups are still present in mitosis (Güttinger et al. 2009).

We used two different microscopy technics to detect Ad5 genome in mitotic cells. Both technics in our systems relies on the detection of pVII exposure, but the way of detection used was different from fixed to living cells (Komatsu et al. 2015). In fixed cells, pVII was detected by immunostaining using anti-pVII antibodies. Therefore, this detection requires an epitope recognition via antibodies. In living cells, pVII was indirectly detected by the oligomerisation of an interacting partner of pVII, TAF-I (Haruki et al. 2003). Upon infection of U2OS cells constitutively expressing TAF-I fused to GFP, exposure of pVII on incoming genomes can be identified by the formation of GFP dots (Komatsu et al. 2015). However, to characterize capsid disassembly, it is important to distinguish three different “shapes” of capsids: intact capsids, partially disassembled capsids exposing their genome and totally disassembled capsid, free from genome. Intact Ad5 capsids do not show fluorescent signal for the Ad5 genome, while partially disassembled capsids show both capsid and genome signals. On the other hand, genomes totally released from the dismantled capsid do not show capsid signals. The Figure 17 illustrates the different signals observed by fluorescence microscopy.

When viruses reached the MTOC, although several minor changes occurred in the capsid shell after cell entry (Greber et al. 1993), Ad5 genomes were still protected in “intact” capsids. Thus, viral cores were not exposed and could not be detected neither via pVII antibody nor TAF-I stain. In contrast, analysis of fixed mitotic cells showed Ad5 genome exposure, detectable after 1 h pi. Capsid disassembly, followed by complete genome release and chromatin-anchoring of the Ad5 DNA molecule could also be followed by live cell imaging of mitotic cells expressing the TAF-I GFP construct. Thus, infection and genome delivery of Ad5 can occur in mitotic cells. Moreover, this result indicates that intact NE and assembled NPCs are not required for capsid disassembly and genome release from the capsid. Thus, our established model of infection in mitotic cell was reliable to follow Ad5 capsid disassembly, until total genome release.

II.2 CRM1 is involved in genome release

Ad5 genome release in mitotic cells has never been reported. Such observations have only been performed on cells that entered in mitosis after infection (Komatsu et al. 2018), which differ from our model of infection, where cells were synchronised in mitosis *prior to* infection. In order to analyse the role of CRM1 in capsid disassembly, we performed infections of mitotic cells upon inhibition of CRM1, via LMB treatment. In our model of infection in mitotic cells, accumulation of Ad5 capsids at the mitotic spindle pole in the presence of LMB was not observed, which is in contradiction with a previous study showing this type of accumulation (Strunze et al. 2005). Strunze et al. synchronised cells in mitosis via a thymidine treatment, to block cells in S phase. This treatment does not impair mitotic spindle assembly. In our study, U2OS cells were synchronised in mitosis by depolymerization of microtubules via colcemid treatment, leading to a defect in the mitotic spindle assembly. Therefore, both studies analysed infection of mitotic cells but the integrity of mitotic spindles was different between these two studies, which may explain the differences observed in accumulation or not of Ad5 capsids at the mitotic spindle poles. However, we did observed accumulation of Ad5 at the mitotic spindle poles upon infection with a higher number of particles after a longer time of infection (data not shown). After a longer time of infection, the formation of mitotic spindles was then probably complete and comparable to the conditions described in the study of Strunze et al.

In mitotic cells, when LMB was added, Ad5 genomes were not detectable in fixed cells, suggesting an inhibition of capsid disassembly. However, upon the expression of a mutant of CRM1, insensitive to LMB (CRM1 C528S-HA), the capsid disassembly was restored and even enhanced. Cellular factors compartmentalized in the nucleus in interphase cells are homogeneously distributed in mitotic cells, i.e available for Ad5. Inhibition of CRM1 strongly impaired capsid disassembly, despite the presence of nuclear factors.

This result confirmed observations from interphase cells (discussed in section I.3 CRM1 is essential for translocation of Ad5 from the MTOC to the NE), about a direct role of CRM1 and the necessity of an NES interaction to perform genome delivery. Interestingly, after LMB treatment, TAF-I GFP dots were observed in mitotic cells upon live-cell imaging, showing that genome exposure was not inhibited in the presence of LMB. Every TAF-I GFP dot was found to colocalize with Ad5 capsids, showing partially disassembled capsids. No free TAF-I GFP dot was detected upon inhibition of CRM1, suggesting a role of CRM1 in the total dismantling of capsid, i.e genome release. Since the detection of Ad5 genome in our systems were different from mitotic to fixed cells, the sensibility of detection in those system was also not the same (Komatsu et al. 2015).

Exposure of pVII detected in living-cells may not be sufficient for epitope recognition by the antibody in fixed cells, which probably requires a further dismantling of the capsid. The Ad5 DNA is known to be more decondensed once it is released from the capsid (Wang et al. 2013). Thus, pVII antibody recognition may require a larger exposure of this core protein, i.e decondensation sate of viral DNA, promoted by CRM1. In their study, Wang et al. used A549 cells and detected Ad5 DNA in interphase cells (i.e with an intact NE) using the deoxythymidine analog 5-ethynyl-20 -deoxyuridine (EdU) staining. Upon LMB treatment, a higher number of genome capsid-associated was detected at the NE, compared to non-treated cells, suggesting a role of CRM1 in genome release. Moreover, in our live-cell imaging analysis, in the absence of LMB, every capsid-free genomes were observed at the vicinity of chromatin, i.e in a RanGTP environment (Carazo-Salas et al. 1999). Taken together, these results suggest a role of CRM1, in combination with RanGTP, in the total dismantling of Ad5 capsids, promoting then genome release.

However, we cannot exclude formation of a complex between CRM1 and a supra-physiological NES (Engelsma et al. 2004) in the cytoplasm, i.e at the MTOC. Such NESs have a very high affinity for CRM1 even in the absence of RanGTP. In parvoviruses, the NS2 protein has been shown to hold a supra-physiological NES, able to bind CRM1 in the cytoplasm (Engelsma et al. 2008). Nonetheless, the requirement of an NES-protein in addition of CRM1 or the direct interaction of CRM1 with a viral NES for capsid disassembly is still not clear.

In this study, we generated U2OS cell lines, constitutively expressing mutants of CRM1, insensitive to LMB. We showed by several biochemical assays the ability of these CRM1 mutants to form a trimeric complex with NES and RanGTP, leading to a functional export. Moreover, the localization of overexpressed CRM1 in those cells was nuclear, but cytoplasmic signals were also detected in most of the cells. Despite the cytoplasmic localization of those CRM1 mutants, we were not able to detect pVII signals before the nuclear targeting of Ad5.

These results show that CRM1 alone is probably not sufficient to promote Ad5 capsid dismantling, but may act as an intermediate to concentrate Ad5 in an environment suitable for the dismantling of the capsid, i.e at the nuclear edge. CRM1 is known to interact with FG-repeats located on the C-terminal part of Nup358 (Ritterhoff et al. 2016) and Nup214 (Port et al. 2015). Moreover, the interaction of Ad5 with the N-terminal part of Nup214 is a prerequisite step for Ad5 docking at the NE (Cassany et al. 2015). We also recently showed that Nup358 is dispensable for Ad5 genome import but its absence induces a delay in the kinetic of import (Carlon-Andres et al. 2020). Accumulation of capsids exposing their genome were observed, showing a delay in the total dismantling of Ad5 capsids, upstream of genome import. Nup358 provides a platform highly enriched in transport factors (Hutten et al. 2008; Hutten et al. 2009; Wälde et al. 2012), promoting genome nuclear import. The delay observed in genome import upon Nup358 deletion is probably due to a lower availability of transport factors at the NE. The docking of Ad5 to the N-terminal part of Nup214 is essential for Ad5 genome release (Trotman et al. 2001; Cassany et al. 2015). Moreover, this docking can also induce further dismantle of the capsid. Thus, the docking of Ad5 to Nup214 and the high concentration of transport factors at the NE may promote the capsid disassembly. CRM1 would then act as a factor transporting the Ad5 capsid at the NPC, where its interaction with the FG-repeats of Nup214 and/or Nup358 could facilitate the docking of Ad5 to Nup214. Moreover, it has already been shown that transport factors can have a role in the viral capsid disassembly, such as transportin-1 which trigger the disassembly of the HIV-1 capsid (Fernandez et al. 2019).

In absence of an intact NE in mitotic cells, Ad5 cores were released from the capsid. We showed that inhibition of CRM1 leads to a defect in genome release. In this scenario, CRM1 would act again as an intermediate, to concentrate Ad5 capsids at the vicinity of soluble Nups (Nup214 and Nup358). Moreover, overexpression of CRM1 binding fragments of Nup358 in mitotic cells have been shown to promote Ad5 capsid disassembly, only in absence of LMB (PhD thesis Irene Carlón-Andrés, 2017). On the other hand, overexpression of CRM1 binding fragments of Nup214 in mitotic cells did no show an effect in promoting Ad5 capsid disassembly. Nup358 would thus indirectly promote genome release, by providing transport factors (transportin-1, importin-β…) necessary for the genome release of the Ad5.

II.3 Partially disassembled capsids are targeted to chromatin in mitotic cells for genome release

We just discussed the role of CRM1 in the indirect recruitment of cellular factors to perform Ad5 genome release. Moreover, we showed that partially disassembled capsids, exposing their genome, were targeted and anchored to the chromatin. Thus, these partially disassembled capsids might expose a core protein promoting targeting and anchoring to the chromatin. Early studies showed an association of DNA from the AdV serotype 12 with chromosomes (Zur Hausen 1968). Our groups showed indeed an association of Ad5 core-DNA with sub-nuclear structures (Komatsu et al. 2015). Using the TAF-I system in interphase cells, we observed confined movements of Ad5 DNA in the nucleus, suggesting an association of Ad5 DNA with sub-nuclear structures. More recently, we published a new technic of detection of Ad5 genomes (Komatsu et al.2018). This system, called the ANCHOR technology, is a bi-partite system. On one hand, it consists of a DNA sequence inserted into the vDNA of Ad5 (sequence ANCH), containing ~10 nucleation sites for the protein OR3. On the other hand, the expression of OR3 fused to GFP leads to the oligomerisation of this protein around the ANCH sequence. The detection of GFP signals, thanks to this oligomerisation, is detected by fluorescence microscopy, and is specific to the Ad5 DNA. Using this technics, we detected Ad5 genomes anchored to the chromatin of cells entered in mitosis after infection. Ad5 DNA molecules were distributed equally between daughter cells during division.

However, the role of such association is still unclear. pVII is known to associate with chromatin (Lee et al. 2003; Avgousti et al. 2016) but the kinetic of association with Ad5 DNA remains unclear (Giberson et al. 2012). Moreover, TP, a core protein covalently bound to both extremities of the Ad5 DNA molecule, has been shown to induce viral DNA attachment to the nucleoplasmic protein network (nuclear matrix), to promote viral transcription and replication (Schaack et al. 1990). We confirmed the association of TP with chromatin, and unpublished data from our group in collaboration with Dr. M. Okuwaki and Dr. K. Nagata in Japan, identified the chromatin binding domain on TP. Attachment of viral DNA to the nuclear matrix, and more specifically to the heterodimer H2A/H2B has been shown for some viruses such as human Cytomegalovirus (hCMV) (Fang et al. 2016), Kaposi's sarcoma-associated herpesvirus (KSHV) (Barbera et al. 2006) or Prototype foamy virus (PFV) (Lesbats et al. 2017). The predicted chromatin binding site of TP showed sequence similarities with those proteins. Thus, anchoring of Ad5 DNA observed in our live-cell imaging analysis could be triggered via TP.

After cell entry, Ad5 capsids escape endosomal degradation pathway and are subjected to a first reorganisation of capsid structure (a first partial disassembly step). This structural change in the capsid leads to the exposure of certain proteins, as it has been shown for pVI (Wiethoff et al. 2005). TP is covalently bound to each end of the genome but mechanisms of DNA packaging and organisation of the core-DNA inside the capsid are not well defined (San Martin 2012). Thus, TP could be oriented in a way that allows its partial exposure after capsid reorganisation in the endosome, for a rapid and coordinated exit of the genome from the capsid, at the nuclear pore.

II.4 Conclusion

NE disruption occurring in mitosis creates a good model to study the requirement of intact NPCs to promote Ad5 capsid disassembly and genome release. Infection of mitotic U2OS cells led to the detection of intermediate partially disassembled capsids and capsid-free genomes, indicating that intact NPCs embedded in the NE are dispensable for Ad5 genome delivery. Using live-cell imaging, we showed that addition of LMB did not prevent genome exposure but instead blocked total dismantling of Ad5. Thus, CRM1 is required to release Ad5 genomes from their capsid. Moreover, genome release occurred at the vicinity of chromatin, in a RanGTP environment. Partially disassembled capsids exposing their genome were targeted and anchored to the nuclear matrix.

As it was shown for several other viruses, this anchoring can be triggered by a specific motif. This motif is also present in the core-protein TP. Therefore, chromatin anchoring of Ad5 could be mediated via exposure of TP, in partially disassembled capsids, independently of CRM1 while complete disassembly and liberating the genome from the capsid may be promoted by transport factors at the vicinity of Nups, where CRM1 would be the factor bringing the Ad5 in a suitable environment for capsid dismantling.

III. Terminal Protein as a potential partner for CRM1

As just discussed above, CRM1 is essential to promote Ad5 NE translocation in interphase cells (Strunze et al. 2005), and genome release in mitotic cells. We also observed that addition of LMB did not prevent genome exposure, nor chromatin anchoring in mitotic cells. During the first steps of infection, gradual events of capsid dismantling are observed, with the loss of external capsid proteins and exposure of internal components (Ortega-Esteban et al. 2013). Thus, we can assume that after endosomal escape and microtubule transport, once at the MTOC, disassembled capsids expose core proteins.

Observations about partially disassembled capsids anchored to the chromatin in mitotic cells in the presence of LMB are in favour of exposed core proteins to trigger targeting to the nuclear matrix. We proposed TP as the core-protein mediating this association. To follow this hypothesis, exposure of TP might already occurs at the MTOC. The addition of LMB blocks Ad5 at the MTOC, showing the requirement of an interaction between CRM1 and an NES. Using a bioinformatics tool, we found a predicted consensus NES in TP. This sequence shows a pattern of basic amino-acids with slight deviations compared to the NES consensus pattern $\Phi^0\Phi^1$-$(x)_{2-3}$-Φ^2-$(x)_{2-3}$-Φ^3-x-Φ^4 (Güttler et al. 2010). We showed the functionality of this NES, responsible for the export of overexpressed TP via its interaction with CRM1. If partially disassembled capsids that arrive at the MTOC also expose TP, is becomes feasible that CRM1 uses the NES in TP to bind to Ad5 capsid. We performed biochemical assays to analyse the binding of CRM1 with Ad5 capsids (data from this study not shown, and data from PhD thesis Irene Carlón-Andrés, 2017). Under our conditions, we were never able to detect such interactions. That can be explained by the fact that we artificially induced a partial disassembly of Ad5, mimicking the disassembly observed during endosomal escape. However, it is difficult to reconstitute *in vitro* the exact level of disassembly of the Ad5.

In addition to functional CRM1, genome release occurs in a RanGTP environment in mitotic cells. CRM1 and RanGTP have been shown to be located at the centrosome (Liu et al. 2009; Keryer et al. 2003). Therefore, we can speculate about the formation of a ternary complex at the centrosome, between CRM1, RanGTP and Ad5, mediated by TP, to promote NE translocation, either assisted by a motor protein like the Kinesin-1 or by simple diffusion.

The deletion of the Kif5B has been shown to induce accumulation of Ad5 capsids at the MTOC (Zhou et al. 2018). Kif5B could thus promotes Ad5 nuclear translocation, via the binding on Ad5 capsid. NPC arrival would then be facilitated by the binding of CRM1 with FG-repeats of Nup358 and/or Nup214, before the final docking of Ad5 on Nup214. Then, final dismantling of Ad5 capsid and genome import would be a simultaneous step involving several factors, concentrated at the nuclear edge, such as Nup214, importin-β, importin-7, transportin-1, histone H1 or Hsc 70 (Wodrich et al. 2006; Hindley et al. 2007; Saphire et al. 2000; Trotman et al. 2001; Carlon-Andres et al. 2020; Cassany et al. 2015).

Furthermore, during genome replication, AdV pol is imported into the nucleus by pTP, thanks to the NLS presents on pTP (Zhao and Padmanabhan 1988). Cleavage of pTP into TP upon maturation, does not remove this NLS, situated downstream of the cleavage site (Webster et al. 1994). Thus, viral DNA of incoming particles is bound to TP, holding both NLS and NES. Nuclear import of Ad5 genome is facilitated by NLSs of pVII (Wodrich et al. 2006), but the implication of the TP-NLS has not been studied in detail.

Although further analysis are required, we can hypothesis that exposure of TP might also trigger genome import. In our model, CRM1 would interact directly with Ad5, via the NES of TP. However, an indirect interaction, via an NES-protein as intermediate between Ad5 and CRM1 cannot be excluded. Nucleophosmin is involved in the centrosomal duplication and this protein maintains its centrosomal location thanks to the CRM1-RanGTP complex (Wang et al. 2005). Addition of LMB induces nucleophosmin dissociation from the centrosome, leading to a premature duplication. Nucleophosmin has also been shown to interact with the Ad5 core protein V (Samad et al. 2012). Thus, such interaction with an intermediate partner between CRM1 and Ad5 could also potentially occurs at the MTOC.

IV. Generation of a mutant of CRM1 to study Ad5 infection

In order to analyse the role of CRM1 in Ad5 genome delivery, we first analysed the impact of point mutations on CRM1 in Ad5 capsid disassembly in mitotic cells. We performed a screening of several mutants of CRM1, all insensitive to LMB (to inhibit the endogenous CRM1) but holding additional point mutations. We found an interesting candidate, with two point mutations in its N-terminal domain, CRM1 W142 P143 C528S-HA. We infected mitotic cells upon expression of this mutant, and we observed that this mutant was not able to rescue the Ad5 genome release. We then monitored genome import and gene expression, upon expression of this triple mutant. During the first 2 h of infection, we observed an accumulation of Ad5 at the MTOC, same phenotype that was observed in control cells treated with LMB, without expression of CRM1 constructs. However, at 2 h pi, nuclear Ad5 genomes started to be detected, showing a delay in genome import. Same results were obtained in the analysis of Ad5 gene expression by RNAscope, the expression of E1A mRNA were delayed compare to cells expressing the simple mutant CRM1 C528S-HA. Interestingly, 6 days pi, no difference between CRM1 528S and the triple mutant were observed. This mutant was showing a striking defect only during the first steps of Ad5 infection.

The point mutations W142A P143A introduced in CRM1 are located close to the binding site of Nup214 FG-repeats (Port et al. 2015). To better explain the defects observed upon Ad5 infections, we performed several *in vitro* and *in vivo* biochemical assays. We generated U2OS cells constitutively expressing this mutant and we monitored the export of several known cargoes of CRM1. Our results show a functional export of CRM1, able to rescue the LMB effect. We then purified recombinant CRM1 proteins, and we performed *in vitro* export assays. Our results confirmed a functional export mediated by this mutant. However, slight defects in the kinetics of export, as well as in the binding with the PKI-NES were observed.

The Kd was measured three times higher compared to CRM1 wild type, showing a defect in the affinity of CRM1 W142A 143A C528S for the PKI-NES.

In conclusion, our results showed that we generated a mutant of CRM1 functional for export, but inducing a clear defect in Ad5 genome delivery. Ad5 are not physiological cargoes for the cell. Viruses highjack cellular pathways to perform they infection cycle. CRM1 export cargoes form the nucleus to the cytoplasm (Fornerod, et al. 1997b; Fornerod,Kehlenbach et al. 1998; Fukuda et al. 1997) but upon Ad5 infection, CRM1 promotes upstream events of genome import, such as NE translocation (Strunze et al. 2005) or capsid release, as we just discussed. The clear differences observed in the triple mutant of CRM1, between the physiological export function of CRM1 and its role in Ad5 genome delivery raise some question about its role, its structure and potential new interacting partners.

W142A P143A point mutations are located in the CRIME domain of CRM1, site of binding with RanGTP (Fornerod et al. 1997a). Formation of a trimeric complex between RanGTP-CRM1 and an NES occurs in a cooperative manner, inducing structural conformation changes in CRM1 (Fornerod et al. 1997b; Monecke et al. 2013). A lower affinity of CRM1 for RanGTP or NES could thus impair binding of the second partner. We showed a lower affinity of CRM1 W142A P143A for PKI-NES, compared to CRM1 wild type. This result could be explained by a lower affinity of CRM1 for the NES itself, but we cannot exclude a lower affinity for RanGTP, thus impairing binding with PKI-NES.

Moreover, we observed degradation products of the CRM1 mutant during its purification. Mutations introduced in the N-terminal part of CRM1 could destabilize the protein, leading to a misfolded recombinant product. The expression level of CRM1 mutant in the newly generated U2OS cell lines are comparable to those in control cells. Recombinant CRM1 is also correctly expressed in bacteria. Thus, the higher yield of degradation product in newly synthetized CRM1 may be explained by less stable proteins, due to a misfolded structure. Slight defects observed in export kinetics and NES binding assays could thus be due to conformational conflicts during the binding of RanGTP and NES. Further structural studies are required to characterize effect of these point mutations.

CRM1 has a centrosomal location, driven by its CRIME domain (Liu et al. 2009). Point mutations W142A P143A are part on this domain. We cannot exclude that these mutations impair the centrosomal localization of CRM1, by decreasing the portion of CRM1 at the MTOC. Therefore, the amount of CRM1 W142 P143A C528S would be less available for the Ad5, explaining the blocking of Ad5 capsids at the MTOC, observed in CRM1 triple mutant cells.

However, the CRM1 mutant was available in mitotic U2OS CRM1-HA expressing cells but capsid disassembly was still impaired.

We generated a tool to help to understand CRM1 function and the nature of Ad5-CRM1 interaction during Ad5 infection. Despite the functionality of this mutant, the observations of accumulation of Ad5 the MTOC in CRM1 mutant cells are in favour of a requirement for the virus to pass by the MTOC. Delay in capsid disassembly despite a functional export are also in favour of a direct interaction of CRM1 with Ad5, rather than an interaction mediated by an exported cargo. Finally, our results point the importance of the structural organisation of CRM1 to form a stable ternary complex with RanGTP and the requirement of a proper folding to maintain the strength of interactions.

V. Model

In this work, we studied the role of CRM1 in Ad5 genome delivery. Infections of interphase or mitotic cells, different imaging technics used for the detection of Ad5 genomes and the generation and characterization of a mutant of CRM1 were used to provide more insight into the role of this exportin in Ad5 infection. Taken together our data suggest a role of CRM1 in MTOC translocation of Ad5, via an interaction with TP, to further promote capsid disassembly and genome release. In our model, a first partial disassembly step taking place in the endosome would lead to the exposure of TP, one of the core protein covalently linked to both ends of the viral genome. The fraction of CRM1 and RanGTP concentrated at the MTOC could then provide an environment to form a ternary complex between CRM1, RanGTP and the NES of TP. This would promote the translocation to the NE, via a mechanism that remains unclear. A simple diffusion or a movement assisted by a motor protein such as Kif5B can be envisaged. The docking of Ad5 to NPCs via binding between the hexon protein and the Nup214 would induce a further dismantling of the capsid to then expose the Ad5 genome. The binding of CRM1 to the FG-repeats of Nup358 would restrict the capsids to an environment rich in transport factors, promoting the final dismantling of capsids and nuclear import of the viral DNA. Unlike Nup214, Nup358 is not a prerequisite necessary for capsid disassembly (Cassany et al. 2015; Carlon-Andres et al. 2020). However, the presence of Nup358 would promote genome import by providing a high concentration of import factors (Wälde et al. 2012) to the Ad5 (importin-β, importin-7, transportin-1), thus enhancing nuclear import of Ad5 genome.

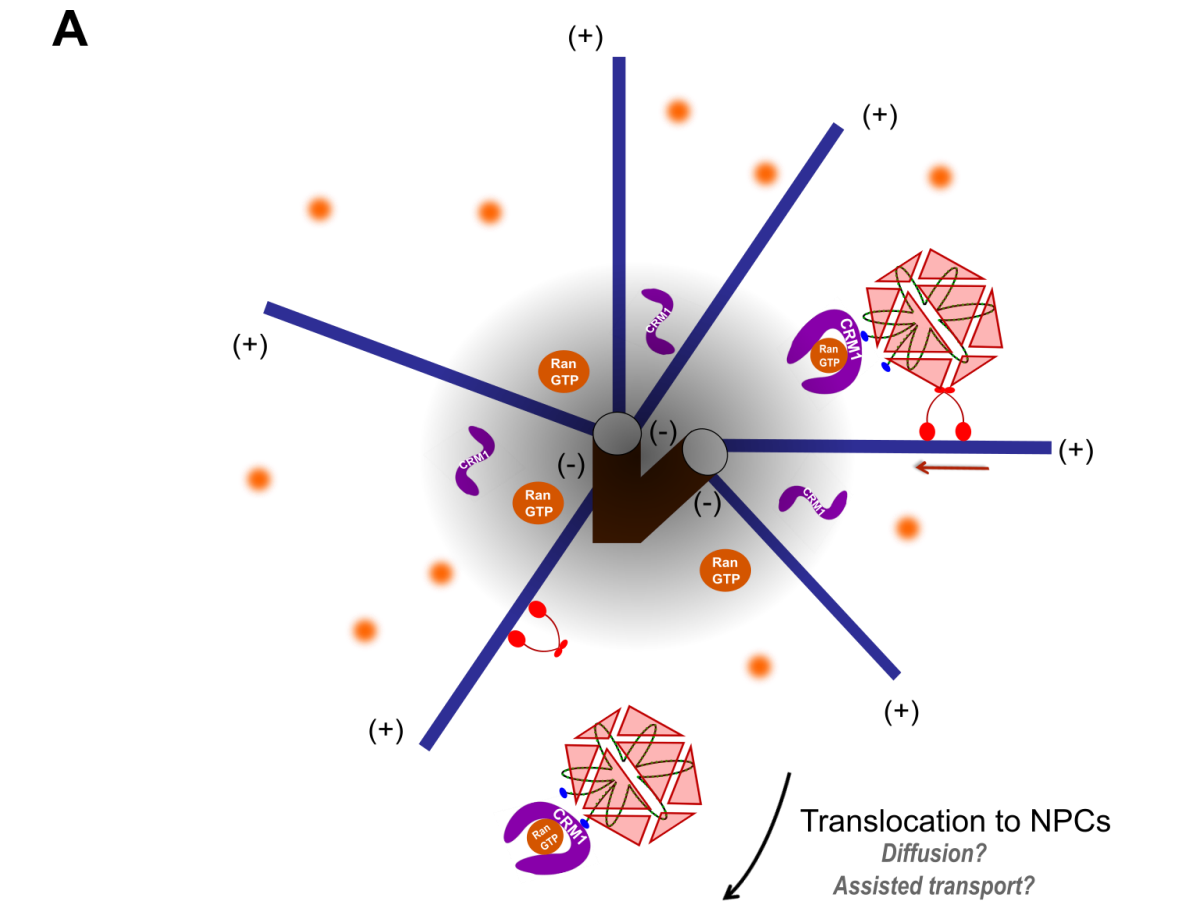
A
(+)
(+)
(+)
(+)
(+)
(-)
(-)
(-)
Ran GTP
Ran GTP
Ran GTP
Ran GTP
CRM1
CRM1
CRM1
CRM1
Translocation to NPCs
Diffusion?
Assisted transport?

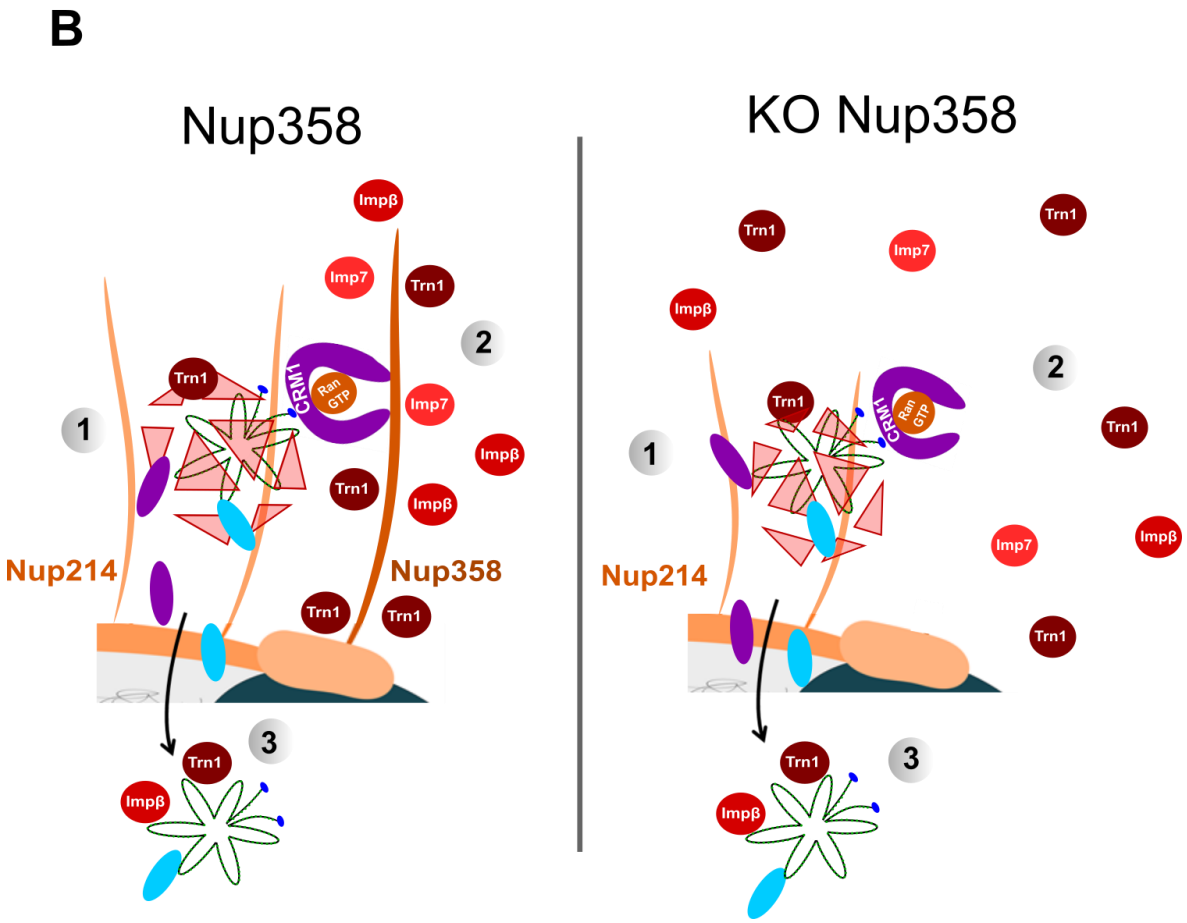
B
Nup358
KO Nup358
Impβ
Imp7
Trn1
CRM1
Ran GTP
Nup214
Nup358
1
2
3

Figure 43. Model for the role of CRM1 in promoting Ad5 genome delivery. (previous page) (A) The first partial disassembly step induced by the pH acidity in the endosome leads to the exposure of Ad5 proteins, such as TP. After endosomal escape, Ad5 is transported to the MTOC via the microtubule motor dynein. The centrosomal fraction of CRM1 recognizes the NES of TP (in blue) and together with RanGTP, forms a ternary complex inducing a conformational change in CRM1, from and extended to a ring like structure. This ternary complex is then translocated to the nuclear pore, via an unknown mechanism either simple diffusion or assisted by a motor protein. (B) Ad5 bound to CRM1 reach the NE where the binding of CRM1 to the FG-repeats of Nup214 and/or Nup358 promotes the interaction of the hexon protein with the Nup214. This interaction induces (1) the docking and the final dismantling of the capsid, exposing pVII. The binding of CRM1 to the FG-repeats of Nup358 (2) enhances the availability of transport receptors for Ad5. The absence of Nup358 delays the import due to a lower direct availability of these receptors. The binding of different factors induces the (3) final genome release from the capsid and the nuclear import of the Ad5 genome.

Outlook

Further assays are required to prove the necessity of every newly infectious Ad5 particles to pass by the MTOC before their nuclear targeting. An assay involving enzymatic modification of labelled Ad5 capsids once at the MTOC or Fluorescence Resonance Energy Transfer (FRET) assay between the Ad5 and one component of the MTOC can be considered to prove this idea. Using another model of differentiated epithelial cells, harbouring a different organisation in their microtubule network (Tang and Marshall 2012) could provide more insights into the role of Ad5-MTOC localization *prior to* their nuclear targeting. Deletion of centrosomal components, known to interact with CRM1 (Kirli et al. 2015) may also show the requirement of PCM or centriolar satellites in the interaction of Ad5 at the MTOC.

Identification of CRM1 and RanGTP at the MTOC in U2OS cells should also be performed, perhaps using Proximity Ligation Assay. The detection of TP in partially disassembled capsids, at the MTOC or in the presence of LMB are required to show the exposure of TP. We generated TP antibodies in this studies that will further help to study this hypothesis. *In vitro* binding experiments between TP and CRM1 are required, to prove that TP is an interacting partner of CRM1. Several pull down have been performed in this work, with recombinant TP or Ad5 particles (data not shown), but optimal conditions showing the binding of recombinant CRM1 have not been determined yet. It is a technical challenge to reproduce *in vitro* the partial disassembled state of the capsid and genome exposure after the endosomal escape. To go further, interaction experiments with partially disassembled capsids and CRM1 could also be performed, in the presence or absence of TP antibodies, to confirm the interaction of these two partners.

Further biochemical studies on the CRM1 mutant W142A P143A should be performed, to explain the defect that we observed in our infection assays. Additional anisotropy assays with different NESs or with increase concentrations of RanGTP could provide a better idea on the formation of a ternary complex in this mutant.

Finally, it will be of interest to confirm the binding of TP with nucleosomes and more specifically with H2A/H2B as it has been shown for several other viral proteins (Fang et al. 2016; Barbera et al. 2006; Lesbats et al. 2017). Preliminary data have been obtained in this work (data not shown), in collaboration with Dr. M. Okuwaki, Dr. K. Nagata, Dr. P. Lesbats and Dr. V. Parissi and further experiments are required to confirm our observations. The replication of Ad5 DNA is stabilized via its interaction with the nuclear matrix (Schaack et al. 1990). If CRM1 is interacting with TP, we can then speculate about the role of CRM1 in the stabilization of the Ad5 replication complex, mediated by TP, or in later step, like in Ad5 assembly.

Appendix

In order to perform biochemical analysis of TP, we purified the recombinant TP wild type and mutated for the CBS, both GST-tagged. The GST tag was inserted at the N-terminal part of TP. In addition to the band at ~70 kDa, degradation products were observed in the final purification products. GST signals were detected upon Western blotting analysis with anti-GST antibodies (Figure 44).

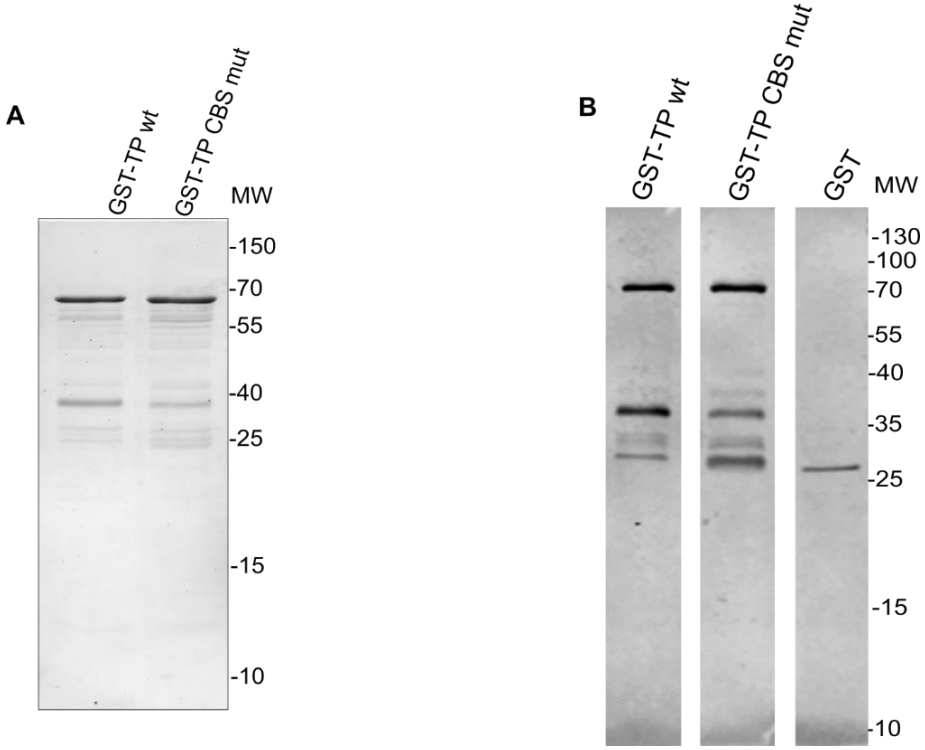

Figure 44. Purification of recombinant Terminal Protein. Purification of recombinant GST-TP wild type of mutated for the CBS was done using Glutathione beads. (A) Coomassie staining of the purification products. (B) Western blot using anti-GST antibodies for detection of recombinant GST tagged proteins.

There is no commercial anti-TP available. In order to generate those antibodies, we used the recombinant TP (see above), to generate monoclonal antibodies (see section IV.5.b TP antibody in Material and Methods). Briefly, mice were immunised with GST-TP wild type and around 15 days later, B-cells were extracted and fused with myelomas (performed by Dr. D. Dacheux). Hybridomas resulting from this fusion were then grown and their supernatant were tested with immunofluorescence and Western blotting against recombinant TP and infected cells. Dr. H. Wodrich performed a first screen by testing hybridomas supernatant on infected cells, during the replication phase of Ad5 genomes (data not shown). 18 to 24 h pi, replication centers with high concentrations of replicative Ad5 genomes are formed in the nucleus of an infected cell.

Thus, high concentration of pTP, can be observed by fluorescence microscopy (Komatsu et al. 2015; Komatsu et al. 2018). The hybridomas, which gave a strong signal for those replication centers were selected, and further tested on transfected cells.

U2OS cells were then transfected with a construct coding for GFP-TP wild type or mutated for the CBS, and immunofluorescence staining was performed using hydridoma supernatants, containing antibodies secreted in the culture medium (Figure 45A). The clone #8.1.5 gave specific signals comparable to GFP signals observed in transfected cells, without unspecific signal. TP wild type was also detected by Western blotting (Figure 45B), using hybridomas supernatant containing antibodies. This clone gave specific signals for TP: therefore, we chose to purified them on a Protein-G sepharose affinity column. The purification was performed by Dr. B Roger and the characterization of these purified antibodies are ongoing.

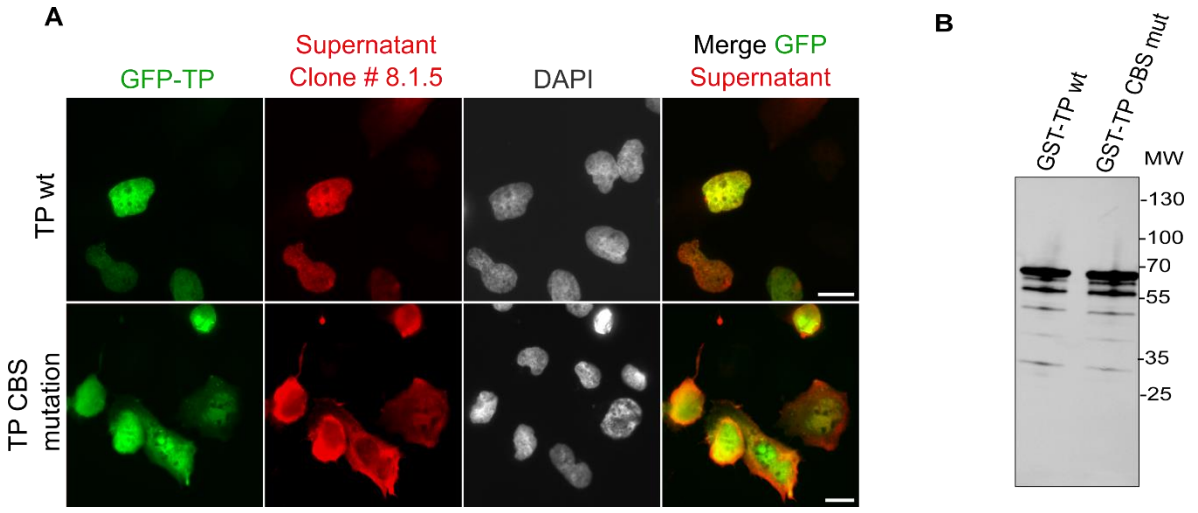

Figure 45. Anti-TP antibodies generated give a specific signal. (A) U2OS cells were transfected with constructs coding for GFP-TP wild type or mutated for the CBS. 24 h later, cells were fixed and stained with supernatant containing antibodies, generated from the culture of the hybridoma clone #8.1.5 (red), and with DAPI (grey) for chromatin staining. GFP-TP signals are depicted in green. Cells were imaged by fluorescence microscopy and one plane is shown. (Scale bars, 50 µm). (B) Detection of recombinant GST-TP by Western blotting, using the supernatant of culture of the hybridoma clone #8.1.5.

References

Adachi, Y., and M. Yanagida. 1989. 'Higher order chromosome structure is affected by cold-sensitive mutations in a Schizosaccharomyces pombe gene crm1+ which encodes a 115-kD protein preferentially localized in the nucleus and its periphery', *J Cell Biol*, 108: 1195-207.

Akhmanova, A., and M. O. Steinmetz. 2015. 'Control of microtubule organization and dynamics: two ends in the limelight', *Nat Rev Mol Cell Biol*, 16: 711-26.

Akhtar, A., and S. M. Gasser. 2007. 'The nuclear envelope and transcriptional control', *Nat Rev Genet*, 8: 507-17.

Akusjarvi, G. 2008. 'Temporal regulation of adenovirus major late alternative RNA splicing', *Front Biosci*, 13: 5006-15.

Alzaid, F., F. Lagadec, M. Albuquerque, R. Ballaire, L. Orliaguet, I. Hainault, C. Blugeon, S. Lemoine, A. Lehuen, D. G. Saliba, I. A. Udalova, V. Paradis, F. Foufelle, and N. Venteclef. 2016. 'IRF5 governs liver macrophage activation that promotes hepatic fibrosis in mice and humans', *JCI Insight*, 1: e88689.

Arnaoutov, A., Y. Azuma, K. Ribbeck, J. Joseph, Y. Boyarchuk, T. Karpova, J. McNally, and M. Dasso. 2005. 'Crm1 is a mitotic effector of Ran-GTP in somatic cells', *Nat Cell Biol*, 7: 626-32.

Avgousti, D. C., C. Herrmann, K. Kulej, N. J. Pancholi, N. Sekulic, J. Petrescu, R. C. Molden, D. Blumenthal, A. J. Paris, E. D. Reyes, P. Ostapchuk, P. Hearing, S. H. Seeholzer, G. S. Worthen, B. E. Black, B. A. Garcia, and M. D. Weitzman. 2016. 'A core viral protein binds host nucleosomes to sequester immune danger signals', *Nature*, 535: 173-7.

Bailey, C. J., R. G. Crystal, and P. L. Leopold. 2003. 'Association of adenovirus with the microtubule organizing center', *J Virol*, 77: 13275-87.

Bao, X. X., C. Spanos, T. Kojidani, E. M. Lynch, J. Rappsilber, Y. Hiraoka, T. Haraguchi, and K. E. Sawin. 2018. 'Exportin Crm1 is repurposed as a docking protein to generate microtubule organizing centers at the nuclear pore', *Elife*, 7.

Barbera, A. J., J. V. Chodaparambil, B. Kelley-Clarke, K. Luger, and K. M. Kaye. 2006. 'Kaposi's sarcoma-associated herpesvirus LANA hitches a ride on the chromosome', *Cell Cycle*, 5: 1048-52.

Beaudouin, J., D. Gerlich, N. Daigle, R. Eils, and J. Ellenberg. 2002. 'Nuclear envelope breakdown proceeds by microtubule-induced tearing of the lamina', *Cell*, 108: 83-96.

Benevento, M., S. Di Palma, J. Snijder, C. L. Moyer, V. S. Reddy, G. R. Nemerow, and A. J. Heck. 2014. 'Adenovirus composition, proteolysis, and disassembly studied by in-depth qualitative and quantitative proteomics', *J Biol Chem*, 289: 11421-30.

Berciaud, S., F. Rayne, S. Kassab, C. Jubert, M. Faure-Della Corte, F. Salin, H. Wodrich, M. E. Lafon, and Members Typadeno Study. 2012. 'Adenovirus infections in Bordeaux University Hospital 2008-2010: clinical and virological features', *J Clin Virol*, 54: 302-7.

Bergelson, J. M., J. A. Cunningham, G. Droguett, E. A. Kurt-Jones, A. Krithivas, J. S. Hong, M. S. Horwitz, R. L. Crowell, and R. W. Finberg. 1997. 'Isolation of a common receptor for Coxsackie B viruses and adenoviruses 2 and 5', *Science*, 275: 1320-3.

Berget, S. M., C. Moore, and P. A. Sharp. 1977. 'Spliced segments at the 5' terminus of adenovirus 2 late mRNA', *Proc Natl Acad Sci U S A*, 74: 3171-5.

Berk, A. J., F. Lee, T. Harrison, J. Williams, and P. A. Sharp. 1979. 'Pre-early adenovirus 5 gene product regulates synthesis of early viral messenger RNAs', *Cell*, 17: 935-44.

Bernad, R., D. Engelsma, H. Sanderson, H. Pickersgill, and M. Fornerod. 2006. 'Nup214-Nup88 nucleoporin subcomplex is required for CRM1-mediated 60 S preribosomal nuclear export', *J Biol Chem*, 281: 19378-86.

Binger, M. H., and S. J. Flint. 1984. 'Accumulation of early and intermediate mRNA species during subgroup C adenovirus productive infections', *Virology*, 136: 387-403.

Bischoff, F. R., H. Krebber, E. Smirnova, W. Dong, and H. Ponstingl. 1995. 'Co-activation of RanGTPase and inhibition of GTP dissociation by Ran-GTP binding protein RanBP1', *EMBO J*, 14: 705-15.

Bischoff, F. R., and H. Ponstingl. 1991. 'Catalysis of guanine nucleotide exchange on Ran by the mitotic regulator RCC1', *Nature*, 354: 80-2.

Bodakuntla, S., A. S. Jijumon, C. Villablanca, C. Gonzalez-Billault, and C. Janke. 2019. 'Microtubule-Associated Proteins: Structuring the Cytoskeleton', *Trends Cell Biol*, 29: 804-19.

Bremner, K. H., J. Scherer, J. Yi, M. Vershinin, S. P. Gross, and R. B. Vallee. 2009. 'Adenovirus transport via direct interaction of cytoplasmic dynein with the viral capsid hexon subunit', *Cell Host Microbe*, 6: 523-35.

Burg, J. L., J. Schweitzer, and E. Daniell. 1983. 'Introduction of superhelical turns into DNA by adenoviral core proteins and chromatin assembly factors', *J Virol*, 46: 749-55.

Carazo-Salas, R. E., G. Guarguaglini, O. J. Gruss, A. Segref, E. Karsenti, and I. W. Mattaj. 1999. 'Generation of GTP-bound Ran by RCC1 is required for chromatin-induced mitotic spindle formation', *Nature*, 400: 178-81.

Carlon-Andres, I., F. Lagadec, N. Pied, F. Rayne, M. E. Lafon, R. H. Kehlenbach, and H. Wodrich. 2020. 'Nup358 and transportin 1 cooperate in adenoviral genome import', *J Virol*.

Cassany, A., J. Ragues, T. Guan, D. Begu, H. Wodrich, M. Kann, G. R. Nemerow, and L. Gerace. 2015. 'Nuclear import of adenovirus DNA involves direct interaction of hexon with an N-terminal domain of the nucleoporin Nup214', *J Virol*, 89: 1719-30.

Centres for Disease Control and Prevention. Adenovirus transmission, https://www.cdc.gov/adenovirus/

Challberg, M. D., and T. J. Kelly, Jr. 1981. 'Processing of the adenovirus terminal protein', *J Virol*, 38: 272-7.

Chardonnet, Y., and S. Dales. 1970. 'Early events in the interaction of adenoviruses with HeLa cells. I. Penetration of type 5 and intracellular release of the DNA genome', *Virology*, 40: 462-77.

Chen, C., and H. Okayama. 1987. 'High-efficiency transformation of mammalian cells by plasmid DNA', *Mol Cell Biol*, 7: 2745-52.

Chow, L. T., R. E. Gelinas, T. R. Broker, and R. J. Roberts. 1977. 'An amazing sequence arrangement at the 5' ends of adenovirus 2 messenger RNA', *Cell*, 12: 1-8.

Christensen, J. B., S. A. Byrd, A. K. Walker, J. R. Strahler, P. C. Andrews, and M. J. Imperiale. 2008. 'Presence of the adenovirus IVa2 protein at a single vertex of the mature virion', *J Virol*, 82: 9086-93.

Chroboczek, J., F. Bieber, and B. Jacrot. 1992. 'The sequence of the genome of adenovirus type 5 and its comparison with the genome of adenovirus type 2', *Virology*, 186: 280-5.

Conti, E., C. W. Muller, and M. Stewart. 2006. 'Karyopherin flexibility in nucleocytoplasmic transport', *Curr Opin Struct Biol*, 16: 237-44.

Cook, J., and J. Radke. 2017. 'Mechanisms of pathogenesis of emerging adenoviruses', *F1000Res*, 6: 90.

Coutavas, E., M. Ren, J. D. Oppenheim, P. D'Eustachio, and M. G. Rush. 1993. 'Characterization of proteins that interact with the cell-cycle regulatory protein Ran/TC4', *Nature*, 366: 585-7.

Crenshaw, B. J., L. B. Jones, C. R. Bell, S. Kumar, and Q. L. Matthews. 2019. 'Perspective on Adenoviruses: Epidemiology, Pathogenicity, and Gene Therapy', *Biomedicines*, 7.

Crisostomo, L., A. M. Soriano, M. Mendez, D. Graves, and P. Pelka. 2019. 'Temporal dynamics of adenovirus 5 gene expression in normal human cells', *PLoS One*, 14: e0211192.

Dales, S., and Y. Chardonnet. 1973. 'Early events in the interaction of adenoviruses with HeLa cells. IV. Association with microtubules and the nuclear pore complex during vectorial movement of the inoculum', *Virology*, 56: 465-83.

Desiderio, S. V., and T. J. Kelly, Jr. 1981. 'Structure of the linkage between adenovirus DNA and the 55,000 molecular weight terminal protein', *J Mol Biol*, 145: 319-37.

Di Fiore, B., M. Ciciarello, R. Mangiacasale, A. Palena, A. M. Tassin, E. Cundari, and P. Lavia. 2003. 'Mammalian RanBP1 regulates centrosome cohesion during mitosis', *J Cell Sci*, 116: 3399-411.

Döhner, K., A. Wolfstein, U. Prank, C. Echeverri, D. Dujardin, R. Vallee, and B. Sodeik. 2002. 'Function of dynein and dynactin in herpes simplex virus capsid transport', *Mol Biol Cell*, 13: 2795-809.

Dong, X., A. Biswas, K. E. Suel, L. K. Jackson, R. Martinez, H. Gu, and Y. M. Chook. 2009. 'Structural basis for leucine-rich nuclear export signal recognition by CRM1', *Nature*, 458: 1136-41.

Doxsey, S. J., P. Stein, L. Evans, P. D. Calarco, and M. Kirschner. 1994. 'Pericentrin, a highly conserved centrosome protein involved in microtubule organization', *Cell*, 76: 639-50.

DuRaine, G., T. W. Wisner, P. Howard, and D. C. Johnson. 2018. 'Kinesin-1 Proteins KIF5A, -5B, and -5C Promote Anterograde Transport of Herpes Simplex Virus Enveloped Virions in Axons', *J Virol*, 92.

Enders, J. F., J. A. Bell, J. H. Dingle, T. Francis, Jr., M. R. Hilleman, R. J. Huebner, and A. M. Payne. 1956. 'Adenoviruses: group name proposed for new respiratory-tract viruses', *Science*, 124: 119-20.

Engelsma, D., R. Bernad, J. Calafat, and M. Fornerod. 2004. 'Supraphysiological nuclear export signals bind CRM1 independently of RanGTP and arrest at Nup358', *EMBO J*, 23: 3643-52.

Engelsma, D., N. Valle, A. Fish, N. Salome, J. M. Almendral, and M. Fornerod. 2008. 'A supraphysiological nuclear export signal is required for parvovirus nuclear export', *Mol Biol Cell*, 19: 2544-52.

Epstein, M. A. 1959. 'Observations on the fine structure of type 5 adenovirus', *J Biophys Biochem Cytol*, 6: 523-6.

Fang, Q., P. Chen, M. Wang, J. Fang, N. Yang, G. Li, and R. M. Xu. 2016. 'Human cytomegalovirus IE1 protein alters the higher-order chromatin structure by targeting the acidic patch of the nucleosome', *Elife*, 5.

Fernandez, J., A. K. Machado, S. Lyonnais, C. Chamontin, K. Gartner, T. Leger, C. Henriquet, C. Garcia, D. M. Portilho, M. Pugniere, L. Chaloin, D. Muriaux, Y. Yamauchi, M. Blaise, S. Nisole, and N. J. Arhel. 2019. 'Transportin-1 binds to the HIV-1 capsid via a nuclear localization signal and triggers uncoating', *Nat Microbiol*, 4: 1840-50.

Fischer, U., J. Huber, W. C. Boelens, I. W. Mattaj, and R. Luhrmann. 1995. 'The HIV-1 Rev activation domain is a nuclear export signal that accesses an export pathway used by specific cellular RNAs', *Cell*, 82: 475-83.

Forgues, M., M. J. Difilippantonio, S. P. Linke, T. Ried, K. Nagashima, J. Feden, K. Valerie, K. Fukasawa, and X. W. Wang. 2003. 'Involvement of Crm1 in hepatitis B virus X protein-induced aberrant centriole replication and abnormal mitotic spindles', *Mol Cell Biol*, 23: 5282-92.

Fornerod, M., M. Ohno, M. Yoshida, and I. W. Mattaj. 1997b. 'CRM1 is an export receptor for leucine-rich nuclear export signals', *Cell*, 90: 1051-60.

Fornerod, M., J. van Deursen, S. van Baal, A. Reynolds, D. Davis, K. G. Murti, J. Fransen, and G. Grosveld. 1997a. 'The human homologue of yeast CRM1 is in a dynamic subcomplex with CAN/Nup214 and a novel nuclear pore component Nup88', *EMBO J*, 16: 807-16.

Fu, S. C., H. Y. J. Fung, T. Cagatay, J. Baumhardt, and Y. M. Chook. 2018. 'Correlation of CRM1-NES affinity with nuclear export activity', *Mol Biol Cell*, 29: 2037-44.

Fukuda, M., S. Asano, T. Nakamura, M. Adachi, M. Yoshida, M. Yanagida, and E. Nishida. 1997. 'CRM1 is responsible for intracellular transport mediated by the nuclear export signal', *Nature*, 390: 308-11.

Gaggar, A., D. M. Shayakhmetov, and A. Lieber. 2003. 'CD46 is a cellular receptor for group B adenoviruses', *Nat Med*, 9: 1408-12.

Gazzola, M., C. J. Burckhardt, B. Bayati, M. Engelke, U. F. Greber, and P. Koumoutsakos. 2009. 'A stochastic model for microtubule motors describes the in vivo cytoplasmic transport of human adenovirus', *PLoS Comput Biol*, 5: e1000623.

Gerace, L., and G. Blobel. 1980. 'The nuclear envelope lamina is reversibly depolymerized during mitosis', *Cell*, 19: 277-87.

Ghebremedhin, B. 2014. 'Human adenovirus: Viral pathogen with increasing importance', *Eur J Microbiol Immunol (Bp)*, 4: 26-33.

Ghosh, S. S., P. Gopinath, and A. Ramesh. 2006. 'Adenoviral vectors: a promising tool for gene therapy', *Appl Biochem Biotechnol*, 133: 9-29.

Giannakakou, P., M. Nakano, K. C. Nicolaou, A. O'Brate, J. Yu, M. V. Blagosklonny, U. F. Greber, and T. Fojo. 2002. 'Enhanced microtubule-dependent trafficking and p53 nuclear accumulation by suppression of microtubule dynamics', *Proc Natl Acad Sci U S A*, 99: 10855-60.

Giberson, A. N., A. R. Davidson, and R. J. Parks. 2012. 'Chromatin structure of adenovirus DNA throughout infection', *Nucleic Acids Res*, 40: 2369-76.

Glenn, G. M., and R. P. Ricciardi. 1988. 'Detailed kinetics of adenovirus type-5 steady-state transcripts during early infection', *Virus Res*, 9: 73-91.

Glotzer, J. B., A. I. Michou, A. Baker, M. Saltik, and M. Cotten. 2001. 'Microtubule-independent motility and nuclear targeting of adenoviruses with fluorescently labeled genomes', *J Virol*, 75: 2421-34.

Görlich, D., S. Kostka, R. Kraft, C. Dingwall, R. A. Laskey, E. Hartmann, and S. Prehn. 1995. 'Two different subunits of importin cooperate to recognize nuclear localization signals and bind them to the nuclear envelope', *Curr Biol*, 5: 383-92.

Görlich, D., N. Pante, U. Kutay, U. Aebi, and F. R. Bischoff. 1996. 'Identification of different roles for RanGDP and RanGTP in nuclear protein import', *EMBO J*, 15: 5584-94.

Greber, U. F., M. Suomalainen, R. P. Stidwill, K. Boucke, M. W. Ebersold, and A. Helenius. 1997. 'The role of the nuclear pore complex in adenovirus DNA entry', *EMBO J*, 16: 5998-6007.

Greber, U. F., P. Webster, J. Weber, and A. Helenius. 1996. 'The role of the adenovirus protease on virus entry into cells', *EMBO J*, 15: 1766-77.

Greber, U. F., M. Willetts, P. Webster, and A. Helenius. 1993. 'Stepwise dismantling of adenovirus 2 during entry into cells', *Cell*, 75: 477-86.

Guarguaglini, G., L. Renzi, F. D'Ottavio, B. Di Fiore, M. Casenghi, E. Cundari, and P. Lavia. 2000. 'Regulated Ran-binding protein 1 activity is required for organization and function of the mitotic spindle in mammalian cells in vivo', *Cell Growth Differ*, 11: 455-65.

Guimet D, Hearing P. Adenovirus Replication Adenoviral Vectors For Gene Therapy: Second Edition. 59-84. DOI: 10.1016/B978-0-12-800276-6.00003-6

Güttinger, S., E. Laurell, and U. Kutay. 2009. 'Orchestrating nuclear envelope disassembly and reassembly during mitosis', *Nat Rev Mol Cell Biol*, 10: 178-91.

Güttler, T., T. Madl, P. Neumann, D. Deichsel, L. Corsini, T. Monecke, R. Ficner, M. Sattler, and D. Görlich. 2010. 'NES consensus redefined by structures of PKI-type and Rev-type nuclear export signals bound to CRM1', *Nat Struct Mol Biol*, 17: 1367-76.

Hamamoto, T., S. Gunji, H. Tsuji, and T. Beppu. 1983. 'Leptomycins A and B, new antifungal antibiotics. I. Taxonomy of the producing strain and their fermentation, purification and characterization', *J Antibiot (Tokyo)*, 36: 639-45.

Harel, A., and D. J. Forbes. 2004. 'Importin beta: conducting a much larger cellular symphony', *Mol Cell*, 16: 319-30.

Haruki, H., B. Gyurcsik, M. Okuwaki, and K. Nagata. 2003. 'Ternary complex formation between DNA-adenovirus core protein VII and TAF-Ibeta/SET, an acidic molecular chaperone', *FEBS Lett*, 555: 521-7.

Hasson, T. B., D. A. Ornelles, and T. Shenk. 1992. 'Adenovirus L1 52- and 55-kilodalton proteins are present within assembling virions and colocalize with nuclear structures distinct from replication centers', *J Virol*, 66: 6133-42.

Hasson, T. B., P. D. Soloway, D. A. Ornelles, W. Doerfler, and T. Shenk. 1989. 'Adenovirus L1 52- and 55-kilodalton proteins are required for assembly of virions', *J Virol*, 63: 3612-21.

Hatfield, L., and P. Hearing. 1991. 'Redundant elements in the adenovirus type 5 inverted terminal repeat promote bidirectional transcription in vitro and are important for virus growth in vivo', *Virology*, 184: 265-76.

Hetzer, M., D. Bilbao-Cortes, T. C. Walther, O. J. Gruss, and I. W. Mattaj. 2000. 'GTP hydrolysis by Ran is required for nuclear envelope assembly', *Mol Cell*, 5: 1013-24.

Hilleman, M. R., and J. H. Werner. 1954. 'Recovery of new agent from patients with acute respiratory illness', *Proc Soc Exp Biol Med*, 85: 183-8.

Hindley, C. E., F. J. Lawrence, and D. A. Matthews. 2007. 'A role for transportin in the nuclear import of adenovirus core proteins and DNA', *Traffic*, 8: 1313-22.

Hinshaw, J. E., B. O. Carragher, and R. A. Milligan. 1992. 'Architecture and design of the nuclear pore complex', *Cell*, 69: 1133-41.

Hoebeke, J., G. Van Nijen, and M. De Brabander. 1976. 'Interaction of oncodazole (R 17934), a new antitumoral drug, with rat brain tubulin', *Biochem Biophys Res Commun*, 69: 319-24.

Hoeben, R. C., and T. G. Uil. 2013. 'Adenovirus DNA replication', *Cold Spring Harb Perspect Biol*, 5: a013003.

Honda, T., H. Saitoh, M. Masuko, T. Katagiri-Abe, K. Tominaga, I. Kozakai, K. Kobayashi, T. Kumanishi, Y. G. Watanabe, S. Odani, and R. Kuwano. 2000. 'The coxsackievirus-adenovirus receptor protein as a cell adhesion molecule in the developing mouse brain', *Brain Res Mol Brain Res*, 77: 19-28.

Hutten, S., A. Flotho, F. Melchior, and R. H. Kehlenbach. 2008. 'The Nup358-RanGAP complex is required for efficient importin alpha/beta-dependent nuclear import', *Mol Biol Cell*, 19: 2300-10.

Hutten, S., and R. H. Kehlenbach. 2006. 'Nup214 is required for CRM1-dependent nuclear protein export in vivo', *Mol Cell Biol*, 26: 6772-85.

Hutten, S., S. Wälde, C. Spillner, J. Hauber, and R. H. Kehlenbach. 2009. 'The nuclear pore component Nup358 promotes transportin-dependent nuclear import', *J Cell Sci*, 122: 1100-10.

Imelli, N., Z. Ruzsics, D. Puntener, M. Gastaldelli, and U. F. Greber. 2009. 'Genetic reconstitution of the human adenovirus type 2 temperature-sensitive 1 mutant defective in endosomal escape', *Virol J*, 6: 174.

Irene Carlón-Andrés. Functional implications of the nucleoporin Nup358/RanBP2 and transport receptors in adenoviral genome delivery. Human health and pathology. Université de Bordeaux, 2017. English. ⟨NNT : 2017BORD0807⟩. ⟨tel-02444535v2⟩

Izaurralde, E., U. Kutay, C. von Kobbe, I. W. Mattaj, and D. Görlich. 1997. 'The asymmetric distribution of the constituents of the Ran system is essential for transport into and out of the nucleus', *EMBO J*, 16: 6535-47.

Jaffe, H. A., C. Danel, G. Longenecker, M. Metzger, Y. Setoguchi, M. A. Rosenfeld, T. W. Gant, S. S. Thorgeirsson, L. D. Stratford-Perricaudet, M. Perricaudet, and et al. 1992. 'Adenovirus-mediated in vivo gene transfer and expression in normal rat liver', *Nat Genet*, 1: 372-8.

Jiang, H., M. V. Olson, D. R. Medrano, O. H. Lee, J. Xu, Y. Piao, M. M. Alonso, C. Gomez-Manzano, M. C. Hung, W. K. Yung, and J. Fueyo. 2006. 'A novel CRM1-dependent nuclear export signal in adenoviral E1A protein regulated by phosphorylation', *FASEB J*, 20: 2603-5.

Jiang, H., E. J. White, C. I. Rios-Vicil, J. Xu, C. Gomez-Manzano, and J. Fueyo. 2011. 'Human adenovirus type 5 induces cell lysis through autophagy and autophagy-triggered caspase activity', *J Virol*, 85: 4720-9.

Joseph, J., S. T. Liu, S. A. Jablonski, T. J. Yen, and M. Dasso. 2004. 'The RanGAP1-RanBP2 complex is essential for microtubule-kinetochore interactions in vivo', *Curr Biol*, 14: 611-7.

Joseph, J., S. H. Tan, T. S. Karpova, J. G. McNally, and M. Dasso. 2002. 'SUMO-1 targets RanGAP1 to kinetochores and mitotic spindles', *J Cell Biol*, 156: 595-602.

Kalab, P., A. Pralle, E. Y. Isacoff, R. Heald, and K. Weis. 2006. 'Analysis of a RanGTP-regulated gradient in mitotic somatic cells', *Nature*, 440: 697-701.

Kalderon, D., W. D. Richardson, A. F. Markham, and A. E. Smith. 1984. 'Sequence requirements for nuclear location of simian virus 40 large-T antigen', *Nature*, 311: 33-8.

Karen, K. A., and P. Hearing. 2011. 'Adenovirus core protein VII protects the viral genome from a DNA damage response at early times after infection', *J Virol*, 85: 4135-42.

Kehlenbach, R. H., A. Dickmanns, and L. Gerace. 1998. 'Nucleocytoplasmic shuttling factors including Ran and CRM1 mediate nuclear export of NFAT In vitro', *J Cell Biol*, 141: 863-74.

Kehlenbach, R. H., A. Dickmanns, A. Kehlenbach, T. Guan, and L. Gerace. 1999. 'A role for RanBP1 in the release of CRM1 from the nuclear pore complex in a terminal step of nuclear export', *J Cell Biol*, 145: 645-57.

Kelkar, S. A., K. K. Pfister, R. G. Crystal, and P. L. Leopold. 2004. 'Cytoplasmic dynein mediates adenovirus binding to microtubules', *J Virol*, 78: 10122-32.

Keryer, G., B. Di Fiore, C. Celati, K. F. Lechtreck, M. Mogensen, A. Delouvee, P. Lavia, M. Bornens, and A. M. Tassin. 2003. 'Part of Ran is associated with AKAP450 at the centrosome: involvement in microtubule-organizing activity', *Mol Biol Cell*, 14: 4260-71.

Kindsmüller, K., P. Groitl, B. Hartl, P. Blanchette, J. Hauber, and T. Dobner. 2007. 'Intranuclear targeting and nuclear export of the adenovirus E1B-55K protein are regulated by SUMO1 conjugation', *Proc Natl Acad Sci U S A*, 104: 6684-9.

Kirli, K., S. Karaca, H. J. Dehne, M. Samwer, K. T. Pan, C. Lenz, H. Urlaub, and D. Görlich. 2015. 'A deep proteomics perspective on CRM1-mediated nuclear export and nucleocytoplasmic partitioning', *Elife*, 4.

Klebe, C., F. R. Bischoff, H. Ponstingl, and A. Wittinghofer. 1995. 'Interaction of the nuclear GTP-binding protein Ran with its regulatory proteins RCC1 and RanGAP1', *Biochemistry*, 34: 639-47.

Komatsu, T., D. Dacheux, F. Kreppel, K. Nagata, and H. Wodrich. 2015. 'A Method for Visualization of Incoming Adenovirus Chromatin Complexes in Fixed and Living Cells', *PLoS One*, 10: e0137102.

Komatsu, T., H. Haruki, and K. Nagata. 2011. 'Cellular and viral chromatin proteins are positive factors in the regulation of adenovirus gene expression', *Nucleic Acids Res*, 39: 889-901.

Komatsu, T., C. Quentin-Froignant, I. Carlon-Andres, F. Lagadec, F. Rayne, J. Ragues, R. H. Kehlenbach, W. Zhang, A. Ehrhardt, K. Bystricky, R. Morin, J. M. Lagarde, F. Gallardo, and H. Wodrich. 2018. 'In Vivo Labelling of Adenovirus DNA Identifies Chromatin Anchoring and Biphasic Genome Replication', *J Virol*, 92.

Komatsu, T., D. R. Robinson, M. Hisaoka, S. Ueshima, M. Okuwaki, K. Nagata, and H. Wodrich. 2016. 'Tracking adenovirus genomes identifies morphologically distinct late DNA replication compartments', *Traffic*, 17: 1168-80.

Kubo, A., H. Sasaki, A. Yuba-Kubo, S. Tsukita, and N. Shiina. 1999. 'Centriolar satellites: molecular characterization, ATP-dependent movement toward centrioles and possible involvement in ciliogenesis', *J Cell Biol*, 147: 969-80.

Kudo, N., N. Matsumori, H. Taoka, D. Fujiwara, E. P. Schreiner, B. Wolff, M. Yoshida, and S. Horinouchi. 1999. 'Leptomycin B inactivates CRM1/exportin 1 by covalent modification at a cysteine residue in the central conserved region', *Proc Natl Acad Sci U S A*, 96: 9112-7.

Kudo, N., B. Wolff, T. Sekimoto, E. P. Schreiner, Y. Yoneda, M. Yanagida, S. Horinouchi, and M. Yoshida. 1998. 'Leptomycin B inhibition of signal-mediated nuclear export by direct binding to CRM1', *Exp Cell Res*, 242: 540-7.

Lavia, P. 2016. 'The GTPase RAN regulates multiple steps of the centrosome life cycle', *Chromosome Res*, 24: 53-65.

Lee, C. S., E. S. Bishop, R. Zhang, X. Yu, E. M. Farina, S. Yan, C. Zhao, Z. Zheng, Y. Shu, X. Wu, J. Lei, Y. Li, W. Zhang, C. Yang, K. Wu, Y. Wu, S. Ho, A. Athiviraham, M. J. Lee, J. M. Wolf, R. R. Reid, and T. C. He. 2017. 'Adenovirus-Mediated Gene Delivery: Potential Applications for Gene and Cell-Based Therapies in the New Era of Personalized Medicine', *Genes Dis*, 4: 43-63.

Lee, T. W. R., G. E. Blair, and D. A. Matthews. 2003. 'Adenovirus core protein VII contains distinct sequences that mediate targeting to the nucleus and nucleolus, and colocalization with human chromosomes', *J Gen Virol*, 84: 3423-28.

Lefkowitz, E. J., D. M. Dempsey, R. C. Hendrickson, R. J. Orton, S. G. Siddell, and D. B. Smith. 2018. 'Virus taxonomy: the database of the International Committee on Taxonomy of Viruses (ICTV)', *Nucleic Acids Res*, 46: D708-D17.

Leopold, P. L., G. Kreitzer, N. Miyazawa, S. Rempel, K. K. Pfister, E. Rodriguez-Boulan, and R. G. Crystal. 2000. 'Dynein- and microtubule-mediated translocation of adenovirus serotype 5 occurs after endosomal lysis', *Hum Gene Ther*, 11: 151-65.

Lesbats, P., E. Serrao, D. P. Maskell, V. E. Pye, N. O'Reilly, D. Lindemann, A. N. Engelman, and P. Cherepanov. 2017. 'Structural basis for spumavirus GAG tethering to chromatin', *Proc Natl Acad Sci U S A*, 114: 5509-14.

Li, E., D. Stupack, G. M. Bokoch, and G. R. Nemerow. 1998b. 'Adenovirus endocytosis requires actin cytoskeleton reorganization mediated by Rho family GTPases', *J Virol*, 72: 8806-12.

Li, E., D. Stupack, R. Klemke, D. A. Cheresh, and G. R. Nemerow. 1998a. 'Adenovirus endocytosis via alpha(v) integrins requires phosphoinositide-3-OH kinase', *J Virol*, 72: 2055-61.

Lindsay, M. E., J. M. Holaska, K. Welch, B. M. Paschal, and I. G. Macara. 2001. 'Ran-binding protein 3 is a cofactor for Crm1-mediated nuclear protein export', *J Cell Biol*, 153: 1391-402.

Liu, H., L. Jin, S. B. Koh, I. Atanasov, S. Schein, L. Wu, and Z. H. Zhou. 2010. 'Atomic structure of human adenovirus by cryo-EM reveals interactions among protein networks', *Science*, 329: 1038-43.

Liu, Q., Q. Jiang, and C. Zhang. 2009. 'A fraction of Crm1 locates at centrosomes by its CRIME domain and regulates the centrosomal localization of pericentrin', *Biochem Biophys Res Commun*, 384: 383-8.

Lodish H, Berk A, Zipursky SL, et al. Molecular Cell Biology. 4th edition. New York: W. H. Freeman; 2000. Section 19.2, Microtubule Dynamics and Associated Proteins. Available from: https://www.ncbi.nlm.nih.gov/books/NBK21522/

Lui, K., and Y. Huang. 2009. 'RanGTPase: A Key Regulator of Nucleocytoplasmic Trafficking', *Mol Cell Pharmacol*, 1: 148-56.

Lukic, Z., A. Dharan, T. Fricke, F. Diaz-Griffero, and E. M. Campbell. 2014. 'HIV-1 uncoating is facilitated by dynein and kinesin 1', *J Virol*, 88: 13613-25.

Ma, Y., and M. B. Mathews. 1996. 'Structure, function, and evolution of adenovirus-associated RNA: a phylogenetic approach', *J Virol*, 70: 5083-99.

Mabit, H., M. Y. Nakano, U. Prank, B. Saam, K. Döhner, B. Sodeik, and U. F. Greber. 2002. 'Intact microtubules support adenovirus and herpes simplex virus infections', *J Virol*, 76: 9962-71.

MacLean-Fletcher, S., and T. D. Pollard. 1980. 'Mechanism of action of cytochalasin B on actin', *Cell*, 20: 329-41.

Mahajan, R., C. Delphin, T. Guan, L. Gerace, and F. Melchior. 1997. 'A small ubiquitin-related polypeptide involved in targeting RanGAP1 to nuclear pore complex protein RanBP2', *Cell*, 88: 97-107.

Maier, O., S. A. Marvin, H. Wodrich, E. M. Campbell, and C. M. Wiethoff. 2012. 'Spatiotemporal dynamics of adenovirus membrane rupture and endosomal escape', *J Virol*, 86: 10821-8.

Mangel, W. F., W. J. McGrath, D. L. Toledo, and C. W. Anderson. 1993. 'Viral DNA and a viral peptide can act as cofactors of adenovirus virion proteinase activity', *Nature*, 361: 274-5.

Mangel, W. F., and C. San Martin. 2014. 'Structure, function and dynamics in adenovirus maturation', *Viruses*, 6: 4536-70.

Martin-Gonzalez, N., M. Hernando-Perez, G. N. Condezo, M. Perez-Illana, A. Siber, D. Reguera, P. Ostapchuk, P. Hearing, C. San Martin, and P. J. de Pablo. 2019. 'Adenovirus major core protein condenses DNA in clusters and bundles, modulating genome release and capsid internal pressure', *Nucleic Acids Res*, 47: 9231-42.

Martinez, R., P. Schellenberger, D. Vasishtan, C. Aknin, S. Austin, D. Dacheux, F. Rayne, A. Siebert, Z. Ruzsics, K. Gruenewald, and H. Wodrich. 2015. 'The amphipathic helix of adenovirus capsid protein VI contributes to penton release and postentry sorting', *J Virol*, 89: 2121-35.

Mathias, P., T. Wickham, M. Moore, and G. Nemerow. 1994. 'Multiple adenovirus serotypes use alpha v integrins for infection', *J Virol*, 68: 6811-4.

Matthews, D. A., and W. C. Russell. 1998. 'Adenovirus core protein V is delivered by the invading virus to the nucleus of the infected cell and later in infection is associated with nucleoli', *J Gen Virol*, 79 (Pt 7): 1671-5.

McDonald, D., M. A. Vodicka, G. Lucero, T. M. Svitkina, G. G. Borisy, M. Emerman, and T. J. Hope. 2002. 'Visualization of the intracellular behavior of HIV in living cells', *J Cell Biol*, 159: 441-52.

McIntosh, J. R. 2016. 'Mitosis', *Cold Spring Harb Perspect Biol*, 8.

Melchior, F., D. J. Sweet, and L. Gerace. 1995. 'Analysis of Ran/TC4 function in nuclear protein import', *Methods Enzymol*, 257: 279-91.

Miles, B. D., R. B. Luftig, J. A. Weatherbee, R. R. Weihing, and J. Weber. 1980. 'Quantitation of the interaction between adenovirus types 2 and 5 and microtubules inside infected cells', *Virology*, 105: 265-9.

Mittereder, N., K. L. March, and B. C. Trapnell. 1996. 'Evaluation of the concentration and bioactivity of adenovirus vectors for gene therapy', *J Virol*, 70: 7498-509.

Mohr, D., S. Frey, T. Fischer, T. Güttler, and D. Görlich. 2009. 'Characterisation of the passive permeability barrier of nuclear pore complexes', *EMBO J*, 28: 2541-53.

Monecke, T., A. Dickmanns, and R. Ficner. 2014. 'Allosteric control of the exportin CRM1 unraveled by crystal structure analysis', *FEBS J*, 281: 4179-94.

Monecke, T., T. Güttler, P. Neumann, A. Dickmanns, D. Görlich, and R. Ficner. 2009. 'Crystal structure of the nuclear export receptor CRM1 in complex with Snurportin1 and RanGTP', *Science*, 324: 1087-91.

Monecke, T., D. Haselbach, B. Voss, A. Russek, P. Neumann, E. Thomson, E. Hurt, U. Zachariae, H. Stark, H. Grubmuller, A. Dickmanns, and R. Ficner. 2013. 'Structural basis for cooperativity of CRM1 export complex formation', *Proc Natl Acad Sci U S A*, 110: 960-5.

Montespan, C., S. A. Marvin, S. Austin, A. M. Burrage, B. Roger, F. Rayne, M. Faure, E. M. Campell, C. Schneider, R. Reimer, K. Grunewald, C. M. Wiethoff, and H. Wodrich. 2017. 'Multi-layered control of Galectin-8 mediated autophagy during adenovirus cell entry through a conserved PPxY motif in the viral capsid', *PLoS Pathog*, 13: e1006217.

Moore, M. S., and G. Blobel. 1993. 'The GTP-binding protein Ran/TC4 is required for protein import into the nucleus', *Nature*, 365: 661-3.

Moore, W., C. Zhang, and P. R. Clarke. 2002. 'Targeting of RCC1 to chromosomes is required for proper mitotic spindle assembly in human cells', *Curr Biol*, 12: 1442-7.

Murnane, J. P. 1990. 'Influence of cellular sequences on instability of plasmid integration sites in human cells', *Somat Cell Mol Genet*, 16: 195-209.

Mysiak, M. E., C. Wyman, P. E. Holthuizen, and P. C. van der Vliet. 2004. 'NFI and Oct-1 bend the Ad5 origin in the same direction leading to optimal DNA replication', *Nucleic Acids Res*, 32: 6218-25.

Nachury, M. V., T. J. Maresca, W. C. Salmon, C. M. Waterman-Storer, R. Heald, and K. Weis. 2001. 'Importin beta is a mitotic target of the small GTPase Ran in spindle assembly', *Cell*, 104: 95-106.

Nemergut, M. E., C. A. Mizzen, T. Stukenberg, C. D. Allis, and I. G. Macara. 2001. 'Chromatin docking and exchange activity enhancement of RCC1 by histones H2A and H2B', *Science*, 292: 1540-3.

Neuber, A., J. Franke, A. Wittstruck, G. Schlenstedt, T. Sommer, and K. Stade. 2008. 'Nuclear export receptor Xpo1/Crm1 is physically and functionally linked to the spindle pole body in budding yeast', *Mol Cell Biol*, 28: 5348-58.

Nevins, J. R., and J. E. Darnell. 1978. 'Groups of adenovirus type 2 mRNA's derived from a large primary transcript: probable nuclear origin and possible common 3' ends', *J Virol*, 25: 811-23.

Nilsson, J., K. Weis, and J. Kjems. 2002. 'The C-terminal extension of the small GTPase Ran is essential for defining the GDP-bound form', *J Mol Biol*, 318: 583-93.

Nishi, K., M. Yoshida, D. Fujiwara, M. Nishikawa, S. Horinouchi, and T. Beppu. 1994. 'Leptomycin B targets a regulatory cascade of crm1, a fission yeast nuclear protein, involved in control of higher order chromosome structure and gene expression', *J Biol Chem*, 269: 6320-4.

Orjalo, A. V., A. Arnaoutov, Z. Shen, Y. Boyarchuk, S. G. Zeitlin, B. Fontoura, S. Briggs, M. Dasso, and D. J. Forbes. 2006. 'The Nup107-160 nucleoporin complex is required for correct bipolar spindle assembly', *Mol Biol Cell*, 17: 3806-18.

Ortega-Esteban, A., A. J. Perez-Berna, R. Menendez-Conejero, S. J. Flint, C. San Martin, and P. J. de Pablo. 2013. 'Monitoring dynamics of human adenovirus disassembly induced by mechanical fatigue', *Sci Rep*, 3: 1434.

Ossareh-Nazari, B., and C. Dargemont. 1999. 'Domains of Crm1 involved in the formation of the Crm1, RanGTP, and leucine-rich nuclear export sequences trimeric complex', *Exp Cell Res*, 252: 236-41.

Ostapchuk, P., M. Suomalainen, Y. Zheng, K. Boucke, U. F. Greber, and P. Hearing. 2017. 'The adenovirus major core protein VII is dispensable for virion assembly but is essential for lytic infection', *PLoS Pathog*, 13: e1006455.

Ostapchuk, P., J. Yang, E. Auffarth, and P. Hearing. 2005. 'Functional interaction of the adenovirus IVa2 protein with adenovirus type 5 packaging sequences', *J Virol*, 79: 2831-8.

Pante, N., and M. Kann. 2002. 'Nuclear pore complex is able to transport macromolecules with diameters of about 39 nm', *Mol Biol Cell*, 13: 425-34.

Paraskeva, E., E. Izaurralde, F. R. Bischoff, J. Huber, U. Kutay, E. Hartmann, R. Luhrmann, and D. Görlich. 1999. 'CRM1-mediated recycling of snurportin 1 to the cytoplasm', *J Cell Biol*, 145: 255-64.

Patel, S. S., B. J. Belmont, J. M. Sante, and M. F. Rexach. 2007. 'Natively unfolded nucleoporins gate protein diffusion across the nuclear pore complex', *Cell*, 129: 83-96.

Patterson, S., and W. C. Russell. 1983. 'Ultrastructural and immunofluorescence studies of early events in adenovirus-HeLa cell interactions', *J Gen Virol*, 64: 1091-9.

Perez-Berna, A. J., R. Marabini, S. H. Scheres, R. Menendez-Conejero, I. P. Dmitriev, D. T. Curiel, W. F. Mangel, S. J. Flint, and C. San Martin. 2009. 'Structure and uncoating of immature adenovirus', *J Mol Biol*, 392: 547-57.

Persson, B. D., D. M. Reiter, M. Marttila, Y. F. Mei, J. M. Casasnovas, N. Arnberg, and T. Stehle. 2007. 'Adenovirus type 11 binding alters the conformation of its receptor CD46', *Nat Struct Mol Biol*, 14: 164-6.

Petosa, C., G. Schoehn, P. Askjaer, U. Bauer, M. Moulin, U. Steuerwald, M. Soler-Lopez, F. Baudin, I. W. Mattaj, and C. W. Muller. 2004. 'Architecture of CRM1/Exportin1 suggests how cooperativity is achieved during formation of a nuclear export complex', *Mol Cell*, 16: 761-75.

Petry, S. 2016. 'Mechanisms of Mitotic Spindle Assembly', *Annu Rev Biochem*, 85: 659-83.

Pied, N., and H. Wodrich. 2019. 'Imaging the adenovirus infection cycle', *FEBS Lett*, 593: 3419-48.

Plafker, K., and I. G. Macara. 2000. 'Facilitated nucleocytoplasmic shuttling of the Ran binding protein RanBP1', *Mol Cell Biol*, 20: 3510-21.

Port, S. A., T. Monecke, A. Dickmanns, C. Spillner, R. Hofele, H. Urlaub, R. Ficner, and R. H. Kehlenbach. 2015. 'Structural and Functional Characterization of CRM1-Nup214 Interactions Reveals Multiple FG-Binding Sites Involved in Nuclear Export', *Cell Rep*, 13: 690-702.

Pronk, R., and P. C. van der Vliet. 1993. 'The adenovirus terminal protein influences binding of replication proteins and changes the origin structure', *Nucleic Acids Res*, 21: 2293-300.

Prosser, S. L., and L. Pelletier. 2020. 'Centriolar satellite biogenesis and function in vertebrate cells', *J Cell Sci*, 133.

Quentin Osseman. Analyse du transport intracytoplasmique de la capside du virus de l'hépatite B : analyse des interactions entre les capsides du VHB et les chaînes du complexe de la dynéine. Immunologie. Université de Bordeaux, 2014. Français. ⟨NNT : 2014BORD0304⟩. ⟨tel-01176843⟩

Rancourt, C., H. Keyvani-Amineh, S. Sircar, P. Labrecque, and J. M. Weber. 1995. 'Proline 137 is critical for adenovirus protease encapsidation and activation but not enzyme activity', *Virology*, 209: 167-73.

Raper, S. E., N. Chirmule, F. S. Lee, N. A. Wivel, A. Bagg, G. P. Gao, J. M. Wilson, and M. L. Batshaw. 2003. 'Fatal systemic inflammatory response syndrome in a ornithine transcarbamylase deficient patient following adenoviral gene transfer', *Mol Genet Metab*, 80: 148-58.

Reddy, V. S., S. K. Natchiar, P. L. Stewart, and G. R. Nemerow. 2010. 'Crystal structure of human adenovirus at 3.5 A resolution', *Science*, 329: 1071-5.

Reddy, V. S., and G. R. Nemerow. 2014. 'Structures and organization of adenovirus cement proteins provide insights into the role of capsid maturation in virus entry and infection', *Proc Natl Acad Sci U S A*, 111: 11715-20.

Rekosh, D. M., W. C. Russell, A. J. Bellet, and A. J. Robinson. 1977. 'Identification of a protein linked to the ends of adenovirus DNA', *Cell*, 11: 283-95.

Rexach, M., and G. Blobel. 1995. 'Protein import into nuclei: association and dissociation reactions involving transport substrate, transport factors, and nucleoporins', *Cell*, 83: 683-92.

Ribbeck, K., and D. Görlich. 2002. 'The permeability barrier of nuclear pore complexes appears to operate via hydrophobic exclusion', *EMBO J*, 21: 2664-71.

Ribbeck, K., G. Lipowsky, H. M. Kent, M. Stewart, and D. Görlich. 1998. 'NTF2 mediates nuclear import of Ran', *EMBO J*, 17: 6587-98.

Ritterhoff, T., H. Das, G. Hofhaus, R. R. Schroder, A. Flotho, and F. Melchior. 2016. 'The RanBP2/RanGAP1*SUMO1/Ubc9 SUMO E3 ligase is a disassembly machine for Crm1-dependent nuclear export complexes', *Nat Commun*, 7: 11482.

Robbins, J., S. M. Dilworth, R. A. Laskey, and C. Dingwall. 1991. 'Two interdependent basic domains in nucleoplasmin nuclear targeting sequence: identification of a class of bipartite nuclear targeting sequence', *Cell*, 64: 615-23.

Roelvink, P. W., A. Lizonova, J. G. Lee, Y. Li, J. M. Bergelson, R. W. Finberg, D. E. Brough, I. Kovesdi, and T. J. Wickham. 1998. 'The coxsackievirus-adenovirus receptor protein can function as a cellular attachment protein for adenovirus serotypes from subgroups A, C, D, E, and F', *J Virol*, 72: 7909-15.

Roloff, S., C. Spillner, and R. H. Kehlenbach. 2013. 'Several phenylalanine-glycine motives in the nucleoporin Nup214 are essential for binding of the nuclear export receptor CRM1', *J Biol Chem*, 288: 3952-63.

Rout, M. P., J. D. Aitchison, M. O. Magnasco, and B. T. Chait. 2003. 'Virtual gating and nuclear transport: the hole picture', *Trends Cell Biol*, 13: 622-8.

Rout, M. P., and S. R. Wente. 1994. 'Pores for thought: nuclear pore complex proteins', *Trends Cell Biol*, 4: 357-65.

Rowe, W. P., R. J. Huebner, L. K. Gilmore, R. H. Parrott, and T. G. Ward. 1953. 'Isolation of a cytopathogenic agent from human adenoids undergoing spontaneous degeneration in tissue culture', *Proc Soc Exp Biol Med*, 84: 570-3.

Russell, W. C. 2009. 'Adenoviruses: update on structure and function', *J Gen Virol*, 90: 1-20.

Russell, W. C., W. G. Laver, and P. J. Sanderson. 1968. 'Internal components of adenovirus', *Nature*, 219: 1127-30.

Ryan, K. J., and S. R. Wente. 2000. 'The nuclear pore complex: a protein machine bridging the nucleus and cytoplasm', *Curr Opin Cell Biol*, 12: 361-71.

Saib, A., F. Puvion-Dutilleul, M. Schmid, J. Peries, and H. de The. 1997. 'Nuclear targeting of incoming human foamy virus Gag proteins involves a centriolar step', *J Virol*, 71: 1155-61.

Samad, M. A., T. Komatsu, M. Okuwaki, and K. Nagata. 2012. 'B23/nucleophosmin is involved in regulation of adenovirus chromatin structure at late infection stages, but not in virus replication and transcription', *J Gen Virol*, 93: 1328-38.

San Martin, C. 2012. 'Latest insights on adenovirus structure and assembly', *Viruses*, 4: 847-77.

Sanchez, A. D., and J. L. Feldman. 2017. 'Microtubule-organizing centers: from the centrosome to non-centrosomal sites', *Curr Opin Cell Biol*, 44: 93-101.

Saphire, A. C., T. Guan, E. C. Schirmer, G. R. Nemerow, and L. Gerace. 2000. 'Nuclear import of adenovirus DNA in vitro involves the nuclear protein import pathway and hsc70', *J Biol Chem*, 275: 4298-304.

Schaack, J., W. Y. Ho, P. Freimuth, and T. Shenk. 1990. 'Adenovirus terminal protein mediates both nuclear matrix association and efficient transcription of adenovirus DNA', *Genes Dev*, 4: 1197-208.

Schaak, J., P. Schedl, and T. Shenk. 1990. 'Transcription of adenovirus and HeLa cell genes in the presence of drugs that inhibit topoisomerase I and II function', *Nucleic Acids Res*, 18: 1499-508.

Schwartz, T. U. 2005. 'Modularity within the architecture of the nuclear pore complex', *Curr Opin Struct Biol*, 15: 221-6.

Smith, A., A. Brownawell, and I. G. Macara. 1998. 'Nuclear import of Ran is mediated by the transport factor NTF2', *Curr Biol*, 8: 1403-6.

Smith, J. G., A. Cassany, L. Gerace, R. Ralston, and G. R. Nemerow. 2008. 'Neutralizing antibody blocks adenovirus infection by arresting microtubule-dependent cytoplasmic transport', *J Virol*, 82: 6492-500.

Sodeik, B., M. W. Ebersold, and A. Helenius. 1997. 'Microtubule-mediated transport of incoming herpes simplex virus 1 capsids to the nucleus', *J Cell Biol*, 136: 1007-21.

Strunze, S., M. F. Engelke, I. H. Wang, D. Puntener, K. Boucke, S. Schleich, M. Way, P. Schoenenberger, C. J. Burckhardt, and U. F. Greber. 2011. 'Kinesin-1-mediated capsid disassembly and disruption of the nuclear pore complex promote virus infection', *Cell Host Microbe*, 10: 210-23.

Strunze, S., L. C. Trotman, K. Boucke, and U. F. Greber. 2005. 'Nuclear targeting of adenovirus type 2 requires CRM1-mediated nuclear export', *Mol Biol Cell*, 16: 2999-3009.

Sundquist, B., E. Everitt, L. Philipson, and S. Hoglund. 1973. 'Assembly of adenoviruses', *J Virol*, 11: 449-59.

Suomalainen, M., M. Y. Nakano, S. Keller, K. Boucke, R. P. Stidwill, and U. F. Greber. 1999. 'Microtubule-dependent plus- and minus end-directed motilities are competing processes for nuclear targeting of adenovirus', *J Cell Biol*, 144: 657-72.

Tang, N., and W. F. Marshall. 2012. 'Centrosome positioning in vertebrate development', *J Cell Sci*, 125: 4951-61.

Tedeschi, A., M. Ciciarello, R. Mangiacasale, E. Roscioli, W. M. Rensen, and P. Lavia. 2007. 'RANBP1 localizes a subset of mitotic regulatory factors on spindle microtubules and regulates chromosome segregation in human cells', *J Cell Sci*, 120: 3748-61.

Thakar, K., S. Karaca, S. A. Port, H. Urlaub, and R. H. Kehlenbach. 2013. 'Identification of CRM1-dependent Nuclear Export Cargos Using Quantitative Mass Spectrometry', *Mol Cell Proteomics*, 12: 664-78.

Tollefson, A. E., A. Scaria, T. W. Hermiston, J. S. Ryerse, L. J. Wold, and W. S. Wold. 1996. 'The adenovirus death protein (E3-11.6K) is required at very late stages of infection for efficient cell lysis and release of adenovirus from infected cells', *J Virol*, 70: 2296-306.

Trotman, L. C., N. Mosberger, M. Fornerod, R. P. Stidwill, and U. F. Greber. 2001. 'Import of adenovirus DNA involves the nuclear pore complex receptor CAN/Nup214 and histone H1', *Nat Cell Biol*, 3: 1092-100.

Vayda, M. E., A. E. Rogers, and S. J. Flint. 1983. 'The structure of nucleoprotein cores released from adenovirions', *Nucleic Acids Res*, 11: 441-60.

Wälde, S., K. Thakar, S. Hutten, C. Spillner, A. Nath, U. Rothbauer, S. Wiemann, and R. H. Kehlenbach. 2012. 'The nucleoporin Nup358/RanBP2 promotes nuclear import in a cargo- and transport receptor-specific manner', *Traffic*, 13: 218-33.

Walkiewicz, M. P., N. Morral, and D. A. Engel. 2009. 'Accurate single-day titration of adenovirus vectors based on equivalence of protein VII nuclear dots and infectious particles', *J Virol Methods*, 159: 251-8.

Wang, F., J. Flanagan, N. Su, L. C. Wang, S. Bui, A. Nielson, X. Wu, H. T. Vo, X. J. Ma, and Y. Luo. 2012. 'RNAscope: a novel in situ RNA analysis platform for formalin-fixed, paraffin-embedded tissues', *J Mol Diagn*, 14: 22-9.

Wang, I. H., C. J. Burckhardt, A. Yakimovich, M. K. Morf, and U. F. Greber. 2017. 'The nuclear export factor CRM1 controls juxta-nuclear microtubule-dependent virus transport', *J Cell Sci*, 130: 2185-95.

Wang, I. H., M. Suomalainen, V. Andriasyan, S. Kilcher, J. Mercer, A. Neef, N. W. Luedtke, and U. F. Greber. 2013. 'Tracking viral genomes in host cells at single-molecule resolution', *Cell Host Microbe*, 14: 468-80.

Wang, K., S. Huang, A. Kapoor-Munshi, and G. Nemerow. 1998. 'Adenovirus internalization and infection require dynamin', *J Virol*, 72: 3455-8.

Wang, R., and M. G. Brattain. 2007. 'The maximal size of protein to diffuse through the nuclear pore is larger than 60kDa', *FEBS Lett*, 581: 3164-70.

Wang, W., A. Budhu, M. Forgues, and X. W. Wang. 2005. 'Temporal and spatial control of nucleophosmin by the Ran-Crm1 complex in centrosome duplication', *Nat Cell Biol*, 7: 823-30.

Webster, A., I. R. Leith, and R. T. Hay. 1994. 'Activation of adenovirus-coded protease and processing of preterminal protein', *J Virol*, 68: 7292-300.

Weigel, S., and M. Dobbelstein. 2000. 'The nuclear export signal within the E4orf6 protein of adenovirus type 5 supports virus replication and cytoplasmic accumulation of viral mRNA', *J Virol*, 74: 764-72.

Wen, W., J. L. Meinkoth, R. Y. Tsien, and S. S. Taylor. 1995. 'Identification of a signal for rapid export of proteins from the nucleus', *Cell*, 82: 463-73.

Wiethoff, C. M., H. Wodrich, L. Gerace, and G. R. Nemerow. 2005. 'Adenovirus protein VI mediates membrane disruption following capsid disassembly', *J Virol*, 79: 1992-2000.

Wodrich, H., A. Cassany, M. A. D'Angelo, T. Guan, G. Nemerow, and L. Gerace. 2006. 'Adenovirus core protein pVII is translocated into the nucleus by multiple import receptor pathways', *J Virol*, 80: 9608-18.

Wodrich, H., T. Guan, G. Cingolani, D. Von Seggern, G. Nemerow, and L. Gerace. 2003. 'Switch from capsid protein import to adenovirus assembly by cleavage of nuclear transport signals', *EMBO J*, 22: 6245-55.

Wodrich, H., D. Henaff, B. Jammart, C. Segura-Morales, S. Seelmeir, O. Coux, Z. Ruzsics, C. M. Wiethoff, and E. J. Kremer. 2010. 'A capsid-encoded PPxY-motif facilitates adenovirus entry', *PLoS Pathog*, 6: e1000808.

Wolff, B., J. J. Sanglier, and Y. Wang. 1997. 'Leptomycin B is an inhibitor of nuclear export: inhibition of nucleo-cytoplasmic translocation of the human immunodeficiency virus type 1 (HIV-1) Rev protein and Rev-dependent mRNA', *Chem Biol*, 4: 139-47.

Woodruff, J. B., O. Wueseke, and A. A. Hyman. 2014. 'Pericentriolar material structure and dynamics', *Philos Trans R Soc Lond B Biol Sci*, 369.

Wu, E., L. Pache, D. J. Von Seggern, T. M. Mullen, Y. Mikyas, P. L. Stewart, and G. R. Nemerow. 2003. 'Flexibility of the adenovirus fiber is required for efficient receptor interaction', *J Virol*, 77: 7225-35.

Wu, Z., Q. Jiang, P. R. Clarke, and C. Zhang. 2013. 'Phosphorylation of Crm1 by CDK1-cyclin-B promotes Ran-dependent mitotic spindle assembly', *J Cell Sci*, 126: 3417-28.

Xu, D., N. V. Grishin, and Y. M. Chook. 2012. 'NESdb: a database of NES-containing CRM1 cargoes', *Mol Biol Cell*, 23: 3673-6.

Yamada, J., J. L. Phillips, S. Patel, G. Goldfien, A. Calestagne-Morelli, H. Huang, R. Reza, J. Acheson, V. V. Krishnan, S. Newsam, A. Gopinathan, E. Y. Lau, M. E. Colvin, V. N. Uversky, and M. F. Rexach. 2010. 'A bimodal distribution of two distinct categories of intrinsically disordered structures with separate functions in FG nucleoporins', *Mol Cell Proteomics*, 9: 2205-24.

Yea, C., J. Dembowy, L. Pacione, and M. Brown. 2007. 'Microtubule-mediated and microtubule-independent transport of adenovirus type 5 in HEK293 cells', *J Virol*, 81: 6899-908.

Zhang, W., and R. Arcos. 2005. 'Interaction of the adenovirus major core protein precursor, pVII, with the viral DNA packaging machinery', *Virology*, 334: 194-202.

Zhang, W., and M. J. Imperiale. 2003. 'Requirement of the adenovirus IVa2 protein for virus assembly', *J Virol*, 77: 3586-94.

Zhao, L. J., and R. Padmanabhan. 1988. 'Nuclear transport of adenovirus DNA polymerase is facilitated by interaction with preterminal protein', *Cell*, 55: 1005-15.

Zhou, J., J. Scherer, J. Yi, and R. B. Vallee. 2018. 'Role of kinesins in directed adenovirus transport and cytoplasmic exploration', *PLoS Pathog*, 14: e1007055.

Zur Hausen, H. 1968. 'Association of adenovirus type 12 deoxyribonucleic acid with host cell chromosomes', *J Virol*, 2: 218-23.